RRFM

EUROPEAN RESEARCH REACTOR CONFERENCE 2011

Transactions

Rome, Italy
20 -24 March 2011

EUROPEAN NUCLEAR SOCIETY

ENS CONFERENCE

organised in collaboration with:

ENEA · IAEA International Atomic Energy Agency · Università di Pavia · INFN Istituto Nazionale di Fisica Nucleare · Consiglio Nazionale delle Ricerche

European Nuclear Society
Rue Belliard 65
1040 Brussels, Belgium
Phone + 32 2 505 30 54
Fax +32 2 502 39 02
E-mail ens@euronuclear.org
Internet www.euronuclear.org

ISBN 978-92-95064-11-9

These transactions contain all contributions submitted by 18 March 2011.

Monday 21 March 2011

THE SUPPLY OF MEDICAL ISOTOPES - AN ASSESSMENT OF THE MARKET ECONOMICS, ALTERNATIVE TECHNOLOGIES AND PROPOSED POLICY APPROACH TO ACHIEVING SUSTAINABILITY

R. CAMERON, A. Y. LOKHOV, C. WESTMACOTT
Nuclear Development Division
OECD Nuclear Energy Agency
12, boulevard des Îles
92130 Issy-les-Moulineaux
France

ABSTRACT

At the request of its member countries, the OECD Nuclear Energy Agency (NEA) has become involved in global efforts to ensure a reliable supply of molybdenum-99 (^{99}Mo) and its decay product, technetium-99m (^{99m}Tc), the most widely used medical radioisotope. The NEA established the High-level Group on the Security of Supply of Medical Radioisotopes (HLG-MR).

The main objective of the HLG-MR is to strengthen the reliability of ^{99}Mo and ^{99m}Tc supply in the short, medium and long term. In order to reach this objective, the group has been reviewing the ^{99}Mo supply chain, working to identify the key areas of vulnerability, the issues that need to be addressed and the mechanisms that could be used to help resolve them. The collective efforts of HLG-MR members and nuclear medicine stakeholders have allowed for a comprehensive assessment of the key areas of vulnerability in the supply chain and an identification of the issues that need to be addressed.

As a result of the work undertaken to date, the NEA has released three reports under the new *The Supply of Medical Radioisotopes* series. These reports discuss the uneconomical situation of the supply chain, other vulnerabilities within the supply chain and alternative technologies to produce ^{99}Mo/^{99m}Tc. From this work, the NEA Secretariat and the HLG-MR have started to develop the policy approach and recommendations for governments, industry and other stakeholders that will outline the foundation for ensuring the long-term supply of ^{99}Mo/^{99m}Tc.

1. Introduction

At the request of its member countries, the OECD Nuclear Energy Agency (NEA) has become involved in global efforts to ensure a reliable supply of molybdenum-99 (^{99}Mo) and its decay product, technetium-99m (^{99m}Tc), the most widely used medical radioisotope. The NEA established the High-level Group on the Security of Supply of Medical Radioisotopes (HLG-MR), which is currently comprised of 22 experts who are representatives from the governments of 13 nations, the European Commission and the International Atomic Energy Agency (IAEA). The main objective of the HLG-MR is to strengthen the reliability of ^{99}Mo and ^{99m}Tc supply in the short, medium and long term.

Throughout the first year and a half of its two-year mandate, the HLG-MR has examined the major issues that affect the short-, medium- and long-term reliability of ^{99}Mo/^{99m}Tc supply. The collective efforts of HLG-MR members and nuclear medicine stakeholders have allowed for a comprehensive assessment of the key areas of vulnerability in the supply chain and an identification of the issues that need to be addressed. Significant progress has already been achieved on improving the supply situation through increased communication, co-ordination of reactor schedules and a better understanding of demand-management opportunities. Continued action is required on the part of all stakeholders.

As a result of the work undertaken to date, the NEA has released three reports under the new *The Supply of Medical Radioisotopes* series (accessible at www.oecd-nea.org/med-radio). The first, subtitled *An Economic Study of the Molybdenum-99 Supply Chain,* offers a

unique analysis of the ^{99}Mo/^{99m}Tc supply chain. The second, subtitled *Interim Report of the OECD/NEA High-level Group on the Security of Supply of Medical Radioisotopes,* presents findings related to the main issues affecting security of supply including reactor and processing capacity constraints, transport, demand management, communications and other supply chain problems. The third, subtitled *Review of Potential Molybdenum-99/Technetium-99m Production Technologies,* presents and reviews potential alternatives for the production of ^{99m}Tc and ^{99}Mo.

From this work, the NEA Secretariat and the HLG-MR have started to develop the policy approach and recommendations for governments, industry and other stakeholders that will outline the foundation for ensuring the long-term supply of ^{99}Mo/^{99m}Tc. This policy approach, as well as the full findings of the HLG-MR, is expected to be published by August 2011.

This paper briefly discusses the findings from these three papers and introduces the policy approach that could address the issues affecting the long-term sustainable supply.

2. Economics of the ^{99}Mo supply chain

2.1 Historical development of the supply chain and its economic implications

Within the current ^{99}Mo supply chain, all the major producers irradiate targets using multipurpose research reactors, which were originally constructed and operated with 100% government funding, mainly for research and materials testing purposes. When ^{99}Mo production started, the reactors' original capital costs had been paid or fully justified for other purposes. As a result, ^{99}Mo was seen as a by-product that provided another mission for the reactor that could generate extra revenue to support research. This resulted in:

- Reactor operators originally only requiring payment of *direct* short-run marginal costs.
- ^{99}Mo prices not covering any significant share of costs of overall reactor operations and maintenance, nor of capital costs or allowances for replacement or refurbishment costs.
- The by-product status remaining with no substantive pricing changes even as the importance of ^{99}Mo production increased within reactor operating activities.

As a result, reactor prices were too low to sustainably support the ^{99}Mo-attributable portion of reactor operations, did not even cover short-run marginal costs in some cases, and did not provide enough financial incentive to support replacing or refurbishing ageing reactors. In addition, even with uncertainty on costs of conversion for a major ^{99}Mo producer, it is clear that the current pricing structure provides insufficient financial incentive for the development and operation of low enriched uranium (LEU) based infrastructure.

The processing component, originally funded by governments, was commercialized in the 1980s and 1990s. Commercialisation was originally thought to be beneficial to all parties; however, contracts were based on historical perceptions of costs and pricing. This resulted in long-term contracts with favourable terms for commercial processing firms, with no substantial change to the prices for irradiation. Once these contracts were established, they set the standard for new processors and reactors that entered the market.

An unintended effect of commercialisation was establishing market power for processors. The contracts, in some cases, created a situation where the reactor had only one avenue for selling its ^{99}Mo irradiation services. Barriers to entry (both natural and created, such as aggressive pricing strategies) sustained the market power balance and contributed to maintaining low prices for irradiation services.

A complicating factor was the historical existence of excess capacity of irradiation services. Some excess capacity is necessary to provide back-up at times when reactors are not operating, or when unexpected or extended shutdowns occur. However, operators were not compensated for maintaining reserve capacity, creating an incentive for reactor operators to use the capacity to gain revenue rather than leaving it idle, driving down the prices of irradiation services further, reducing reliability, and perpetuating processor market power.

Further downstream, pricing strategies of generator manufacturers were focused on encouraging sales of their cold kits. These strategies had a feedback effect upstream, with profits not flowing back up through the ^{99}Mo supply chain and limiting the flexibility to absorb proposed upstream price increases.

However, reactors continued to provide irradiation services even under these uneconomical conditions given the social contract between governments and the medical imaging community. Governments subsidised the development and operation of research reactors and related infrastructure, including radioactive waste management. Using part of this funding, reactor operators irradiated targets to produce ^{99}Mo. In return, citizens would receive an important medical isotope for nuclear medicine diagnostic procedures.

Although reactor operators were aware that government financial support was increasingly used for ^{99}Mo production, this may not have been transparent to governments. In some cases, the magnitude of the change did not become clear until there were requests for specific funding to refurbish a reactor or construct a new reactor. These subsidies were also supporting the production of ^{99}Mo that was exported to other countries.

Recently, governments from almost all current major producing countries have indicated that they are reconsidering or no longer interested in subsidising new or ongoing production of ^{99}Mo at the reactor level at historical levels (or at all), some more formally than others – questioning whether it remains in the public interest. With a changed social contract, the economics have to become sustainable on a full-cost basis or the availability of a long-term reliable supply of ^{99}Mo will be threatened.

2.2 Economically sustainable pricing and impacts

Starting from a representative cost and pricing structure developed by the NEA, based on information from supply chain participants, levelised unit cost of ^{99}Mo (LUCM) calculations determined the magnitude of the price changes needed for economic sustainability. Their impact, based on various capital investment scenarios, was also examined. These scenarios range from using existing reactors to building a fully dedicated isotope reactor and processing facilities. Under all the scenarios, prices must increase; the analysis of the current economic situation found that, for existing reactors, the marginal revenue from production was lower than the marginal costs, with reactors facing a loss on every unit of ^{99}Mo produced.

The LUCM calculations indicated that significant price increases are necessary in the upstream supply chain in order to be economically sustainable (up to a maximum increase of 900%). However, the analysis finds that there is very little effect on the prices per patient dose; at pre-shortage prices, the irradiation price from the reactor is calculated to be only 0.11% of the final reimbursement rate. Even at the most extreme price increase from the reactor, the value of irradiation would increase to only represent 0.97% of the final reimbursement rate.

The analysis indicates that, while prices will increase for the downstream components, these should be able to be absorbed. However, this issue may require further study and possible assessment by hospitals and medical insurance plans, especially in the context of continued downward pressure on reimbursement rates or in cases where the health system provides fixed budgets to hospitals for radioisotope purchases.

The study makes a number of recommendations and investigates options to assist decision-makers to restructure the supply chain. These recommendations have been considered and integrated, where appropriate, in on-going HLG-MR work to develop a comprehensive policy approach to encourage a long-term secure supply of ^{99}Mo/^{99m}Tc. This policy approach is discussed further below.

3. Supply chain vulnerability beyond economics

In addition to the economic issues being faced by the supply chain, there are a number of other related areas of vulnerability that the HLG-MR has been able to identify. These are discussed in-depth within the *Interim report*.

The Canadian and Dutch reactors have come back on line, providing for production of ^{99}Mo to return to levels seen before the 2009-2010 supply shortage. While this is positive news, the current capacity remains fragile and further supply shortages could be expected. A number of the producing reactors within the current ageing fleet are scheduled to be removed from the supply chain over the next decade, with the earliest scheduled for 2015 (OSIRIS) and 2016 (NRU). Coupling these shutdowns with growing demand, there is the possibility that supply would fail to be able to meet demand within the next few years.

Since the shortage, there have been a number of new projects that have been discussed and a few that have started to irradiate targets to produce ^{99}Mo. For example, the MARIA reactor in Poland, the Rez reactor in the Czech Republic, and the Russian reactors have all entered the supply chain. Even with these new additions and a consideration of the other new projects that are under development or discussion, growing demand and the removal from the supply chain of current reactors means that there could still be a supply-insufficient situation as early before the end of the current decade.

This concern on future supplies is partly as a result of regional limitations on processing capacity, which is essential for extracting and purifying the ^{99}Mo from the irradiated targets. These targets are very difficult to transport long distances, requiring processing capacity to be located reasonably close to ^{99}Mo producing reactors. There are some regions where processing capacity is not currently sufficient to support increased production of ^{99}Mo, to meet increasing demand, to deal with possible reactor outages globally or to address the changing supply structure as older reactors are retired. These processing limitations can be a significant barrier to developing new irradiation capacity and can exacerbate regional supply imbalances in shortage situations.

The necessity to transport radioactive material is another area of vulnerability affecting the reliable supply of ^{99}Mo/^{99m}Tc. At each stage of the supply chain, radioactive material is transported, sometimes across a number of borders or even half-way around the world. In a number of cases, this transportation requires multiple approvals in multiple jurisdictions. There is also the concern that shipments of these vital medical radioisotopes are sometimes denied or delayed by carriers or are refused entry by national authorities. These issues have significant impacts on the economics of the supply chain (delay of one day reduces the amount of ^{99}Mo available by about 23%) as well as affecting the patient that is waiting for their essential medical imaging diagnostic procedure. The IAEA, among other players, continues to undertake important efforts to address these concerns.

4. Alternative Technologies

The importance of nuclear medicine and diagnostics in the world, and also the recent shortage of ^{99}Mo supply, has motivated investigations of alternative technologies. Alternative technologies could be reactor-based (like neutron activation of ^{98}Mo) or accelerator-based (direct cyclotron production of ^{99m}Tc, photofission, etc.) and they are currently at very different development stages.

In order to get a sense of the potential of alternative technologies for producing ^{99}Mo/^{99m}Tc, the NEA, with the help of its HLG-MR and other experts, developed a common set of criteria that could be used to compare all the technologies. The physical and economic criteria were then applied to the alternative technologies. For convenience, these alternative technologies were classified as short-, medium-, and long-term technologies based on an assessment of their timeframe for potential availability.

The assessment of the various alternative technologies has been done using a three-grade rating system (low, medium and high) derived from the application the common estimation methodology. The set of criteria used within the methodology is:

- Technology maturity
- Production yield
- Available irradiation capacity
- Distribution range and logistics
- Simplicity of processing
- Waste management
- Proliferation resistance
- Other isotope co-production potential
- Normalized capital costs
- Commercial compatibility
- Estimated levelised unit cost
- Ease of nuclear regulatory approval
- Ease of health regulatory approval
- Units required to supply world market

The review defines short-term technologies as those that have already been used for ^{99}Mo/^{99m}Tc production, or for which nuclear imaging test have been performed. Today, the list of short-term technologies includes uranium fission route (irradiation of solid targets in research reactors), neutron activation route and direct cyclotron production of ^{99m}Tc. These technologies were considered in detail in the review.

The review highlighted that the use of low enrichment uranium (LEU) targets for ^{99}Mo production has some advantages over HEU, including: proliferation resistance; easier availability of the target material; and easier compliance for target transportation and processing. However, it currently has lower production yield than HEU and may require more targets to be irradiated with correspondingly increased volumes of waste. Increasing the uranium content of the targets (e.g. of the existing high density LEU targets, or using metallic foil targets), to counteract the lower production yield will be a key factor for LEU-based production, but there seems to be no technological or economic reasons not to deploy this technology.

The review also found that neutron activation in a research reactor has advantages in terms of safety, waste management and proliferation resistance, but has low specific activity and, with current technologies, would require the recycling of the highly enriched molybdenum in order to be cost-effective. This is currently not done. Also, more development and experience is needed in (gel) generator technology prior to eventual larger scale deployment.

Direct ^{99m}Tc production using cyclotrons has potential advantages in terms of cost, waste management, proliferation resistance and ease of approval but can only provide local needs (^{99m}Tc is a very-short lived isotope). The technology also requires significant amounts of highly enriched molybdenum (^{100}Mo). As a result, a large number of cyclotrons would be required to meet the world demand and the product would not be able to be shipped far or exported to supply global needs.

5. Policy Approach

The HLG-MR is currently developing a cohesive policy approach to address the issues being faced by the supply chain, in order to move towards a long-term secure supply of ^{99}Mo and ^{99m}Tc. At its last meeting, the HLG-MR agreed on many necessary aspects of this approach.

In order to address the problems being faced by the industry, the HLG-MR agreed that the final policy approach will have to address the following four central pillars of reform:

- Market economics need to be improved.
- Structural changes are necessary.
- The government role has to be clearly defined.
- An effective co-ordinated international approach is necessary.

The HLG-MR agreed that the policy approach most likely to be able to achieve the necessary reforms in a coherent and comprehensive manner is as follows:

- Markets should do what they can, but there are limits to what may be possible.

- Governments have an essential role in supporting market operations by ensuring the proper environment for investment and addressing market failures, while recognising the commercial nature of the supply chain.
- International collaboration is necessary, particularly to avoid policy approaches at the domestic and regional levels that could negatively affect global ^{99}Mo/^{99m}Tc supply security.
- Transparency of market operation is important to ensure that the market continues its evolution to an economically sustainable system.

In order to ensure the consistent fulfilment of responsibilities by the various communities and stakeholders of the supply chain, the HLG-MR is presently working to formulate the policy approach necessary to address the key issues affecting the ability to realise a long-term secure ^{99}Mo/^{99m}Tc supply. This approach will suggest addressing the main issues by:

- Implementing full-cost recovery.
- Sourcing, valuing and paying for reserve capacity.
- Fulfilling the essential government role in setting the proper environment for safe and efficient market operations
- Encouraging the conversion to using LEU targets for ^{99}Mo production.
- Collaborating internationally to ensure a globally consistent approach to addressing security of supply of ^{99}Mo/^{99m}Tc.
- Periodically reviewing progress to implementing an economically sustainable supply chain.

The HLG-MR is currently working to finalise the policy approach, including developing recommendations on how to implement the necessary actions. The policy approach will be finalised in June 2011.

6. Conclusions

The work of the HLG-MR and the associated stakeholders has been important in determining the issues affecting the ability of the supply chain to ensure a long-term secure supply of ^{99}Mo and ^{99m}Tc. It has also undertaken some significant actions already that have made on impact; however, there are still a number of actions that need to be taken to ensure a long-term reliable supply. Even though the current supply situation has stabilised (at the time of writing the article), it is important to stress that the underlying problem – the unsustainable economic structure – has not yet been addressed; supply shortages could become commonplace over the next decade unless longer-term actions are taken to secure supplies.

It is clear that without ongoing financial support from governments, commercial pricing is required for the continued supply of reactor-based ^{99}Mo in the medium to longer term and the conversion to LEU-based production. Changes are necessary to arrive at a ^{99}Mo/^{99m}Tc supply chain that is economically sustainable and reliable.

The policy approach currently being developed by the HLG-MR will set the foundation for consistent and comprehensive steps forward to ensuring the long-term security of supply of the vital medical radioisotopes molybdenum-99 and its decay product technetium-99m.

THE JULES HOROWITZ REACTOR: A NEW EUROPEAN MTR (MATERIAL TESTING REACTOR) OPEN TO INTERNATIONAL COLLABORATION: DESCRIPTION AND STATUS

G.BIGNAN, P.M. LEMOINE, X. BRAVO
French Atomic Energy Commission
Nuclear Energy Division
Research Centre of Cadarache and Saclay
Bâtiment 707 13108 St Paul lez Durance France
Bâtiment 121 91191 Gif sur Yvette France
gilles.bignan@cea.fr; patrick-marie.lemoine@cea.fr ; xavier.bravo@cea.fr

ABSTRACT

The Jules Horowitz Reactor (JHR) is a new Material Testing Reactor currently under construction at CEA Cadarache research centre in the south of France.
It will represent a major Research Infrastructure for scientific studies dealing with material and fuel behaviour under irradiation (and is consequently identified for this purpose within various European road maps and forums; ESFRI, SNE-TP…).
The reactor will also be devoted to medical isotope production.
The reactor will perform R&D programs for the optimization of the present generation of NPP, support the development of the next generation of NPP (mainly LWR) and also offer irradiation possibilities for future reactors.
JHR is designed, built and will be operated as an international user-facility open to international collaboration. Moreover, the preparation of the experimental capacity is in progress with the development of “hosting experimental devices” to be “on the shelves” for the start of operation.
This paper gives an up-to-date status of the construction and of the developments of the future experimental capacity.

INTRODUCTION

European Material Testing Reactors (MTR) have provided an essential support for nuclear power programs over the last 40 years within the European Community. However, these Material Test Reactors (MTRs) will be more than 50 years old in this decade and will face increasing probability of shut-down due to the obsolescence of their safety standards and of their experimental capability. Such a situation cannot be sustained long term since “nuclear energy is a competitive energy source meeting the dual requirements for energy security and the reduction of greenhouse gas emissions, and is also an essential component of the energy mix” [1].
Associated with hot laboratories for the post irradiation examinations, MTRs are structuring research facilities for the European Research Area in the field of nuclear fission energy.
MTRs address the development and the qualification of materials and fuels under irradiation with sizes and environment conditions relevant for nuclear power plants in order to optimise

and demonstrate safe operations of existing power reactors as well as to support future reactor design:

- Nuclear plants will follow a long-term trend driven by the plant life extension and management, reinforcement of the safety, waste and resource management, flexibility and economic improvement. These stakes require in depth technical assessment of material and fuel behaviour under irradiation so that industry and safety bodies need a permanent access to irradiation experimental capabilities and associated technical expertise.
- In parallel to extending performance and safety for existing and coming power plants, R&D programs are taking place in order to assess and develop new reactor concepts (Generation IV reactors) that meet sustainability purposes. A variety of aspects need to be addressed in this context, regarding economics, safety, resources management, waste management and nuclear proliferation criteria. Development of new fuels and material are mandatory for these reactor concepts, leading to challenging scientific and technical issues.
- **In addition, for most European countries, keeping competences alive is a strategic cross-cutting issue**; developing and operating a new and up-to-date research reactor appears to be an effective way to train a new generation of scientists and engineers. This goal is presently carried out by various joint developments (notably through FP projects) of a new generation of experimental processes and devices, with increased instrumentation capabilities consistent with advanced modelling in material and fuel science.

This analysis was already made by a thematic network of Euratom 5th FP, involving experts and industry representatives, in order to answer the question from the European Commission on the need for a new Material Testing Reactor (MTR) in Europe [2,3].
The conclusions were the following:

- « There is clearly a need as long as nuclear power provides a significant part of the mix of energy production sources »
- « Given the age of current MTRs, there is a strategic need to renew MTRs in Europe; At least one new MTR shall be in operation in about a decade from now ».

This entire preparatory work leads to the fact that the **JHR research infrastructure has been identified on the ESFRI Roadmap since 2008.**

1] The JHR project in this context

JHR will offer modern irradiation experimental capabilities to study material & fuel behaviour under irradiation. JHR will be a flexible experimental infrastructure to meet industrial and public needs within the European Union related to present and future Nuclear Power Reactors.
JHR is designed to provide high neutron flux (twice as large as the maximum available today in MTRs), to run highly instrumented experiments to support advanced modelling giving prediction beyond experimental points, and to operate experimental devices giving environment conditions (pressure, temperature, flux, coolant chemistry, …) relevant for water reactors, for gas cooled thermal or fast reactors, for sodium fast reactors, …

These irradiation experimental capabilities will address

- Power plant operation of existing and coming reactors (Gen 2 & 3) for material ageing and plant life management,
- Design evolutions for Gen 3 power reactors (in operation for the whole century) such as performance improvement and evolution in the fuel cycle,

- Fuel performance and safety margin improvements with a strong continuous positive impact on Gen 2 & 3 reactor operating costs and on fuel cycle (burn-up and duty-cycle increase for UOX and MOX fuel)
- Fuel qualification in incidental or accidental situations
- Fuel optimisation and qualification for High Temperature Reactors
- Innovative material & fuel development for Gen 4 systems in various environments (very high temperature, fast neutron gas cooled systems, various coolants such as supercritical water, lead, sodium…). The development of these systems raises challenges to be addressed by a modern experimental irradiation infrastructure like JHR.

These objectives require representative tests of structural materials and fuel components as well as in-depth investigations with “separate effects” experiments coupled with advanced modelling.
For example, the JHR design accommodates improved on-line monitoring capabilities such as the fission product laboratory directly coupled to the experimental fuel sample under irradiation. This monitoring can be used to get key information on the fission gas source term during transients related to incidents. It can also provide time-dependant data on the fuel microstructure evolution during the irradiation, which is of course a valuable input for modelling developments.

As a modern research infrastructure, JHR will contribute to the development of expertise and know-how, and to the training of the next generation of scientists and operators with a positive impact on nuclear safety, competitiveness and social acceptance. The JHR is mainly designed to meet these technical objectives.

As another important objective, **the JHR will contribute to secure the production of radioisotope for medical application. This is a key public health stake.**

JHR, as a future international User Facility, is driven by an international consortium gathering industry (Utilities, Fuel vendors…) and public bodies (R&D centres, TSO, Regulator…).

The present members list of JHR consortium is the following:
CEA (France),EDF (France), AREVA(France),Euratom, SCK.CEN (Belgium),UJV (Czech Republic),VTT(Finland),CIEMAT(Spain),Vattenfall(Sweden),DAE(India), JAEA(Japan)

The JHR facility description and the development of the first experimental capacity is described in detailed in previous RRFM and IGORR conferences (see for examples ref 4], 5] and 6]) and we will only focus now on an update status.

2] JHR construction update

The construction of JHR which was started in 2007 is going-on in a nominal way and some major milestones have been achieved in 2010 regarding the construction:
- Discharge structure of the water tertiary circuit into EDF canal (Fig.1)
- Completion of upper basement concrete for the Nuclear Auxiliary Building (NAB) and for the Reactor Building (RB) (Fig. 2, 3, 4)

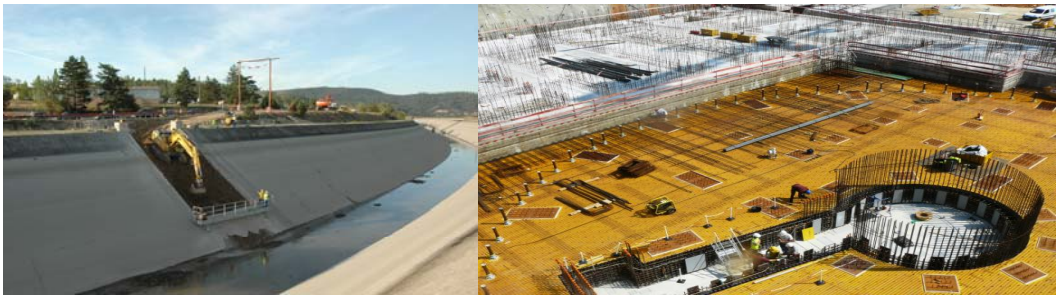

Fig.1: water circuit work on EDF canal; Fig.2: Nuclear Auxiliary Building upper basement concrete and preparation for Reactor Building upper basement

Fig.3: Pouring concrete for RB upper basement; Fig.4: view of Building site-January 2011

Qualification Program is also continuing and, at the end of 2010, the choice of the forging process for the material of JHR core rack (Al-T6061) was done (two-beaked anvil process)

Fig.5: JHR core rack and mock-up manufacturing

It is interesting to quote that some members of JHR consortium have an in-kind contribution which is also progressing in a nominal way;

- CIEMAT who represent a Spanish consortium is designing and launching the manufacturing of the three Heat exchangers of the primary circuit
- VTT who represent a Finnish consortium is designing and manufacturing various NDE equipment (see ref 6] presentation at this conference)
- SCK.CEN Mol from Belgium is performing JHR fuel qualification under irradiation in the EVITA loop (see EVITA presentation in RRFM 2010)
- NRI from Czech Republic is designing, performing qualification tests and manufacturing JHR Hot Cells (see photos below):

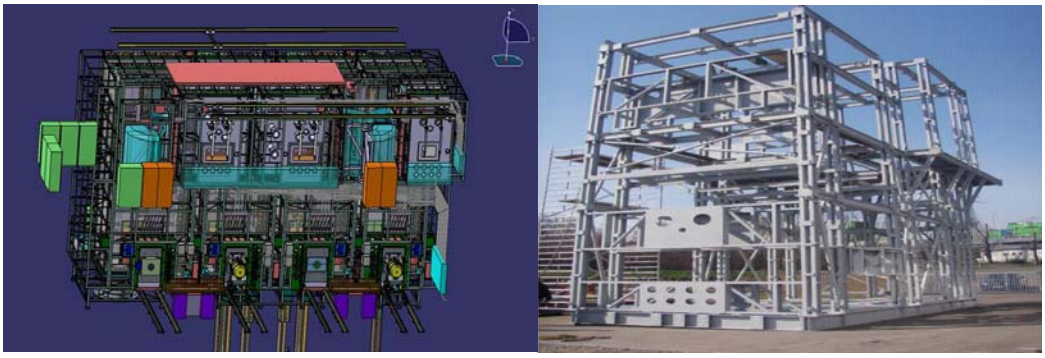

Fig.6: JHR Hot Cells design and manufacturing by NRI

3] JHR as an International Scientific User Facility

In parallel to the construction, the preparation of an international community around JHR is continuing; this is an important topic because, as indicated in the introduction, building and gathering a strong international community in support to MTR experiments is a key-issue for the R&D in nuclear energy field.
CEA is welcoming scientists –secondee- from various organisations who are integrated within the JHR team for the development of the experimental devices.
At the present time, scientists from Australia (ANSTO) Austria (ATI), Italy (ENEA), Poland (POLATOM) and USA (INL) are integrated in JHR team and some are working for JHR while staying in their institutes (eg. Vattenfall from Sweden).

Building an international joint program: the JHIP (Jules Horowitz International Program)
According to the consortium agreement, JHR is aimed to become a user reactor at international level on the model of the Halden Reactor Project with multinational project and proprietary experiments. Consequently, CEA is preparing, with the support of the OECD/NEA, a joint program called Jules Horowitz International Programme (JHIP) which has been thought with the strategic scope to address fuel and material issues of common interest that are key for operating plants and future NPP (mainly focused on LWR).

2010 has been a very active year for the preparation of this International Joint Program with a scientific proposal made by CEA to the expert community on Fuel Safety and Reliability and the venue of an expert meeting mid-September 2010 at the OECD headquarters to debate on the judiciousness of the CEA proposals. The overall objective of the proposed program is to increase the understanding of the mechanisms that govern fuel reliability and safety throughout the entire fuel service time and to assess design improvements aimed at enhancing the flexible, reliable and safe operation of nuclear fuel. This objective is to be pursued through a suitable hot cell and in-reactor experimentation program combined with analytical work in support of the data interpretation and model development.
The intended programme is to be carried out as an international OECD-NEA project:

- Hence it will consist of an internationally agreed scope and be run according to a given cost sharing arrangement

- The programme is meant to complement the work performed at other establishments, notably those involved with OECD projects, such as SCIP, STEP…

The CEA proposals deal with the following topics:

- Fuel reliability, assessed through power ramps tests and PIE
- LOCA tests, done out of-pile in a first phase and in-pile in a possible second phase
- Source Term tests addressing fission products release in a variety of fuel failure conditions.

A tentative planning for setting-up the JHIP is as follows:

- 2009-2011: Project preparation
- 2012-2015: Project Phase 1 with Experimentation in existing facilities (OSIRIS, LECA…)
- 2016-2019: Project Phase 2 with experimentation in JHR.

Around 50 experts from various origin (Safety Authorities-CSN, SRSA… and/or Technical Support Organisation to regulatory bodies-NRC,IRSN, …Utilities-EDF, ENUSA, GDF Suez, VATTENFALL, GE…Engineering companies –AREVA…, Research Organisation- VTT, AECL, NRI, AEKI, PSI, CEA…) from 15 countries have participated in this meeting.
Following positive feedback from this meeting, CEA is preparing the test matrix for each topic (Ramps, LOCA and Source Term) to be discussed in detail with each potential partner.
The target is to get a nearly completed JHIP OECD agreement by the end of 2011 in order to launch scientific programs up to 2012.

Conclusion

As indicated JHR building is going-on in a nominal way and its first criticality is scheduled for 2014. This facility –regarding the experimental capacity- is already open and will be more and more so to international collaboration. It is clear that within a context of nuclear renewal, the JHR will be a key infrastructure in the European Research Area for R&D in support to the use of nuclear energy.

References

1] The Green Paper, “Towards a European Energy Security Strategy”, published by the European Commission in November 2000
2] FEUNMARR, Future European Union Needs in Material Research Reactors, 5th FP thematic network, Nov. 2001 – Oct 2002
3] C. Vitanza, D. Iracane, D. Parrat, Future needs for materials test reactors in Europe (FEUNMARR Findings), 7th International Topical Meeting on Research Reactor Fuel Management, ENS, RRFM 2003.
4] The Jules Horowitz Reactor Project:” A new High Performances European and International Material Testing Reactor for the 21st century”- G. Bignan, D.Iracane Nuclear Energy International (NEI-Dec 2008)
5] “Sustaining Material Testing Capacity in France: From OSIRIS to JHR” G. Bignan, D. Iracane, S. Loubière, C. Blandin CEA (France) IGORR 2009 Conference (Beijing)
6] “Status of the MELODIE experiment, an advanced device for on-line biaxial study of the irradiation creep of LWR cladding” P. Guimbal et al (This conference)

MYRRHA, A FLEXIBLE FAST SPECTRUM IRRADIATION FACILITY

P. BAETEN, R. FERNANDEZ, D. DE BRUYN, G. VAN DEN EYNDE, E. MALAMBU, P. BENOIT & H. AÏT ABDERRAHIM
Belgian Nuclear Research Centre (SCK•CEN)
Boeretang 200, BE-2400 Mol – Belgium

ABSTRACT

MYRRHA (Multi-purpose hYbrid Research Reactor for High-tech Applications) is the flexible experimental accelerator-driven system (ADS) in development at SCK•CEN in replacement of its material testing reactor (MTR) BR2. The MYRRHA-facility, currently developed with the aid of the FP7-project "Central Design Team" is conceived as a flexible irradiation facility, able to work in both subcritical and critical modes. In this way, MYRRHA will allow fuel developments for innovative reactor systems, material developments for GEN IV systems, material developments for fusion reactors, radioisotope production for medical and industrial applications, and Si-doping.
MYRRHA will also demonstrate the ADS full concept by coupling the three components (accelerator, spallation target and subcritical reactor) at reasonable power level to allow operation feedback, scalable to an industrial demonstrator and allow the study of efficient transmutation of high-level nuclear waste. Since MYRRHA is based on the heavy liquid metal technology, lead-bismuth eutectic, it will be able to significantly contribute to the development of Lead Fast Reactor Technology and in critical mode, MYRRHA will play the role of European Technology Pilot Plant in the roadmap for LFR.
In this paper the historic evolution, international positioning and the set-up of the international members' consortium of the MYRRHA-project and the rationale behind the design choices are presented. Also, the latest configuration of the reactor system is described together with the different irradiation capabilities. More specifically, the possibilities and performances for fuel irradiations are presented in more detail.

1. Introduction

One of the flagships of the nuclear infrastructure of the Belgian Nuclear Research Centre (SCK•CEN) is the BR2 reactor[1], a flexible irradiation facility known as a multipurpose materials testing reactor. This reactor is in operation since 1962 and is, after being refurbished twice, now licensed for operating until 2016 with a possible extension for another ten-year period until 2026. Therefore, the Belgian Nuclear Research Centre is working since 1998 at the pre- and conceptual design of a multi-purpose flexible irradiation facility, called MYRRHA, that can replace BR2 MTR and that is innovative to support future oriented research projects needed to sustain the future of the research centre. MYRRHA has been designed as a multipurpose Accelerator Driven System (ADS) for R&D applications, and consists of a proton accelerator delivering its beam to a spallation target that in turn couples to a sub-critical fast core, also cooled with Lead-Bismuth.
MYRRHA has started from the ADONIS project (1995-1997). ADONIS was the first SCK•CEN project where the coupling between an accelerator, a spallation target and a subcritical core was studied. The ADONIS project, since 1998 named MYRRHA, evolved to a larger installation. In 2005, MYRRHA has been offered as a starting base for the XT-ADS design. XT-ADS is a short-term (operational around 2020) small-scale (50 to 100 MW_{th} experimental facility that should demonstrate the technical feasibility of transmutation in an accelerator driven system. The history of MYRRHA from ADONIS to FASTEF is discussed in section 2. The present design of the project in section 3. Of this present design, the following components are discussed in detail: the primary cooling system (3.1), the sub-critical core (3.2) and the in-vessel fuel handling machine (3.3). At last, the performances of the fuel irradiations are described in section 4.

2. Historical evolution of MYRRHA: from ADONIS to XT-ADS

The coupling between an accelerator, a spallation target and a subcritical core has been studied for the first time at SCK•CEN in collaboration with Ion Beam Applications (IBA, Louvain-la-Neuve) in the frame of the ADONIS project (1995-1997). ADONIS was a small irradiation facility, based on the ADS concept, having the single objective to produce radioisotopes for medical purposes and more particularly ^{99}Mo as a fission product from highly enriched ^{235}U fissile targets. The proposed design was of limited size with an accelerator of 150 MeV and a core with a power of around 1.5 MW_{th}. The system was a thermal spectrum machine and therefore water was used as coolant and moderator.

The ad-hoc scientific advisory committee recommended extending the purpose of the ADONIS machine to become a material testing reactor for material and fuel research, to study the feasibility of transmutation of the minor actinides and to demonstrate at a reasonable power scale the principle of the ADS. Since 1998, the project is named MYRRHA. In its 2005 version, MYRRHA consisted of a proton accelerator of the cyclotron type delivering a 350 MeV * 5 mA beam to a windowless liquid Pb-Bi spallation target that in turn couples to a Pb-Bi cooled, subcritical fast core of 50 MW_{th}. This 2005 design is also called 'Draft – 2' design[2].

The MYRRHA 2005 design was offered as a starting base for the XT-ADS design in the FP6 EUROTRANS integrated project[3]. The XT-ADS is a pool-type ADS cooled by lead-bismuth eutectic (LBE). The XT-ADS accelerator is a linear accelerator delivering a 600 MeV * 3.2 mA beam into the spallation target. The reactor power is 57 MW_{th}. The primary heat exchangers have been dimensioned to 70 MW_{th} in order to incorporate the beam power output as well as the decay heat and some extra margin.

At the end of the EUROTRANS project, the XT-ADS design has complied with the project main requirements[4]. However, the objectives of the XT-ADS did not fully correspond with the objectives of MYRRHA. Therefore, it's clear that future design work is needed to bring the design of MYRRHA-FASTEF in line with the objectives, application catalogue and rationale for implementation.

First of all, since the objective of MYRRHA-FASTEF is to operate both in a sub-critical mode and a critical mode, an analysis was be performed to establish to which extent the design of XT-ADS (which only considered sub-critical mode operation) needs to be modified to respond to the objective to operate also in critical mode. In this respect, it is clear that reactivity control and scram systems have to be included in the design. Also, an analysis had to be performed to determine the advantages and disadvantages linked to windowless target concept. Working in critical mode modifies significantly the safety characteristics of the facility and the impact of the safety feedback on the design needs to be implemented.

A second major topic for the update of the MYRRHA design is to obtain the targets set in the applications catalogue. The XT-ADS concept is not able to reach all the different targets in terms of irradiation conditions listed in the applications catalogue. To increase the flux level, it is obvious that the total power and power density will have to be increased.

3. Current FASTEF design

The main components/systems of FASTEF are of the same XT-ADS type with only increased size. The primary and secondary systems have been designed to evacuate a maximum core power of 100 MW_{th}. All the FASTEF components are optimized for the extensive use of the remote handling system during components replacement, inspections and handling.

Figure 1 presents a vertical cut inside the reactor vessel, showing its main internal components. The main parameters are listed in Table 1.

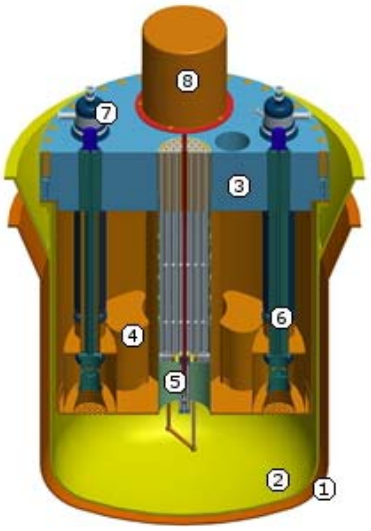

1. Outer vessel
2. Inner vessel
3. Cover
4. Diaphragm
5. Core
6. Primary Pump
7. Primary Heat Exchanger
8. In-vessel fuel handling machine

Figure 1: Vertical cut of FASTEF

FA Length	2000 mm
Nominal Power	100 MW
Core inlet temperature	270 °C
Core outlet temperature	410 °C
Coolant velocity in core	2 m/s
Coolant pressure drop	2.5 bar
Secondary coolant	Saturated water/steam
Tertiary coolant	Air

Table 1: Main FASTEF parameters

3.1. The primary cooling system

As stated earlier in this paper, the primary and secondary systems have been designed to evacuate a maximum thermal core power of 100 MW. The average coolant temperature increase in the core in nominal conditions is 140 °C with a coolant flow of 2 m/s. The primary cooling system exists of two pumps and four heat exchangers.

The pumps are axial or mixed-type pumps with a mass flow 3500 kg/s per pump. The pumps are designed for a working pressure of 3 bar.

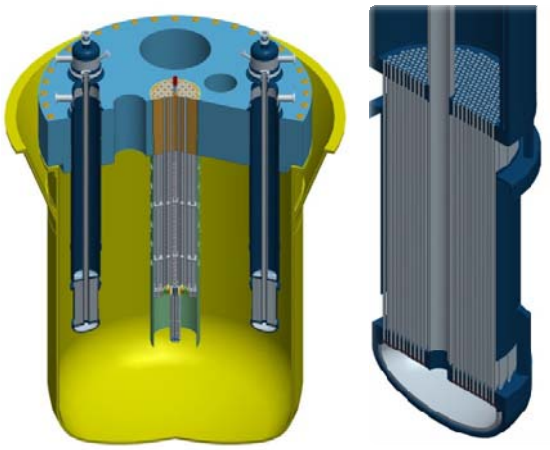

Figure 2: Heat exchangers

The heat exchangers (Figure 2) are from the shell and tube, single-pass and counter-current type. The heat exchangers are using pressurized water as secondary coolant, flowing through 700 tubes, to evacuate the heat. The heat exchangers are double walled to avoid pre-heating of the secondary coolant and to prevent water leaking in the LBE when a failure occurs.

In case of loss of primary flow (primary pumps failure), the primary heat exchangers aren't able to extract the full heat power. In such cases, the beam must be shut off in the subcritical case and the shutdown rods inserted in the critical case.

The decay heat removal (DHR) is achieved by natural convection. Ultimate DHR is done through a reactor vessel coolant system, also by natural convection.

3.2. The core

At the present state of the design, the reactor core consists of mixed oxide (MOX) fuel pins, typical for fast reactors. The Fuel Assemblies (FA) size is a little bit increased in order to accommodate the window target in the core centre. Consequently the In-Pile test Sections (IPS), which will be located in dedicated FA positions, are larger in diameter giving more flexibility for experiments. Thirty seven positions can be occupied by IPS's or by the spallation target (the central one of the core in sub-critical configuration) or by control and shutdown rods (in the core critical configuration). This gives a large flexibility in the choice of the more suitable position (neutron flux) for each experiment.

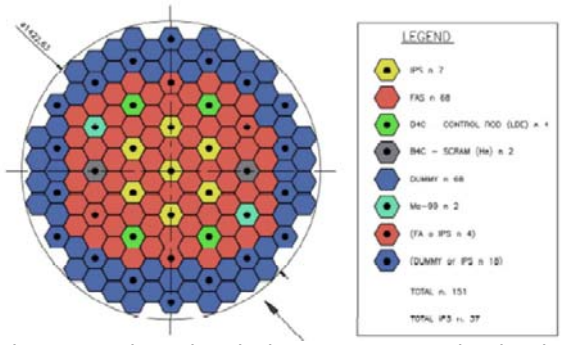

Figure 3: Horizontal cut in the FASTEF core, showing the central target, the different types of fuel assemblies and dummy components

The requested high fast flux intensity has been obtained optimizing the core configuration geometry (fuel rod diameter and pitch) and maximizing the power density. We will be using, for the first core loadings, 15-15Ti as cladding material instead of T91 that will be qualified progressively further on during MYRRHA operation. Thanks to the use of LBE as coolant, it permits to lower the core inlet operating temperature (down to 270 °C) decreasing the risk of corrosion and allowing to increase the core ΔT. This together with the adoption of reliable and passive shut down systems will permit to meet the high fast flux intensity target.

3.3. The in-vessel fuel handling machine

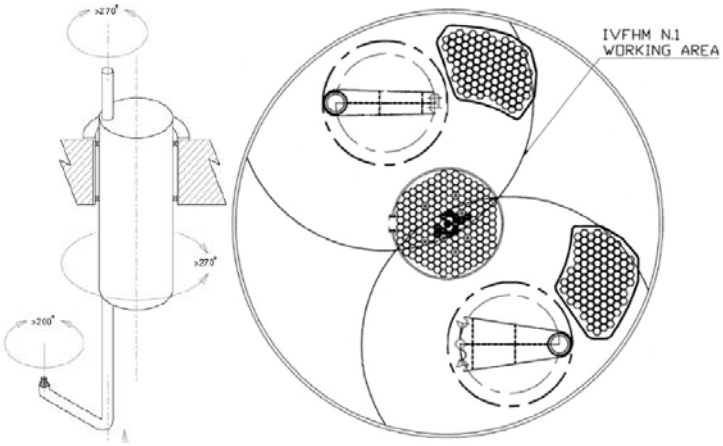

Figure 4: The in-vessel fuel handling machine

The interference of the core with the proton beam, the fact that the room situated directly above the core will be occupied by lots of instrumentations and IPS penetrations, and core compactness result in insufficient space for fuel handling to (un)load the core from above. Therefore, fuel handling is performed from underneath the core. The fuel assemblies are kept by buoyancy under the core support plate.

The in-vessel fuel handling machine is based on two SCARA robots, each covering one side of the core, as shown in Figure 4. The robot can move up and down for about 2 m, to extract the fuel assemblies from the core. A guide is used for handling the FA, while a plate prevents the surrounding FA's to be extracted from the core. An ultrasonic sensor is used to uniquely identify the FA's. With its diameter of just above 2 meters, the two SCARA robots determine together with the core the diameter of the reactor vessel.

4. Irradiation performances

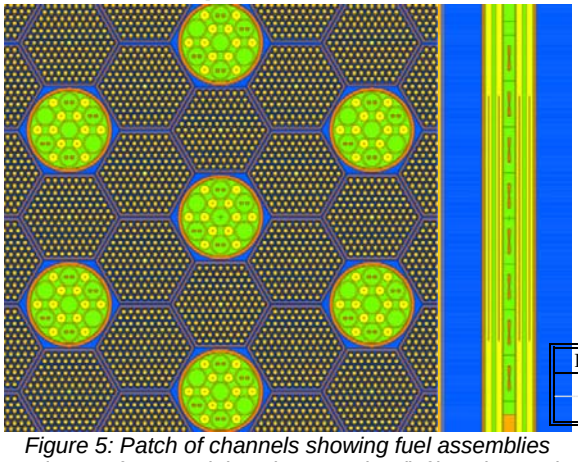

Figure 5: Patch of channels showing fuel assemblies and 7 IPS for material testing samples (left) and a stack of steel specimen (right)

As described in the design of the core, thirty seven positions can be occupied by In-Pile test Sections to perform experiments. Figure 5 shows a MCNPX plot-view displaying a patch of channels in the MYRRHA/FASTEF critical core. Besides the driving fuel assemblies, seven IPS are loaded, each one having seven channels wherein stacks of various steel specimen for material testing as regards to irradiation damage are placed.

In

FA centre	[1 0 0]	[1 2 0]	[3 0 0]	[4 0 0]
Φ_{tot}	3.42E+15	2.93E+15	2.71E+15	2.05E+15
$\Phi_{>0.75\ MeV}$	6.44E+14	5.59E+14	5.15E+14	3.71E+14

Table 2, the achievable neutron flux levels and the accumulated DPA damage over one effective full power year at 100 MW_{th} are

given for the typical stack of 8 specimens, as shown on the right side of Figure 5. Both values of the IPS loaded in the central core channel [0 0 0] as a IPS loaded in ring #2 are listed. In terms of fuel irradiation performances, the flux levels are given at different fuel assembly positions. The values for the flux levels given in the second table are for the flux in the central fuel pin of the considered fuel assembly at the mid-plane of the core.

	IPS in Chan [0 0 0]		IPS in Chan [2 0 0]	
Sample n°	dpa/EFPY	Φ_{tot}	dpa/EFPY	Φ_{tot}
8	18.1	2.38E+15	16.2	2.12E+15
7	23.0	2.85E+15	20.7	2.54E+15
6	25.9	3.19E+15	23.3	2.85E+15
5	27.5	3.37E+15	24.5	3.02E+15
4	27.2	**3.39E+15**	24.5	**3.03E+15**
3	25.7	3.23E+15	22.9	2.89E+15
2	22.3	2.92E+15	19.9	2.62E+15
1	17.3	2.50E+15	15.5	2.23E+15

FA centre	[1 0 0]	[1 2 0]	[3 0 0]	[4 0 0]
Φ_{tot}	3.42E+15	2.93E+15	2.71E+15	2.05E+15
$\Phi_{>0.75\ MeV}$	6.44E+14	5.59E+14	5.15E+14	3.71E+14

Table 2: Fluxes and accumulated DPA over one effective full power year at 100 MW_{th}

Conclusion

SCK•CEN is proposing to replace its ageing flagship facility, the Material Testing Reactor BR2, by a new flexible irradiation facility, MYRRHA. Considering the international and European needs, MYRRHA is conceived as a flexible fast spectrum irradiation facility able to work in both sub-critical and critical mode. With the CDT project, we are modifying the existing XT-ADS design into a new concept, called FASTEF, for this purpose.

MYRRHA is now foreseen to be in full operation by 2023 and it will be operated as an Accelerator Driven Systems to demonstrate the ADS technology and the efficient demonstration of MA in sub-critical mode and will be able to be run in critical mode. As a fast spectrum irradiation facility, it will address fuel research for innovative reactor systems, material research for GEN IV systems and for fusion reactors, radioisotope production for medical and industrial applications and industrial applications, such as Si-doping. Being based on heavy liquid metal coolant technology, MYRRHA will also act as the European Technology Pilot Plant for the development of the Lead Fast Reactor.

Acknowledgements

The XT-ADS design work has been performed under the Integrated Project EUROTRANS (Ref. FI6W-CT-2004-516520) co-funded by the European Union in its 6th Framework Programme. The FASTEF design work is being performed under the Collaborative Project CDT (Ref. FP7-232527) co-funded by the European Union in its 7th Framework Programme. Acknowledgment is also due to all the colleagues of all partner institutes for their contributions in many different topics associated with the XT-ADS and FASTEF design and operation.

References

1. BR2 reactor, (http://www.sckcen.be/en/Our-Research/Scientific-Institutes-Expert-Groups/Nuclear-Materials-Science/Belgian-Reactor-2).
2. H. Aït Abderrahim, D. De Bruyn, e.a., "MYRRHA Project – Technical description", SCK•CEN Report reference ANS/HAA/DDB/3900.B043000/85/07-17bis, April 2007, 57 p
3. EU Integrated Project EUROTRANS, contract nr. FI6W-CT-2004-516520.
4. D. De Bruyn, S. Larmignat, A. Woaye Hune, L. Mansani, G. Rimpault and C. Artioli, "Accelerator Driven Systems for Transmutation: Main Design Achievements of the XT ADS and EFIT Systems within the FP6 IP-EUROTRANS Integrated Project", International Congress on Advances in Nuclear Power Plants (ICAPP'10), San Diego (California, USA), paper 10112, 1808 – 1816 (2010).

THE INFRASTRUCTURE FOR PALLAS, THE NEW NUCLEAR REACTOR IN THE NETHERLANDS

B. VAN DER SCHAAF, K. BROEKHAUS, N. VAN DER LINDEN, F. WIJTSMA
PALLAS project, NRG
Westerduinweg 3,PO box 5, 1755ZG Petten, The Netherlands
E.M: vanderschaaf@pallasreactor.eu

ABSTRACT

The High Flux Reactor (HFR) in Petten, The Netherlands, is one of the world's main isotope production and research reactors. Given the advanced age of this reactor (operational since 1961), the Nuclear Research and consultancy Group (NRG) has taken the initiative to build PALLAS, a flexible and high capacity research reactor. PALLAS will become part of the dense network of adjacent facilities on site – for instance the hot-cell laboratories. Besides the construction of the facility, the layout of its periphery and infrastructure is a challenge to build and operate PALLAS without affecting the ongoing activities. This paper explains the major options for the secondary cooling system that should determine an uninterrupted operation for the next half century, and it discusses the anticipated utilization of remnant heat with measures for continuing delivery during maintenance outages. In June 2010 the Dutch government issues its guidelines for the Environmental Impact Assessment (EIA) of PALLAS. At the end PALLAS will satisfy the necessary regulatory requirements. The infrastructure of experiments and isotope capsules in the core shall enable to use the neutrons most efficiently. At the same time these devices should satisfy the regulatory demands for the operating license boundaries of PALLAS. Therefore PALLAS will be commissioned with a fixed number of reference experiments and isotope production capsules that fully meet all requirements, and boundary conditions.

1. Introduction

In 1956 Petten was chosen from four allowable locations as the site for the High Flux Reactor, HFR. Presently the HFR together with its associated hot cell laboratories, isotope production and, waste treatment facilities is one of the world's main isotope production and research center combinations in the world. As the historic data indicate the site selection was made before the IAEA entered into force in 1957. Given the advanced age of the reactor (operational since 1961), the Nuclear Research and consultancy Group (NRG) has taken the initiative to build a new research and isotope reactor: PALLAS. This reactor will be a flexible and high capacity facility, that will utilize the surrounding infrastructure which is on the average of a younger age, but that is being renewed as well. In 2010 the Petten site was selected as the most likely location for the new research and isotope reactor. The Borssele site lacks the Petten infrastructure, and would therefore require much more investment. PALLAS will be a flexible and high capacity facility, that will fully utilize the existing infrastructure at Petten.
The paper explains in section 2 the off plot scope activities accompanying the building of PALLAS. The secondary cooling facilities design, and choices, also part of the off plot scope, are treated in section 3. Comments on the environmental impact assessment, EIA, and the "Richtlijnen" [2] for the EIA are presented in section 4, explaining the Netherlands rules for the EIA. The design and commissioning development for the nuclear infrastructure inside PALLAS,

consisting of comprehensive sets of isotope production, and experimental devices with their support equipment, are treated in the final section.

2. Off plot scope

The PALLAS site is part of the research location Petten, where next to NRG, also ECN, COVIDIEN and JRC-IE have their offices, workshops and laboratories. The total site population counts nearly 1400 persons travelling daily to and from the site, mainly by private cars. One of the key challenges, besides the construction of the facility itself, is the layout of its periphery and infrastructure on this intensively used terrain. Fig 1 shows the present location of the HFR and nearby hot-cell facilities and isotope laboratories. PALLAS will be located close to the hot cell and isotope laboratory for logistic and security reasons. This nearby arrangement facilitates the prevention, and mitigation of the Design Basis Threats.

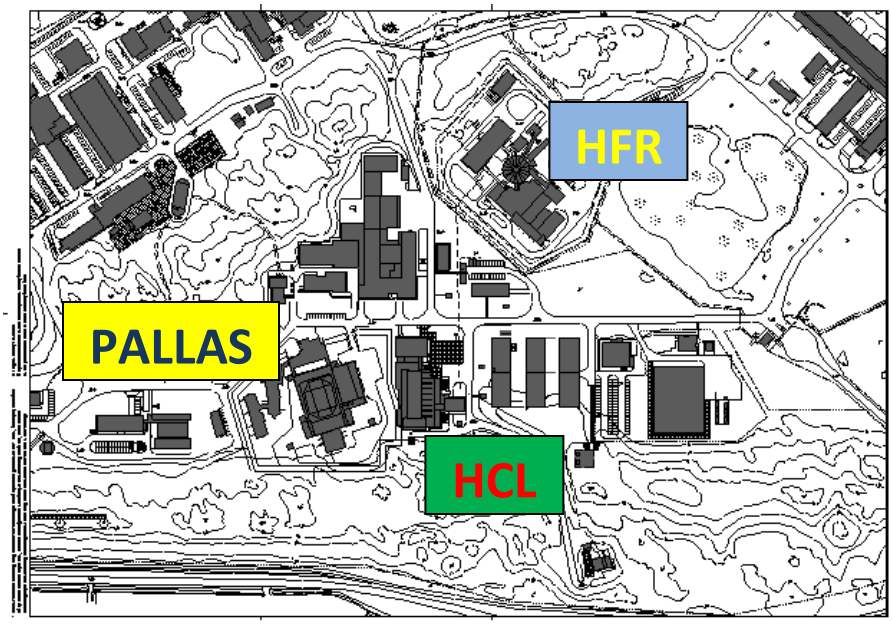

Fig 1. The location of the Petten facilities with the PALLAS projection [north to the right]

The security level of the building site will be increased stepwise during the building process reaching its highest level during the installation phase. The infrastructure has been designed in such a way that the HFR and PALLAS can be operated in parallel for a long period of time with independent secondary cooling water, normal and emergency power supply, and other utility facilities. These separate services are necessary, because of the age and capacity of the HFR utilities, but most important they are essential for the safety of operation of both research reactors.
The density of buildings on the Petten site is low because of the present dunes, which have functions as landscape dominating shapes, host for the rich fauna and flora and sea defense.
Finding the proper location for the PALLAS building on the site for the operation phase was rather simple compared to the site utilization during the building phase. Traffic analyses has shown that creating a dedicated entrance gate, doubling the capacity of the present one, is needed for safe and secure handling of the additional “construction” traffic. Some more or less level surfaces on the site will have to be used for temporary workshops, warehouses, depots, offices, and parking sites.

3. Secondary cooling system

The options for the secondary cooling system are in the range from sea or sweet surface water, see Fig 2, to air cooled heat exchangers. The North Sea coastal waters area is rather shallow [3], therefore intake from seawater requires high investments and operating costs. The nearby Noord-Hollands Kanaal offers abundant intake of sweet water 10 months of a year. Experience over the past decade shows the non-availability of insufficient water supply in the months July and August, which leads to the hybrid option with additional cooling capacity from air blown heat exchangers. This hybrid solution is the most reliable solution for the secondary cooling system.

Fig 2. Coastal defense possibly needs more dunes rows in front of present beach.

On many occasions the question arose: Are there viable options for reusing the residual heat of PALLAS? Considered possibilities are amongst others crop growth, biomass, shrimp and fish farms, and heating of expanding high pressure natural gas. With the exception of natural gas heating all options require limited fractions of heat. For all these customers the continuity of delivery is essential. The solution to this requirement can be found underneath the PALLAS site where wet sand layers can accumulate remnant heat during operation and can deliver heat during planned and unplanned outages of PALLAS.

4. Environmental Impact Study

Since changes in the design or infrastructure can affect the license application and the Environmental Impact Assessment (EIA), licensing and infrastructure activities keep a close relation in the project design phase. Based upon the submitted EIA-start notice for PALLAS [4], the PALLAS project team received its final EIA-guidelines in June 2010 from the Dutch government. The major issues are in line with the EU directives [5] and are centred on:

- justification of the initiative for PALLAS;
- description of the total lifecycle including de-commissioning of PALLAS and HFR;
- description of the complete fuel cycle;
- safety during normal operation and postulated accident scenario’s;
- Impact on nearby nature reserves.

The fauna and flora populations on the site have to be identified and the impact of the building and operation phase must be estimated with an effect mitigation plan. In addition an impact analyses of PALLAS on the Dutch society by analysing costs and benefits should be provided to the authorities. A visual impact plan of PALLAS will be developed with cooperation of the community of Zijpe, involving the local inhabitants and authorities. Since the holiday season attracts many tourists, local entrepreneurs in the tourist sector expect the rural-nature characteristics of the region to be preserved.

Fig 3. Example of images used in the view quality planning

Fig 3 shows a panorama view of the research site Petten, with a comparison between the PALLAS contours and the HFR horizon impact

5. Nuclear infrastructure

The PALLAS operator and customers are primarily interested in the infrastructure for experiments and isotope production capsules, in order to use the PALLAS neutrons to their best advantage, at least as good as in the HFR [6]. The irradiation infrastructure is defined in terms of the number, volume and neutronic properties of irradiation positions. The flexibility of the utilization requires the possibility to exchange the number of experimental and isotope positions depending on the customers' demand. For this reason the PALLAS reactor will be commissioned with a fixed number of reference experimental devices, RED, and Reference Isotope Devices, RID. They must all fully meet the requirements and objectives of a wide range of customers. At the same time the reference devices should satisfy the regulatory boundaries of PALLAS operation. The devices will also validate the utilization of the support systems, such as tooling and storage, control gas supply and handling, off-gas processing, measurement devices, data collection and data-management.

The "hot" commissioning of the reactor will start with aluminium filler pieces in the irradiation positions followed by a schedule of gradual introduction of irradiation devices. The reference devices shall demonstrate:

- the reactivity effects of fuel experiments and certain isotope capsules during insertion and removal from the core;
- the capabilities of the PALLAS reactivity control system to cope with loading and unloading of experiments, and production facilities;
- the effectiveness of the interface for control and protection of the reactor in relation to the functioning of the irradiation devices;

- validity of the operating limits for irradiation devices;
- the safe use of pressurized water and gas in static devices and loops;
- flux distribution and peaking in experimental devices;
- performance (yield) with respect to isotope production;
- modelling of experiments, and isotope production devices, and in-core behaviour;
- ease and economy of device use and handling of devices in and out of the core;
- correct use and operation of support systems.

The RED will amongst others most likely include a pressurized helium cooled loop intended for the research and development programs needed for AGR, (V)HTR, GFR, and fusion cooled blanket components. The safe in core operation is challenging, but also the support system (feeding and analysing the gases into the loop with the required pressure and composition) needs a lot of attention to assure proper functioning operation and safety systems, effectively connected to the reactor protection system.

Most probably the Tc-production in PALLAS will be based on Low Enriched Uranium, LEU. Developing and testing this production chain and accompanying RID's with the HFR before use in PALLAS, will provide a flying start in this domain. Another RID that needs attention is the production facility for doted silicon for half-conductor properties. The trend of continuously increasing sizes of silicon ingots, and the wish to offer flexible irradiation facilities in Petten require clever use of the space in the core.

7. Conclusions

1. By putting great effort in the EIA and in monitoring during the construction phase, PALLAS is expected to be completed without irreversible environmental impact.
2. Sweet water supply will be sufficient for cooling, because using a hybrid secondary system, cooling is also secured when water supply would be limited in July or August.
3. The site offers sufficient space for the operating phase of PALLAS, but during the building phase the site will be stretched to its limits.
4. During the cold and hot commissioning stages the operating license will be validated utilizing the reference experiments and radioisotope production facilities.
5. The systems and facilities for the experiments and isotope production capsule with support facilities have to be designed and planned with high accuracy in an early stage, because of their impact on the safety and space in the reactor building.

8. References

[1] M. Bustraan, J. Pelser, Selection of a site for a nuclear reactor centre in The Netherlands, Proc. of the IAEA Symposium of 11-15 March 1963, IAEA, Vienna 1963, p. 381 – p. 391.
[2] Ministerie van Volkshuisvesting, Ruimtelijke Ordening en Milieu beheer, Richtlijnen Milieueffectrapport, juni 2010: www.ikregeer.nl/document/blg-71804
[3] Noordzeekust IJmuiden tot den Helder, Mercator projectie (WGS84), 1801.9, Uitgegeven in 2011 door de Chef der Hydrografie, Den Haag, editie 2010.
[4] Startnotitie PALLAS: www.rijksoverheid.nl/documenten-en-publicaties/rapporten/2009/11/17/startnotitie-pallas.html
[5] EUROPEAN COMMISSION. Environmental Assessment. Council Directive 85/337/EEC of 27 June 1985 and amendment Council Directive 97/11/EEC of 3 March 1997. O.J. No. L73, 14.3, 1997. P.5.
[6] J. Ahlf, A. Zurita, HFR Petten characteristics, EUR15151, ECC, Brussel-Luxemburg, 1993.

Jordan's First Research Reactor Project: Driving Forces, Present Status and the Way Ahead

Ned Xoubi

Jordan Atomic Energy Commission (JAEC)
P.O.Box 70, Shafa Badran, 11934 Amman, Jordan

Ned@Xoubi.com

Abstract

In a gigantic step towards establishing Jordan's nuclear power program, Jordan Atomic Energy Commission (JAEC) is building the first nuclear research and test reactor in the Kingdom. The new reactor will serve as the focal point for Jordan Center for Nuclear Research (JCNR), a comprehensive state of the art nuclear center not only for Jordan but for the whole region, the center will include in addition to the reactor a radioisotopes production plant, a nuclear fuel fabrication plant, a cold neutron source (CNS), a radioactive waste treatment facility, and education and training center.

The JRTR reactor is the only research reactor new build worldwide in 2010, it is a 5 MW light water open pool multipurpose reactor, The reactor core is composed of 18 fuel assemblies, MTR plate type, with 19.75% enriched uranium silicide (U_3Si_2) in an aluminum matrix. It is reflected on all sides by beryllium and graphite blocks. Reactor power is upgradable to 10 MW with a maximum thermal flux of 1.45×1014 cm-2s-1. The reactor reactivity is controlled by four Hafnium Control Absorber Rods (CAR) .

Jordan Center for Nuclear Research is located in Ramtha city, it is owned by Jordan Atomic Energy Commission (JAEC), and is contracted to Korea Atomic Energy Research Institute (KAERI) and Daewoo E&C, The JCNR project is a 56 months EPC fixed price contract for the design engineering, construction, and commissioning the JCNR reactor, and other nuclear facilities. The project presents many challenges for both the owner and the contractor, being the first nuclear reactor for Jordan, and the first nuclear export for Korea. The driving forces, present status and the way ahead will be presented in this paper.

1. Introduction

The building and construction of a research and test reactor is a gigantic step towards establishing a nuclear power program in Jordan and a landmark of its nuclear technology infrastructure. The reactor will become the focal point for Jordan Center for Nuclear Research (JCNR) that is intended to play the primary role in educating the upcoming generations of nuclear engineers and scientists in Jordan [1], and provide irradiation services in support of the Jordanian industrial, agricultural and health/medical infrastructure [2].

Jordan Center for Nuclear Research (JCNR) is a comprehensive nuclear technology center for Jordan & the Region that is designed to include in addition to the nuclear reactor, a radioisotopes production facility (RIP), an educational and training center, a

radioactive waste treatment facility, a cold neutrons facility (CNS), and a fuel fabrication plant, a layout view of JCNR is shown in Figure 1.
JCNR is located in Ramtha approximately 70 km. north of Amman, within the Jordan University of Science and Technology (JUST) campus, one of the largest universities in Jordan. With about 20 000 students from more than 50 nations, the university is home to the only Nuclear Engineering Department (NED) in Jordan [3]. Currently, Jordan serves as a regional educational centre, a medical hub for the Middle East and a supplier of know-how in the various areas of education, engineering and science. It is anticipated that the established nuclear center JCNR will support these efforts and complement and solidify the objective of instituting nuclear energy as a viable option for fulfilling the Jordanian electricity and water needs in the 21st century

Figure 1. Birds Eye View of Jordan Centre for Nuclear Research in Ramtha

2. JRTR Design Features

Jordan Research and Training Reactor (JRTR) is a multipurpose isotope production, research and training reactor, with a designed power of 5 MW upgradable to 10 MW. It is light water moderated and cooled open-tank-in-pool type reactor; the core (shown in Fig 2) consists of 18 MTR plate type fuel assemblies, surrounded by beryllium and graphite reflector blocks. The core is flexible and can be reconfigured by replacing the fuel assemblies with beryllium blocks and vice versa.

The fuel is MTR plate type, aluminum clad, 19.75% enriched uranium silicide (U_3Si_2) dispersed in an aluminum matrix. The nominal fuel loading is 18 fuel assemblies containing 7.0 kg of ^{235}U, and each assembly is a bundle of 21 fuel plates. The operating cycle is 50 days. When one fuel assembly is reloaded; the average discharge burn-up is 70%.

The compact core design is optimized to produce the highest thermal neutron fluxes at in-core and external irradiation facilities. The maximum in-core thermal-flux-to-power ratio is 2.9×10^{13} $cm^{-2}s^{-1}MW^{-1}$, producing a maximum thermal flux of 1.45×10^{14} $cm^{-2}s^{-1}$, and the maximum external thermal flux to power ratio is 1.4×10^{13} $cm^{-2}s^{-1}MW^{-1}$ producing a maximum thermal flux of 6.78×10^{13} $cm^{-2}s^{-1}$.

Forced convection cooling is used to cool the reactor under normal operating conditions. The coolant flows downward at a rate of 146 kg/s, with an inlet temperature of around 35 °C and exits the core with an outlet temperature of 44.2 °C. The average heat flux is 17.3 W/cm^2, with a maximum of 51.9 W/cm^2 [4].

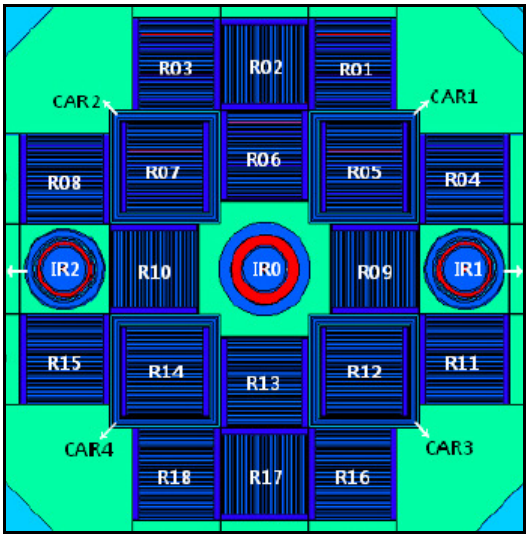

Figure 2 JRTR Core showing the Fuel Assemblies and Beryllium blocks

3. Licensing and Regulations

The existence of a well developed and clear nuclear regulatory framework is fundamental to the success of any nuclear project. In 2007 Jordan enacted the radiation protection and nuclear safety and security Law (No. 43), which was amended in 2008 leading to the establishment of an independent nuclear regulator in the country. In March 2008 the Regulatory Commission for Nuclear & Radiation work (JNRC) was established, as the authority to regulate, control and to establish Regulations and Guidance on rules and procedures for the safe use of nuclear energy and the safety and security of radiation sources. The lack of any nuclear regulations in Jordan presented additional challenges, and introduced new risks to the project.

To overcome these challenges an agreement between JAEC and JNRC was made, stating that the Korean nuclear regulation will be used for the JRTR project, the agreement was added as an appendix to the EPC contract.
Two step licensing procedures consistent with the Korean regulations will be adopted for the JRTR project. Uppon the submittal of the PSAR and FSAR reports, JNRC with the help of KINS will review and issue the construction permit and operating license respectively.

4. Driving Forces

Nuclear energy is not a luxury for Jordan, it is a necessity, with the lack of conventional energy resources, Jordan currently imports over 95% of its energy needs. With increasing and fluctuating oil prices this dependence on energy imports is becoming a huge burden on Jordan economy and is hindering our development, and economic growth.
Nuclear energy offers a promising approach to meet Jordan's energy needs, an approach that would reduce dependence on oil imports, create jobs, raise the standard of living, and alleviate the burden on the national budget. It will also provide electricity for energy demanding mega projects that Jordan is aspiring to build; such as water desalination, the red-dead canal, and electric trains. JRTR is a major milestone on the road to establishing a nuclear power program in Jordan.

5. Future Issues and Considerations

JRTR is the first nuclear reactor project in Jordan, JAEC will be facing many challenges that have to be overcome and issues that have consider as the project progress. Project management team that is capable of following schedule, budget, reporting, design reviews, construction and quality control. Management of environmental obligations, management of regulatory obligations, international obligations, safety and licensing, ethics & confidentiality, stakeholders involvement, public awareness and acceptance, strategic plan for effective utilization, building of user groups, financial concerns, funds for essential facilities that is not part of the contract.

6. Project Status

Despite the challenges of first experience, by being Jordan's first nuclear reactor, and Korea's first nuclear export, the JRTR reactor project has been progressing on schedule as shown in figure 3.
Jordan Atomic Energy Commission (JAEC) is the owner and operator of the reactor that is being designed and constructed by a Korean consortium of Korea Atomic Energy Research Institute and Daewoo E&C (KDC). The EPC contract includes the design,

engineering, construction, and commissioning of the reactor and its associated facilities, as well as training and technology transfer.
The project which started in August 2010 will take 56 months to complete, making the reactor ready for operation in March 2015. Allowing no less than five years before the introduction of Jordan's first nuclear power plant; a period necessary for building and qualifying indigenes human resources and developing the necessary nuclear infrastructure.

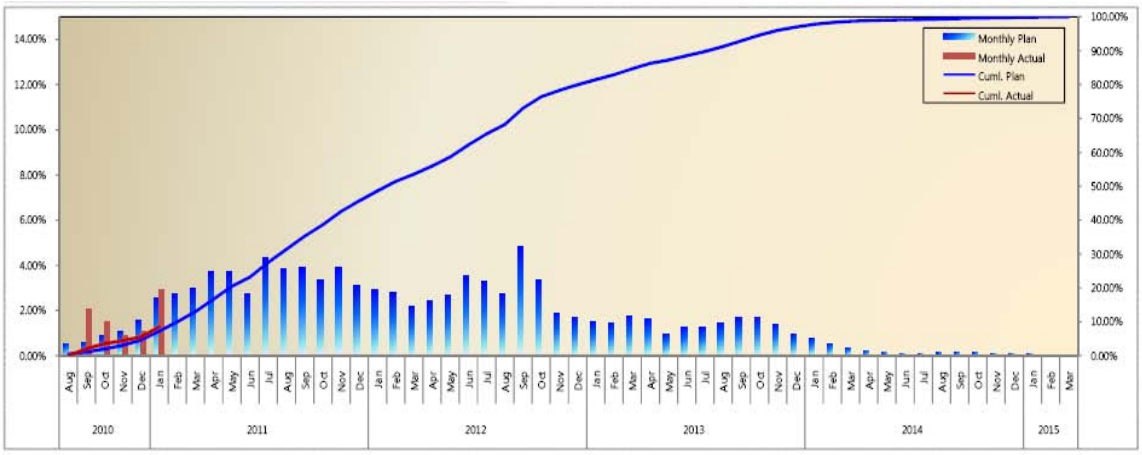

Figure 3. Project Progress Status (S-Curve)

Site studies have been completed, including seismotectonics, active faults, structural geology and soil investigation. The basic design of the Reactor Island and other balance-of-plant systems is underway. The Preliminary Safety Analysis Report (PSAR) is expected to be completed in July of this year and presented to Jordan Nuclear Regulatory Commission (JNRC), for review and approval. First concrete of nuclear construction is planed to start in April 2012, upon the issuance of construction permit. Detailed design of the training center and reactor school is underway; construction will start in June 2011, and will be completed in March 2012.

References

[1] N. Xoubi, "Proposal of a Nuclear Reactor at Jordan University of Science & Technology", College of Engineering - JUST University, Irbid, JUST/NE/2007-103 (2007)

[2] N. Xoubi, RR.Committee, "Request for Proposals for the Design and Construction of Research and Training Reactor", Jordan Atomic Energy Commission, Amman 15-01-2009 (2009)

[3] N. Xoubi, "Development of Nuclear Engineering Education in Jordan", International Conference on Knowledge Management in Nuclear Facilities, 18–21 June 2007, Vienna, Austria, IAEA-CN-153-4-P-14 (2007)

[4] KAERI, Daewoo "Technical Proposal for the Design and Construction of Research and Training Reactor" Korea Atomic Energy Research Institute, October 25, 2009

2011 PROGRESS REPORT ON HEU MINIMIZATION ACTIVITIES IN ARGENTINA

A. Bonini, P.Cristini, L. De Lio, L. Dell'Occhio, D. Gil, A. G. Gonzalez, R. González, C. Komar Varela, M. López, O. Novara, H. Taboada

COMISIÓN NACIONAL DE ENERGÍA ATÓMICA
Av. Del Libertador 8250 (1429) Buenos Aires, Argentina

After the core conversion of the RA-6 reactor finished in March 2008, an extension of the original CNEA-NNSA DoE contract was signed to enhance the final national HEU inventories minimization. Before this process, CNEA reserved a small inventory of HEU for R&D uses in fission chambers, neutronic probes and standards. This minimization comprises that all fresh and irradiated HEU remnant inventories coming from fuels and Mo99 irradiation targets fabrication and irradiated HEU-oxides retained in production filters and solutions will be recovered, down-blended into LEU and purified or dispose as waste whenever its recovery would not be advisable due to cost-benefit consideration.

CNEA has a R&D program to develop the fabrication technology of both dispersed U-Mo (Al-Si matrix and Al cladding) and monolithic (Zry-4 cladding) miniplates to support the qualification activities of the RERTR program. Some monolithic 58% enrichment and LEU 8%Mo and U10%Mo miniplates and plates were and are being delivered to INL-DoE to be irradiated in the ATR reactor core.

CNEA, a worldwide leader on LEU technology for fission radioisotope production is providing Brazil with 1/3 of the national requirements on Mo99 by weekly deliveries. Australia has started the fission radioisotope production through several batches by week, based on CNEA's LEU technology provided by INVAP SE. CNEA is also committed to improve the diffusion of LEU target and radiochemical technology for radioisotope production and target and process optimization.

Future plans include:

1. Plans to recover and purify the LEU based inventories in Mo99 production filters, once the HEU to LEU campaign is over.
2. Fabrication and delivering to INL to be irradiated in the ATR core of U-8%Mo and U-10%Mo monolithic miniplates and development and fabrication of LEU very high density monolithic and dispersed U-Mo fuel plates with Zr cladding for the FUTURE-MONO experiment in the frame of the RERTR program.
3. Optimization of LEU target and radiochemical techniques for radioisotope production.

1. Introduction:

On October 30th, 2005 the signature of two contracts between CNEA and NNSA-DoE gave rise to the RA-6 reactor core conversion from HEU to LEU. The RA-6 reactor is a pool-type one sited at San Carlos de Bariloche city, Province of Río Negro, Argentina. A special project named UBERA-6 enabled the realization of several tasks:

- Swapping of HEU-LEU inventories,
- Exportation of HEU SNF US-origin to USA,
- Fabrication of the conversion core and new graphite reflectors
- Improvements on primary and secondary loops.

This core conversion process ended in May, 2008 when first criticallity of the new core was achieved.

In March 2010, a supplementary agreement between CNEA and NNSA-DoE was signed by both parties, in the frame of the HEU minimization for civilian uses. A strategic small amount

of HEU inventory for R&D purposes, as fission chambers, neutronic probes and standard fabrication was reserved by CNEA.

This minimization means the recovery, blending down and purification of fresh and irradiated HEU inventories contained in scraps from fuel and target fabrication and in fission Mo99 production filters, or the disposition as waste of those inventories whenever its recovery is not advisable due to a cost-benefit consideration. These tasks are taking place and the expected deadline is December 2012.

2. New tasks on HEU minimization

These inventories were classified into 6 groups, as it is shown in Table 1

Description	Group Number	Form	U Mass (kg)	Enrichment	235 U Mass (kg)
Irradiated Mo-99 Targets And Solutions	**1**	**Solid and Liquid**	**1.928**	**89.73%**	**1.73**
UF6 Cylinder	**2**	**Gas / Solid (UO2F2)**	**0.65**	**90.14%**	**0.59**
Miscellaneous Solids (alloys, metal)	**3**	**Solid**	**0.397**	**87.15%**	**0.346**
Miscellaneous Solutions	**4**	**Liquid**	**0.228**	**89.91%**	**0.205**
Materials declared waste to dispose	**5**	**Solid**	**0.505**	**89.97%**	**0.453**
Ingot for MEU-Mo/Zr Miniplates Fabrication	**6**	**Solid**	**0.344**	**88.66%**	**0.305**
TOTAL			**4.05**		**3.63**

Tab. 1 HEU inventories

Group 1 comprises the refurbishment of a radiochemical laboratory (LFR lab), licensing of two transport casks, for irradiated solutions and solids contained in cartridge filters, among of the proper recovery, downblending and purification of the HEU inventory in the hot cells of the LFR lab. This task is ongoing and the deadline is December 2012.

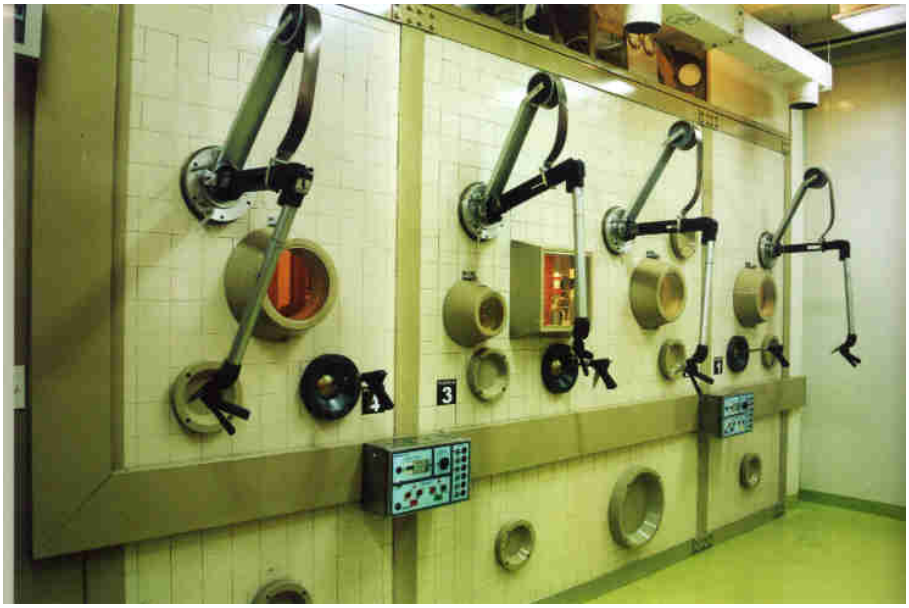

Fig. LFR laboratory front of hot cells

Group 2 comprised the opening of a valve stucked 5A type cylinder containing a partial hydrolized UF6 inventory, and the recovery, downblending and purification of the HEU inventory into LEU. This task was finished on October 2010[I]

Fig. 2 Glove box al LTA lab where the 5A cylinder was punctured

GROUP 2	ID DESCRIPTION	HEU MASS (g)	U235 MASS (g)	PARTIAL %	TOTAL %

	5A CYLINDER DECLARED VALUES	**649,3**	**585,29**		**100**
TOTAL RECOVERY	**TOTAL HEU DOWNBLENDED**	**602,72**	**543,41**	**92,8**	**95,1**
	SAMPLES	**15,05**	**13,57**	**2,3**	
TOTAL WASTE	**SOLID WASTE**	**0,80**	**0,72**	**0,1**	**3,2**
	TREATED CYLINDER	**12**	**10,82**	**1,9**	
	ANALYTICAL WASTE	**2,26**	**2,04**	**0,4**	
	SUPERNATE FROM WASHES AND PRECIPITATES	**5,46**	**4,92**	**0,8**	
TOTAL ACCOUNTED MATERIAL		**638,29**	**575,48**		**98,3**
NOT ACCOUNTED MATERIAL		**11,01**	**9,81**		**1,7**

Tab. 2 HEU-F6 processed from the 5A cylinder

Group 3 implied the downblending of an HEU-Al inventory through cast melting. This task was finished during September 2010.
Group 4 is made of several HEU solutions in acqueous and organic media. It was characterized and is being downblended, expecting its finalization on May 2011.
Group 5: this inventory will be managed after a consultation made by the Argentinean Nuclear Regulatory Authority (ARN) to IAEA on a specific disposal proposal.

GROUP	**DESCRIPTION**	**HEU MASS (Kg)**	**REMNANT HEU (Kg)**
1	**IRRADIATED MATERIAL**	**1,928**	**1,928**
2	**5A CYLINDER CONTAINING HEU-F6**	**0,649**	**0**
3	**SOLIDS**	**0,397**	**0**
4	**LIQUIDS**	**0,228**	**0,078**
5	**MATERIAL TO DECLARE WASTE**	**0,505**	**0,505**
6	**HEU FOR MEU-Mo MINIPLATES & LEU-Mo PLATE FABRICATION**	**0,344**	**0,300**
TOTAL		**4,051**	**2,811**

Tab.3 HEU remnant up to January, 2011

Group 6 includes the blending down of a HEU ingot to 58% enrichment (at U235) to make ME U-10%Mo and U-8%Mo based miniplates with Zr cladding. The agreement includes the exportation to INL of miniplates for irradiation testing under the RERTR program. This task is being accomplished with a first delivery made in April, 2010 and a final second one scheduled for May 2011[II]. Finally, the remaining 58% enrichment inventory will be downblended to LEU-10%Mo or LEU-8%Mo for full scale plate fabrication in the frame of the RERTR programme.

3. R&D on VHD fuels

The development of CNEA miniplates using monolithic UMo alloy cores involves the use of the well known Zircalloy-4. Zry-4 is commonly used as nuclear fuels cladding for nuclear power plants (uranium alloyed or not). In this case Zry-4 is employed as cladding in top, cover and frame. The fuel material in the core is UMo alloy with different contents of Mo (between 7-10% wt/wt). It was decided to employ a content of Molybdenum between 5 to 10% enough to retain the gamma phase at low temperature but also not to penalize the reactor neutronics due to the capture cross section of Mo95 isotope. Regarding hot rolling temperature between 575º - 660ºC analyses showed the presence of some amount of alpha plus delta phases, while hot rolling at 800-850ºC will take place in gamma phase which has a metastable bcc crystal structure.

Experimental set-up: an 89.24 % (at. U235) enriched U ingot was downblended to 58 %. This process took place in a vaccum inductive furnace, using enrichment and depleted uranium. Crucible employed was made of Zirconia – Ytria. This ingot was splitted into two parts that were employed for U-8%Mo and U-10% Mo ingot preparation with the same equipment used before. Also DU was employed to prepare DU-8%Mo and Du-10%Mo for use in developing tests. Slices were cut from each ingot. Edges and surfaces were polished using grinding paper # 1000. The core final dimensions were (in general):19.5 mm wide, 19.5 mm long and 1.1 mm thick. They were placed inside Zry-4 frames with dimensions of 1.1 mm thick, 35 mm wide and 47 mm long. Two sheets (cladding) of the same material and planar dimensions, but 2.7 mm thick, were placed under and over the frame containing the core. All sheets have the same surface finishing as the slice. The bottom, top and frame Zry-4 material were TIG welded under He atmosphere. Miniplates were co-rolled to final thickness of 1- 1,4 mm.

Miniplates hot co-rolled at 800°C were performed in 8 steps with intermediate heating between 785/810 °C during 15 minutes in a furnace without controlled atmosphere. Miniplates having cores containing alloys with U58% enrichment (at.U235) and DU were sent to INL for RERTR experiment and were analyzed in order to decide if their were admissible for the irradiation experiment.

Results: the microscopic observation of the material co-rolled at 800ºC shows clearly the presence of an interlayer (IL) (figure 1). The dark zone of the micrograph is Zr, as it can be observed in cross1, cross 2 is in the beginning of the interlayer and the SEM revealed only Zr. Cross 3 that is in the middle of the IL shows a zone with 50% of Zr/U each in weight, when it was quantified; no evidence of Mo can be observed. Cross 4 shows a very low quantity of Zr, a considerable quantity of U and an increased quantity of Mo (regarding the uranium). Cross 5, which is in the limit of the IL in the UMo alloy side shows the presence of Zr in low quantity; it is richer in Mo (7 times more than cross 4) and poorly in Uranium. Crosses 6 and 7 are clearly UMo alloy.

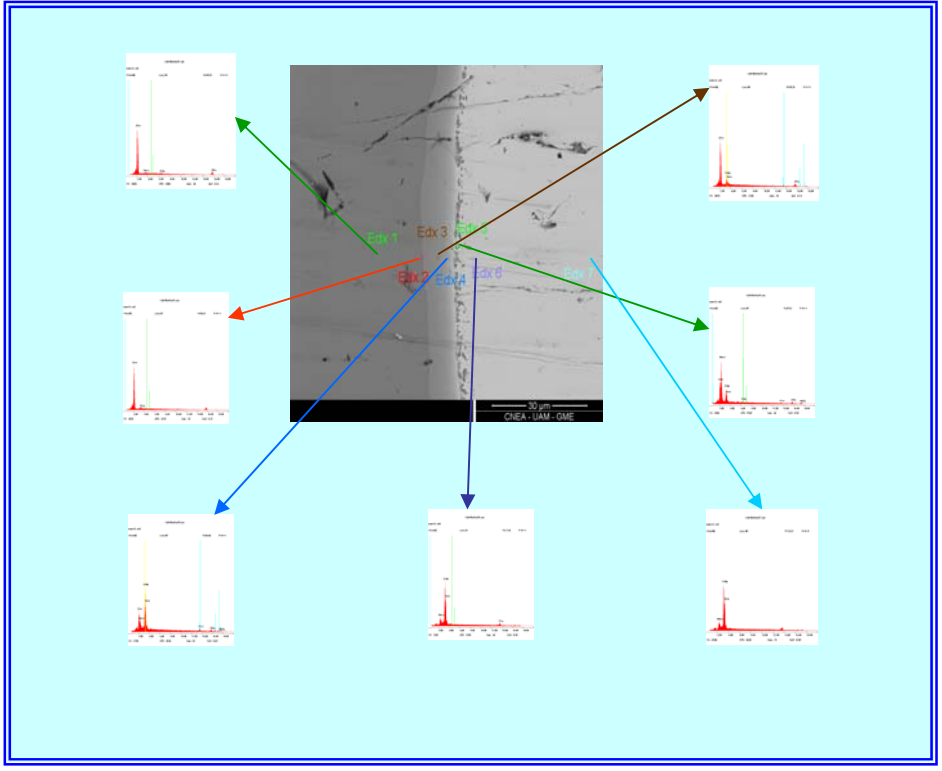

Figure 1: Miniplate Zry-4/U8Mo/Zry-4 hot co-rolled at 800 ºC

The miniplates fabricated for the RERTR-13 experiment underwent three non-destructive evaluation tests to assess the viability to be included in the experiment. The ultrasonic testing revealed that several of them were not candidate for the experiment. NDE evaluation provided characterization information.
Radiography studies confirmed the lack of uniform thickness (dogbone) at fuel ends.
Thermography studies on some miniplates were performed to determine if this non-destructive and portable experiment method was acceptable for debonding determination. Results showed that this technology is an acceptable method.
Destructive examinations of plate made of depleted Uranium-10%Mo ARD10Mo1 were performed to verify clad and fuel thickness of the data generated using UT and radiography. An OM examination of the thickest end of this plate confirmed the UT data for the min-clad value indicated and provided a correction factor for the density data provided by radiography.
Conclusions: hot rolling at 800°C was intended to assess an adequate bonding, looking for U-Mo and Zry-4 more compatible crystallographic structures and for a more plastic state to reduce rolling passes. However it was found that a relevant interlayer zone between U-Mo and Zry-4 was formed, where Mo agglomerates after migrating from U-Mo side, also the alpha-U phase appeared, debonding presence mainly at miniplate borders and dogbone at front and end of core were observed.
Future plans: a compromise between thermal plasticity and inadequate phases formation (Mo agglomeration, alpha-U phase) will be seek. An adequate number for co-rolling passes and rolling speed to avoid dog-bone formation and debonding will be tested.

LEU target and radiochemical technology for Mo99 and other radioisotopes production: it is the largest contribution of CNEA to HEU minimizationin civilian uses. It was already informed about the circumstances of the final cutoff to HEU supply for Mo99 production and how CNEA found abn adequate LEU replacement without changing its radiochemical technology. CNEA has developed and is using high-density LEU-aluminum dispersion targets. The target meat has a density of 2.9 gU/cm3 obtained by increasing the ratio of uranium aluminide to aluminum in the target meat. The mass of U-235 in the target meat is about twice that of conventional uranium-aluminum alloy targets. CNEA was able to convert to LEU-based production in the same set of hot cells that were being used for HEU-based production, without interrupting Mo-99 production. Targets are irradiated in the RA-3 reactor at CNEA's Ezeiza Atomic Center near Buenos Aires. Target processing is carried out

in a hot cell facility at the Ezeiza site. Process wastes are also managed at the site. CNEA's development showed that there are no technical barriers to conversion of Mo-99 production from HEU targets to LEU targets. Production using LEU targets is technically feasible and is being carried out by CNEA in Argentina and by the Australian National Nuclear Science and Technology Organisation. ANSTO is using CNEA's radiochemical technology and LEU targets to produce Mo-99. This new LEU technology satisfies the most stringent requirements of quality for its use in nuclear medicine applications. Mo-99 purity has been consistently higher than that produced using HEU targets[III]. Also in September 2005, CNEA began the regular production of high quality fission I-131, a by-product of Mo-99 production, meeting also international quality standards. HEU-LEU production process comparison costs reveal that this new technology has no significant overall cost of 5% [IV]. Since CNEA has duplicated the LEU-based radioisotope weekly production rate to provide Mo99 to Brazil covering 1/3 of the Brazilian market.

.

4. Conclusions:

FINAL HEU MINIMIZATION: CNEA is minimizing the remnants HEU inventories, both fresh and irradiated from fuel and target fabrication scraps and fission RI production solutions and filters. All these tasks are scheduled to finish during December 2012.

R&D ON LEU VHD FUELS: CNEA is actively supporting both R&D activities to achieve solutions for core conversions.

LEU TECHNOLOGY FOR FISSION RI PRODUCTION: No technical, quality or financial reasons make disadvantageous changing from HEU to LEU for fission Mo99 and other RI production. CNEA leads LEU based isotope production technology, and with INVAP built all LEU-based production systems in Australia and Egypt. This is by far the largest contribution of CNEA to the HEU minimization for civilian uses.

[I] L. N. Aldave, H. Blanco Bello, A. A. Bonini, L. I. De Lio, L. A. Dell'Occhio, M. Falcón, T. Feijoo, A. Gauna, D. A. Gil, A. Rodriguez y J. Valdez. 2010 RERTR International Meeting, Lisbon, Portugal, 10-14 October 2010.

II M.López, A. González, R. González, F. Rice, H. Taboada, D. Wachs. 2010 RERTR International Meeting, Lisbon, Portugal, 10-14 October 2010.

III Durán,A. 2005. Radionuclide Purity of Fission Mo-99 Produced from LEU And HEU. A Comparative Study. 2005 International RERTR Meeting, Boston, Massachusetts, USA, November 6-10, 2005. Available at http://www.rertr.anl.gov/RERTR27/PDF/S8-3_Duran.pdf.

IV Cestau D., A. Novello, P. Cristini, M. Bronca, R. Centurión, R. Bavaro, J. Cestau, E. Carranza. HEU and LEU cost comparison in the production of molybdenum-99. 2008 International RERTR Meeting, Washington, DC, USA, 5-9 October 2008, and Cestau D., A. Novello, P. Cristini, M. Bronca, R. Centurión, R. Bavaro, J. Cestau, E.Carranza. 2007. HEU and LEU comparison in the production of molybdenum-99. 2007 International RERTR Meeting, Prague, Czech Republic, Sep. 23-27, 2007. Available at http://www.rertr.anl.gov/RERTR29/PDF/6-4_Cestau.pdf

MICROSTRUCTURAL CHARACTERIZATION OF BURNABLE ABSORBER MATERIALS BEING EVALUATED FOR APPLICATION IN LEU U-MO FUEL PLATES

D. KEISER, JR.[1], J. JUE [1], I. GLAGOLENKO[1], G. MOORE[1], C. CLARK[1], B. RABIN[1], D WACHS[1], A. EWH[2], B. YAO[2], Y. H. SOHN[2], T. TOTEV[3], AND T. WIENCEK[3]

[1] *Nuclear Fuels and Materials Division, Idaho National Laboratory*
P. O. Box 1625, Idaho Falls, Idaho 83403 USA

[2] *University of Central Florida*
P. O. Box 162450, Orlando, FL 32816 USA

[3] *Argonne National Laboratory, Argonne, Illinois 60439 – USA*

ABSTRACT

The starting microstructure of a fuel plate will impact how it performs during irradiation. This includes any burnable absorber materials that may be added to a dispersion or monolithic fuel plate to compensate for excess reactivity and/or to flatten the radial power profile. The borated compounds B_4C, ZrB_2, and Al-B alloys have been selected for testing in the ATR as part of the RERTR-13 test, and to support completion of this test, microstructural characterization has been performed on the samples in the as-fabricated condition. This paper will discuss the results of optical metallography, scanning electron microscopy, and transmission electron microscopy analyses that have been performed. Overall, there was a fairly significant difference in how the boron-containing phases were distributed in the various samples. The ZrB_2 and B_4C samples had the most uniform distribution of the boron-containing phases. The HIP process used to fabricate the final plate samples effectively closes porosity that was present in some of the foil samples in the as-rolled condition.

1. Introduction

Burnable absorbers (BA) are used in a reactor fuel plate when it is necessary to suppress excess initial reactivity in a fuel and/or to flatten the radial power profile within a fuel element. In ATR and HFIR fuel elements, B_4C is currently used as the burnable absorber [1,2]. As part of the development of low-enriched U-Mo fuel, it is of interest to identify BA material(s) that can be employed for the reactors where the use of such a material is required and also to identify the best methodology of incorporating the material into the fuel plate (particularly for the monolithic fuel) such that there will be no impact of the BA material on the mechanical integrity of the fuel plate during irradiation.

The RERTR-13 reactor experiment being performed in the Advance Test Reactor (ATR) (see Table 1) will test BA-containing samples where the phases that contain boron (B), are B_4C, ZrB_2, or AlB_2. The test is comprised of 28 plates (8 non-fueled material test plates, 8 dispersion plates, and 12 monolithic plates). The B-10 concentrations employed in the materials are prototypic of what would be employed in LEU ATR plates [1]. The prime phenomena of interest in these plates are helium behavior, fuel swelling, blister anneal failure temperature and interaction layer behavior. In order to understand the effects of irradiation, it is necessary to perform detailed pre-test characterization on as-fabricated samples. The pre-test characterization was comprised of optical metallography (OM), scanning electron microscopy (SEM), and transmission electron microscopy (TEM) analyses. This paper will describe the microstructures that were observed and will focus on the morphology and distribution of the phases that contain the boron.

Table 1. RERTR-13 Experiment Matrix.

ID	Capsule	Column 1	Column 2	Column 3	Column 4
13-A	Top	A-1	A-2	A-3	A-4
		U-7Mo + B_4C dispersion in Al-4 wt% Si, U235-25%	U-7Mo + B_4C dispersion in Al-4 wt% Si, U235-69%	U-7Mo + ZrB_2 dispersion in Al-4 wt% Si, U235-69%	U-7Mo + ZrB_2 dispersion in Al-4 wt% Si, U235-25%
	Bottom	A-5	A-6	A-7	A-8
		Aluminum Dummy	Aluminum Dummy	U-10Mo monolithic + B_4C-Al dispersion, U235-66%	U-10Mo monolithic + Al-1.5B alloy U235-66%
13-B	Top	B-1	B-2	B-3	B-4
		U-10Mo monolithic + ZrB_2-Al dispersion, U235-19.7%	U-10Mo monolithic + ZrB_2-Al dispersion, U235-66%	U-10Mo monolithic + B_4C-Al dispersion, U235-66%	U-10Mo monolithic + B_4C-Al dispersion, U235-19.7%
	Bottom	B-5	B-6	B-7	B-8
		Al-4.5B dispersion	Al-1.5B dispersion	ZrB_2-Al dispersion (Enriched B)	B_4C-Al dispersion
13-C	Top	C-1	C-2	C-3	C-4
		U-10Mo monolithic + ZrB_2-Al dispersion, U235-19.7%	U-10Mo monolithic + ZrB_2-Al dispersion, U235-66%	U-10Mo monolithic + B_4C-Al dispersion, U235-66%	U-10Mo monolithic + B_4C-Al dispersion, U235-19.7%
	Bottom	C-5	C-6	C-7	C-8
		Aluminum Dummy	Aluminum Dummy	U-10Mo monolithic + B_4C-Al dispersion, U235-66%	U-10Mo monolithic + Al-4.5B alloy, U235-66%
13-D	Top	D-1	D-2	D-3	D-4
		U-7Mo + B_4C dispersion in Al-4 wt% Si, U235-25%	U-7Mo + B_4C dispersion in Al-4 wt% Si, U235-69%	U-7Mo + ZrB_2 dispersion in Al-4 wt% Si, U235-69%	U-7Mo + ZrB_2 dispersion in Al-4 wt% Si, U235-25%
	Bottom	D-5	D-6	D-7	D-8
		Al-4.5B dispersion	Al-1.5B dispersion	ZrB_2-Al dispersion	B_4C-Al dispersion

2. Experimental

Table 2 enumerates the six samples that were characterized, their form, the specific analyses that have been performed to date, and the B-containing phase in the material. The laminate samples were fabricated by blending 400 mesh (< 37 μm) powders of B_4C and ZrB_2 powders (supplied by Ceradyne, Inc.) and aluminum powders, followed by compacting of the

powders, and then rolling of the material to a desired thickness inside of an aluminum can. The edges of
the can were then trimmed, leaving a layer of boron-bearing material sandwiched between two thin layers of AA6061 cladding. The single layer samples were fabricated by commercially procuring boron-bearing ingots from Ceradyne, Inc. and then rolling them to the desired thickness. The Al-4.5B (nominal wt% composition) ingot was manufactured by adding a boron halide to molten aluminum, and the Al-1.5B ingot was manufactured by adding a mixture of boron-halide and titanium-halide compounds to molten aluminum [1]. The single layer and laminate materials were inserted into fuel plates that were fabricated using the hot isostatic pressing (HIP) method [3]. All four samples (Al-1.5B, Al-4.5B, B_4C, and ZrB_2) were characterized in the unassembled (free foil) condition, and two samples (Al-1.5B and ZrB_2) were also analyzed in the as-HIPed condition.

The SEM analyses were conducted using a JEOL 7000F FEG SEM with energy-dispersive and wavelength-dispersive spectrometers (EDS/WDS) and a Zeiss Ultra-55 field emission SEM with X-ray energy dispersive spectroscopy (XEDS). Backscattered electron (BSE) imaging and X-ray mapping was performed on transverse cross sections of the samples to identify the microstructures and partitioning of the sample constituents amongst different phases. Specimens for TEM were prepared with a focused ion beam (FIB) in-situ (INLO) technique using a FEI™ TEM 200 FIB. The TEM analyses were performed using a FEI/Tecnai F30 300keV TEM/STEM equipped with a Fischione high-angle annular dark field (HAADF) detector. Electron diffraction was performed in the TEM to accurately identify the constituent phases based on crystal structure.

Table 1. Samples Employed for Microstructural Characterization

Label	Sample Form	Nominal B Loading (wt%)	Percentage of B that is B-10	Analysis Performed	B-Containing Phase
Al-1.5B	Single Layer	1.5	95.90	OM, SEM	AlB_2
Al-4.5B	Single Layer	4.5	98.50	OM, SEM	AlB_2
ZrB_2	Laminate	9.6	75.17	OM, SEM, TEM	ZrB_2
B_4C	Laminate	1.9	97.58	OM, SEM	B_4C
Al-1.5B HIP	HIP plate	1.5	95.90	OM, SEM, TEM	AlB_2
ZrB_2 HIP	HIP plate	9.6	75.17	OM, SEM	ZrB_2

3. Results

3.1 Al-1.5B and Al-1.5B HIP Sample

Figure 1 shows a BSE image of the microstructure observed for a section of the Al-1.5B sample. A heterogeneous distribution of precipitates was observed in the sample, along with relatively large areas of porosity. X-ray mapping of the sample demonstrated that the dark-contrast precipitates are enriched in Al, and the bright-phase precipitates are enriched in Ti. The Al-1.5B HIP sample had a similar microstructure without relatively large regions of porosity. TEM analysis was performed on the Al-1.5B HIP sample. The bright contrast phases in the microstructure were comprised of Al_3Ti (larger particles) and $AlTi_3$ and Al_3Fe (smaller particles). The dark precipitates were AlB_2.

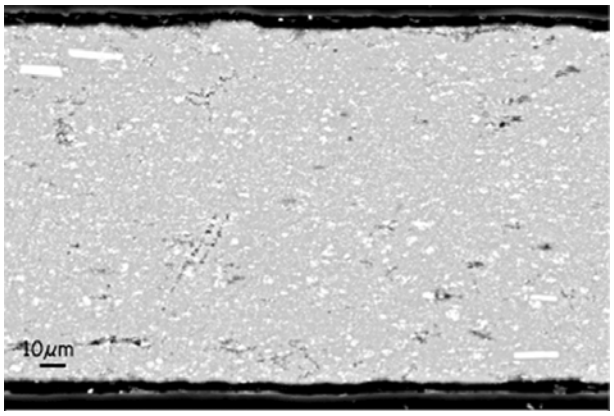

Fig. 1. BSE images of the microstructure observed for the Al-1.5B sample.

3.2 Al-4.5B Sample

Figure 2 shows a BSE image of the microstructure observed for a transverse cross section of the Al-4.5B sample. A heterogeneous distribution of precipitates were observed in the sample, along with relatively large areas of porosity. X-ray mapping of the microstructure demonstrated that the dark-contrast phases are enriched in Al and B.

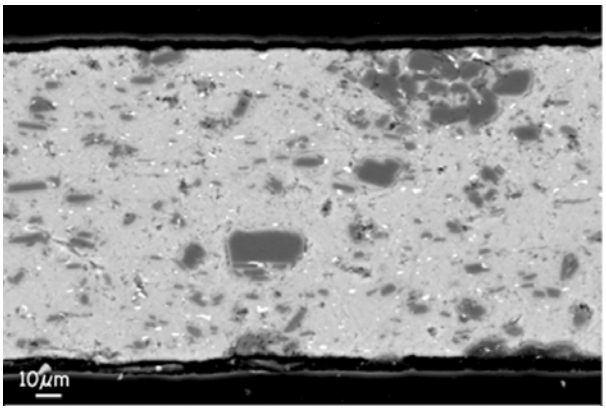

Fig. 2. BSE image of the microstructure observed for the Al-4.5B sample.

3.3 ZrB_2 and ZrB_2 HIP Sample

BSE images of the ZrB_2 sample microstructure are presented in Fig. 3. A generally uniform microstructure was observed with some areas of porosity. In the ZrB_2 HIP sample a similar microstructure was observed without any relatively large regions of porosity. TEM characterization of the ZrB_2 sample confirmed the presence of the ZrB_2 precipitate (bright contrast) and identified a minor $(Al,Si)_{12}Mg_{17}$ precipitate (dark contrast).

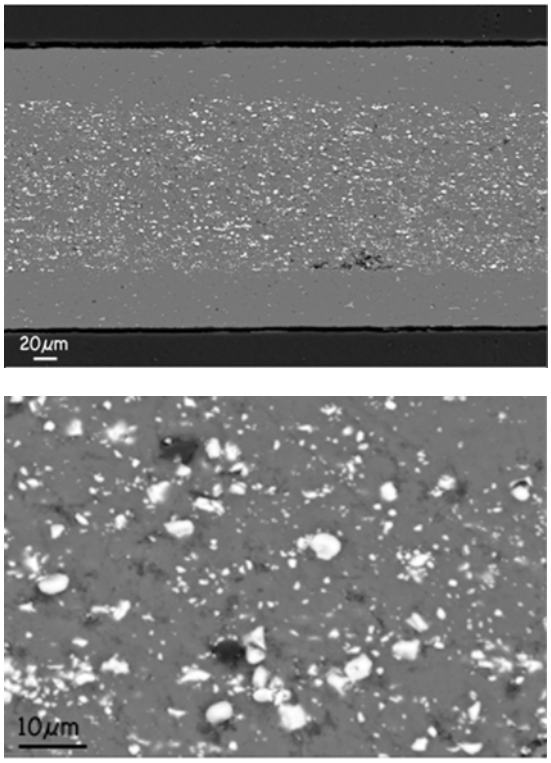

Fig. 3. BSE images of the microstructure observed for the ZrB_2 sample.

3.4 B_4C Sample

In Fig.4, the BSE image indicates that a fairly uniform microstructure was observed for the B_4C sample. The dark-contrast precipitates are the B_4C phase.

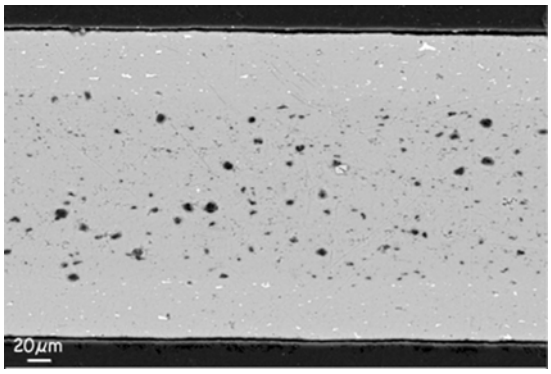

Fig. 4. BSE image of the microstructure observed for the B_4C sample.

4. Discussion

Microstructural characterization of Al-1.5B, Al-4.5B, ZrB_2, B_4C samples indicated that each sample has a very unique microstructure. The Al-1.5B sample has a significant fraction of

Ti-containing precipitates and a minority AlB_2 phase that contains the boron. The Al-4.5B sample microstructure displays the AlB_2 phase as the majority phase, but there is a wide range in the size of the precipitates. The ZrB_2 sample has fairly uniform distribution of the ZrB_2 phase, but there is a fairly significant variation in the size of the precipitates. The B_4C sample also has a fairly uniform distribution of the B_4C phase and a farily significant variation in the size of the precipitates.

When microstructural analysis is performed on the as-irradiated samples, it will be of particular interest to track the development of the porosity in the microstructure due to the generation of He from nuclear reactions with the boron contained in the different phases.

5. Conclusions

Based on the microstructural analyses performed on the BA samples that will be tested in the RERTR-13 experiment, there was a fairly significant difference in how the boron-containing phases were distributed in the various samples. The ZrB_2 and B_4C samples had the most uniform distribution of the boron-containing phases. The HIP process used to fabricate the final plate samples effectively closes porosity that was present in some of the foil samples in the as-rolled condition.

Acknowledgments

This work was supported by the U.S. Department of Energy, Office of Nuclear Materials Threat Reduction (NA-212), National Nuclear Security Administration, under DOE-NE Idaho Operations Office Contract DE-AC07-05ID14517.

References

[1] I. Glagolenko et al., RERTR 2010, Lisbon, Portugal, Oct. 10-14, 2010.
[2] A. Richt et al., Oak Ridge National Laboratory Report, ORNL-4714, (December, 1971).
[3] Jan-Fong Jue et al., Nucl. Tech. 172 (2010) 204-210.

COATED PARTICLE PRODUCTION IN THE SELENIUM PROJECT

S. VAN DEN BERGHE, A. LEENAERS
Nuclear Materials Science Institute, SCK•CEN
Boeretang 200, B-2400 Mol, Belgium

C. DETAVERNIER
Solid State Sciences, University of Ghent
Krijgslaan 281, 9000 Ghent – Belgium

ABSTRACT

Within the "Surface Engineering of Low EnrIched Uranium-Molybdenum" (SELENIUM) research reactor fuel development program, initiated by SCK•CEN in 2008, the coating of atomised U(Mo) fuel particles has been successfully completed in 2010. This paper reports on the results of the coating and will show some initial results of the annealing experiments of coated particles in an Al matrix.
Currently, fuel plates are being produced by CERCA using the coated particles provided by SCK•CEN. Test productions, based on coated natural uranium kernels will be completed first, after which LEU based plates will be produced. As much as possible, standard production parameters are applied in this production.
The irradiation experiment is planned for this year and consists of 4 flat, full size LEU fuel plates which will be irradiated in BR2 in the FUTURE-device. Three fuel plates will contain U(Mo) kernels coated with Si (~300 nm and ~600 nm) and one with ZrN (~1 µm). The 4th fuel plate contains a U(Mo) dispersion in an Al-5w%Si "alloy" matrix made from atomised Al-5w%Si particles. This 4th plate is a reference plate and a direct comparison with the plates irradiated in the E-FUTURE experiment of the European LEONIDAS qualification program. Irradiation conditions will be kept as similar as possible to this experiment.

1 Introduction

Introduction of Si in the Al matrix of LEU(Mo) dispersion fuels is now generally accepted as beneficial to the fuel in-pile behaviour with respect to its interaction with the Al dispersion matrix [1, 2, 3, 4, 5, 6]. The presence of Si improves the properties of the interaction product and reduces the formation kinetics of the interaction product. Although a number of questions still surround the optimal concentration of Si [5] and the requirement for pre-irradiation thermal formation of Si-rich layers at the fuel kernel-matrix interface [7], the U(Mo)-Al(Si) system is now considered sufficiently mature to warrant qualification to start, an effort which is currently in progress in the frame of the LEONIDAS program [8]. The first experiment in this program, called E-FUTURE, concerns the irradiation of 4 flat, full size U(Mo) 8g_U/cc fuel plates with 4 and 6 w% Si in the matrix [9]. These fuel plates have undergone different pre-irradiation heat treatments to generate Si enriched layers around the fuel kernels. Results of the pre-irradiation characterisation were presented at the RERTR conference in 2010 [10] and at present the irradiation, done at high heat fluxes, is finished without fuel plate failure. The plates are cooling down and awaiting post-irradiation characterisation.
Indications exist that the Si addition to the matrix in the concentration range currently selected for the qualification may not prevent, at high heat fluxes, an important fraction of the matrix from being consumed by the interaction with the fuel [11]. Furthermore, Si is an undesireable element for the reprocessing of irradiated fuels, which provides an incentive to minimise its concentration or to attempt to eliminate it altogether. Finally, heat treatments of fuel plates as part of the production process may have an influence on the number of rejected fuel plates.

The heat treatments are aimed at concentrating the Si on the fuel kernel-matrix interface. In addition, minimising Si is best accomplished by using the Si inventory as effectively as possible, namely by introducing it only at the location where it can be considered most effective. An alternative way to reach these goals is to deposit a coating of Si on the U(Mo) kernel surface. If the process chosen to accomplish this allows sufficient flexibility, it can be used to deposit other coating materials to avoid Si altogether. Generally speaking, coated U(Mo) fuel particles may in this way allow higher heat fluxes to be demanded from U(Mo) fuels, which is in the interest of future reactor systems, allowing operation at higher fuel powers with a sufficient safety margin.
The use of coatings on U(Mo) is the subject of the "Surface Engineering of Low EnrIched Uranium-Molybdenum" (SELENIUM) fuel development project at SCK•CEN [12, 13]. The project consists of the production, irradiation and post-irradiation examination of coated U(Mo) atomised powders in flat, full size plate configuration in the BR2 reactor at similar powers as those used in the E-FUTURE experiment of the LEONIDAS program. In 2009, a sputter deposition coater was built for this purpose [13] and in 2010 the production of 16 batches of NU and LEU based U(Mo) powders was completed. This paper reports on the results of this production, discusses preliminary results of a number of out-of-pile tests and introduces the matrix established for the irradiation, scheduled for this year.

2 Coatings and the fuel-matrix interaction process

Even if a nuclear fuel system cannot be considered in thermodynamic equilibrium, the basic principles of solid state reactions also apply to the U(Mo)-Al(Si) interaction as it occurs in pile. As for most reactions, the interaction mechanism of the U(Mo) fuel kernels and the Al-Si matrix has chemical and physical components. For a solid state reaction to occur thermodynamically, a net Gibbs energy gain is required. However, the reaction products will also need to be in direct contact to allow them to react with formation of a new compound. In solid state reactions, this is accomplished by diffusion, which is temperature driven in most cases. Finally, the reaction kinetics or the speed at which the reaction will occur are obviously also influenced by temperature, both directly (chemical kinetics) and indirectly (diffusion speed).
The formation of the glassy U-Al-Si interaction phase requires diffusion to allow direct interaction of the Al(Si) and the U. The presence of Si in the Al matrix has an influence on both the chemistry and the diffusion kinetics of the interaction process [14]. The higher affinity of U for Si, compared to Al, as seen from the formation enthalpies of the silicides versus the aluminides, directly affects the interaction chemistry. At the same time, the presence of Si in Al reduces the Al diffusivity, also effectively affecting the interaction product formation speed.
As the operation temperatures of the fuel are relatively low, the major driving force for the in-pile diffusion will be the fission product recoils, which generate 2 main effects in the U(Mo) and the Al(Si) matrix [15]. Ballistically, they will displace the U, Mo, Al and Si atoms, then called primary knock-on atoms, by direct interaction. Secondly, and more importantly at the high energies of the fission products, fission tracks create a temporary thermal spike in their passage through the material. This effectively creates a tubular path around each fission track, a few nm in diameter, in which the material locally can be considered molten. Both effects leave behind defects in the material, which also influence its diffusion characteristics over the longer term as damage accumulates.

How then, can coatings affect the interaction process and possibly improve on the addition of Si to the Al matrix ? Using Si coatings, the effects generated by the addition of Si to the matrix as a dispersion, namely playing on the affinity of U for Si and the reduction of the Al diffusion kinetics, are still the major goals. The Si coatings will be particularly effective in accomplishing the former, being in direct contact with the U kernel and consisting of pure Si, without Al present. The latter effect requires mixing of the Si into the Al, which will gradually also occur by displacement of the Si atoms as they are displaced into the Al by the fission

products or mixed at the Si-Al interface by the fission product spikes or thermally, even at the moderate operation temperature.
However, since the detrimental properties of the interaction product are directly related to the U-Al interaction, coatings succeed in accomplishing one more important effect : keeping the Al and U physically separated, i.e. they act as a diffusion barrier. Since in-pile diffusion is governed by the effect of the fission product tracks, we need to evaluate if coatings can effectively stop the ballistically created knock-on atoms and if they can withstand the thermal spikes. Also, as defects are accumulating in the coating materials, their diffusion barrier properties should not break down.
With this reasoning, an opportunity is created to move away from Si, which has the advantage of its effect on the physico-chemistry of the U-Al reaction, to other coating materials, which may be chemically inert, but can provide more interesting diffusion barrier properties. Literature review shows particularly promising behaviour of the nitrides for diffusion reduction. Gold coloured sputter deposited ZrN coatings [16] are used frequently to prevent diffusion, for example between Al and Si [17]. Zr based solutions have the additional advantage that Zr addition to the U(Mo) has been shown to reduce the interaction layer formation rate too [18]. For this reason, it was decided to try ZrN as a diffusion barrier coating. Results obtained in the irradiation of ZrN coated U(Mo) fuels by Russian colleagues have shown good behaviour of 2-3 µm thick ZrN coatings in the reduction of U(Mo)-Al interaction layer formation in pin-type fuels [19].
While the Zr interlayers used in the monolithic fuel development [20] are sufficiently thick (>10µm) to stop the fission fragments completely, this is not the case for the coatings around the U(Mo) kernels. However, not so much the fission fragments themselves, but the recoiled U and Al atoms need to be stopped from interacting. The energy of these knock-on atoms is usually much lower than the ~80 MeV of the fission fragments. Simulations using the TRIM [21] code show that they have an average energy of ~2-3 keV (Al) and ~4-6 keV (U) and are stopped within the first ~50 nm of their original location. The simulation was done using a randomly oriented (0-90°) influx of fission fragments, taken at random as Mo and Xe ions with random energies ranging from 75-85 MeV, originating randomly from 0-5 µm deep in the U(Mo). The simulation was set up to stop most fission fragments in the simulated interface (5 µm U(Mo) – 1 µm ZrN – 10 µm Al). Per fission event in the simulation, a few hundred atoms are displaced (directly by the incident ion or indirectly by the knock-on atoms), but less than 0.1% of the recoil atoms gain an energy of >1MeV and are displaced over larger distances.

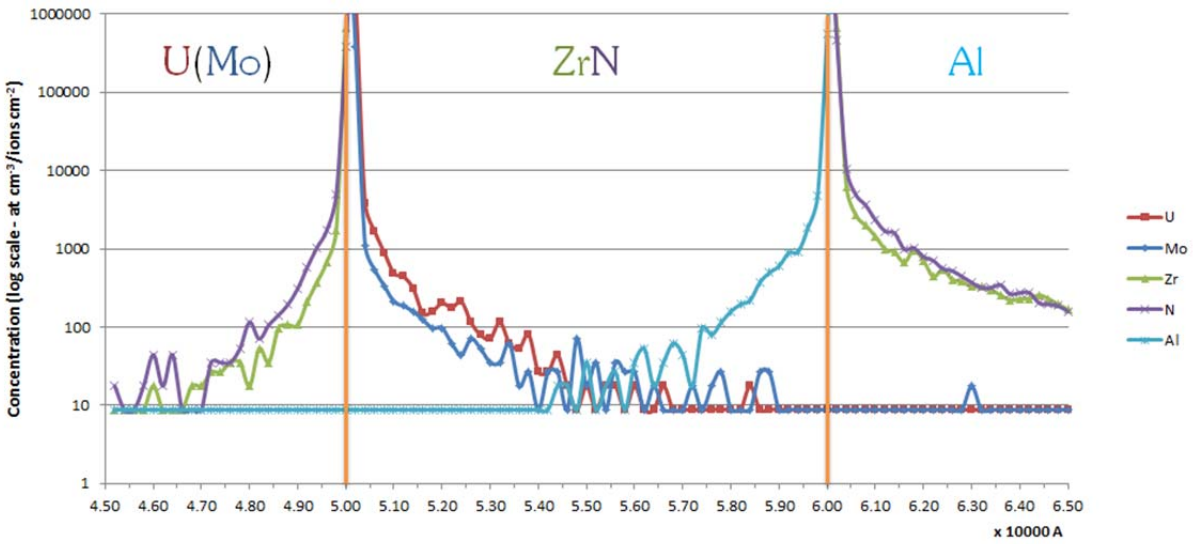

Figure 1 : Distribution of final recoil positions in a simulation of ion bombardment of a ZrN layer of 1µm wide between U(Mo) and Al after 56000 ions. The interfaces are located at the positions 5.00 and 6.00 in the graph. The graph shows the effect of the ZrN layer on the reduction of the U-Al interdiffusion under the ballistic effects of the ion bombardment.

The distribution of the recoiled U, Zr and Al atoms in a typical simulation is shown in Figure 1. The effectiveness of the coating to reduce very significantly the ballistically driven diffusion is clear from this figure. A similar result is obtained with Si coatings, although the range of the recoils in the coating is slightly larger, as can be expected and therefore the Si coatings, which are also thinner, will have a less pronounced barrier effect. However, for Si coatings, the effects of the chemical interactions with the U and the interdiffusion of Al and Si, even at moderate temperature, will be more important effects. Concerning the effect of the irradiation, what remains to be evaluated is the resistance of the coating to the thermal spike effects, which are very important at the energies of the fission fragments, and the deterioration of its properties as defects are accumulated.
Thermal spikes may be simulated using molecular dynamics calculations, but no data on the ZrN-U(Mo) system is presently available in open literature. Some experimental data on irradiation damage in ZrN exists, since it is a candidate ceramic for use in inert matrix fuels. Ion and proton bombardment studies have shown [22, 23] that dislocation loops and point defects develop in ZrN under irradiation, causing a hardening of the material, but no important lattice expansion, void formation or amorphisation was found. These studies were carried out at significantly higher temperatures than what is to be expected in research reactor fuels, but no open literature data was found on low temperature irradiation behaviour of ZrN, particularly related to changes in its diffusion behaviour. The stability of the strong covalent Zr-N bond and its B1 (NaCl) crystal structure provides some support for the assumption that ZrN coatings resist the effects of the thermal spikes and do not suffer from major breakdowns in their diffusion properties by the defects created under irradiation.

Resulting from these considerations, a choice for the particle coatings to be applied in the SELENIUM project was decided. The following matrix was established :

Plate	Coating	Matrix	Coating thickness	Purpose
1	Si	Al	300	Retain >5at% Si in IL at 5 µm IL thickness
2	Si	Al	600	Equivalent to Al+4w% Si matrix (E-FUTURE)
3	ZrN	Al	1000	Diffusion barrier coating
4	n/a	Al5Si	n/a	Reference plate (E-FUTURE comparison)

The reference plate n°4 has a composition close to the E-FUTURE plates, but it contains atomised Al-Si 'alloy' powder instead of a mixture of Al and Si powders and it will not undergo specific heat treatments during production, so only 'standard' hot rolling and blister anneal temperatures and times for AG3 cladded fuel plates are applied.

3 Coated kernel production

The STEPS&DRUMS ("Sputtering Tool for Enhancing Powder Surfaces" & "Deposition Reactor for Uranium based Model Surfaces") sputter deposition reactor, presented previously [13], was used to produce the coated U(Mo) kernels. The vacuum vessel, containing a rotating drum, is loaded with the powder to be coated in batches of around 200g. The reactor is pumped down to the 10^{-6} mbar range and high-purity Ar gas is admitted in the chamber by a gas flow controller at a rate of 80 cc per minute. In the case of ZrN deposition [16], high purity nitrogen is added at a rate of 6 cc per minute, while reducing the Ar flow to 76 ccm. Deposition of Si or Zr from ultra high purity metallic targets is performed using 2 sources operated simultaneously at powers of 1kW (for Si) or 800W (Zr) each. The U(Mo) powder is kept in motion by rotation of the drum at roughly 2-5 rotations per minute.
Sputter speed calibrations were performed by sputter depositing the desired material on stainless steel atomised powder and taking samples of the coated powder every hour. As such, the gradual increase in coating thickness could be used to calibrate the deposition speed on powders and determine the sputtering time required to achieve the desired coating thickness on the U(Mo) powders, as shown in Figure 2. Because the STEPS&DRUMS setup

is a research tool, sputter geometries are optimised for flexibility, rather than for production, which leads to relatively long sputter times, up to 7 hours. The determined sputter times were then used to deposit coatings on natural uranium based U(Mo) atomised powder to verify their validity. After a successful preparation of 2 batches (a batch corresponds to the amount required for 1 full size fuel plate) of coated U(Mo) powders with acceptable thicknesses, 2 batches of LEU(Mo) powder were coated under the established conditions. The coatings on the LEU were always performed in a single run, so the coating process was never interrupted.

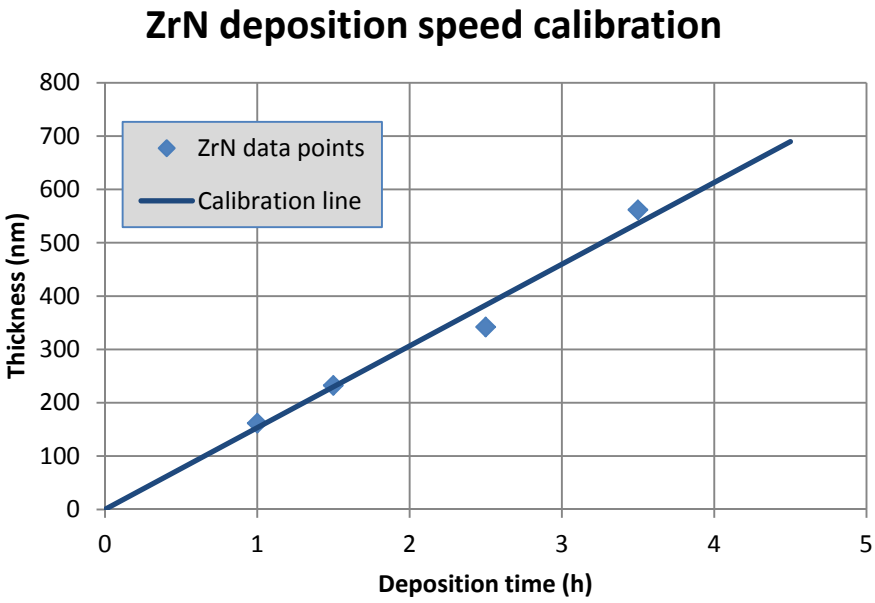

Figure 2 : Typical deposition speed calibration line obtained on stainless steel atomised powder, in this case for depostion of ZrN.

Measurements of coating thicknesses are performed by Scanning Electron Microscopy (SEM), using a Jeol JSM6310 microscope. Coated powder particles are embedded in a special matrix and polished to 1µm finish using SiC paper and diamond paste. Average thicknesses are determined by measuring >100 coating thicknesses on a number of particles, taking ~4 measurements per particle. Variations in the results are governed mainly by stereologic variations (level at which a particle is sectioned in the observed plane) and variations in the kernel sizes, which lead to different coverages. The observations show that the average coating thicknesses are in fair agreement with the intended thicknesses. More importantly, it is clearly observed that all particles are covered by a continuous coating with a homogeneous thickness around the circumference of each particle, even where deviations from the spherical shape are observed. Several examples of the coating results can be observed in Figure 3 and the results of a thickness determination are shown in Figure 4. Using EDX and/or WDX mapping, the coating can be visualised. However, because the coating thicknesses and the electron beam interaction volume have comparable sizes, the mappings should not be used directly to determine the coating thicknesses.
Additionally, flat surfaces (Si wafers) have been coated in identical conditions as used in the kernel coating and have been used to assess the crystallography of the coatings. Si coatings are amorphous, as is expected, but their densities as measured by X-ray reflectometry are close to the theoretical density for Si. The ZrN coatings are dense and cristalline, with a good correspondence with the theoretical lattice parameter for ZrN. The evolution of the as-deposited ZrN coatings with exposure to air has been followed in the XRD for 12 hours, but no evolution, eg. due to oxidation, was observed.

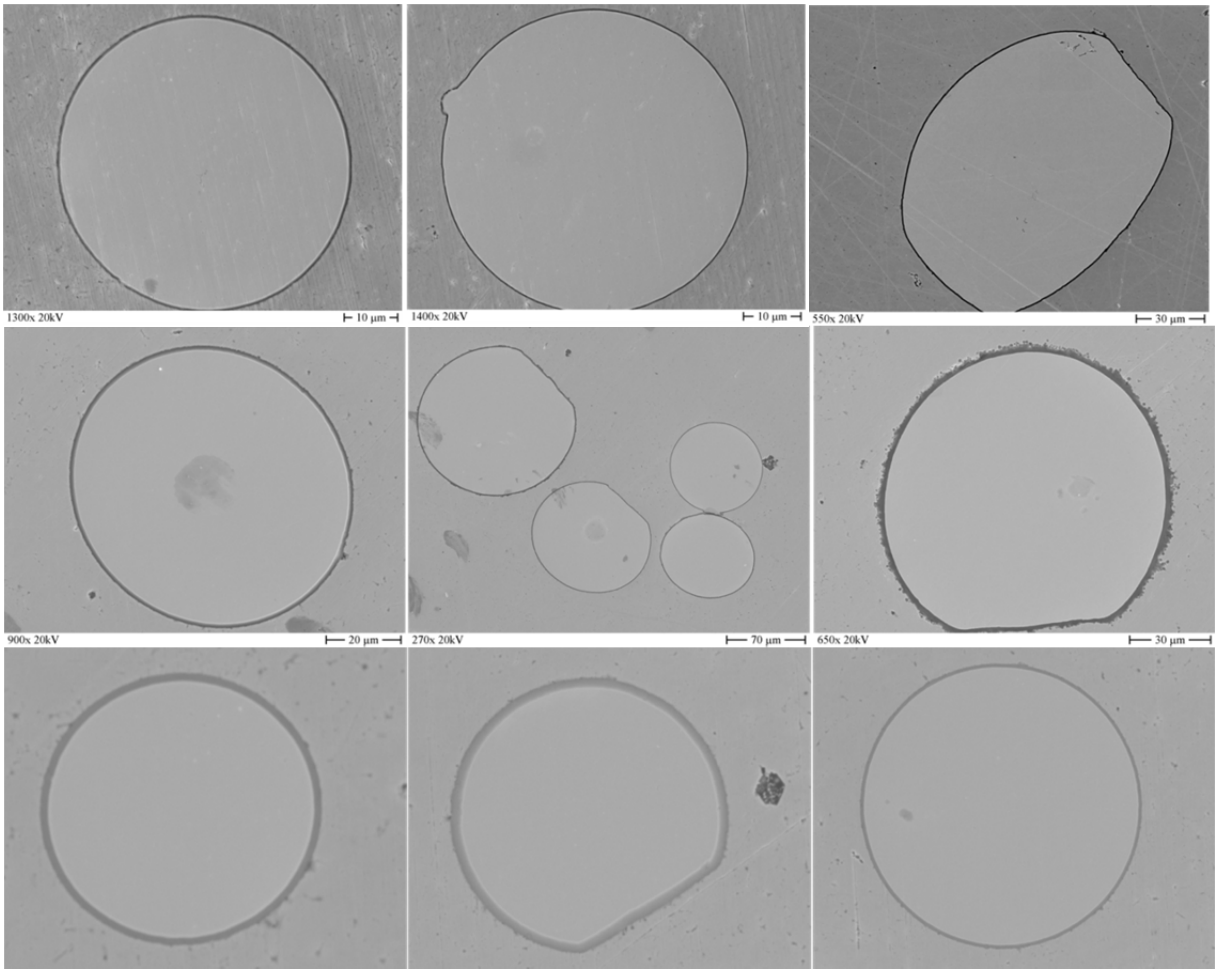

Figure 3 : Scanning electron microscopy images of typical coated kernels. From top to bottom : Si coating (~300 nm), Si coating (~800 nm) and ZrN coating (~1150 nm).

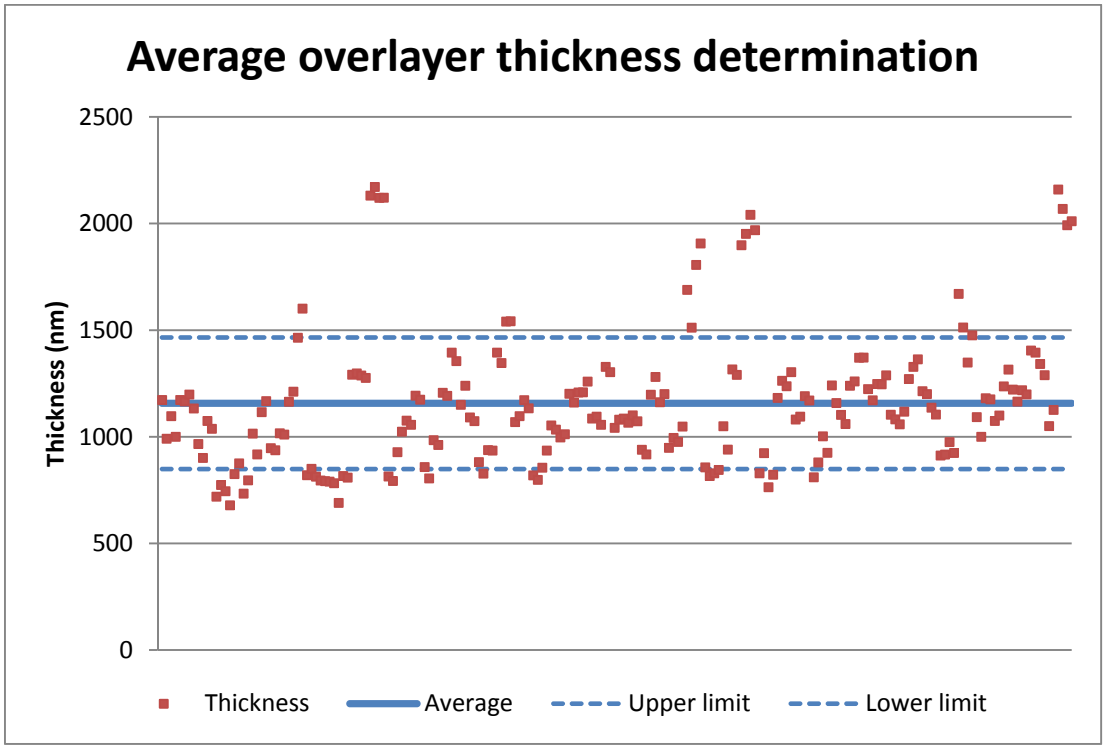

Figure 4 : Typical result of a coating thickness determination by SEM, in this case for depostion of ZrN.

Out-of-pile thermal treatment studies of the coated particles and their interaction with Al were carried out as well. Pellets were pressed to make a dispersion of U(Mo) particles in a pure Al or Al-Si matrix. A test plan was established for these studies as follows :

ID	Anneal T	A	B	C	D	E
		U(Mo) + Al	[U(Mo)]Si +Al	[U(Mo)]ZrN +Al	U(Mo) +Al5Si	U(Mo) +Al+Si
1	340 °C	130 d	130 d	130 d	130 d	130 d
2	450 °C	4 h	4 h	4 h	4 h	4 h
3	550 °C	4 h	4 h	4 h	4 h	4 h
4	550 °C	2 h	2 h	2 h	2 h	2 h

The 3 temperatures are chosen to simulate to some degree 1) the thermal component of the in-pile diffusion (340°C), 2) the fabrication behaviour (450°C) and 3) the enhanced diffusion due to fission product recoils (550°C). At the same time, they have been chosen at values where literature data exists for comparison. Although only the true in-reactor behaviour can provide final conclusions, the results of these out-of-pile tests provide some good indications on the expected behaviour.

While the B and C batches are based on coated particles, the A, D and E batches contain kernels without coatings. Where the A batch is the reference and contains no Si, the D and E batches differ in the way Si is introduced in the matrix. For D, the matrix consists of an atomised Al-Si 'alloy', while for E, an Al-Si powder mixture is used. Both batches have matrix Si concentrations of 5w%. The anneals are on-going, but the first results are reported at this conference in a paper by A. Leenaers [24].

An important preliminary conclusion for the SELENIUM project is the excellent behaviour of the ZrN coating as a diffusion barrier, as seen by the absence of Al inside the U(Mo) kernels even after 4 hours at 550°C in Figure 5. The images show the typical microstructure, as observed for the majority of kernels. The coatings remain intact and only local transformation of the U(Mo) to alpha phase and the associated volume change is capable of locally affecting their integrity. Such transformations are not expected to occur under irradiation, as the irradiation enhances gamma phase stability. Compared to the U(Mo)-Al reference batch A, where the U-Al interaction has consumed the majority of the kernels at least partially, the differences are striking. Also the Si coatings behave very well during the thermal treatment at 550°C : there is a distinct difference in behaviour with the U(Mo) in Al-Si matrix. The D and E type samples evidence the well-known formation of Si-free zones around the kernels, with a prominent Si-rich layer at the outer kernel surface, in many cases even presence of Si throughout the kernel. These Si rich layers do however, contain important amounts of Al. In the case of the Si coatings in batch B, no Al in the kernels was observed and only localised interactions of the U(Mo) with the Si overlayers is seen, in which the Si penetrates the U(Mo), even after 4h at 550°C. Further details can be found in [24].

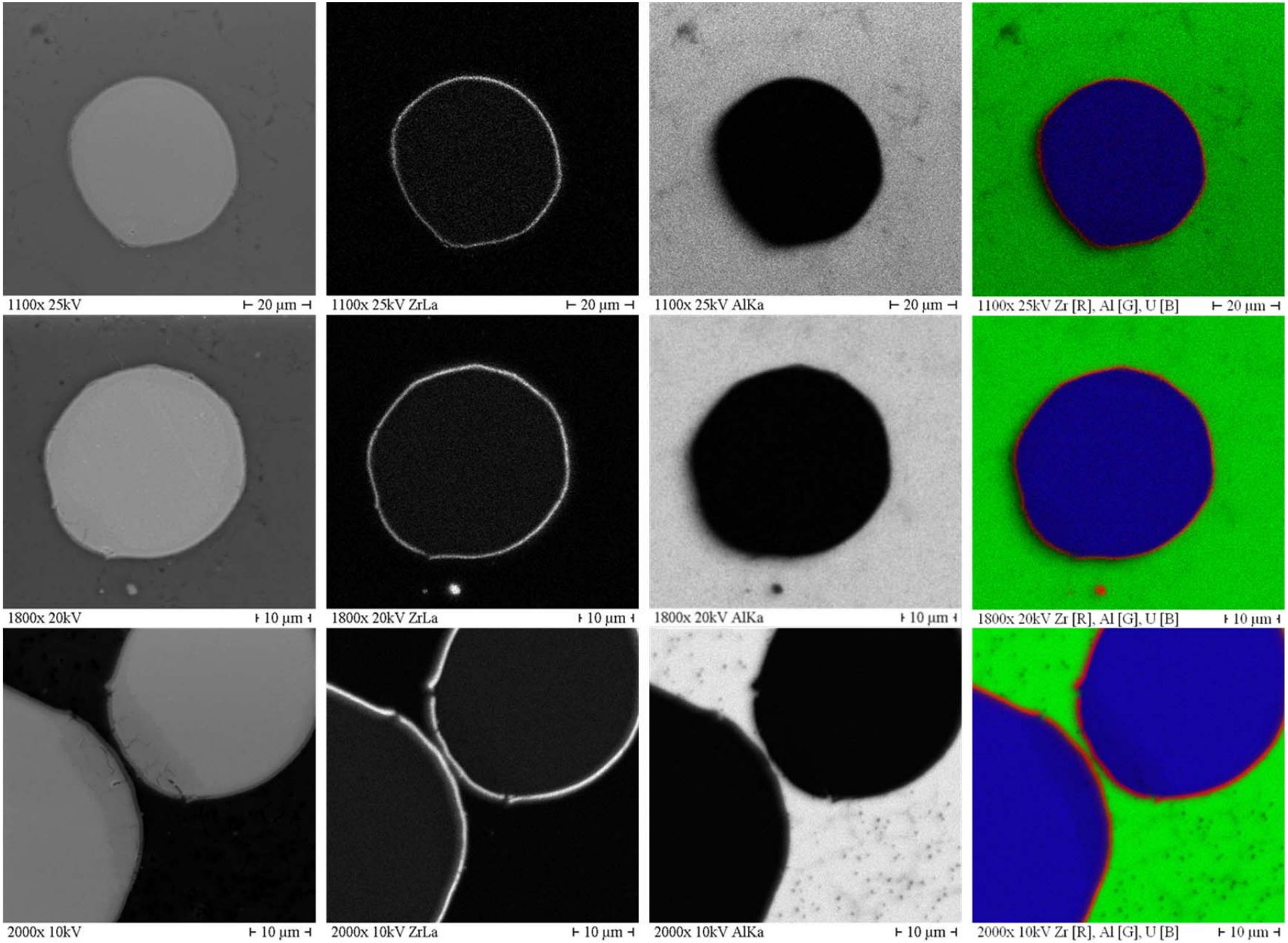
1100x 25kV
20 µm
1100x 25kV ZrLa
20 µm
1100x 25kV AlKa
20 µm
1100x 25kV Zr [R], Al [G], U [B]
20 µm
1800x 20kV
10 µm
1800x 20kV ZrLa
10 µm
1800x 20kV AlKa
10 µm
1800x 20kV Zr [R], Al [G], U [B]
10 µm
2000x 10kV
10 µm
2000x 10kV ZrLa
10 µm
2000x 10kV AlKa
10 µm
2000x 10kV Zr [R], Al [G], U [B]
10 µm

4 Conclusions

Within the SELENIUM project at SCK•CEN, coated LEU(Mo) particles have been produced and characterised in 2010 and are currently at CERCA for fuel plate production. Start of the irradiation is planned for the second half of 2011.
The SELENIUM irradiation matrix contains 2 types of coatings on the U(Mo) particles : Si and ZrN. Where the former is expected to have mostly an effect on the chemistry of the interaction process, the latter is expected to act as a diffusion barrier. Ion bombardment simulations provide support for this behaviour.
Out-of-pile annealing tests of coated and uncoated U(Mo) powder embedded in Al and Al-Si matrices have been started. The initial results show a very promising behaviour of the coated particles, with a virtual absence of interaction of U and Al even after 4h at 550°C.

References

[1] S. Van den Berghe, A. Leenaers, E. Koonen and L. Sannen, Adv. Sci. Techn. 73 (2010) 78-90.
[2] G. L. Hofman, Y. S. Kim, H. J. Ryu, J. Rest, D. M. Wachs and M. R. Finlay in: Proceedings of the 10th International Topical Meeting on Research Reactor Fuel Management (RRFM), Sofia, Bulgaria (2006).
[3] A. Leenaers, S. Van den Berghe, F. Charollais, P. Lemoine, C. Jarousse, A. Rohrmoser and W. Petry in: Proceedings of the 31th International Meeting On Reduced Enrichment For Research And Test Reactors, Beijing, China (2009).
[4] Y. S. Kim, G. L. Hofman, P. G. Medvedev, G. V. Shevlyakov, A. B. Robinson and H. J. Ryu in: Proceedings of the 29th International Meeting On Reduced Enrichment For Research And Test Reactors, Prague, Czech Republic (2007).
[5] Y. S. Kim, G. Hofman and A. B. Robinson in: Proceedings of the International Topical Meeting on Research Reactor Fuel Management (RRFM), Vienna, Austria (2009).
[6] D. D. Keiser Jr, J. F. Jue, A. B. Robinson and P. Medvedev in: Proceedings of the 32nd International Conference on Reduced Enrichment for Research and Test Reactors (RERTR), Lisbon, Portugal (2010).
[7] M. Cornen, M. Rodier, X. Iltis, S. Dubois and P. Lemoine in: Proceedings of the International Topical Meeting on Research Reactor Fuel Management (RRFM), Hamburg, Germany (2008).
[8] E. Koonen, H. Guyon, P. Lemoine, C. Jarousse, D. M. Wachs and J. Stevens in: Proceedings of the 31th International Meeting On Reduced Enrichment For Research And Test Reactors, Beijing, China (2009).
[9] F. Fréry, H. Guyon, E. Koonen, S. Van den Berghe, P. Lemoine, F. Charollais, C. Jarousse and D. Geslin in: Proceedings of the 32nd International Meeting on Reduced Enrichment for Research and Test Reactors (RERTR), Lisbon, Portugal (2010).
[10] X. Iltis, F. Charollais, M. C. Anselmet, P. Lemoine, A. Leenaers, S. Van den Berghe, E. Koonen, C. Jarousse, D. Geslin, F. Frery and H. Guyon in: Proceedings of the 32th International Meeting on Reduced Enrichment for Research and Test Reactors (RERTR), Lisbon, Portugal (2010).
[11] D. D. Keiser Jr, J. F. Jue and A. B. Robinson in: Proceedings of the 32nd International Conference on Reduced Enrichment for Research and Test Reactors, Lisbon, Portugal (2010).
[12] S. Van den Berghe, A. Leenaers, E. Koonen and L. Sannen in: Proceedings of the 12th International Conference on Modern Materials and Technologies (CIMTEC), Montecatini Terme (Italy) (2010).
[13] S. Van den Berghe, A. leenaers and C. Detavernier in: Proceedings of the International Conference on Research Reactor Fuel Management (RRFM), Marrakech, Marocco (2010).
[14] A. Leenaers, C. Detavernier and S. Van den Berghe, J. Nucl. Mater. 381 (2008) 242-248.

[15] P. Süle, M. Menyhàrd and K. Nordlund, Nucl. Instr. Meth. Phys. Res. B 226 (2004) 517-530.
[16] M. Del Re, R. Gouttebaron, J.-P. Dauchot, P. Leclère, G. Terwagne and M. Hecq, Surf. Coat. Techn. 174-175 (2003) 240-245.
[17] M. Östling, S. Nygren, C. S. Petersson, H. Norström, R. Buchta, H. O. Blom and S. Berg, Thin Solid Films 145 (1) (1986) 81-88.
[18] J. M. Park, H. J. Ryu, S. J. Oh, D. B. Lee, C. K. Kim, Y. S. Kim and G. L. Hofman, Journal Of Nuclear Materials 374 (3) (2008) 422-430.
[19] A. L. Izhutov, V. V. Alexandrov, N. A.E., V. A. Starkov, V. E. Fedoseev, V. V. Pimenov, A. V. Sheldyakov, V. Y. Shishin, V. V. Yakovlev, I. V. Dobrikova, A. V. Vatulin, V. B. Suprun and K. G.V. (2010). The main results of investigation of modified dispersion LEU U-Mo fuel tested in the MIR reactor. 32nd International Meeting on Reduced Enrichment for Research and Test Reactors (RERTR). Lisbon, Portugal.
[20] G. Moore, B. Rabin, J.-F. Jue, C. Clark, N. Woolstenhulme, B. Park, S. Steffler, M. Chapple, M. Marshall, J. Green and B. Mackowiak in: Proceedings of the 32nd International Conference on Reduced Enrichment for Research and Test Reactors, Lisbon, Portugal (2010).
[21] J. F. Ziegler (2000). SRIM-2000 computer code. The Stopping and Range of Ions in Solids. J. F. Ziegler, J. P. Biersack and U. Littmark, Pergamon Press (1985).
[22] Y. Yang, C. A. Dickerson and T. R. Allen, J. Nucl. Mater. 392 (2009) 200-205.
[23] J. Gan, Y. Yang, C. Dickson and T. R. Allen, J. Nucl. Mater. 389 (2009) 317-325.
[24] A. Leenaers, S. Van den Berghe and C. Detavernier in: Proceedings of the International Conference on Research Reactor Fuel Management (RRFM), Rome, Italy (2011).

MONTE CARLO MODEL OF TRIGA REACTOR TO SUPPORT NEUTRON ACTIVATION ANALYSIS

G. ŽEROVNIK, L. SNOJ, A. TRKOV
Reactor Physics Department, Jožef Stefan Institute
Jamova cesta 39, SI-1000 Ljubljana, Slovenija

ABSTRACT

The TRIGA reactor at Jožef Stefan Institute is used as a neutron source for neutron activation analysis. The accuracy of the method depends on the accuracy of the neutron spectrum characterization. Therefore, computational models on different scales have been developed: Monte Carlo full reactor model, model of an irradiation channel and deterministic code for self-shielding factor calculations. The models have been validated by comparing against experiment and thus provide a very strong support for neutron activation analysis of samples irradiated at the TRIGA reactor.

1. Introduction

The TRIGA Mark II reactor at Jožef Stefan Institute (JSI) [1] is among others, used as a neutron source for neutron activation analysis (NAA). The accuracy of the method depends on the accuracy of the neutron spectrum characterization. Calculated spectra based on full-core model in combination with activation measurements of monitor materials can be used. Computational model of the reactor has been developed and validated [2]. This MCNP5 [3] model includes core, reflector and all irradiation facilities, which are well characterized. This enables accurate determination of relative reaction rates for samples with negligible flux feedback effect. Additionally, self-shielding effect has to be taken into account for strong absorbers. Since using brute-force (whole-core model) for self-shielding calculations is numerically inefficient, a simplified MCNP model is used, retaining merely the irradiation channel with the associated moderator. An isotropic source is placed in the moderator, with the spectrum and axial distribution as calculated by the detailed model. For quick calculations, a deterministic method for self-shielding factor (SSF) determination for cylindrical samples, based on the Bondarenko equivalence principle, has been developed and verified [4]. The code MATSSF enables reliable routine SSF calculations for homogenous samples of almost any mixture of materials. The code is not limited to the TRIGA reactor, but is not as accurate as the MCNP model, especially when the self-shielding correction is large. Altogether, the combination of the flux distribution calculation with the whole-core MCNP model, SSF calculation with the simplified model, and planned accurate reactor power calibration, which is already in progress [5], will significantly increase the accuracy and predictability of the NAA at the JSI TRIGA reactor.

2. TRIGA reactor at JSI

The research reactor at the Jožef Stefan Institute (JSI) is a typical 250 kW TRIGA Mark-II reactor [1]. In addition to training purposes, it is extensively used for NAA.

2.1 Computational methods

Accurate knowledge of spectral characteristics of the irradiation facilities is crucial for the accuracy of the NAA and the assessment of the experimental uncertainties. Computational methods, particularly full three-dimensional models of the facility using Monte Carlo methods (e.g. the commonly used MCNP code [3]), are very powerful in providing information on the detailed shape of the neutron spectrum, but the results require careful validation to eliminate modelling errors, biases due to model simplifications, approximations in the methods and uncertainties in nuclear data. Self-shielding calculations of small samples using the whole reactor model is not impossible, but numerically very inefficient. Therefore, in addition to the full MCNP model, a simplified model, including only the observed irradiation channel and its immediate surroundings, has been developed. Finally, self-shielding factors can routinely be calculated using a simple deterministic code MATSSF [4].

2.1.1 Full reactor MCNP model

A detailed geometrical model of the TRIGA reactor was developed, in order to accurately calculate physical parameters of the TRIGA reactor. Our model is based on the criticality benchmark model, which is thoroughly described and published in [1]. This model can be used in calculations of the effective multiplication factor k_{eff} [6], power peaking factors [7], or reactor kinetic parameters [8].

The model has been further refined by adding the following structure elements: irradiation channels in the core, carrousel in the reflector with explicitly modelled irradiation tubes, and other components. This extension of the model is required to accurately calculate neutron spectra and flux distributions in irradiation channels, located both inside and around the core [2]. The model corresponds to fresh fuel, zero power, room temperature conditions. A sensitivity study has been performed in order to show that the influence of burnup, xenon, and fuel temperature on the flux distribution in irradiation channels is almost negligible [9].

2.1.2 MCNP model of the irradiation channel

In order to speed up the calculation procedure of reaction rates and self-shielding factors for samples in irradiation channels, the MCNP model has been simplified, retaining merely the chosen irradiation channel with its immediate surroundings. The neutrons can no longer be obtained from multiplication in fuel, therefore an external neutron source has to be defined explicitly. First, an isotropic source (its spectrum and axial distribution is calculated by the full reactor model) was put on the edge of the irradiation channel tube. Later we found that the flux on the channel-edge is slightly anisotropic. This can be correctly taken into account by moving the neutron source into the moderator outside the channel.

2.1.3 Deterministic self-shielding factor calculations by MATSSF code

The MATSSF code (available at: http://www-nds.iaea.org/naa/matssf/) was developed for routine calculations of approximate thermal and epithermal (resonance) self-shielding factors in samples for NAA. Self-shielding factors can be calculated for arbitrary cylindrical samples and different neutron source configurations assuming a Maxwellian spectrum for thermal and a $1/E$ spectrum for resonance factors. The algorithm for the resonance self-shielding calculations is based on the Bondarenko equivalence principle, while the thermal flux depression is calculated using a simple semi-empirical formula. Details can be found in [4].

3. Results

A neutron activation experiment was performed, simultaneously irradiating foils (5 mm diameter, 0.2 mm thick) of aluminium (99.9 w/o) - gold (0.1 w/o) alloy in 33 locations; 6 in the

core and 27 in the reflector. Through activity measurements of individual samples, relative reaction rates for ^{197}Au(n,γ) (representing mostly thermal flux) and ^{27}Al(n,α) (representing fast flux) reactions have been determined experimentally and compared to calculations obtained from the full MCNP model. The agreement between the calculated and measured reaction rate distribution in both the reflector and in the core is within the experimental error and Monte Carlo standard deviation [8]. However, the ratio between the calculated ^{197}Au(n,γ) reaction rates in the reflector and the core is overpredicted by around 7 % [2]. The main reasons are incomplete material and geometry data of the reflector and possibly inaccurate thermal scattering data. The differences are considered small enough to consider the full MCNP model validated.

Rhodium foils of about 5 mm diameter, 0.006 mm and 0.112 mm thick, were irradiated in the core and in the reflector of the JSI TRIGA reactor. The foils were irradiated enclosed in small cadmium boxes of 1 mm thickness. The resonance self-shielding corrections for the 0.006 and 0.112 mm thick samples were calculated by the MCNP model of the irradiation channel and amount to about 10% and 60%, respectively. The agreement with the measurements was within 1 % for the thin and within 4 % for the thick foil, confirming the validity of self-shielding factors calculated by the simplified MCNP model of the irradiation channel [10].

Isotropic neutron field on the inner edge of the irradiation channel in the original simplified MCNP model cause angular flux anisotropy in the centre of the channel (and consequently self-shielding factor dependence on the sample orientation) due to the streaming effect [4]. However, it was observed experimentally [11] that there is no measurable flux anisotropy in the centre of any TRIGA irradiation channel. Refining the model by moving the neutron source surface out of the channel into the surrounding moderator, the calculated result agrees with the measurements. Actually, the anisotropy on the inner edge of the irradiation channel (Fig 1) almost exactly compensates the channel streaming effect, rendering an almost isotropic neutron field in the centre of the channel (within the experimental and calculational precision of less than 1 %). The relative anisotropy is generally increasing with distance from the centre of the reactor core (Fig 2). The isotropy of the flux in the centre of the channel can be explained by the fact that the active core height is only 38 cm. If the core was much higher, one would expect the streaming effect to prevail, thus inducing neutron field anisotropy in the centre.

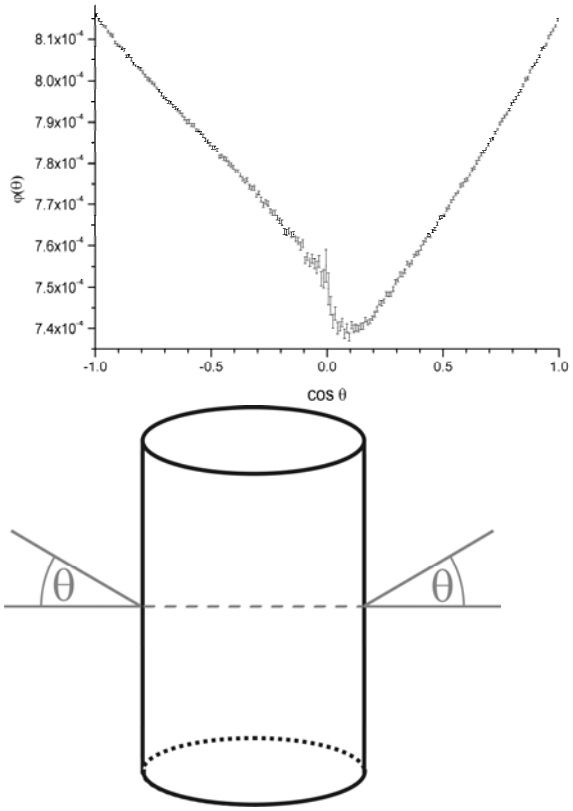

Fig 1: Angular flux $\varphi(\theta)$ on the edge of the TRIGA central irradiation channel (left). θ is the angle relative the positive normal of the irradiation channel tube (right).

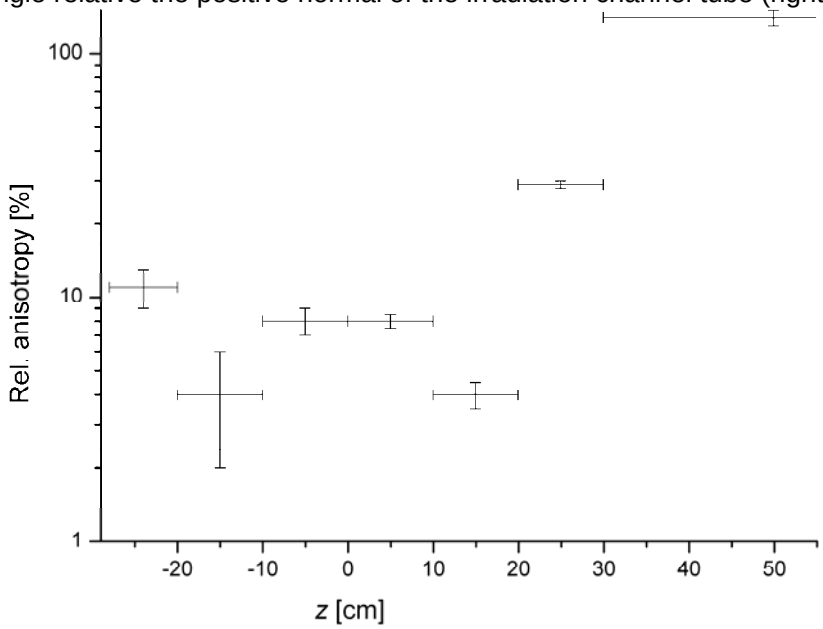

Fig 2: Axial dependence of the relative anisotropy (relative variation of the angular flux) on the edge of the channel. z is the axial position relative to the centre of the reactor core (active core height corresponds to $z \in$ [-19.05 cm,19.05 cm]). Axial asymmetry is a consequence of the irradiation channel asymmetry (graphite in bottom half and air in top half of the channel).

Though in MATSSF all geometry is parameterised merely by the sample mean chord length, it gives surprisingly good results compared to the rigorous Monte Carlo method [4]. It also takes into account approximately the interference between resonances of different nuclides

present in the sample material. MATSSF has been verified by comparison against MCNP calculated self-shielding factors for a number of different monitor materials [4]. In Tab 1, comparison between MATSSF resonance self-shielding factors for nuclides in the mixture (G_f) and reference MCNP full sample self-shielding factors (G_{f0}) for a 1 mm thick and about 3.8 mm long wire of Ni(80.93 w/o) Mo(15.16 w/o) W(2.76 w/o) Fe(0.45 w/o) Mn(0.41 w/o) Au(0.29 w/o) alloy with density of 9.21 g/cm^3, is shown as an example of good agreement of the simplified MATSSF results with the more rigorous Monte Carlo method.

nuclide	**MATSSF (G_f)**	**MCNP (G_{f0})**	$(G_f - G_{f0})/G_{f0}$ [%]
^{55}Mn	0.9902	0.993 ± 0.000	-0.3
^{56}Fe	0.9930	0.994 ± 0.001	-0.1
^{58}Fe	0.9904	0.986 ± 0.002	0.4
^{58}Ni	0.9863	0.991 ± 0.000	-0.5
^{64}Ni	0.9934	0.995 ± 0.000	-0.2
^{92}Mo	0.9880	0.990 ± 0.001	-0.2
^{98}Mo	0.9347	0.952 ± 0.001	-1.8
^{100}Mo	0.9369	0.952 ± 0.002	-1.6
^{184}W	0.9651	0.977 ± 0.001	-1.2
^{186}W	0.7860	0.817 ± 0.001	-3.8
^{197}Au	0.9213	0.940 ± 0.001	-2.0

Tab 1: Resonance self-shielding factors for the constituents of the nickel-alloy wire.

4. Conclusion

The full TRIGA reactor MCNP model has been verified on a benchmark based on a neutron activation experiment. Furthermore, simplified MCNP model and deterministic MATSSF code allow to explicitly and accurately take into account the self-shielding effect, if necessary. In addition to the undergoing project of the reactor power calibration, these computational tools offer a very strong support for neutron activation analysis of samples irradiated at the TRIGA Mark II reactor at the Jožef Stefan Institute.

5. References

[1] R. Jeraj, M. Ravnik, TRIGA Mark II reactor: U(20) - Zirconium Hydride fuel rods in water with graphite reflector, IEU-COMP-THERM-003, International Handbook of Evaluated Critical Safety Benchmark Experiments, Organization for Economic Cooperation and Development - Nuclear Energy Agency, NEA/NSC/DOC(95)03, Paris, 1999.

[2] L. Snoj, A. Trkov, R. Jaćimović, P. Rogan, G. Žerovnik, M. Ravnik, Analysis of neutron flux distribution for the validation of computational methods for the optimization of research reactor utilization, Appl. Rad. Isotopes, 69 (2011) 136-141.

[3] X-5 Monte Carlo Team, MCNP - A general Monte Carlo N-particle Transport code, Version 5, LA-UR-03-1987, April 24, 2003 (revised June 30, 2004).

[4] A. Trkov, G. Žerovnik, L. Snoj, M. Ravnik, On the self-shielding factors in neutron activation analysis, Nucl. Instr. Meth. A, 610 (2009) 553-565.

[5] L. Snoj, G. Žerovnik, A. Trkov, T. Žagar, B. Smodiš, Improving the accuracy of the absolute power calibration of TRIGA Mark II reactor, European Research Reactor Conference RRFM 2011, 20-24 March, Rome.

[6] Ravnik, M., Jeraj, R., 2003. Research reactor benchmarks. Nucl. Sci. Eng., 145, 145-152.

[7] L. Snoj, M. Ravnik, Power peakings in mixed TRIGA cores, Nucl. Eng. Des., 238 (2008) 2473-2479.

[8] L. Snoj, A. Kavčič, G. Žerovnik, M. Ravnik, Calculation of Kinetic Parameters for Mixed TRIGA Cores with Monte Carlo. An. Nucl. Ene., 37 (2010) 223-229.

[9] G. Žerovnik, Karakterizacija nevtronskega polja v obsevalnih kanalih reaktorja TRIGA, diploma work, Faculty of Mathematics and Physics, University of Ljubljana, 2007 (In Slovene).

[10] R. Jaćimović, A. Trkov, G. Žerovnik, L. Snoj, P. Schillebeeckx, Validation of calculated self-shielding factors for Rh foils, Nucl. Instr. Meth. A, 622 (2010) 399-402.

[11] G. Kennedy, C. Chilian, R. Jaćimović, G. Žerovnik, L. Snoj, A. Trkov, Neutron Self-Shielding in Irradiation Channels of Small Reactors is Isotropic, 13th International Conference on Modern Trends in Activation Analysis, Texas A&M University, 13-18 March, 2011.

OPTIMIZATION OF A POTENTIAL NEW CORE OF THE TRIGA MARK II REACTOR VIENNA

R. KHAN, M. VILLA, H. BÖCK, H. ABELE, G. STEINHAUSER
Vienna University of Technology-Atominstitut

The TRIGA Mark II Vienna is one of the last TRIGA reactors utilizing a mixed core with High Enrich Uranium (HEU) fuel. Due to the US Fuel Return Program, the Vienna University of Technology/Atominstitut (ATI) is obliged to return its HEU fuel by 2019. There is no final decision on any further utilization of the Vienna research reactor beyond that point. However, of all possible scenarios of the future, the conversion of the current core into Low Enriched Uranium (LEU) fuel and the complete replacement of all existing 83 burned FE(s) by new fresh FE(s) are investigated herein. This paper presents detailed reactor design calculations for three different reactor cores. The core 1 employs 104-type, core 2 uses 108-type and core 3 is loaded with mixed TRIGA fuels (i.e. 104 and 108). The combination of the Monte Carlo based neutronics code MCNP5, Oak Ridge Isotope Generation and depletion code ORIGEN2 and diffusion theory based reactor physics program TRIGLAV is used for this study. On the basis of this neutronics study, the amount of fuel required for a possible future reactor operation and its cost minimization is presented in this paper. The criticality, core excess reactivity, length of initial life cycle and thermal flux density distribution is simulated for three different cores. Keeping the utilization of existing fourteen 104-type FE(s) (i.e. six burned and eight fresh FE(s)) in view, the core 3 is found the most economical, enduring and safe option for future of the TRIGA Mark II reactor in Vienna.

1. Introduction

The Atominstitut (ATI) hosts the 250 kW TRIGA Mark II research reactor. Its cylindrical core lattice is surrounded by a Al-encased graphite reflector. This reflector has penetrations and cut-outs for beam tubes and the rotator rack etc. The whole core structure is submerged into a light water tank. The current core is loaded with 83 FE(s) of three different types of FE(s). Out of 83, 54 are 102 (20% enriched Al clad), 21 are 104 (20% enriched SS clad) and the rest 8 are 110 (or FLIP) FE(s). The 110 or FLIP fuel is Highly Enrich Uranium (HEU), 70% enriched.

The TRIGA Mark II reactor Vienna is still utilizing Highly Enrich Uranium (HEU) fuel. Due to the US Fuel Return Program, the Vienna University of Technology-ATI is obliged to return its 9 HEU FE(s) by 2019. Moreover, most of the 102-types FE(s) in the current core are close to achieve their maximum burn-up values. Therefore, it is also an option to return the FE(s) with maximum burn up numbers along with HEU fuel. Until now, there is no final decision on any further utilization of the Vienna research reactor beyond this limit of 2016. However, of all possible scenarios of the future, the conversion of the current core into Low Enriched Uranium (LEU) fuel and the replacement of the most of the burned FE(s) by fresh FE(s) are investigated in this paper.

Keeping in view the local, European and international research/training demands [2], the safe operation of the reactor is indispensable for next few decades. This paper consider following three possible options for the future of reactor operation i.e. core no. 1, core no. 2 and core no. 3 (mixed core)

1.1. Core No. 1

The core no. 1 is uniform and employed with 104-type fuel. This Zirconium Hydride (U-ZrH) fuel contains 8.5 w/o Uranium (U) and is enriched with 20% U-235. The 104-type FE has a central zirconium (Zr) rod, fuel meat (U-ZrH), lower Molybdenum disc and top & bottom graphite reflectors with Stainless Steel (SS) fixings. The geometrical and material characteristics of this fuel are given in Table 1[3].

1.2. Core No. 2

The core no. 2 is composed of only 108-type fuel. This is also called 20/20 fuel which refers to 20 w/o fuel content with 20% enrichment. This U-ZrH fuel is encased into the SS-304 cladding. There is no moly disc but 0.44 w/o Erbium is mixed homogeneously in the fuel meat to compensate the additional excess reactivity in the fresh core. The 108 type FE has fuel meat, upper & lower graphite reflectors and top & bottom SS fixings. The schematic

diagram of 108-type FE is given in Figure 1 and exact geometrical and material characteristics are provided in Table 1.

Table 1: The material and geometrical characteristics of the two TRIGA fuels.

Fuel Type	**104-type Fuel**	**108-type Fuel**
Fuel meat		
Material	U-$ZrH_{1.65}$	U-$ZrH_{1.65}$-Er
density	5.889	6.68
radius/length (cm)	1.82245/38.1	1.82245/38.1
mass of alloy	2259.84	2462
mass of U/U-235	192/38.2	492.4/98.5
Wt.% of fuel	8.5	20
Central Zr-rod		
Radius cm/Length	0.3175/38.1	0.3175/38.1
Burnable poison		
Material	Lower Molybdenum disc	0.44 w/o of Er homogeneously mixed in fuel meat
Radius/ length	0.0794/1.82245	

1.3. Core No. 3 (mixed core)

The core 3, containing 54 FE(s), is a mixed core of two different types of fuels i.e. 104-type and 108 (20/20) fuel types. Out of total 54 FE(s), the forty 108-type FE(s) are needed for initial criticality while the 14 FE(s) are 104-type FE(s). These 14 FE(s) include six burned FE(s) existing in the current core and 8 FE(s) fresh FE(s) present in the dry storage. The burn up of 6 burned FE(s) has been calculated by ORIGEN2 and given in Table 2 [1].

Table 2: The burn up (MWD) of 6 burned FE(s) in the current core.

FE ID	Burn up (MWD)	FE ID	Burn up (MWD)
9200	0.322539	10196	0.808415
10198	0.385086	10145	0.859611
10197	0.642366	10144	1.16768

In addition to FE(s) loadings, all three suggested cores use three control rods (shim, safety and regulating), one Am-Be neutron source, graphite elements in empty positions and two pneumatic transfer systems in the F-ring.

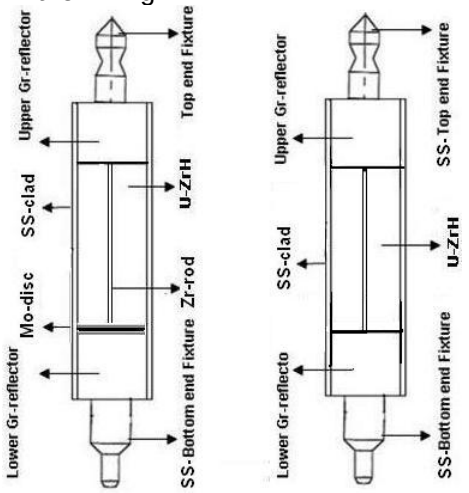

Figure 1: TRIGA 104-type FE (left) and 108-type FE (right).

2. Methodology

Reactor physics tools have gained key importance in the nuclear energy sector as they predict the microscopic and macroscopic behaviors of the reactor core considered in the given situation. Keeping the nature of calculations in view, a combination of probabilistic and deterministic tools has been selected for this research paper. The static part of the work is calculated by Monte Carlo N-Particle general purpose radiation transport code MCNP5 [4]

while the dynamic study is performed by diffusion theory based reactor physics program TRIGLAV [5] and Oak Ridge Isotope Generation and depletion code ORIGEN2 [6].

2.1. The ATI reactor MCNP Model

A detailed three dimensional MCNP model of the TRIGA mark II reactor is developed [1] to perform the neutronics calculations for the three proposed cores (core no. 1, 2, 3). However, only the structural importance for the parameters has been modeled. For example, irradiation holes inside the core due to their least effect on the core reactivity are neglected in this model. Similarly, the exact geometry of the top and bottom Aluminum fixing is simplified into simple cylindrical geometry.

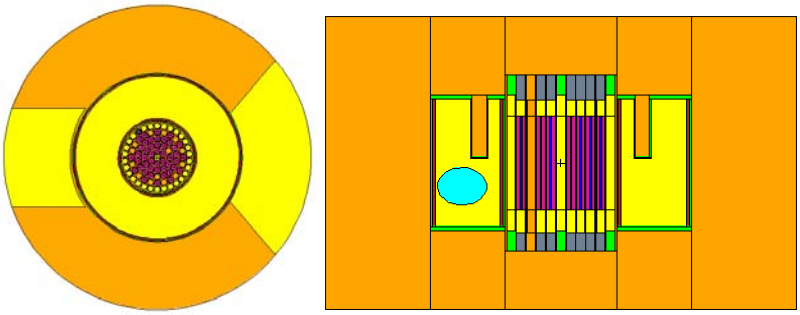

Figure 2: Top or XY-view (left side) and Side or YZ-view (right side) of the MCNP model of the TRIGA Mark II reactor.

The MCNP model is equipped with JEFF 3.1 neutronics data libraries. It incorporates all the necessary core components e.g. FE(s), central irradiation channel, three control rods, graphite elements, Be-Am source element inside the core. While annular graphite reflector, four beam tubes, thermal column and radiographic collimator are modeled outside the reactor core. All these components inside and outside the core are shown in Figure 2.

2.2. Validation

The MCNP model has been validated through initial criticality, reactivity distribution and thermal flux mapping experiments on the first core configuration [1]. The burn-up calculations (from initial core to the current core (30-06-2009) have been confirmed through gamma spectroscopic experiment on six 102-type FE(s) [7]. The burned fuel material composition is applied to the MCNP model to develop the current core MCNP model which is verified by three different experiments on the current core [1].

3. Reactor Physics Calculations

3.1. Initial Criticality

The verified MCNP model is applied for criticality calculations with a source size of 100000 particles and 150 active cycles. The criticality results are described in Table 3. With the core loading of 56 FE(s), the core 1 remains subcritical while on addition of 57th FE, it achieves its initial criticality which is agreed with the experimental results of initial criticality experiment performed on the ATI reactor in March 1962 [1]. The core 2 and core 3 approach their criticality states when 40th FE is loaded to E-ring.

Table 3: The criticality analysis of three possible cores of the TRIGA Mark II reactor.

Case	**FE(s)**	**U235 (kg)**	**K_{eff} MCNP5**
Core 1	57	2.172	1.00255 ± 0.00018
Core 2	40	3.940	1.00081 ± 0.00021
Core 3 (mixed)	40	3.940	1.00081± 0.00021

3.2. Core Excess Reactivity

To keep the reactor into safe operation, it is important to calculate the core excess reactivity that would meet the safety criteria and licensing limits of the reactor. The table 4 presents the excess reactivity of all three proposed cores. In the initial step, the core 1 is loaded with eighty four 104-type FE(s), core 2 with forty six 108-type 46 FE (s) and core 3 which is a mixed core and loaded with 54 FE(s) including forty 108-type, eight 104-type fresh and six 104-type burned FE(s). The results are given in Table 6.

Table 6: The excess reactivity of three different cores.

Core type	Fuel type	No. of FE(s)	ρ_{ex} ($)
Core 1	104	84	7.51
Core 2	108	46	4.85
Core 3	108 and 104	54	7.14

3.3. Core Life Time

The Full Power Day (FPD) refers to the continuous full power reactor operation for 24 hours round the clock. Figure 3 (left) presents the excess reactivity verses FPD(s) of reactor operation for core no. 1. It shows that core no. 1 can be operated for 750 FPD(s) without any reshuffling of FE(s). The different numbers on the graph show the fuel core loadings. The life of the core is extended by applying effective fuel management strategies (sequential reshufflings etc.) after the first cycle.

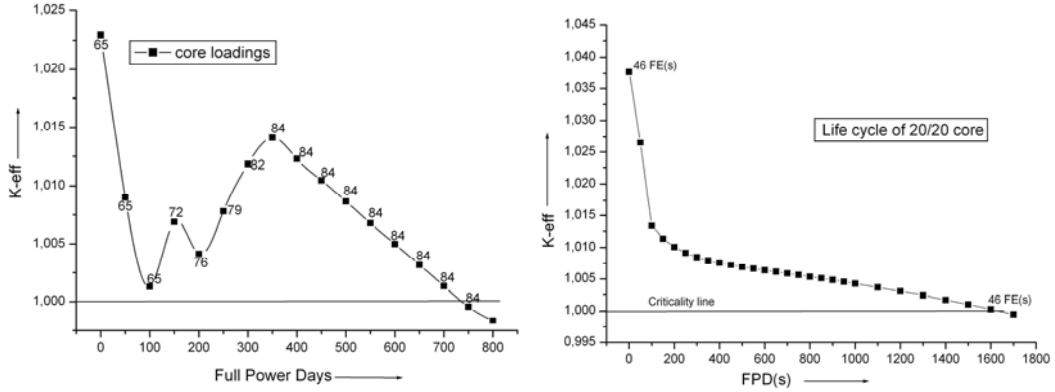

Figure 3: The excess reactivity verses FPD(s) for core 1 (left) and core 2 (right) of the TRIGA Mark II reactor.

Figure 3 (right) reflects the initial life cycle of core 2 which is about 1700 FPD(s) showing that 108-type fuel has more burn up than 104-type fuel. The maximum burn-up numbers of FE(s) in respective core rings for all three cores are provided in Table 7.

Figure 4 gives the first operating cycle length of the core 3. This core can be operated at 250 kW for 1900 FPD(s) for its first operating cycle. This core life is higher than the both previous two cases. This mixed core incorporates total fifty four FE(s). Out of 54, 14 FE(s) are 104-type and loaded to E ring of the core. These fourteen 104-type FE(s) include six burned and eight fresh FE(s). The burn-up numbers of each ring are described in Table 7.

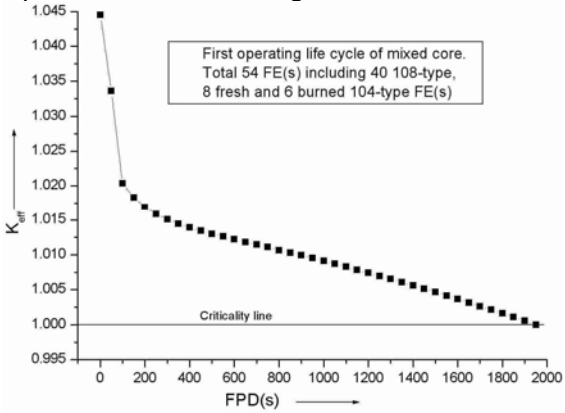

Figure 4: The core 3 excess reactivity verses FPD(s) of the TRIGA Mark II reactor.

Table 7: Burn up comparison of 104-type and 108-type TRIGA fuels.

FE position	**Core 1 Burn up (MWD)**	**Core 2 Burn up (MWD)**	**Mixed core Burn up (MWD)**
B-ring	3.344	11.583	13.50

C-ring	2.821	9.017	10.73
D-ring	2.459	7.961	9.10
E-ring	1.985	8.491	*8.23 **5.25
F-ring	1.473	No FE	No FE

*108-type Fresh FE, **104-type fresh FE

3.4. Thermal Flux Distribution

The MCNP model of core 2 and 3 is applied to calculate radial thermal flux density of the TRIGA reactor keeping all three CR(s) in fully withdrawn positions. The simulated results in comparison with the experimental results of the current core are given in Figure 5. Generally, the results look quite symmetrical as maximum in the centre and decreases along the radial direction. The thermal flux density distribution in core 2 and 3 is quite similar except the values at the F-ring. Thermal flux density at F-ring position of the core 3 is higher than core 2. It may be because of core 3 has 54 FE(s) keeping E-ring is almost filled with 104-type FE(s) while the core 2 has only six filled positions in the E-ring.

Table 11 and Figure 5 show that core 2 and 3 provide respectively the 63 to 71 percent higher thermal flux in F-ring and 12 to 10 percent higher flux in the centre Irradiation channel CIR as compared to the current core. It is due to high density fuel employed in the inner rings of the core lattice. These higher values of thermal flux at F-ring would attract the beam tube scientists for further utilization.

Table 11: Radial thermal flux density (ns/cm2.s) distribution in three different cores.

Radius (cm)	Th. flux Current core	Th. flux Core 2	% -diff. from exp. results	Th. Flux core no. 3 ($x10^{12}$ns/cm.s)	%-diff. from exp. results
0	1.00E+13	1.1218E+13	12	1.100E+13	10
5.3	6.01E+12	1.1123E+13	85	1.084E+13	80
10.6	2.59E+12	8.6249E+12	233	8.548E+12	230
13.5	3.45E+12	9.5693E+12	177	7.316E+12	112
18.5	2.27E+12	4.5768E+12	101	4.835E+12	112
21.3	2.23E+12	3.6543E+12	63	3.815E+12	71

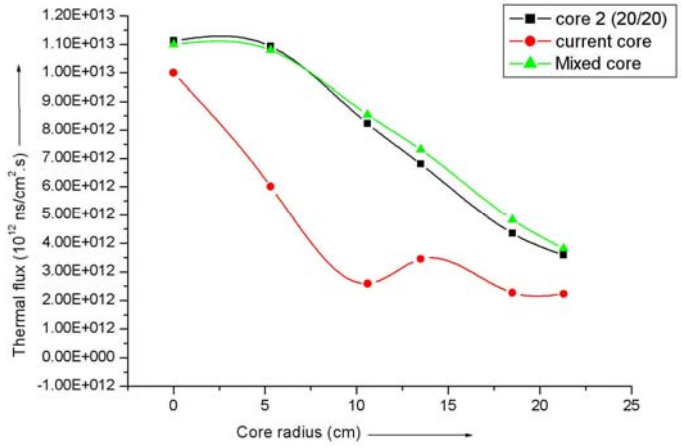

Fig. 5: Graphical comparison of thermal flux of current core with new core.

4. Conclusion

The 104 and 108-type of TRIGA fuels (104 and 108-type) have been employed for their neutronics behaviors in three different core configurations. The core 1 is loaded with eighty four 104-type fresh FE(s), core 2 is employed with forty six 108-type fuel and core 3 is loaded with both fuels (i.e. 104

and 108 type) constituting a mixed core. Though core 2 is more compact and uniform than core 1 and 3, but keeping the economical factor and utilization of fresh fuel on stock in view, the core 3 is determined as safe, economical and long lived option. On the basis these neutronics results, it is concluded that core 3 is the best future option for the TRIGA Mark II Vienna reactor.

Acknowledgement

We are grateful and acknowledge the support from the Austrian Science Fund (FWF) under Contract No. I534-N20 for this research project.

References

1. R. Khan, June 2010, Neutronics Analysis of the TRIGA Mark II Research Reactor and its Experimental Facilities, PhD dissertation, Vienna University of Technology, Vienna, Austria.
2. R. Khan, H. Böck, M. Villa, the Status and Patterns of Nuclear Education in Anti-nuclear Environment, Austria, 2010, International Journal of Nuclear Knowledge Management (IJNKM), Vo. 4, number. 3, 2010.
3. Luka Snoj, 2009, Analysis of Physical Parameters of TRIGA reactor, PhD dissertation, University of Ljubljana, Slovenia.
4. X-5 Monte Carlo Team, 2005, MCNP - A general Monte Carlo N-particle Transport code, Version 5, LA-UR-03-1987.
5. Peršič, A., et al., "TRIGLAV - A Program Package for Research Reactor Calculations", OECD, NEA Data Bank, France.
6. A.G. Croff, 1999. A user's manual for the ORIGEN2 computer code. OAK RIDGE National Laboratory, USA.
7. Khan, R., Karimzadeh, S., Böck, H., 2010. TRIGA fuel burn-up calculations and its confirmation. Nuclear Engineering and Design 240 (2010), 1043–1049.

NEUTRONIC ANALYSIS OF THE PAVIA UNIVERSITY TRIGA MARK II REACTOR CORE

A. BORIO DI TIGLIOLE[1,2], A. CAMMI[3], **D. CHIESA**[4], M. CLEMENZA[4], L. PATTAVINA[4,5], E. PREVITALI[4,5], G. SCIAN [2]

(1) University of Pavia, Department of Nuclear and Theoretical Physics, Via Bassi 4, 27100 Pavia, Italy
(2) University of Pavia, Laboratory of Applied Nuclear Energy, Via Aselli 41, 27100 Pavia, Italy
(3) Polytechnic of Milano, Department of Energy, Via La Masa 34, 20156 Milano, Italy
(4) University of Milano-Bicocca, Physics Department, Piazza della Scienza 3, 20126, Milano, Italy
(5) INFN section of Milano-Bicocca, Piazza della Scienza 3, 20126, Milano, Italy

ABSTRACT

An advanced computational tool based on Monte Carlo code was developed for the neutronic analysis of the TRIGA Mark II research reactor of the University of Pavia and the results from simulations were benchmarked with the experimental data. The neutron analysis was performed by means of the 3-D continuous-energy Monte Carlo codes MCNP4C and MCNP5. All core components were reproduced in good detail and the model allows the description of different core and fuel configurations with good versatility. In a first step, the results from the simulations with fresh fuel at room temperature were compared with the experimental data about critical core parameters at zero power level, quoted in the reactor First Criticality Final Report; a very good agreement was found and the goodness of the model was proved. Afterwards, neutron flux and reactivity dependence on the fuel and moderator temperature was studied in detail; all the available methods for the simulation of thermal effects were analyzed in order to model the reactor in the stationary operating condition at 250 kW. The model was updated to the present configuration and the use of specific S(α,β) cross sections was found to be of primary importance for a correct simulation of low-energy neutrons scattering within moderator.

1. Introduction

The TRIGA Mark II Reactor at Applied Nuclear Energy Laboratory (L.E.N.A.) of the University of Pavia was brought to its first criticality in 1965. Since then, the TRIGA reactor has been used for several scientific activities such as production of radioisotopes, activation of materials for non destructive analysis, development of boron neutron capture therapy in the medical field and reactor physics studies. It is a pool-type research reactor moderated and cooled by light water. Fuel consists of a uniform mixture of uranium (8%wt, enriched 20%wt in ^{235}U), hydrogen (1%wt) and zirconium (91%wt).

The TRIGA reactor of the University of Pavia has a nominal power of 250*kW* in a stationary-state operation. The core shape is a right cylinder and the volume can host 90 locations distributed according 6 concentric rings (see Fig 1) labelled as A (central thimble),B, C, D, E and F. These locations can be filled either with fuel elements (FE) or different core components like graphite elements (dummy), control rods, neutron source and irradiation channels. A 30*cm* thick radial graphite reflector surrounds the core, while the top and bottom reflector is provided by the fuel element itself in which two graphite cylinders are located at the ends of the rod. The neutron flux in the centre of the reactor core in a stationary operating condition at 250*kW* is about $2.2 \cdot 10^{13} cm^{-2} s^{-1}$ and can reach the value of $2.2 \cdot 10^{16} cm^{-2} s^{-1}$ during a pulse mode operation at 250*MW* power peak.

The TRIGA current core contains two different types of fuel elements: the outer rings E and F host 49 FE(s) with aluminium cladding (102-type), while the 34 fuel rods in the inner rings are 104-type FE(s), having stainless steel cladding.

To analyze the critical core parameters and neutron fluxes, a detailed 3D geometry of the TRIGA reactor was reconstructed in a Monte Carlo model. Monte Carlo methods represent an advanced computational tool to perform analysis in nuclear physics. The MCNP code was

chosen due to its capability in general geometrical modelling, correct representation of transport effects, continuous-energy cross sections treatment and suitable nuclear reactor characterization.

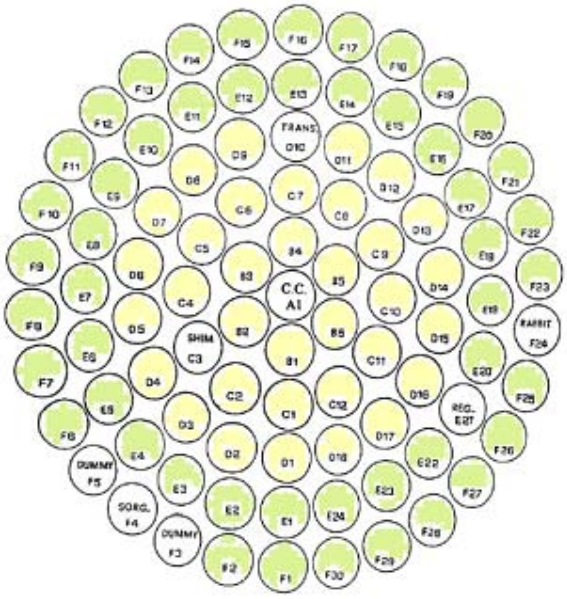

Fig 1: The current core map of the TRIGA Mark II reactor in Pavia: yellow rods are 104-type, while green ones are 102-type.

2. Benchmark analysis of MCNP model

First of all, a benchmark analysis of the model was performed in condition of fresh fuel and zero power (nominally 10*W*), which means that no temperature effects, no nuclear fuel poisoning and burn-up effects were considered. The MCNP simulation results were compared to experimental measurements performed in 1965, during reactor first start-up. Some benchmark comparisons are presented in the next sections.

Total reactivity worth of control rods

The TRIGA reactor has three control rods, called SHIM, REGULATING and TRANSIENT. The total reactivity worth (ρ_{tot}) of each control rod is defined as the difference of reactivity recorded when a rod is completely extracted from the full-inserted position. The data from simulations show a very good agreement with the experimental ones (see Tab 1).

Control rod	ρ_{tot} calculated [$]	ρ_{tot} experimental [$]
SHIM	4,12 ± 0,04	4,10 ± 0,02
TRANSIENT	2,02 ± 0,04	2,05 ± 0,02
REGULATING	1,64 ± 0,04	1,64 ± 0,02

Tab 1: Comparison between calculated and experimental total reactivity worth ρ_{tot} of each control rod.

Reactivity worth of ^{235}U

This parameter is defined as reactivity change per gram of ^{235}U when a fuel element is inserted in the core. The reactivity worth of ^{235}U depends on the rod position in the core and was measured for the B5 and the C9 rods.

Experimentally, a fuel element is removed from the core and the reactivity change ($\Delta\rho$) is evaluated using the calibration curves of the control rods. The reactivity per gram of ^{235}U (ρ_m) is then simply calculated by dividing the absolute value of $\Delta\rho$ by the mass of ^{235}U included in the extracted fuel element. The values calculated with the simulations show a good agreement with the experimental data (see Tab 2), thus the model returns good results not only for global parameters, but also for a single fuel rod.

Ring Position	^{235}U mass [g]	$\rho_{m,exp}$ [$/g]	$\rho_{m,calc}$ [$/g]
B5	37,59	0,0415 ± 0,0005	0,0436 ± 0,0011
C9	37,04	0,0271 ± 0,0005	0,0293 ± 0,0011

Tab 2: Comparison between calculated and experimental reactivity worth of ^{235}U in different rings.

Void reactivity coefficient of moderator

Another important parameter for the reactor core characterization is the void reactivity coefficient of the moderator. The experimental evaluation of this parameter consists in measuring the reactivity change, when a rod filled with the moderator (H_2O) is replaced with an empty one. The void reactivity coefficient is then calculated as:

$$\alpha_V = \frac{\Delta\rho}{V_M}$$

where V_M is the volume of the moderator. In the MCNP simulations the void reactivity coefficients were calculated in the same core positions as the experimental measurements and the results are presented in Tab 3.

Ring Position	$\Delta\rho_{exp}$ [cents of $]	$\Delta\rho_{calc}$ [cents of $]	$\alpha_{v,exp}$ [cents of $/cm^3]	$\alpha_{v,calc}$ [cents of $/cm^3]
C9	-23,5 ± 1,5	-23,1 ± 1,5	-0,065 ± 0,004	-0,063 ± 0,010
D13	-23,0 ± 1,5	-23,4 ± 1,5	-0,063 ± 0,004	-0,064 ± 0,010
E17	-11,1 ± 1,5	-8,38 ± 1,5	-0,030 ± 0,004	-0,023 ± 0,010

Tab 3: Comparison between calculated and experimental void reactivity coefficient in different rings.

3. Simulations and measurements of neutron flux

The following step was the analysis of neutron fluxes, in order to evaluate how close the simulations are respect to measurements. The neutron flux depends on position and energy; since it determines the reaction rate, it's very important to know its spectrum and spatial distribution.

Measurement of Neutron Flux

The flux was measured with the target activation technique using Au, Cu, Fe, Ni, Al and In foils; two more measurements were performed with gold and copper targets placed in a cadmium box. The reactivity induced on targets was measured with gamma ray spectroscopy and the activation rate was determined. Neutron energy spectra were also reconstructed using SANDII software, that performs an iterative spectrum calculation from experimental activation data using a de-convolution algorithm.

Fluxes were measured in the central core thimble, in the pneumatic irradiation system named “Rabbit” (ring F) and in the rotary specimen rack named "Lazy Susan", located in a circular well within the radial reflector. The reactor was kept at a low power level (2,5*kW* and 25*kW*), so that the fuel and the moderator were at room temperature.

MCNP Simulations

First of all, the MCNP geometry input was updated to the current core configuration: some fuel elements were added in the F ring and the geometry of the new 104-type rods in B, C and D rings was described. Afterwards, MCNP simulations were performed and fluxes were estimated in cells where the target foils were exposed to neutrons. Monte Carlo results were normalized by the number of neutrons produced per second in the core.

Comparison between simulated and measured of fluxes

The comparison between experimental measurements and MCNP simulations are reported in Tab 4; all data are normalized to 250*kW* reactor power. Fluxes estimated in simulations are always lower than the measured ones. In particular, the difference is 18% for central thimble, 37% for Rabbit channel and 28% for Lazy Susan. These differences are greater than the

uncertainty associated to the experimental data, that was estimated around 10%.
The reason of these discrepancies has to be investigated in detail, because there are some aspects that are not included in the model. In particular, the ^{235}U content in the model is the same in all fuel rods, not taking into account fuel burnup and poisoning. The real distribution in the core of fissile material and neutron poisons obviously affect the intensity of the neutron flux locally. These effects are not included in the MCNP simulation yet.

Central thimble		
Energy [MeV]	Φ calculated [$cm^{-2}s^{-1}$]	Φ experimental [$cm^{-2}s^{-1}$]
0 - $5{,}5\cdot10^{-7}$ (thermal)	$(6{,}407 \pm 0{,}018)\cdot10^{12}$	$(7{,}3 \pm 0{,}7)\cdot10^{12}$
$5{,}5\cdot10^{-7}$ - 0,1 (epithermal)	$(5{,}388 \pm 0{,}013)\cdot10^{12}$	$(7{,}5 \pm 0{,}7)\cdot10^{12}$
0,1 - 18 (fast)	$(6{,}201 \pm 0{,}013)\cdot10^{12}$	$(6{,}8 \pm 0{,}7)\cdot10^{12}$
Total	**$(1{,}80 \pm 0{,}03)\cdot10^{13}$**	**$(2{,}16 \pm 0{,}22)\cdot10^{13}$**

Rabbit channel		
Energy [MeV]	Φ calculated [$cm^{-2}s^{-1}$]	Φ experimental [$cm^{-2}s^{-1}$]
0 - $5{,}5\cdot10^{-7}$ (thermal)	$(2{,}462 \pm 0{,}007)\cdot10^{12}$	$(3{,}37 \pm 0{,}34)\cdot10^{12}$
$5{,}5\cdot10^{-7}$ - 0,1 (epithermal)	$(2{,}100 \pm 0{,}005)\cdot10^{12}$	$(3{,}52 \pm 0{,}35)\cdot10^{12}$
0,1 - 18 (fast)	$(2{,}088 \pm 0{,}004)\cdot10^{12}$	$(2{,}83 \pm 0{,}28)\cdot10^{12}$
Total	**$(6{,}65 \pm 0{,}01)\cdot10^{12}$**	**$(9{,}72 \pm 0{,}97)\cdot10^{12}$**

Lazy Susan		
Energy [MeV]	Φ calculated [$cm^{-2}s^{-1}$]	Φ experimental [$cm^{-2}s^{-1}$]
0 - $5{,}5\cdot10^{-7}$ (thermal)	$(11{,}665 \pm 0{,}012)\cdot10^{11}$	$(12{,}8 \pm 1{,}3)\cdot10^{11}$
$5{,}5\cdot10^{-7}$ - 0,1 (epithermal)	$(7{,}383 \pm 0{,}008)\cdot10^{11}$	$(10{,}4 \pm 1{,}0)\cdot10^{11}$
0,1 - 18 (fast)	$(3{,}920 \pm 0{,}005)\cdot10^{11}$	$(7{,}1 \pm 0{,}7)\cdot10^{11}$
Total	**$(2{,}297 \pm 0{,}002)\cdot10^{12}$**	**$(3{,}04 \pm 0{,}30)\cdot10^{12}$**

Tab 3: Comparison between calculated and experimental flux in different core positions.

In Fig. 2 the neutron flux spectra, measured and simulated, are shown in 30 energy intervals. Although the results from simulations are generally underestimated, the shape of the spectrum is well reproduced, confirming that the MCNP model can simulate the real energetic distribution with good detail.

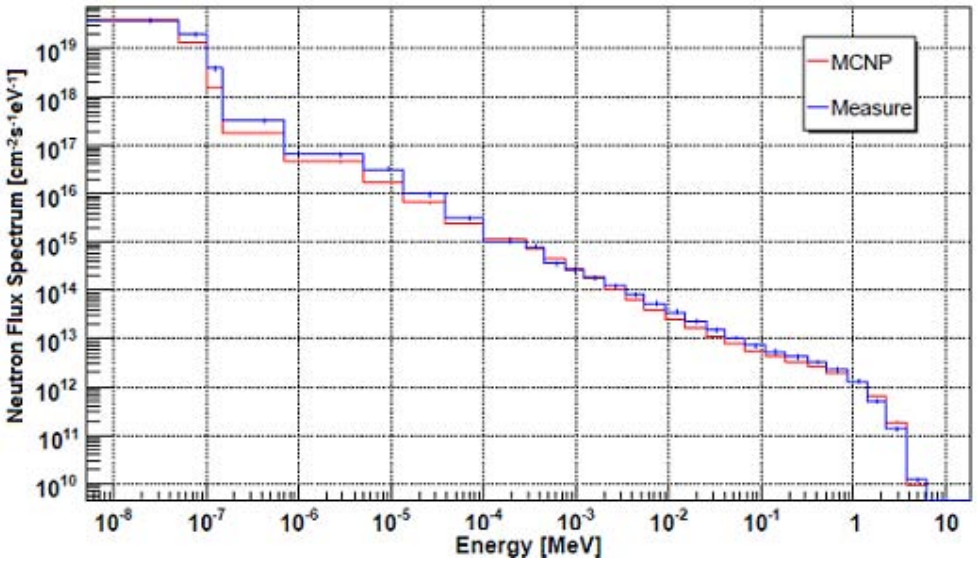

Fig 2: Comparison between calculated and experimental neutron flux spectrum in the central thimble, divided in 30 energy groups.

4. Simulation of Thermal Effects

In order reconstruct the TRIGA reactor conditions in stationary condition at 250*kW* power, a in-depth study was performed about neutron fluxes and the reactivity dependences on fuel temperature. The thermal motion of nuclei affects the values of cross sections that describe the interaction of neutrons at low energy. MCNP provides different methods to simulate these thermal effects, thus some tests were performed to check the answer of the model while introducing different thermal conditions.

The *free gas thermal model* allows to describe the elastic scattering at any temperature: atoms are modelled like a free gas with Maxwell distribution of velocities and low energy cross sections are multiplied by a factor that depends on the temperature of the medium.

Moreover, for some materials, a specific thermal model must be used to correctly simulate the effects due to chemical bindings. This treatment uses specific cross sections below 4*eV* energy, that are usually named *S*(α,β) from the homonymous law that describes thermal neutron anelastic scattering on molecules or lattice solids. *S*(α,β) data are normally available only for some temperatures and for a small number of materials.

Comparison between Free Gas and *S*(α,β) Thermal Treatments

A first set of simulations was performed using the free gas thermal treatment for the Zirconium Hydride (HZr) contained in the fuel. 8 different temperatures were chosen, spacing from 300K to 1200K. These simulations were compared to the ones performed at the same temperatures with the use of the latest *S*(α,β) cross sections for hydrogen bound in the lattice of HZr (ENDF/B-VII Thermal Data).

The flux of neutrons in the fuel was found to be different using *free gas* respect to *S*(α,β) thermal treatment (Fig 3a). In the first case, neutrons have Maxwell distribution of energies corresponding to the temperature at which the fuel is set. The use of *S*(α,β) cross sections show a shift of the spectrum towards higher energies, moreover some spikes appear in the energetic distribution of flux. In simulations at high temperatures, a deformation of the spectrum is observed at the energy of 0.137*eV*, corresponding to the first energy level in which hydrogen atoms are bound in an isotropic 3D harmonic potential well (Fig 3b).

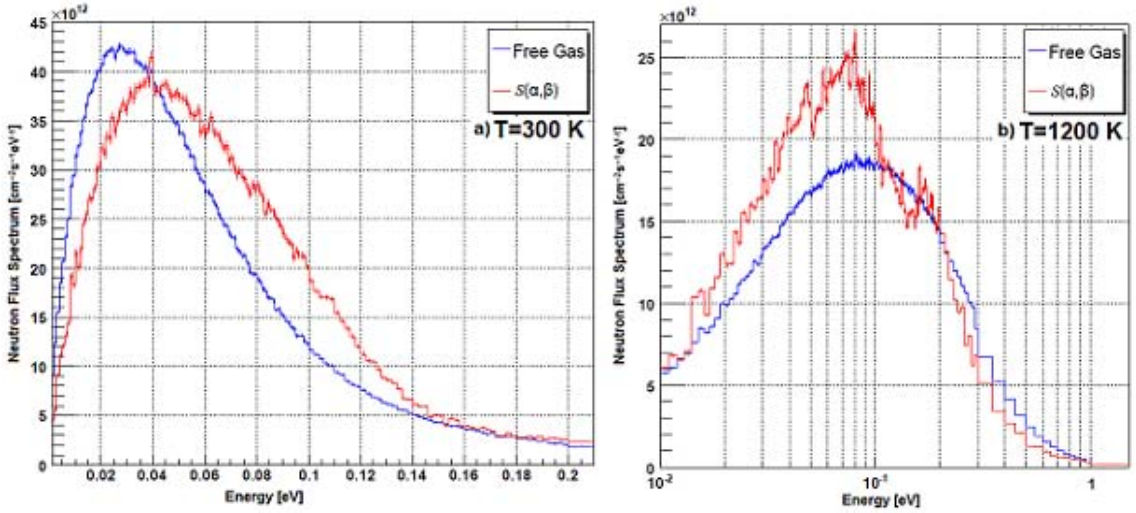

Fig 3: Comparison of the thermal flux spectrum in the fuel of ring B when *free gas* treatment is used instead of *S*(α,β) thermal treatment. a) Fuel temperature: 296.3K; b) Fuel temperature: 1200K.

With these simulations, we highlight that the use of *S*(α,β) thermal treatment affects significantly the results. The application of this treatment involves the modelling of inelastic scattering on lattice: bound hydrogen atoms exchange energy quanta with neutrons modifying their energies. Excited energy level population of bound atoms increases with temperature, producing a shift of the thermal neutron spectrum towards higher energies which affects the reactivity of the core. The mean difference in reactivity between simulations performed with or without *S*(α,β) treatment is equal to (1,93±0,23)$, with a maximum difference of 3,18$ at room temperature.

Comparison between different releases of *S*(α,β) cross sections

Some simulations were performed by using the *S*(α,β) cross sections released either in 1999 (ENDF/B-VI) or in 2004 (ENDF/B-VII); the flux distribution inside the fuel and the reactivity parameter were compared and some differences were found (see Fig 4). In particular, the reactivity worth decreases when using updated libraries with a mean difference of (0,25±0,11)$.

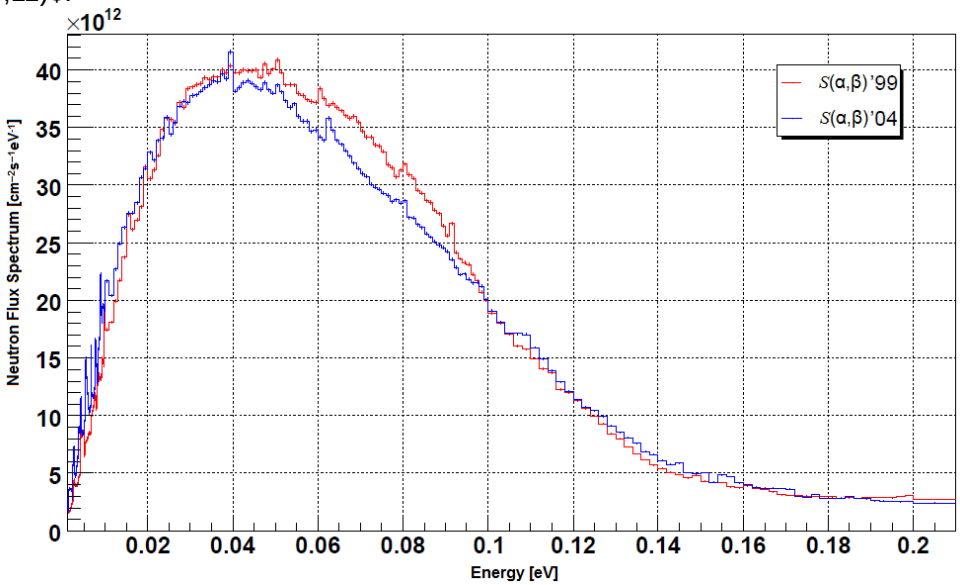

Fig 4: Comparison of the thermal flux spectrum in the fuel of ring B when *S*(α,β) cross sections released in 1999 are used instead of the last ones, dating back to 2004.

5. Conclusion and outlook

The MCNP model for the TRIGA Mark II Reactor of the University of Pavia was benchmarked in first start-up configuration: the simulations were found in good agreement with the measurements performed during the first criticality test. The detailed geometrical description allows to calculate the reactor parameters with good precision.

The model was updated to the current reactor configuration with 83 fuel elements and fluxes were measured by target foils activation. The spectrum shape is well reproduced in the simulation and the next step will be the introduction of burnup and neutron poisons effects in the model to obtain a more precise evaluation of neutron fluxes.

Thermal effects due to the increase of fuel temperature were investigated with various MCNP simulations techniques, highlighting that the *S*(α,β) thermal treatment introduces significant differences in the results.

References

1. A. Borio di Tigliole, A. Cammi, M. Clemenza, V. Memoli, L. Pattavina and E. Previtali. *Benchmark evaluation of reactor critical parameters and neutron fluxes distributions at zero power for the TRIGA Mark II reactor of the University of Pavia using the Monte Carlo code MCNP.* Progress in Nuclear Energy, 2009.
2. Monte Carlo Team. *MCNP - A general Monte Carlo N-Particle Transport Code, Version 5*. LA-UR-03-1987. Los Alamos National Laboratory, April 24, 2003.
3. M.Mattes and J.Keinert. *Thermal Neutron Scattering Data for the Moderator Materials H2O, D2O, and ZrHx in ENDF-6 Format and as ACE Library for MCNP(X) Codes*. INDC/NDS report INDC(NDS)-0470, April 2005.
4. J.R. Lamarsh. *Nuclear Reactor Theory*. Addison-Wesley Publishing Company, 1966.
5. M. Dabbene, *Interpretazione di misure di attivazione per la valutazione del flusso neutronico nel reattore sperimentale TRIGA*, Thesis in Nuclear Engineering, Politechnical University of Tourin, Italy - 2010

EFFECT OF THE NEW WIMSD LIBRARIES ON THE NEUTRONIC PARAMETERS OF THE FIRST AND EQUILIBRIUM CORES OF THE INDONESIAN MULTIPURPOSE RESEARCH REACTOR

T.M. Sembiring, L. Suparlina
Center for Reactor Technology and Nuclear Safety, National Nuclear Energy Agency (BATAN)
Kawasan PUSPIPTEK Gd. No. 80, Serpong, Tangerang Selatan 15310 - Indonesia

Liem Peng Hong
Research Laboratory for Nuclear Reactors, Tokyo Institute of Technology
O-okayama, Meguro, Tokyo 152-8550 - Japan

ABSTRACT

Accurate neutronic parameters are very important in the design and safety analysis of a research reactor. The calculation method and neutron cross-section data play an important role to obtain those neutronic parameters. In this work, we reported our new results on the effects of the recent neutron cross-section data of the WIMSD libraries, JEFF-3.1 and ENDF/B-VII.0, on the criticality parameters of the first and equilibrium cores of the Indonesian multipurpose reactor, RSG-GAS reactor. WIMSD lattice code together with WIMSD libraries, coupled with the in-core fuel management code BATAN-FUEL, has been used routinely in the in-core management analysis since 1996. The objective of this work is to assess the accuracy of the recent WIMSD libraries before being adopted for routine in-core fuel management. As the first step, a series of core calculations were carried out for determining the effective multiplication factor, burn-up swing reactivity and Xenon equilibrium reactivity for the first and equilibrium cores. The results show that WIMSD library based on the evaluated nuclear data ENDF/B-VII.0 gives better agreement with the experimental results for criticality evaluation (underestimation of less than 0.4%). For burn-up swing evaluation, we found relatively large differences among the libraries (max. 5%). However, there is no significant difference among three WIMSD libraries in determining the Xenon equilibrium reactivity.

1. Introduction

Winfrith Improved Multigroup Scheme version-D (WIMS-D) is one of the widely used deterministic computation tools for basic reactor physics computations including burnup calculations for a wide variety of reactor types. In 1998, WIMSD-5B code has been released to replace the old version of WIMS-D/4 code [1,2]. Because the old library is essentially based on the evaluated nuclear data from 1960's, the IAEA through the WIMS-D Library Update Project has provided new WIMSD libraries which are taken from the recent evaluated nuclear data such as ENDF/B-VII.0 and JEFF-3.1 [3-5]. These libraries enable scientists and reactor designers to reflect the enhancements of the recent evaluated nuclear data in their reactor physics calculations.

Up to now, the WIMS-D/4 lattice code has been used to generate the macroscopic cross-sections for all core materials of the Indonesian multipurpose reactor GA Siwabessy, RSG-GAS reactor [6,7]. The cross-section library is arranged in as a public library for the 2-or 3-dimensional neutron diffusion code [8], and 2-D in-core fuel management code BATAN-FUEL [6]. Before we adopt the recent WIMSD libraries, it is necessary to investigate the effects of the use of those WIMSD libraries (ENDF/B-VII.0 and JEFF-3.1) on the calculated neutronic parameters of the RSG-GAS reactor.

In the first step of our investigation, macroscopic cross-section libraries for fuel elements have been generated using the recent WIMSD libraries, while the macroscopic cross-section libraries for non-fission materials have been not changed.

2. Description of RSG-GAS Reactor

The RSG-GAS reactor is a multipurpose open-pool tank type reactor. The reactor has nominal power of 30 MWth using 40 standard fuel elements (FE, each consisting of 21 fuel plates), 8 control fuel elements (CE, each consisting of 15 fuel plates) and 8 fork-type Ag-In-Cd absorbers arranged on the 10 × 10 core grid positions as shown in Fig.1. Beryllium and light water are used as the reflector and the moderator as well as coolant, respectively. At the nominal power, the reactor produces thermal neutron flux in order of 10^{14} n/cm^{2}s. Originally, the core used the oxide fuel (U_3O_8-Al), but, presently, the core uses the silicide fuel (U_3Si_2-Al). Reactor main data are presented elsewhere in Ref.[9].

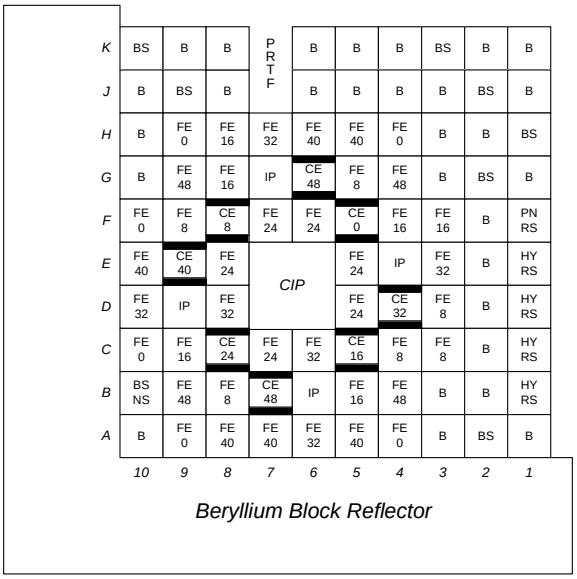

Note: BE = Beryllium Element;BS = Beryllium Element with plug;CIP/IP = Irradiation Position; PNRS/HYRS = Pneumatic/ Hydraulic Rabbit System;

Fig 1. Typical working core configuration of RSG-GAS reactor
(Beginning of cycle; values in the second rows denote burn-up (%^{235}U loss)).

2.1 First core configuration

The full configuration of the first core of RSG GAS consists of 12 fresh FEs and 6 CEs while for the first criticality, the core needs only fresh 9 FEsd and 6 CEs. The configurations for the first criticality and full core of the first core are shown in Fig. 2 and Fig. 3, respectively.

As seen in Fig. 3, the core grid positions B-6, C-7, D-6 and F-4 were used for irradiation positions. There were 15 loading steps for achieving the full core configuration. The maximum power of the first core (full configuration) was 10.17 MWth.

2.2 Equilibrium core configuration (Oxide Fuel)

As seen in Fig. 1, the core-average burn-up at beginning of cycle (BOC) is 23.3% loss of ^{235}U, and the corresponding value at end of cycle (EOC) is 31.3%, i.e. the burn-up step for one core cycle is about 8%. The maximum discharge burn-up of FE or CE is approximately 56%. Hence, the core consists of FEs and CEs with 7 different burn-up classes, i.e. 6 standard FEs and 1 CE for the first 6 classes and 4 FEs and 2 CEs for the 7th class (highest burn-up).

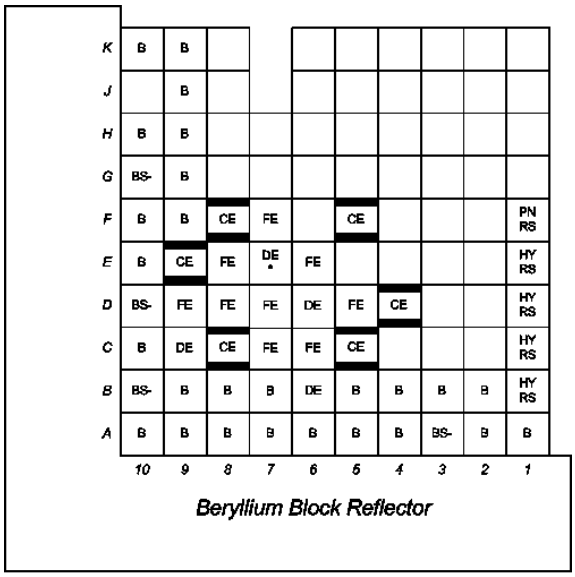

Note : FE = Fuel Element, CE = Control Element, B = Be Reflector Element,
BS = Be Reflector Element with plug, BS- = Be Reflector Element without plug,
DE = Dummy Element, PNRS = Pneumatic Rabbit System, HYRS = Hydraulic
Rabbit System, * = Neutron source (Cf-252)

Fig 2. First criticality configuration of the RSG GAS first core

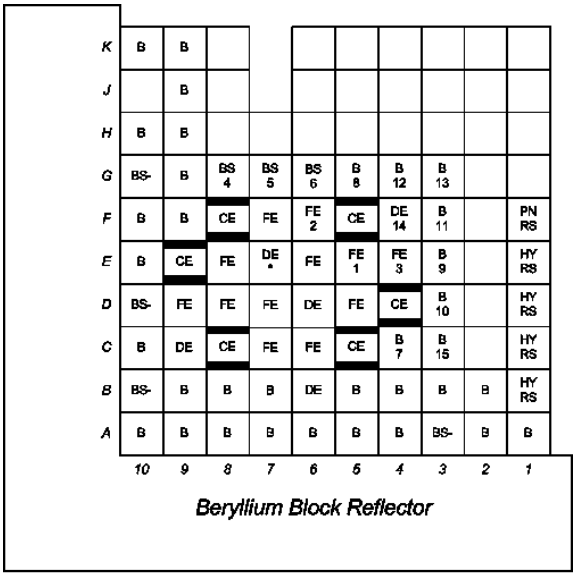

Note : FE = Fuel Element, CE = Control Element, B = Be Reflector Element,
BS = Be Reflector Element with plug, BS- = Be Reflector Element without plug,
DE = Dummy Element, PNRS = Pneumatic Rabbit System, HYRS = Hydraulic
Rabbit System, * = Neutron source (Cf-252)

Fig 3. Full core configuration of the RSG GAS first core

3. Calculation methods

The cell calculations for FE and CE were carried out using WIMSD-5B code with 69 group cross-section ENDF/B-VII.0 and JEFF-3.1 libraries. The macroscopic cross-sections for FE and CE were then prepared in the 4-groups (the neutron energy boundaries: 10 MeV, 0.821

MeV, 5.531 keV, 0.625 eV and 10^{-5} eV) and as a function of burn-up (%loss of ^{235}U), temperature (hot and cold) and the existence of Xe and Sm. Batan-3DIFF and Batan-FUEL will use the libraries for a prescribed condition by cubic interpolation method.

The first and equilibrium cores were modeled in the 2-dimensional X-Y reactor geometry with appropriate group dependent axial buckling values. The core calculations were carried out using the multigroup neutron diffusion method of the BATAN-FUEL code. The criticality, excess reactivity, burn-up swing reactivity (BOC to EOC) and Xenon equilibrium reactivity were evaluated using old (WIMS/D-4), ENDF/B-VII.0 and JEFF-3.1 libraries. In the calculation, we assumed that the mass of ^{235}U in a FE is 250 g (nominal mass).

4. Results and discussions

Table 1 shows the comparison between experimental and calculated results with the three WIMSD libraries for first criticality and excess reactivity of RSG GAS first core. The first criticality predictions by those libraries were very close to the experimental result (underestimation in the range of less than 0.5%). A similar trend can be observed for the excess reactivity. The maximum differences with the experiment occurred in JEFF-3.1 library. Among three libraries, the ENDF/B-VII.0 give better agreement with the experimental result (underestimation of less than 0.4%).

Core Configuration		Experimental results	Calculated results		
			Old	JEFF-3.1	ENDF/B-VII.0
First Criticality	k_{eff}	1.0000	0.996160	0.995308	0.99708
	C/E[a]		0.996	0.995	0.997
Full core (all CRs are withdrawn)	k_{eff}	1.09242	1.086859	1.086034	1.087813
	C/E[a]		0.995	0.994	0.996

[a] Calculated value divided by experimental value

Tab 1: Comparison of the calculation results of the three WIMSD libraries with experimental results

For the equilibrium core (using oxide fuel), the core calculations were performed for determining the burn-up swing reactivity (BOC to EOC) and Xenon equilibrium reactivity. Table 2 shows the comparison of the three WIMSD libraries.

Evaluated Reactivity	Old	JEFF-3.1	ENDF/B-VII.0
Burn-up swing (BOC to EOC), $\%\Delta k/k$ (Xenon free condition)	2.84 (0,981)[a]	3.05 (1.050)[a]	2.90
Xenon equilibrium, $\%\Delta k/k$	3.47 (1.004)[a]	3.49 (1.010)[a]	3.45

[a] Given library value divided by ENDF/B-VII.0 library value

Tab 2: Calculated reactivity parameters based on the three WIMSD libraries

For burn-up swing reactivity, the difference between the old and JEFF-3.1 with ENDF/B-VII.0 library are -2% and -5%, respectively. This shows that the effect of neutron cross sections of heavy metals and fission products involved in the depletion chain is significant. It should be noted, the number of nuclides used in the calculation of fuel burn-up in the old library is 50, while in the JEFF-3.1 and ENDF libraries are 78. However, because some adjustments with empirical data, then the calculation result of the old library is close to the ENDF/B-VII.0 library. It should be noted, in this calculation, we assumed the Xenon free condition.

For the equilibrium xenon (Xe) reactivity, the old library and JEFF-3.1 libraries show overestimation of 0.4% and 1.0%, respectively, compared with the one of the ENDF/B-VII.0 library. There are no significant discrepancies between the three libraries.

5. Conclusions

The results showed that for the first core, where all fuels are un-irradiated fuel, the WIMSD libraries do not show large discrepancies in determining the effective multiplication factor. On the other hand, for the equilibrium core, which uses irradiated fuel, differences among the WIMSD libraries are observed. It is seen in determination of burn-up swing (BOC to EOC). The results showed that among the three libraries, the library WIMSD based on the evaluated nuclear data ENDF/B-VII.0 give better agreement with the experimental results, relatively, with the maximum underestimation of 0.4%.

In the future we will continue the study by changing also the neutron cross section libraries of non-fission materials using the recent WIMSD libraries, especially for beryllium, water and aluminum, to show more precisely the influence of nuclear data in neutronic parameters. Also the reasons of the above-mentioned differences on the burn-up swing reactivity should be further investigated.

References

[1] WIMS-D5, OECD/NEA Data Bank Documentation, Package ID No. 1507/02 (1998), http:// www.nea.fr/html/dbprog/

[2] ASKEW, J.R., FAYERS, F.J., KEMSHELL, P.B., "*A General Description of the Code WIMS"*, J. Br. Nucl. Energy Soc. **5** (1966) 564

[3] IAEA, "*WIMS-D Library Update"*, IAEA, Vienna (2007)

[4] CHADWICK, M.B., *et al*., "*ENDF/B-VII.0: Next Generation Evaluated Nuclear Data Library for Nuclear Science and Technology*", *Nuclear Data Sheets* **107** p. 2931–3060 (2006)

[5] KONING, A., *et al*. (Eds), "*The JEFF-3.1 Nuclear Data Library*", JEFF Report 21, OECD NEA (2006)

[6] LIEM, P.H., "*Batan-FUEL: A General In-Core Fuel Management Code*", Atom Indonesia **22**, No. 2 (1996)

[7] LIEM, P.H., et al., "*Fuel Management Strategy for the New Equilibrium Silicide Core Design of RSG GAS(MPR-30)*", Nuclear Engineering and Design **180**, p. 207–219 (1998)

[8] LIEM, P.H., "*Validation of BATAN Standard 3-D Diffusion Code, BATAN-3DIFF, on the First Core of RSG-GAS*", Atom Indonesia **25**, No. 1 (1999)

[9] BATAN, "*MPR-30 Safety Analysis Report*" , Rev. 7, Jakarta (1987)

Temperature Reactivity Effects Calculations for Needs of Dedicated Instrumentation Design on Zero Power Reactor Using MCNP5

T. BÍLÝ, L. SKLENKA
Department of Nuclear Reactors, Czech Technical University in Prague
V Holesovickach 2, 18000 Prague 8, Czech Republic

Abstract

At the zero power reactor VR-1 a new experimental instrumentation for temperature reactivity effects demonstration and measurement is being designed. To create a credible design and to estimate relatively small reactivity changes with temperature in a precise and accurate way, the calculation scheme for such effects determination was verified through available benchmark at similarly designed reactor. Thus an older well described set of experiments performed at KUCA reactor and dedicated to isothermal temperature coefficient determination in the range from ambient temperatures to some 80°C were recalculated using MCNP5. The effect of employment various data libraries and of the two codes and means of temperature-dependent nuclear data processing was evaluated and compared. Thus, calculations were performed with ENDF/B-VII, JEFF 3.1 a JENDL 3.3 libraries using the same data processing scheme; in the latter case, employment of NJOY and makxsf codes for processing the data to the temperature of interest was compared. Also, attention was paid to thermal-scattering-data temperature dependence and the importance of their proper handling to obtain accurate results was pointed out. Finally it was demonstrated the current status of achievable precision and accuracy of temperature reactivity effects calculations is sufficient for performing reliable design of the experimental instrumentation for zero power reactors.

1. Introduction

The capability of accurate determination of temperature reactivity effects for research reactors applications is a delicate task. The small temperature changes in order of tens of °C induce only small reactivity changes. This puts the necessity on performing high-precision calculations consuming a lot of computer time. On the other hand, the experiments performed at zero power reactors possess a big advantage in evaluating achievable precision and accuracy of temperature reactivity effects determination. As almost no heat is generated during their operation, and so a system of external heating is usually provided to study the temperature reactivity effects, an invariable well-defined temperature profile across the whole core could be obtained. This fact along with the negligible fuel burn-up makes it feasible to perform accurate experimental as well as computational determination of isothermal reactivity coefficient and related quantities. So, the adequacy of various nuclear data libraries and their processing schemes could be assessed in relation to their ability of temperature reactivity effects prediction as well. This was carried out against an older but well described Japanese benchmark experiment at the C-core of the KUCA reactor [1, 2].

Most of nuclear data could be nowadays relatively easily processed for any desired temperature of interest. The situation slightly differs for the thermal scattering data for important moderator materials and its energy and momentum transfer matrices S(α,β). These data could be standardly processed only for a given set of temperatures (e.g. for H in H_2O for 9 temperatures from 20.5°C to 1000°C in case of ENDF/B-VII). However, such a set seems to be insufficient for the investigation of relatively small temperature changes in the range of several tens of °C. In this case, it is possible either to prepare own S(α,β) matrices for desired temperatures and use them for processing the relevant data libraries or to interpolate between already available libraries (or to extrapolate if an interpolation is not possible) [3]; the latter procedure being much easily proceedable from the viewpoint of the calculation code user. Although, on principle, also such kind of data could be processed for any desired temperature, there is a lack of papers dealing with the achievable accuracy of such a procedure and of achievable agreement with experimental data.

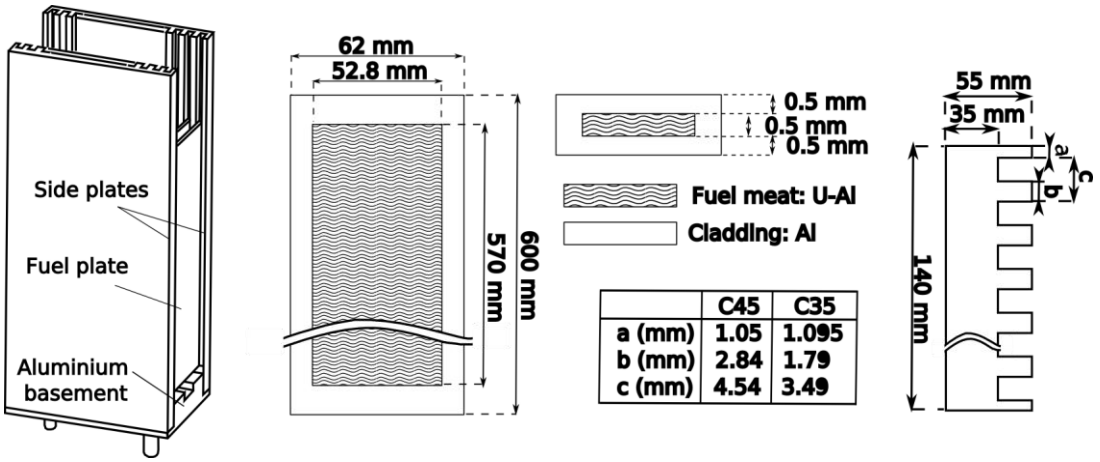

Figure 1: Left: Fuel element. Middle: Fuel plate. Right: Side plate [1].

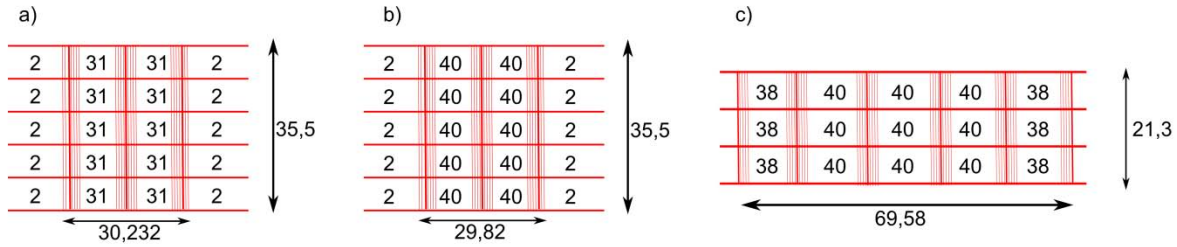

Figure 2: KUCA core configurations: a) C45G0, b) C35G0 - 5 rows, c) C35G0 - 3 rows. Numbers in brackets denote the number of fuel plates in the corresponding fuel element. Also, the dimensions of particular cores are indicated in cm [1].

2. KUCA reactor benchmark

KUCA (Kyoto University Critical Assembly) reactor [1] is a multi-zone zero power reactor. Its C-core is a light-water moderated core with highly enriched fuel of plate shape (enrichment 93,1% on U-235). Fuel plates are of flat shape and consist of U-Al alloy covered in Al cladding. Each fuel plate contains 8.89 g of U-235. The U content in U-Al alloy is 20 %. Fuel plates are assembled to side plates to create fuel element. Within the benchmark, two types of side plates with different pitches and thus with different H/U-235 ratio were used. The side plate grooves for inserting the fuel plates possess pitches of 4.54 mm, and 3.49 mm for core configurations called C45, and C35 respectively. The fuel element pitch was 71 mm in one and 142 mm in the other direction. So, the fuel element could contain up to 31 or 40 fuel plates for core configurations C45, and C35 respectively. The fuel element, fuel and side plates are illustrated in the fig 1. The experiment at the KUCA C-core [1] performed at the end of 80th was devoted to measurement of isothermal temperature coefficient of reactivity in the temperature range from 20° to 70°C. Altogether, three sets of experiments with various pitches of fuel plates (i.e. with various water-to-uranium ratios) and various core configurations (see fig. 2) were carried out. The experiments were carried out by repumping the water at given temperature into the C-core of the reactor; consequently, the reactivity was measured using the positive period method and source multiplication method in super- and sub-critical region respectively. The maximal experimental error of reactivity excess determination was estimated to be ±5 pcm [1]. The description of the core configurations used within the benchmark is given in table 1.

Core configuration	H to U-235 ratio	Lattice pitch (mm)	Nr. of fuel plates
C45G0	315	4.54	330
C35G0 - 5 rows	212	3.43	420
C35G0 - 3 rows	212	3.43	588

Table 1: Description of KUCA core configurations [1]

3. Materials and Methods

All calculations were carried out using MCNP5 code [4] which enables detailed modelling of the particular cores. Three widely used nuclear data libraries were used ENDF/B-VII, JEFF 3.1 and JENDL 3.3. For processing the data for desired temperatures, NJOY v.259 [5, 6] and makxsf [7] codes have been utilized. First aim of the paper was to compare the temperature reactivity effects calculated by above mentioned nuclear data libraries at identical parameters of their processing. To proceed this, data libraries were processed by NJOY code using well described and validated approach standardly used for JEFF 3.1 library [3, 8]. The data describing the thermal scattering on moderators (i.e. on hydrogen in water in the current case) could not be processed for any temperature, but only for a given set of temperatures; thus, they were processed for the given available temperature set; consequently, the data for desired temperatures were obtained by manual interpolation between two closest available data sets, or by extrapolation in the case that interpolation was not possible. This procedure is recommended by [9]. As JENDL 3.3 library does not contain the thermal scattering law data, the corresponding data from ENDF/B-VII was used for calculation with this library.

Second, the influence of nuclear data library processing scheme (code) was accessed; the ENDF/B-VII library was processed by above mentioned procedure and, on the other hand with the help of makxsf code. The makxsf code serves for interpolation between data libraries in ACE format which is used by MCNP code. It utilizes similar procedures as the NJOY code. A very good agreement between the NJOY and makxsf code has been already demonstrated for larger temperature changes [10].

Further the importance of proper utilisation of thermal scattering data for H in H_20 and its temperature dependence for predicting the temperature reactivity effects was assessed. Calculations were performed a) without these data (i.e. using free-gas approximation for all isotopes also in thermal region), b) using the data interpolated to desired temperatures, and c) using the standardly available TSL data set of closest available temperature. The comparison was performed only for ENDF/B-VII library.

As the paper's point of interest was to assess the capability of temperature reactivity effects prediction, it was the reactivity difference of states with two temperatures which was taken as a measure for accessing the accuracy, rather than the k_{eff} or ρ values of individual states. The agreement between calculations and experiment was assessed based on following quantities: first, the difference between calculated and measured reactivity changes $\Delta\rho_C - \Delta\rho_E$ in pcm; the reactivity at temperature corresponding to measured criticality state of particular core configuration was taken as the reference value for evaluating reactivity changes. If the criticality state was not measured, then, the reactivity value at the maximal temperature was taken as the reference one. Further, standard deviation of the difference between calculated and measured reactivity was determined as a measure of calculation results consistency.

4. Results and discussion

The comparison between experimental and calculated values for the KUCA benchmark is presented in figure 3. The upper part indicates the differences between calculated and experimental reactivity change values for particular modes of calculations (uncertainty intervals being at 1σ level, incl. experimental uncertainty); the bottom part shows the temperature reactivity effect calculated via three ways of thermal scattering data utilisation.

As could be seen, particular data libraries give results that are in good mutual accordance; in most cases, moreover, also in accordance with experimental values within their 2σ intervals. The largest deviations show the JEFF 3.1 library. Further, a good agreement was obtained from comparison of the results obtained by the same data library processed in two different ways. Finally, the key requirement for correct prediction of temperature reactivity effects is the utilisation and proper handling of thermal scattering law data libraries for moderator material and their temperature dependence. Obviously, the utilisation of interpolated temperature-dependent TSL data leads to difference between calculation and experiment (C-E) in order of tens of pcm; the reactivity course being in a good accordance with experiments. If only the closest standardly available TSL library is used, the differences from experiment are somehow higher and the reactivity course does not correspond to reality; of

course, this is caused by unavoidable switch from lower to higher temperature TSL library which cause the step reactivity change. In case the TSL data are fully omitted (i.e. application of free-gas model also in thermal region for all materials), the C-E values are an order of magnitude higher, i.e. in the order of hundreds of pcm, compare to the interpolated TSL data utilisation case. It is also profitable to note the close connection between reactivity-temperature-changes determination precision and the size of temperature difference. In the experimental as well as in calculation case, the reactivity change is determined as a reactivity difference in two states of the system. As the precision of experimental reactivity determination at various temperatures is practically invariable, and similarly, the precision of reactivity calculation almost constant for any temperature, it is clear that the higher temperature difference, the more precise prediction of reactivity changes could be achieved. Simultaneously, it is worth to keep in mind that reactivity temperature changes are generally non-linear and are determined not only by the quantities as the fuel composition or water-to-fuel ratio, but also by such factors as for example the core configuration shape.

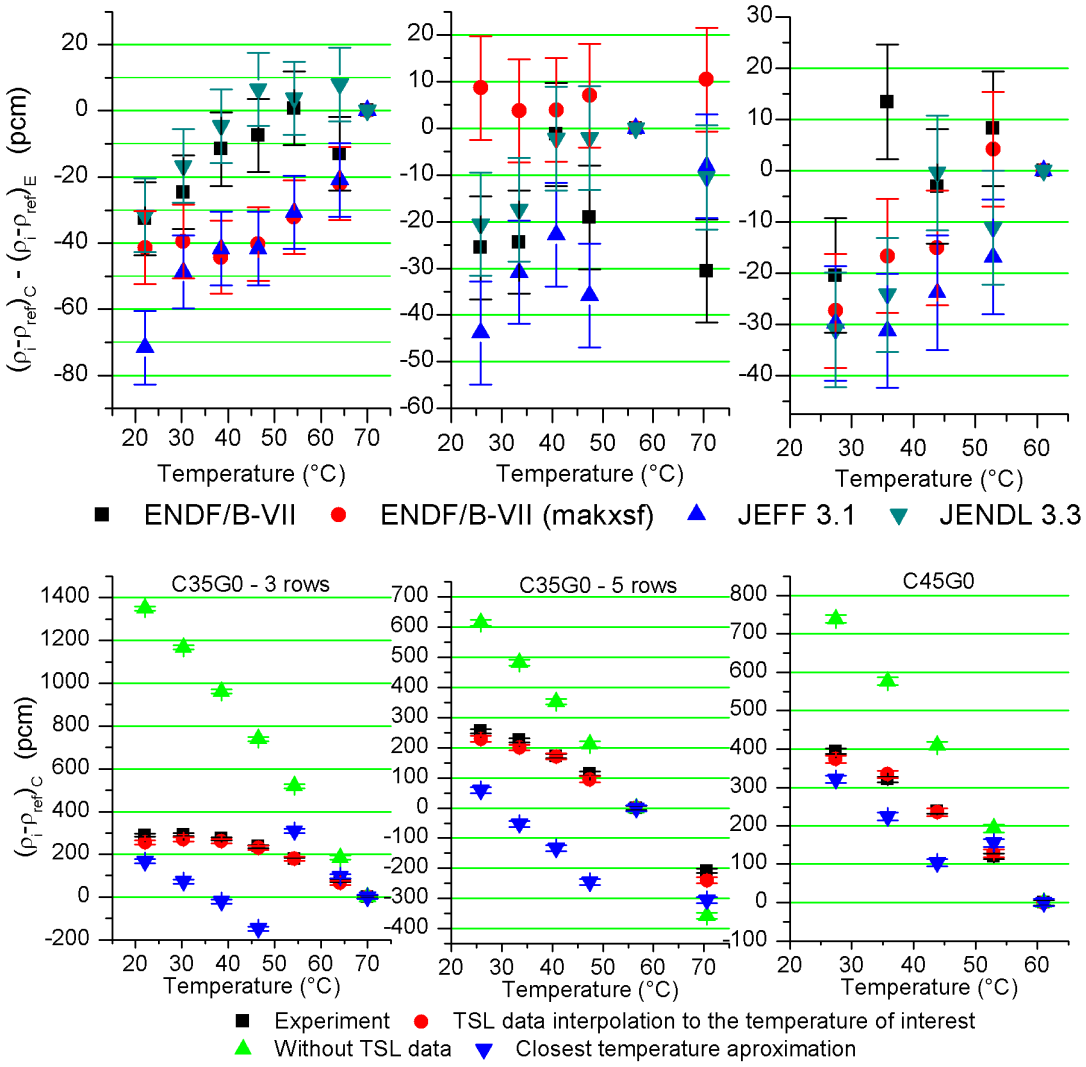

Figure 3: Results of KUCA benchmark: Up: Deviations of C-E temperature reactivity changes for C35G0-3rows, C35G0-5rows and C45G0 core configurations (left to right). Bottom: TSL data handling and utilisation.

Library	**JEFF 3.1**	**JENDL 3.3**	**ENDF/B-VII**	**ENDF/B-VII (makxsf)**
$\Delta\rho_C - \Delta\rho_E$	-27,6 ± 18,8	-8,6 ± 12,4	-10,6 ± 13,8	-13,4 ± 19,8

Table 2: Average $\Delta\rho_C - \Delta\rho_E$ values of KUCA benchmark

5. Conclusions

Based on the performed calculations, the following could be stated. To achieve an accurate prediction of temperature reactivity effects, a proper handling of TSL data for important moderator materials is of key importance. By the interpolation between the available data sets (either manual or using a specialized code like makxsf) a very accurate results could be obtained for temperature differences of few tens of °C. Such accuracy seems to be satisfactory for most applications on research reactors, including the design of new experiments and experimental devices. On the contrary, if the TSL data are omitted or the interpolation is not performed, the calculated reactivity changes will be strongly overpredicted in the former case or will not correspond with the true reactivity dependence on temperature in the latter case. The both last cases seem to be useless, if the accurate temperature reactivity effects prediction is required. Further, it is clear, that temperature-reactivity-effects determination precision level in pcm/°C could not be determined unless the size of temperature difference is given. This stems from the definition of reactivity temperature changes as a difference of the two reactor states at different reactivities and temperatures and from the corresponding uncertainties of experimental as well as computational methods of reactivity determination. Finally, it could be stated that using modern monte-carlo code the temperature reactivity effects could be determined very accurately and consistently. The differences between particular libraries were rather small, only JEFF 3.1 gives slightly different results.

References

[1] M. Mori, S. Shiroya, K. Kanda: “Temperature Coeffcient of Reactivity in Light-Water Moderated and Reected Cores Loaded with Highly-Enriched-Uranium Fuel”, Journal of Nuclear Science and Technology 24[8], pp. 653 667 (August 1987)

[2] S. Shiroya, K. Kanda: “Analyses Reactor of Physics Experiments in the Kyoto University Critical Assembly”, Nuclear Science and Engineering: 100, 525-537(1988)

[3] O. Cabellos: “Processing of the JEFF-3.1 Cross Section Library into a Continuous Energy Monte Carlo Radiation Transport and Criticality Data Library”, OECD NEA Data Bank, NEA/NSC/DOC(2006)18, May 2006

[4] J. F. Briesmeister, Ed.: “MCNP - A General Monte Carlo N-Particle Transport Code”, LA-13709-M (April 2000)

[5] R. E. MacFarlane, D. W. Muir, R. M. Boicourt: “The NJOY Nuclear Data Processing System, Volume 11:The NJOY, RECONR, BROADR,HEATR, and THERMR Modules”, LA-9303-M, vol. II(ENDF-324) , Manual , Issued: May 1982

[6] Understanding NJOY http://t2.lanl.gov/njoy

[7] F. B. Brown: “The makxsf Code with Doppler Broadening”, X-3 Monte Carlo Codes Los Alamos National Laboratory 2006

[8] O. Cabellos and Y. Rugama: “Processing and validation of JEFF3.1 library in ACE format at 10 different temperatures”, International Conference on Nuclear Data for Science and Technology 2007

[9] M. Mattes, J. Keinert: “Thermal Neutron Scattering Data for the Moderator Materials H2O, D2O and ZrHx in ENDF-6 Format and as ACE Library for MCNP(X) Codes”, INDC(NDS)-0470, April 2005

[10] R. D. Mosteller, R. E. MacFarlane, R. C. Little, M. C. White:” Analysis of Hot and Cold Kritz Criticals with MCNP5 and Temperature-Specific Nuclear-Data Libraries”, LA-UR-03-5634, Advances in Nuclear Fuel Management III , Hilton Head Island, SC , October 5-8, 2003

COMPLEMENTARY CHARACTERIZATION OF SI-RICH LAYER IN E-FUTURE FRESH FUEL PLATES

A. BONNIN, H. PALANCHER, F. CHAROLLAIS, MC. ANSELMET
CEA, DEN, DEC
F-13108 St Paul Lez Durance Cedex – France

V. HONKIMÄKI
ESRF
6, rue J. Horowitz, 38500 Grenoble Cedex – France

P. LEMOINE
CEA, DEN, DISN
Saclay, F-91191 Gif-sur-Yvette – France

ABSTRACT

The E-FUTURE in-pile test has been performed in 2010 as a first step towards the qualification of U(Mo)/Al-Si nuclear fuel plates for high power reactors. For each plate, compositions (Si weight fractions) and fabrication conditions have been chosen different to investigate the influence of these parameters on the plate in-pile behavior.
In this paper, complementary analyses regarding the as-fabricated fuels are presented. The Si behavior during the manufacturing step has been accurately characterized: the composition and thickness of the Si-rich layer appeared around U(Mo) particles as well the Si fraction still remaining in the matrix have been quantified.

1. Introduction

High density U(Mo)/Al fuels are considered internationally as the most promising LEU material for converting high performance research reactors. However their development has required many efforts in particular i.e. to limit their swelling during in-pile irradiation. These difficulties were attributed to the growth of a low density interaction layer (IL) at U(Mo)/Al interfaces that was moreover exhibiting low fission gas retention capabilities.
A breakthrough has been recently reached by adding limited concentration of Si to the Al matrix. First in-pile experiments performed under moderate heat fluxes (about 200W.cm^{-2} for the IRIS3 experiment [1]) have demonstrated the interest of these U(Mo)/Al-Si nuclear fuels for low and medium operating conditions (OSIRIS type). However, an optimization was required to qualify this solution for the most powerful reactors such as the BR2 or the RHF in Western Europe. In collaboration with the US GTRI, the LEONIDAS Advanced Technology Group has performed a first in-pile experiment, called E-FUTURE, in order to test the U(Mo)/Al-Si dispersion fuel performance at 470W.cm^{-2} [2].
From a technological point of view, the main objective of this irradiation test was to optimize both the Si concentration added to the matrix and the conditions of the post-fabrication thermal treatments. With this objective, four full sized nuclear fuel plates have been irradiated in the BR2 reactor in 2010.
The microstructures of the as-fabricated fuel plates have already been analysed by optical microscopy, SEM, EPMA and laboratory XRD [3]. To complement these mainly local studies, volume characterizations were needed. A methodology based on high energy synchrotron radiations (87 keV) has been developed: it enables the determination of both the average

thickness of a Si rich layer (written SiRDL in the following) appearing during fabrication around UMo particles and the fraction of Si remaining in the matrix as precipitates.
After having briefly recalled the composition of each E-FUTURE plate and their fabrication conditions, the additional synchrotron radiations characterizations are described. The obtained SiRDL characteristics (crystallographic composition and average thicknesses) and the remaining Si fraction in the Al matrix are then successively discussed as a function of the two main parameters (composition and fabrication conditions). Finally, prospects regarding optimized U(Mo)/Al-Si nuclear fuels are proposed.

2. Experimental methods

2.1. Fuel plate manufacturing and sample preparation

The E-FUTURE nuclear fuel plates were produced by AREVA-CERCA using a mixture of UMo7.4 atomized powders (i.e. about 16.5 at%Mo) and two kinds of AlSi powders (4 and 6 wt%Si). These fuel plates underwent three different heat treatments (at 425°C during 2 hours and at 475°C for 2 or 4 hours). Table 1 summarizes the characteristic of the 4 E-FUTURE fuel plates. They are identified EF4112_4wt%Si, EF6101_6wt%Si, EF4201_4wt%Si and EF6311_6wt%Si respectively.

	U(Mo) powders	Matrix weight fraction in the core (wt%)	Si content in the AlSi matrix (wt%)	Al material	Conditions of the thermal annealing	
	type		Si	Cladding	T (°C)	time (h)
EF4112_4wt%Si	atomized	12.9	4	AlFeNi	425	2
EF6101_6wt%Si	atomized	12.9	6	AG3	425	2
EF4201_4wt%Si	atomized	12.9	4	AG3	475	2
EF6311_6wt%Si	atomized	12.9	6	AlFeNi	475	4

Table 1: Characteristics of the U(Mo)/Al-Si nuclear fuel plates.

For each fuel plate to be tested in-pile, an additional spare item had been produced. In the "twin" item, a square of 10×10mm² has been cut. Note that the sample location in the fuel plate has been chosen far enough from the interface between the core and the frame: it has been shown that particles are often over oxidized in this volume (see for example ref [4]).
The cladding material has been removed on both sides by conventional mechanical polishing techniques to enable the meat analysis.

2.2. Experimental settings

To achieve an accurate, quantitative and volume characterization, the selected technique should have a penetration depth of at least 500µm in the U(Mo)/Al-Si meat and the signal to noise ratio must be high enough to identify trace phases, such as phases constituting the SiRDL (see [6]).
Diffraction using high energy X-rays fulfils both requirements and in a preliminary study it has been shown to provide the quantitative crystallographic composition in the UMo/Al fuel plates [5]. This method has thus been applied to the E-FUTURE fuel plates analysis.

Measurements have been performed at the ID15B beamline at the ESRF (Grenoble, France) in transmission mode using an 87keV X-ray beam. Its footprint on the sample was set to 0.3×0.3mm². In order to obtain good enough statistics, a mapping has been carried out on each of the four E-FUTURE samples, which represents about 200 steps per sample. Figure 1 shows the comparison between the patterns collected on each fuel plate.

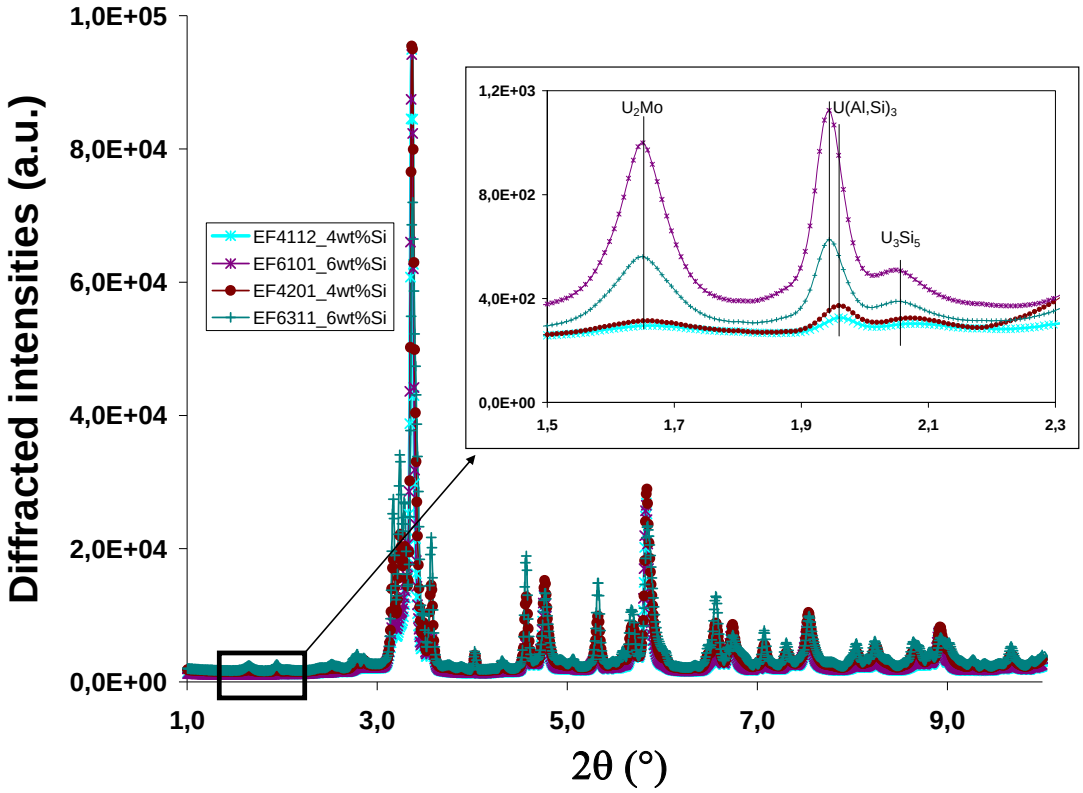

Figure 1: Diffraction patterns collected with high energy X-rays. The inset highlights the presence of U_2Mo and USiAl phases in the E-FUTURE nuclear plates (the background has been subtracted).

At a second step, data have been analyzed with the FullProf software package using the Rietveld method. Nine phases have been included in the refinement. The first five (αU, γU(Mo8), γU(Mo12) or γU(Mo13), UC) are describing the U(Mo) particles themselves, the next three, the UMoSiAl shell surrounding the UMo particles ($U(Al,Si)_3$, U_3Si_5, UO_2) and the last one, the matrix (Al).

3. γ-U(Mo) decomposition in the E-FUTURE fuel plates

In this section, the results of the Rietveld analysis regarding the γ-U(Mo) decomposition (mechanisms, rates) are presented and discussed as a function of post-annealing conditions.

3.1. Atomized powders in fuel plates manufactured at 425°C

Two samples have been considered for this analysis (EF4112_4wt%Si, EF6101_6wt%Si). As shown in Table 2, the decomposition rate of the atomized UMo particles is very limited using a manufacturing process at 425°C. The main products of this decomposition are γU(Mo12) and a phase close to αU. Moreover even if the U_2Mo phase has been unambiguously identified (cf. Figure 1), its amount does never exceed 2.2%.

	αU	U_2Mo	γU(Mo)	UC	$U0_2$	$U(Al,Si)_3$	U_3Si_5	Al
EF4112_4wt%Si	13.5± 0.1	1.2±0.1	71.4 ± 0.7	0.5 ± 0.1	0.1 ± 0.1	0.2	0.5	12.9 ± 0.4
EF6101_6wt%Si	15.6± 0.1	1.9±0.3	68.3 ± 0.8	0.5 ± 0.1	0.2 ± 0.1	0.3	1.3	12.4 ± 0.4
EF4201_4wt%Si	26.1± 0.2	6.0±0.3	54.0 ± 0.7	0.5 ± 0.1	0.2 ± 0.1	0.6	0.8	11.8 ± 0.3
EF6311_6wt%Si	31.7± 0.2	13.8± 0.3	39.8 ± 0.4	0.4 ± 0.1	0.2 ± 0.1	2.0	1.0	11.1 ± 0.3

Table 2: Crystallographic composition (wt%) of the four analyzed fuel plates given by the Rietveld analysis of the diffraction data collected with a high energy X-ray beam.

A quantitative comparison of the results of the Rietveld analysis in this set of samples shows that the decomposition rates of the γU(Mo) phase are extremely close to each other confirming the excellent reproducibility of this manufacturing process (cf. Table 3). Indeed the αU-ratio evolves between 15.6 and 18.1% and γU(Mo)-ratio between 79.2 and 82.7%.

	αU-ratio	U_2Mo-ratio	γU(Mo)-ratio
EF4112_4wt%Si	15.6 ± 0.3	1.3 ± 0.1	82.6 ± 1.8
EF6101_6wt%Si	18.1 ± 0.4	2.2 ± 0.3	79.2 ± 1.9
EF4201_4wt%Si	30.2 ± 0.5	6.9 ± 0.2	62.4 ± 1.5
EF6311_6wt%Si	37.0 ± 0.7	16.1 ± 0.4	46.4 ± 1.7

Table 3: αU, U_2Mo and γU(Mo) (wt%) fractions in UMo particles.

3.2. Atomized powders in fuel plates manufactured at 475°C

Manufacturing nuclear fuel plates at 475°C (EF4201_4wt%Si and EF6311_6wt%Si) clearly favors the destabilization of the γU(Mo8) phase (cf. Figure 1 and Table 3). At this temperature the first step of the destabilization (after 2 hours i.e. for the EF4201_4wt%Si fuel plate) leads to mainly the growth of αU and a Mo enriched γU(Mo) phase (γU(Mo12)), the formation of U_2Mo being however significantly larger to what was observed at 425°C. At a second step (after 4 hours i.e. for the EF6311_6wt%Si fuel plate), the amount of γUMo12 does not evolve much, and the destabilization seems to mainly lead to the growth of U_2Mo and αU, as expected from the TTT diagram.

4. SiRDL composition and thickness

Using the quantitative weight fractions determined for the components ($U(Al,Si)_3$ and U_3Si_5) of the SiRDL and a simple model, the thickness of this layer around UMo atomized particles can be calculated [6]. In this section, the obtained sizes and the elementary compositions are described for each plate of the E-FUTURE experiment and compared with those measured by microscopy and/or micro-analyses.

4.1. At 425°C

At this temperature, the composition of the EF4112_4wt%Si and EF6101_6wt%Si fuel plates can be directly compared. First it can be shown that whatever the Si content in the matrix is, the composition of the SiRDL does not evolve significantly. Two components have been identified: $U(Al, Si)_3$ and U_3Si_5. In each case, the cell parameter of the $U(Al, Si)_3$ has been found to be 4.16Å. As proposed by Dwight, Silicon is inserted in the UAl_3 crystal structure and forms a solid solution: the cell parameter value evolves proportionally with the Si content [7]. In this case, the atomic ratio Si/(Al+Si) can be evaluated to 44.2 at%.
Using this XRD characterization of the SiRDL for the different fuel plates, its elementary composition can be evaluated and compared to the one found by SEM/EDX/EPMA (cf. Table 4 and [3]). Whatever the Si content in the matrix (4 or 6%) is, the Si content in the SiRDL in the as-manufactured fuel plates is almost constant (about 50 at%) and very close to what

has been measured by elementary techniques. This good agreement can be considered as an additional proof for validating this quantitative analysis based on XRD.
Concerning the thickness of the SiRDL, it appears that by increasing the Si content in the Al matrix, the SiRDL becomes thicker. From 0.12µm with 4wt%Si, it increases up to 0.27µm when adding 6wt%Si (EF6101_6wt%Si).
As a conclusion, manufacturing nuclear fuel plates with an overall thermal treatment of 425°C during 2 hours, the SiRDL thickness is directly linked to the Si availability in the matrix.

	SiRDL composition as determined by XRD (wt%)		Si atomic composition in the SiRDL (at%)		Average thickness of the protective layers around UMo particles (µm)	
	$U(Al,Si)_3$	U_3Si_5	XRD	EDX/EPMA	XRD	SEM
E-FUTURE 4112	25.0	75.0	53.4	50	0.12	0,7
E-FUTURE 6101	19.7	80.2	55.2	38	0.27	0,6
E-FUTURE 4201	42.0	57.9	43.5	33	0.34	0,8
E-FUTURE 6311	66.7	33.2	34.3	36	0.87	1,3

Table 4: SiRDL average elementary compositions and thicknesses in the 4 E-FUTURE fuel plates containing UMo atomized powder as determined from high energy XRD.
(The Si atomic ratio has been determined by calculating (Si/(U+Si+Al), since no Mo containing phase has been identified in the SiRDL.)

4.2. At 475°C

The crystallographic composition of the SiRDL formed after fuel plate manufacturing at 475°C, is basically identical to the one obtained at 425°C. Two phases are identified: U_3Si_5 and $U(Al,Si)_3$ with however a higher cell parameter (4.19 Å) thus indicating a lower Si content [7]. The Si/(Al+Si) atomic ratio in $U(Al,Si)_3$ appears to be about 32%. From these crystallographic results, the Si content in the SiRDL has been assessed. It comes that the longer the annealing duration, the higher is the $U(Al,Si)_3$ weight ratio in the SiRDL; therefore the Si content decreases even if the amount of the Si added in the matrix was higher (cf. Table 4). As expected, by increasing the annealing time and the Si weight fraction, the SiRDL thickness becomes significantly thicker.

4.3. Discussion

The comparison between the thicknesses of the SiRDL as determined by 2D techniques (EDX/EPMA) and those obtained from volume techniques (high energy XRD) shows a clear difference, the first being systematically lower than the seconds. However if this difference is very probably resulting from the correction of geometrical artifacts created by the use of a 2D characterization, it should be investigated whether the density of this SiRDL is 100% or lower. A dedicated study is undergoing.
Concerning the composition of the SiRDL, it has been shown that at both tested temperatures, only the $U(Al, Si)_3$ and U_3Si_5 crystallographic phases have been identified. It is therefore very likely that the $U_6Mo_4Al_{43}$, which is supposed to have very poor irradiation performances [8], is not present in theses protective layers. Indeed even if this UMoAl ternary phase is difficult to identify using XRD [4], this phase is generally associated with UAl_3 (Si-free) and which has not been found [9].

5. Si remaining in the Al matrix in the E-FUTURE as fabricated fuel plates

From the knowledge of the average composition and thickness of this SiRDL, it is possible to derive the Si weight fraction in the SiRDL for each fuel plate. However it must be clear that this value is resulting directly from the identification of the Si phase in the high energy XRD patterns. The results demonstrate that even in the most favorable tested annealing conditions (475°C during 4 hours), the fraction of Si in the SiRDL never exceeds 50% (cf Table 5).

	Location of the Si elements in the as-fabricated fuel plates	
	SiRDL	Si precipitates in the matrix
EF4112_4wt%Si	18.8	81.2
EF6101_6wt%Si	33.7	66.3
EF4201_4wt%Si	38.0	62.0
EF6311_6wt%Si	48.4	51.6

Table 5: Fraction of Si located in the SiRDL and in the Si precipitates after fuel plate manufacturing.

To improve the in-pile behavior of this nuclear fuel, this fraction should be optimized. One way to increase this fraction is to add higher Si quantities to the matrix (compare fuel plates EF4112_4wt%Si, EF6101_6wt%Si). However these amounts have to remain limited considering fuel back-end issues [3]. As a consequence, annealing during a larger duration at 425°C nuclear fuel that contains 6wt% Si in the matrix seems to be a very promising solution. Indeed the destabilization of the UMo particles has been found to be very low (below 20wt%), the fraction of Si in the SiRDL is optimal (higher than 50at%) and the ratio of Si located in the SiRDL pretty high (about 30%). As a comparison, annealings at high temperature such as 475°C seems to be less appropriated regarding manufacturing process consideration whatever the Si content and the duration of the thermal treatment.

5. Conclusion

X-ray diffraction using high energy X-ray beams has been shown to be a very powerful technique to characterize the as-fabricated U(Mo)/Al-Si nuclear fuel plates at a macroscopic scale. Note that this method has also been used for analyzing the IRIS and E-FUTURE fresh nuclear fuels. A comparative study is under preparation [10].
In the four E-FUTURE plates, the destabilization level of UMo particles and both the thickness and the compositions (crystallographic and elementary) of the SiRDL have been determined and compared to the results obtained by microscopy. Moreover access to the repartition of the Si between SiRDL and precipitates in the matrix has been obtained. In this communication, the interest of producing these fuels at relative lower temperature (425°C) has been demonstrated, and improvements proposed.

References :

[1] M. Ripert, S. Dubois, P. Boulcourt *et al.*, Proceedings of RRFM 2006, Sofia, Bulgaria, April 30 – May 5, 2006; M.Ripert, V. Marelle, X. Iltis *et al.*, this conference.
[2] F. Frery, H. Guyon, E. Koonen *et al.*, Proceedings of RERTR 2010, Lisbon, Portugal, October 10-14, 2010.
[3] X. Iltis, F. Charollais, M. Anselmet *et al.*, Proceedings of RERTR 2010, Lisbon, Portugal, October 10-14, 2010.
[4] H. Palancher, Ph. Martin, V. Nassif *et al.*, J. Appl. Crystallogr. 40 (2007) 1064.
[5] A. Bonnin, H. Palancher, V. Honkimäki *et al.*, accepted in Zeitschrift für Kristallographie
[6] H. Palancher, A. Bonnin, V. Honkimäki *et al.* in preparation.
[7] A.E. Dwight, ANL 82-14 report, September 1982.
[8] J. Gan, D.D. Keiser Jr., D.M. Wachs *et al.*, J. Nucl. Mater. 396, 2010, p. 234-239.
[9] J. Allenou, H. Palancher, X. Iltis *et al.*, J. Nucl. Mater. 399, 2010, p. 189-199.
[10] A. Bonnin, H. Palancher, V. Honkimäki *et al.*, in preparation, J. Nucl. Mater.

THERMAL STABILITY OF γ U(Mo,X) FUEL ALLOYS WITH X = Ti, Cr AND Zr

J. ALLENOU[1,2], X. ILTIS, F. CHAROLLAIS, M.C. ANSELMET
[1] *CEA, DEN, DEC, Cadarache, F-13108 Saint-Paul-Lez-Durance – France*

O. TOUGAIT, M. PASTUREL, H. NOEL
[2] *Sciences Chimiques de Rennes, UMR-CNRS 6226, Université de Rennes 1, Campus de Beaulieu, 35042 Rennes Cedex – France*

P. LEMOINE
CEA, DEN, DISN, Saclay, F-91191 Gif-sur-Yvette - France

ABSTRACT

The phase transformation γ → α and the thermal stability of U(Mo,X) alloys compared to the thermodynamic behavior of U(Mo) binary phases are studied. For this purpose, samples were prepared by arc-melting the elemental components obeying the atomic ratio (U-Mo)/X of 95/5, with U content ranging from 95 to 59 at. %. Equilibrium state at low temperature was achieved by heat-treatments; the samples were maintained at 900°C for 24 hours to promote homogenization followed by an annealing at 500°C for 72 hours to provoke the eutectoid decomposition of the γ U phase. Thermal analyses were carried out by using differential thermal analysis with heating and cooling cycles from room temperature up to 1400°C and by examination of cooling curves obtained by measuring by pyrometry the temperature of the samples surface heated up to 1800°C and allowed to cool down at various rates. The samples states, before and after thermal experiments were examined by means of microstructural observations coupled with elemental analyses and by X-ray diffraction techniques.
Accurate liquidus and solidus temperatures were determined for all the samples revealing a narrow two-phases domain for X = Ti and Zr, whereas a large liquid-solid domain exists in the case of X = Cr. Regarding the eutectoid decomposition, the temperatures of this invariant reaction remain in a small range around 565(10)°C in the case of Cr, whereas, an increase of 30-40°C is observed in the case of Ti. However, for both elements, Cr and Ti, no significant change in the reaction transformations as well as in the phase appearing can be detected. The case of Zr is more tricky, only one solid-solid transformation is observed at about 610(10)°C, without any evidence of two-phase domain, suggesting a possible diffusionless transformation.

1. Introduction

The valuable irradiation behavior of the high temperature *bcc*-U allotropic form (denoted γ) under neutron fluxes is of particular interest for the development of high density fuels [1]. Fortunately, the phase transformation γ → α can be suppressed by a chemical alloying with Mo for content above 7 wt. % under moderate quenching conditions [2]. γ U(Mo) alloys are thus promising candidates for Low Enriched Uranium fuels working at low temperature (100-300°C), either as dispersed particles in an Al base matrix or in a monolithic form [3,4]. Unlikely, first in-pile irradiation experiments of γ U(Mo) dispersion fuels plates and extruded rods revealed significant swelling, hindering the development of these fissile materials [5]. Improvement of the irradiation behavior may be achieved by modifying the γ U(Mo) alloy by adding a third selected element (X) [6-15]. The ability of various addition metals to reduce the

interdiffusion processes evaluated in out of pile [7-12] as well as in pile studies [13-15], points out promising results in the cases of Ti [8,9,12,14] and Zr [10-11,13]. More recently, parameters such as the microstructure of γ U based alloys, including the solubility of X elements into U(Mo,X) alloys, were identified to play a significant role on the interdiffusion reactions [12]. Moreover, the γ phase stability when adding a third element X is also a factor which seems to control the fuel behaviour under irradiation.

This work is oriented toward X = Ti, Cr and Zr which are characterized by large solubility domains in the γ U phase [16]. Our main goal is to obtain fundamental data on the phase transformation $\gamma \rightarrow \alpha$, and on the thermal stability of U(Mo,X) alloys with X = Ti, Cr or Zr and to compare these results with the thermodynamic behavior of U(Mo) binary alloys. In particular, the influence of a third element on the stability domain of the γ U(Mo) phase is studied.
For this purpose, thermal analyses are carried out by using Differential Thermal Analysis (DTA) on reference binary U(Mo) alloys and ternary U(Mo,X) alloys of atomic ratio (U-Mo)/X of 95/5, with U content ranging from 95 to 59 at. %. The temperatures of liquidus and solidus and the temperature of eutectoid decomposition are determined for all the samples allowing to draw the existing limits of the γ U(Mo,X) domain.

2. Experimental details

Reference binary U(Mo) alloys and ternary U(Mo,X) alloys with X = Ti, Cr or Zr, of atomic ratio (U-Mo)/X of 95/5, with U content ranging from 95 to 59 at. %, were melted in an arc-furnace using a non-consumable tungsten electrode and a cooled copper crucible under partial pressure of argon. High purity metals, uranium piece (99.8 wt.%) molybdenum (99.99 wt.%) and X metal chips : Ti, Cr or Zr (all 99.99 wt.%) were used.
The ingots were introduced into silica tubes, which were sealed under argon cleaned vacuum and underwent two different heat treatments:

- the first heat-treatment was performed by combining an annealing at 900℃ for 24 hours for homogenization, followed by water-quenching of the samples.
- the second heat-treatment was carried out at 900℃ for 24 hours to promote homogenization followed by an annealing at 500℃ for 72 hours to provoke the eutectoid decomposition of γ U based alloys. The samples were then slowly air cooled.

Thermal analyses were carried out by using DTA with heating and cooling cycles from room temperature up to 1400℃ and by examination of cooling curves obtained by measuring the temperature, with a bi-chromatic IR pyrometer, of the surface of samples heated up to 1800℃ and allowed to cool at various rates.

X-ray diffraction (XRD – D8 Advanced Brucker) and scanning electron microscopy coupled with energy dispersive spectroscopy (SEM+EDS - JEOL JSM 6400 + OXFORD EDS system) techniques were used to characterize the homogenized and destabilized U(Mo,X) alloys before and after the thermal analyses.

3. Results

3.1. SEM observations and XRD analyses and of γU(Mo,X) ternary alloys heat-treated at 900℃

Metallographic observations of the microstructure of all the ternary alloys, heat-treated at 900℃, revealed precipitates dispersed in an U-Mo-X matrix, as illustrated by Fig.1. Upon increasing the U content, the density of the precipitates decreases, indicating an improvement of the solubility of the alloying elements into the γ U(Mo) matrix. The

composition of these precipitates are found to be Mo- Zr-, Ti- and Cr-rich phases, and therefore the elemental composition of the matrix was hardly found to be the target composition, but slightly deficient in X-element. Table 1 summarizes the average composition over 3-6 EDS points of analysis of the γ U(Mo,X) main phase, as well as a rough estimation of the composition of the precipitates. In the case of the samples U84Mo11Cr5 and U90Mo5Cr6, the EDS measurements yield inconsistent results, which were therefore omitted. They are symbolized by a question mark in table 1.

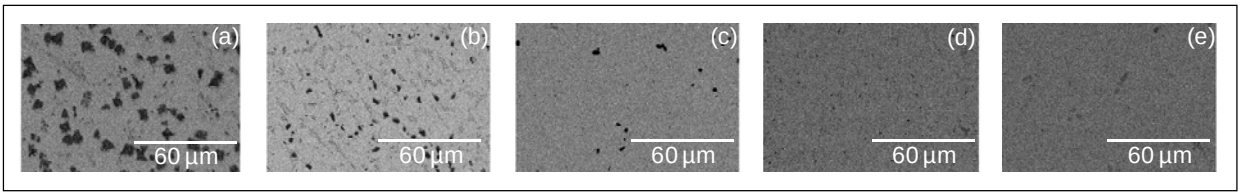

Fig. 1. SEM micrograph (BSE mode) of the sample annealed at 900℃ with nominal composition (a) U59Mo36Cr5, (b) U64.5Mo30.5Cr5, (c) U78Mo17Cr5, (d) U84Mo11Cr5, (e) U90Mo5Cr5. Small dark precipitates are Mo- or Cr- rich phase whereas the white matrix roughly matched the target composition.

Sample composition (at. %)	EDS analyses (at.%), U-Mo-X, (X = Zr, Ti, Cr)	
	Matrix	Precipitates
U59Mo36Zr5	U65Mo33Zr2 ! (U-rich ?)	Mo-rich
U59Mo36Cr5	U61Mo36Cr3	Mo-rich
U64.5Mo30.5Zr5	U69Mo28Zr3	Mo-rich
U64.5Mo30.5Cr5	U69Mo26Cr5	Mo-rich
U78Mo17Cr5	U80Mo15Cr5	Cr-rich
U78Mo17Ti5	U78Mo17Ti5	Ti-rich
U84Mo11Zr5	U84Mo11Zr5	Zr-rich
U84Mo11Cr5	U84Mo11Cr5	?
U84Mo11Ti5	U84Mo11Ti5	Ti-rich
U90Mo5Zr5	U90Mo5Zr5	Zr-rich
U90Mo5Cr5	U89Mo6Cr5	?
U90Mo5Ti5	U90Mo6Ti4	Ti-rich

Table 1. Average elementary composition of U-Mo-X alloys annealed at 900℃ determined by EDS analysis.

The XRD patterns collected on flat surface of the ingots display for all samples ranging in composition from U59Mo36X5 to U84Mo11X5, characteristic peaks of the *bcc*-lattice. They were nicely indexed with a lattice parameter ranging form 4.39Å to 3.48Å. The smallest unit-cell was found for U59Mo36Cr5 sample whereas the largest one was found for U84Mo11Zr5, in agreement with the respective metallic radii of the various components. Regarding the XRD patterns of the U90Mo5X5 samples water quenched from 900℃ (Fig.2), they mainly display diffraction peaks of the orthorhombic α-phase and broad peaks of bcc-phase with lattice parameter of about 3.44Å. Similar experimental unit-cell value was refined for the samples with composition U78Mo17X5, indicating an enrichment in Mo or in X-elements upon phase transformation. For the binary phase diagram the composition U78Mo22

(U78(Mo+X)22) is close to the composition of the eutectoid invariant reaction, γ U(Mo) → α U + U_2Mo, suggesting that quenching from the γ domain gives α phase and the eutectoid microstructure, γ' (α + U_2Mo).

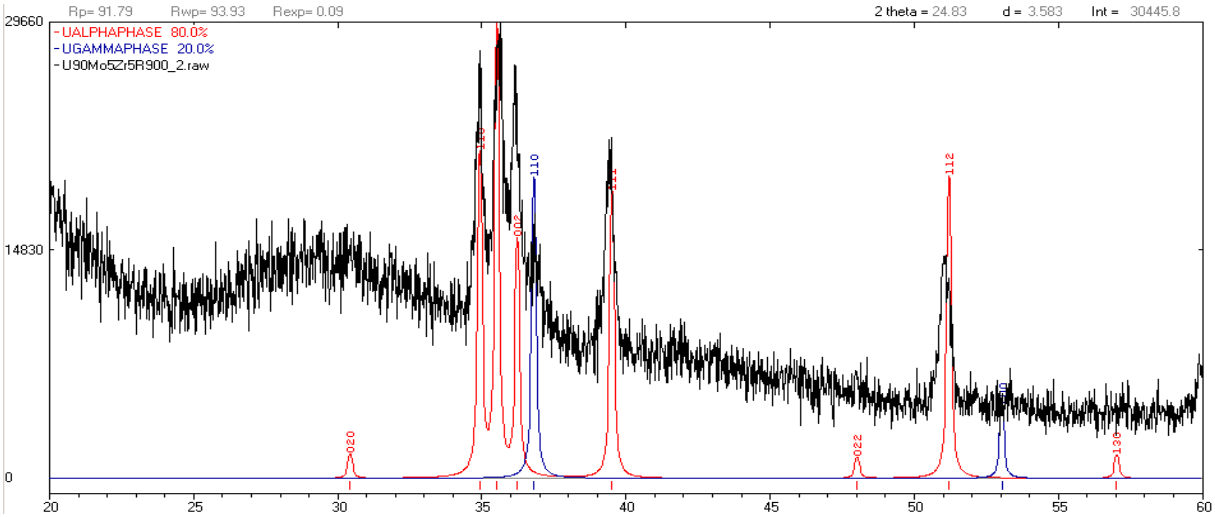

Fig.2. XRD pattern of the sample U90Mo5Zr5 water-quenched from 900℃, showing diffraction peaks corresponding to the α U (in red) and to a γ U based phase (in blue) with a lattice parameter of about 3.43Å.

3.2. SEM observations and XRD analyses and of γ U(Mo,X) ternary alloys heat-treated at 500℃

For the samples with U content above 78 at % (90 wt % of U), the SEM micrographs of the polished surface of all the samples heat-treated at 500℃ for 72h, showed acicular or lamellar microstructures with very fine grains. No direct link was established between the morphology of the microstructure and the effect of the ternary additions X. Fig.3 depicts the microstructure of the sample with nominal composition U84Mo11Zr5, showing the decomposed microstructure of the U(Mo) matrix along with micrometric precipitates. The presence of these precipitates was not detected in the microstructure of the samples heat-treated at 900℃, suggesting that their nucleation is due to oversaturation of the γ phase upon cooling.

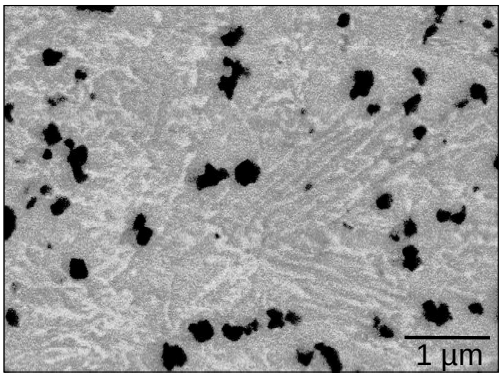

Fig.3. SEM micrograph of the sample with nominal composition U84Mo11Zr5, featuring the eutectoid decomposition of the U(Mo) matrix and the presence of micrometric precipitates.

The X-ray diffraction patterns of these samples displays characteristic peaks of the α phase, and broad peaks with shoulders which may correspond to U_2Mo or to a derivative of the γ phase [17].

3.3. DTA measurements

The work reported here about the ternary additions to U-Mo had the following objectives:

(i) studying the influence on the temperature of the invariant reaction γ→α + U_2Mo.
(ii) studying the influence on the transformation mechanism, especially the sequence of phase appearing at isothermal levels.
(iii) evaluating the temperatures of solid - liquid transformation.

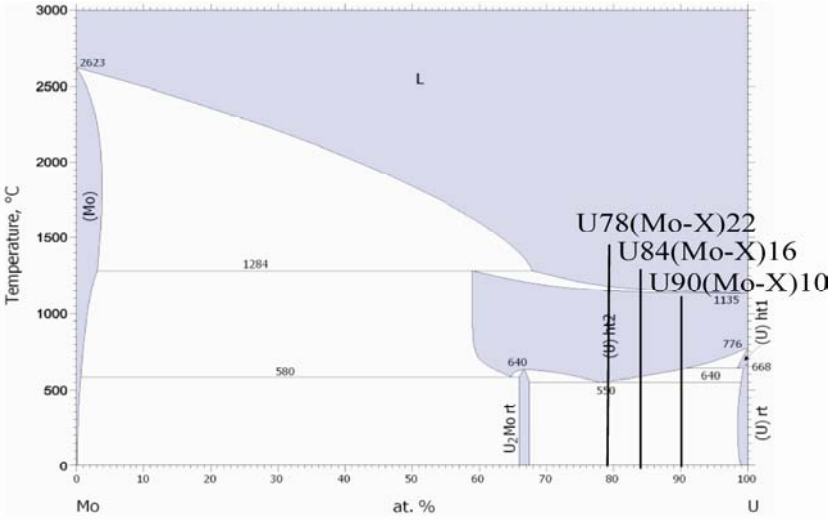

Fig. 5. Uranium-molybdenum phase diagram, according to [16], with superimposed the nominal composition of the examined samples, U78Mo17X5, U84Mo11X5, U90Mo5X5, with X = Cr, Ti, Zr.

Binary samples with nominal compositions U78Mo22, U84Mo16 and U90Mo10 were first measured to validate the sequence of phase appearing as well as evaluating the temperature of the various transformations. Table 2 summarized the results of the DTA measurements and Fig. 6 illustrates the heating and cooling curves of a sample with nominal composition U84Mo16.

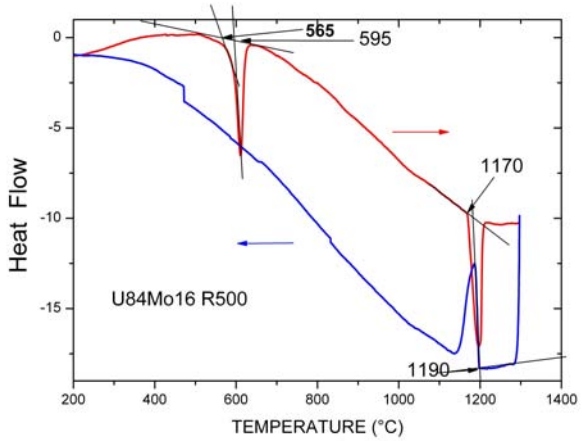

Fig.6 : DTA curves recorded with a heating and cooling rate of 10℃/min of a sample with nominal composition U84Mo16.

Sample	Temperature (℃)	Transformation
U78Mo22	1215(10)	L → S
	1190(10)	S → γ
	580(10)	γ→ α + γ
	562(10)	γ → α + U_2Mo
U84Mo16	1190(10)	L → S
	1170(10)	S → γ
	590(10)	γ→ α + γ
	565(10)	γ → α + U_2Mo
U90Mo10	1160(10)	L ↔ S !
	625(10)	γ → α + γ
	570(10)	γ → α + U_2Mo

Table 2. Experimental temperatures of the observed phase-transformation with the corresponding reaction, for the binary U-Mo samples.

Our results are in good agreement with the experimental works of A.E. Dwight [18] for the temperatures of reaction below 900℃ and of S.P. Ga rg and R.J. Ackermann [19] for the temperature of phase-transformation above 900℃.

Sample	Temperature of reaction (℃)	Possible reacti ons
U78Mo17Cr5	1160(10)	L → S
	1155(10)	S → γ
	588(10)	γ→α + γ
	570(10)	γ → α + U_2Mo
U84Mo11Cr5	1120(10)	L → S
	1090(10)	S → γ
	616(10)	γ→α + γ
	568(10)	γ → α + U_2Mo
U90Mo5Cr5	1084(10)	L → S
	984(10)	S → γ
	605(10)	γ→α + γ
	565(10)	γ → α + U_2Mo
U78Mo17Ti5	1250(10)	L → S
	1195(10)	S → γ
	605(10)	γ → α + U_2Mo
U84Mo11Ti5	1220(10)	L → S
	1181(10)	S → γ
	630(10)	γ→α + γ
	610(10)	α + γ → α + U_2Mo
U90Mo5Ti5	1183(10)	L → S
	1157(10)	S → γ
	640(10)	γ→α + γ
	620(10)	γ → α + U_2Mo
U78Mo17Zr5	1260(10)	L → S
	1210(10)	S → γ
	614(10)	?
U84Mo11Zr5	1195(10)	L → S
	1172(10)	S → γ
	610(10)	?

U90Mo5Zr5	1180(10)	L → S
	1160(10)	S → γ
	605(10)	?

Table 3. Experimental temperatures of the observed phase-transformations with the suggested reaction, for the ternary U-Mo-X (X = Cr, Ti, Zr) samples.

The reactions presented in table 3, for the ternary U-Mo-X alloys, are related to the U(Mo) phase-diagram, they do not consider the nucleation of the micrometric precipitates, which are presumably formed due to oversaturation of the γ phase upon cooling. Due to cooling rates of some degree per minute in DTA measurements, this technique is not suitable to investigate such type of transformation, which therefore was neglected in our analyses.
The ternary additions to the U(Mo) alloys provoke various effects depending on the nature of the alloying element. In the case of Cr and Ti, the sequence of the phase appearing does not seem to be affected: only the temperature of the transformations displays some changes compared to the binary U-Mo alloys. For Cr, the solid-solid transformations remain in a similar range of temperatures, about 565°C for the eutectoid decomposition of the γ phase and between 590-616°C for the two-phase field domain γ + α. The major changes regard the liquid-solid transformations which are lower by 50-100°C than in the case of binary U(Mo), and by the increase of the surface of the two-phase field L + S for the range of composition considered.
For Ti, both the solid-solid and liquid-solid transformations are impacted: a noticeable increase of the temperature of the transformations is measured compared to the binary U(Mo) samples. This increase of temperature is roughly constant by about 50°C in the whole range of composition studied, leading to a kind of shift of the isopleths section (U-Mo)95-Ti5 toward higher temperatures than the binary U(Mo) phase-diagram.
The case of Zr is more tricky, the addition of this element seems to impact the solid-solid phase transformations. Our DTA measurements evidence the modification or the suppression of the expected reactions, $\gamma \rightarrow \alpha + \gamma$ and $\alpha + \gamma \rightarrow \alpha + U_2Mo$. The work is still in progress, we are not able yet to ascribe the thermal effect observed at about 610°C to any transformation. However, based on X-ray diffraction analysis and SEM observations, the intermetallic compound U_2Mo is hardly observed in sample with 5 at % of Zr, suggesting that the Zr element hindered its formation.

4. Conclusion

The objectives of the present work were to evaluate the influence on the phase-transformation of ternary additions, at a constant content of 5 at. %, to U(Mo) alloys. Our main conclusions, derived from the comparison with the binary U(Mo) alloys, can be summarized as follow:

(i) Cr addition doesn't influence the nature of the phase-transformations, especially on the sequence of phase-appearing as well as on the temperature of the solid-solid transformations, which occur below 900°C. Its addition, however, modifies the transformation points above 900°C by reducing the Solidus and Liquidus temperatures and enlarging the two-phase field (S + L).

(ii) The ternary addition of Ti seems to increase the temperature of all the phase-transformations of about 30-40°C, but without any modification of the reaction of transformations and of the sequence of phase appearing.

(iii) In the case of Zr, our observations should be considered as assumptions, more likely. The effect of Zr addition impacts significantly the reactions of transformation in the solid state domain. The DTA curves do not show any evidence of pseudo two-phase field as expected. Only one solid-solid transformation is observed at a temperature about 610(10) °C. The observations suggest the occurrence of a diffusionless transformation (martensitic).

5. Acknowledgments

The authors are grateful to H. El Bekkachi for preparation of samples, and to the Centre de Microscopie Electronique à Balayage et microAnalyse (CMEBA, Université Rennes1) for SEM-EDS analyses.

6. References

[1] J. Snelgrove, G.L. Hofman, M.K. Meyer, C.L. Trybus, T.C. Wiencek, Nucl. Eng. Des. 178 (1997) 119
[2] G. Cabane and G. Donzé, J. Nucl. Mater. 4 (1959) 364
[3] S.L. Hayes, M. K. Meyer, G. L. Hofman, and R. V. Strain, in: Proceedings of the International Meeting on Reduced Enrichment for Research and Test Reactors, Sao Paulo, Brazil, October 18-23, 1998
[4] M.K. Meyer, G. L. Hofman, S. L. Hayes, C. R. Clark, T. C. Wiencek, J. L. Snelgrove, R. V. Strain, K. -H. Kim, J. Nucl. Mater. 304 (2002) 221
[5] A. Leenaers, S. Van den Berghe, E. Koonen, C. Jarousse, F. Huet, M. Trotabas, M. Boyard, S. Guillot, L. Sannen, M. Verwerft, J. Nucl. Mater. 335 (2004) 39
[6] Y.S. Kim, G.L. Hofman, H.J. Ryu, J. Rest, in: Proceedings of the International Meeting on Reduced Enrichment for Research and Test Reactors, Boston, USA, November 6-10, 2005
[7] F. B. Vaz De Oliveira, E.F.U. Carvalho, H.G. Riella, Twelfth International Topical Meeting on Research Reactor Fuel Management, Hamburg, Germany, March 2-5, 2008
[8] M. Rodier, X. Iltis, F. Mazaudier, M. Cornen, S. Dubois, P. Lemoine, Eleventh International Topical Meeting on Research Reactor Fuel Management, Lyon, France, March 11-15, 2007
[9] J.M. Park, H.J. Ryu, J.S. Park, S.J. Oh, C.K. Kim, Y.S. Kim, G.L. Hofman, in: Proceedings of the International Meeting on Reduced Enrichment for Research and Test Reactors, Czech Republic, September 23-27, 2007
[10] J.M. Park, H.J. Ryu, S.J. Oh, D.B. Lee, C.K. Kim, Y.S. Kim, G.L. Hofman, J. Nucl. Mater. 374 (2008) 422
[11] C. Komar Varela, M. Mirandou, S. Aricó, S. Balart, L. Gribaudo, J. Nucl. Mater. 395 (2009) 162
[12] J. Allenou, O. Tougait, M. Pasturel, X. Iltis, F. Charollais, M.C. Anselmet, P. Lemoine, J. Nucl. Mater. (2011), In Press
[13] J.M. Park, H.J. Ryu, Y.S. Lee, B.O. Yoo, Y.H. Jung, C.K. Kim, Twelfth International Topical Meeting on Research Reactor Fuel Management, Hamburg, Germany, March 2-5, 2008
[14] G.L. Hofman, Y.S. Kim, J. Rest, A.B. Robinson, D.M. Wachs, Twelfth International Topical Meeting on Research Reactor Fuel Management, Hamburg, Germany, March 2-5, 2008
[15] D. Kramer et W.V. Johnston, J. Nucl. Mater. 2 (1963) 213
[16] T.B. Massalski, H. Okamoto, P.R. Subramanian, L. Kacprzak (Eds.), Binary Alloy Phase Diagrams, vols. 1–3, second ed., ASM International, 1990.
[17] K. Tangri, G.I. Williams, J. Nucl. Mater., 4 (1961) 226.
[18] A.E. Dwight, J. Nucl. Mater., 2 (1960) 8.
[19] S.P. Garg and R.J. Ackermann, J. Nucl. Mater., 64 (1977) 265.

REMELTING AND THERMAL TREATMENT TO HOMOGENIZE U-Zr-Nb AND U-Nb ALLOYS

B.M.Aguiar[1], C.T.Kniess[1], R.W.D.Pais[4], W.B.Ferraz[4], H.G.Riella[1,2,3]

[1] *Nuclear and Energy Research Institute - IPEN/CNEN*

[2] National Institute of Science and Technology for *Innovating Nuclear Reactor*

Nuclear Fuel Center

Av. Prof. Lineu Prestes, 2242 – Cidade Universitária

CEP 05508-000, São Paulo – SP – Brazil

bmaguiar@ipen.br

[3]*Chemical Engineering Department - Federal University of Santa Catarina*

Campus Universitário – Trindade

CEP 88040-970, Florianópolis – SC – Brazil

[4]*Nuclear Technology Development Center – CDTN/CNEN*

Rua Prof. Mario Werneck s/n

CEP: 31027-901 – Belo Horizonte - MG

Abstract

The high density U-Zr-Nb and U-Nb uranium-based alloys are very promising to be used as a nuclear fuel not only in thermal power pressurized water reactors (PWR) but also in research reactors of low enrichment uranium. These alloys can stabilize the gamma phase, however, at the working coolant temperature of a PWR reactor, all the gamma phase transforms to alpha phase in a few hours. To avoid this type of transformation, the U-Zr-Nb and U-Nb alloy are used in α'' phase. The stability of α'' phase depends on the alloy composition and it's necessary to homogenize the alloy to obtain the correct phase. The homogenization has to be very effective to eliminate the precipitates rich in Zr and Nb to avoid changes in the uranium content of the alloy matrix. In this paper we present a method to homogenize these alloys by remelting in a resistance furnace at a very slow cooling rate. The obtained remelted alloys were characterized in terms of metallographic techniques, scanning electronic microscopy, X-ray diffraction and then the results were discussed.

Introduction

Uranium and its alloys are employed in various applications due to their high density and nuclear properties. The metals Mo, Nb, Ti, Zr, Hf and Re have high solubility in gamma uranium and they do not form any intermetallic compound. However, Zr and Nb have a special advantage because of their low capture cross section for thermal neutrons (1).

The U-Zr-Nb alloys can stabilize the gamma phase (cubic), however, some different martensitic transformations have been found to occurs, depending upon composition and cooling rate. The martensite phases identified with orthorhombic phases having non-equilibrium lattice parameters are called α', and monoclinic modifications, which occurs at even higher alloys contents, are called α'' (2). According some time-temperature-transformation diagrams for these alloys, at the working coolant temperature of a PWR reactor (about 300°C), all the gamma phase transforms to alpha phase in a few hours. To avoid this kind of transformation during

the nuclear reactor operation, and differently of U-Mo alloys, the U-Zr-Nb alloys are used in α'' phase (2-3).

The stability of α'' phase depends on the alloy composition and it's necessary to homogenize the alloy to obtain the correct phase. The homogenization has to be very effective to eliminate the precipitates rich in Zr and Nb, changing the uranium content of the matrix.

However, those precipitates are very stable and it is not easy to eliminate them only by diffusion, even after some day at 1050°C. One solution to remove these precipitates is remelting the alloy and to leave in liquid state for a sufficient time to allow the precipitates to float by density differences. After this process, the upper part of the ingot can be removed. This remelting process cannot be done in an induction furnace because the electrical currents and magnetic fields generated in the metal agitates the liquid metal, not allowing the precipitates (less dense) to float. For this reason, the remelting process was made in a resistance furnace (3).

Experimental

For this work, the U-Zr-Nb alloys (all compositions are reported in weight percent) were obtained by melting cubic pieces of uranium, zirconium sponge and niobium sheets in an induction furnace with the use of graphite crucible under argon atmosphere. The materials stays melted during 10 to 12 minutes and subsequently it was casted into a copper cylindrical mould of 2,5 cm diameter and 15 cm length dimensions. Further, the ingot was cut in samples with thickness of approximately 2mm and whose mass is approximately 5 grams each.

In the as-cast ingot, the homogenization is very poor. To obtain a homogenized alloy, two different thermal treatments were performed and analyzed:

1 - Heat treatment at 1.050°C for 72h under argon flux;

2 - Remelting the alloy under argon.

The first is a typical treatment of homogenization by solid-state diffusional process. However, in U-Zr-Nb and U-Nb alloys, it's common the formation of precipitates very rich (90 to 100%) in zirconium or niobium (or both). This precipitates are very stable and the solid-state diffusional process is not enough to eliminate them.

The remelting procedure was made in a resistance furnace under argon flux, employing yttria stabilized zirconia crucible. The remelting steps were:

a) Heat the sample from room temperature up to 1.570°C, at a rate of 10°C/min, for 15 minutes
b) Cooled from 1.570°C to 1250°C at a rate of 0,2°C/min (or 0,3°C/min)
c) Cooled from 1250°C to 900°C, at a rate of 5°C/min
d) Then, water quenching.

The temperature of 1570°C was chosen because all U-Zr-Nb alloys melts in a lower temperature and the temperature of 1250°C was selected to ensure that all alloys will solidify at this temperature. The cooling from 1250°C to 900°C was used to avoid a thermal stress in the oven's ceramic tube.

For all the electron microscopy examinations, samples were resin mounted into 2,5 cm diameter mould and they were mechanically ground, polished down to 3 μm diamond and 1 μm colloidal silica. Scanning electron microscopy was performed on a JEOL instrument model JSM-5310 equipped with the energy dispersive X-ray spectroscopy system (EDS).

Results and discussions

In this preliminary work, samples of U-5Zr-5Nb and U-3Zr-7Nb were homogenized at 1050°C for 72 hours under an argon flux and cooled to room temperature. Samples of U-6Nb, U-2.5Zr-7.5Nb *(*Mulberry Alloy) and U-5Zr-5Nb was remelted.

Figure 1 shows a typical backscattered electrons micrograph examinations of as cast U-5Zr-Nb (left) and as cast U-3Zr-7Nb (right) alloys.

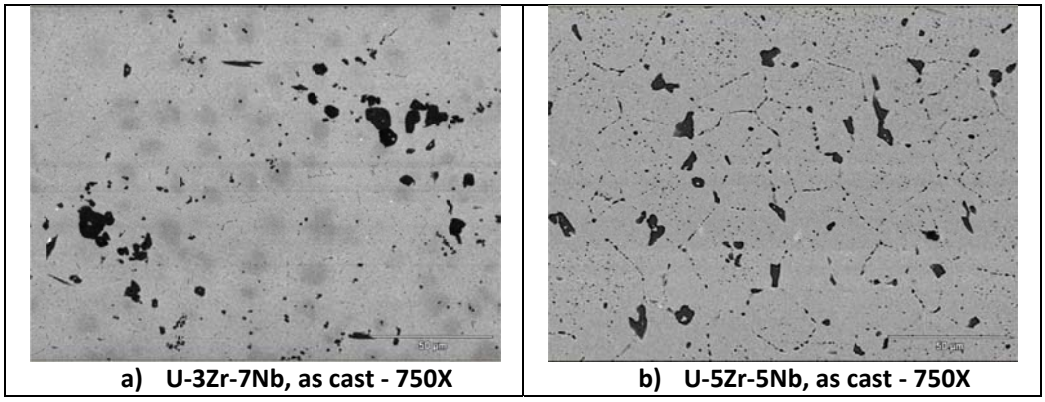

Figure 1 Backscattered electrons micrographs of as-cast alloys (a) U-3Zr-7Nb (b) U-5Zr-5Nb

The U-3Zr-7Nb micrograph shows three different regions of the as-cast alloys (matrix, microsegregation shown in the micrographs as gray spots and precipitates as dark spots) and Table 1 shows the microanalysis of each region. These values are the mean values of several measurements and the value in brackets are the standard deviation. In the matrix, there is a segregation of zirconium and, most intensively, niobium. The precipitates have a very high content of zirconium (63.37%), niobium (33.13%) and a little amount of uranium (3.5%).

Table 1 - EDS microanalysis of U-3Zr-7Nb as-cast alloy.

Region	*% Zr (σ)*	*% Nb (σ)*	*% U (σ)*
Matrix	2,17 (0,66)	4,64 (0,89)	93,19 (1,47)
Microsegregation	3,94 (0,44)	12,56 (1,06)	83,5 (1,44)
Precipitates	63,37 (1,46)	33,13 (0,54)	3,5 (1,99)

Table 2 shows the microanalysis of as-cast U-5Zr-5Nb. The microsegregation in the matrix area it is not intense as in U-3Zr-7Nb, but it is possible to see the same effect in higher magnification. The precipitates has a high zirconium segregation (90,66%) and a low content of niobium (3,95%) and uranium (5,39%).

Table 2 - EDS microanalysis of U-5Zr-5Nb alloy as cast.

Region	*% Zr (σ)*	*% Nb (σ)*	*% U(σ)*
Matrix	3,31 (0,32)	4,74 (0,32)	91,95 (0,38)
Precipitates	90,66 (2,34)	3,95 (0,98)	5,39 (2,89)

Figure 2 shows the backscattered electrons micrograph examinations of U-3Zr-7Nb (left) and U-5Zr-5Nb (right) alloys after heat treated at 1.050°C for 72h under argon flux.

The U-3Zr-7Nb alloy shows, after the heat treatment, a homogeneous matrix, without gray spots regions. In the U-5Zr-5Nb micrograph, the small precipitates in the center of the grains and in grain boundary were vanished.

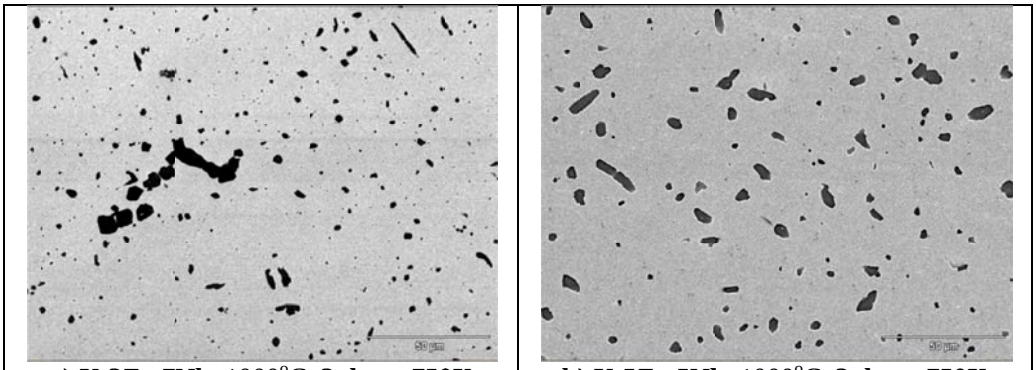

a) U-3Zr-7Nb, 1000°C**, 3 days- 750X** **b) U-5Zr-5Nb,** 1000°C**, 3 days- 750X**

Figure 2 - Backscattered electrons micrographs of (a) U-3Zr-7Nb and (b) U-5Zr-5Nb alloys, heat treated at 1.050°C for 72h

Table 3 shows the EDS microanalysis of U-3Zr-7Nb and U-5Zr-5Nb alloy after heat treated at 1.050°C for 72h. For both alloys, the increase of homogeneity can be inferred by the decrease of standard deviation. However, for the U-3Zr-7Nb alloy, the zirconium and uranium contents in the matrix were decreased and increased in the precipitates, respectively. For the U-5Zr-5Nb alloy, the content of zirconium and uranium were increased in the matrix and the niobium content were decreased (and the opposite way for the precipitates).

Table 3 - EDS microanalysis of U-3Zr-7Nb and U-5Zr-5Nb alloy after heat treated at 1.050°C for 72h.

	U-3Zr-7Nb			*U-5Zr-5Nb*		
Region	***% Zr (σ)***	***% Nb (σ)***	***% U (σ)***	***% Zr (σ)***	***% Nb (σ)***	***% U(σ)***
Matrix	1,88 (0,06)	5,75 (0,21)	92,37(0,15)	3,41 (0,30)	4,10 (0,10)	92,49 (0,26)
Precipitates	84,67 (6,68)	14,1 (6,73)	1,23 (0,52)	80,86 (4,56)	18,2 (4,56)	0,94 (0,54)

Figure 3 shows the backscattered electrons micrograph examinations of U-5Zr-5Nb alloy after it was remelted. The upper part is rich in precipitates and the bottom part practically free of them. The same result was obtained for U-6Nb and U-2.5Zr-7.5Nb. It can be observed also that the grain boundary is denoted as almost imperceptible thin line and do not contain precipitates, as shown in figures one and two.

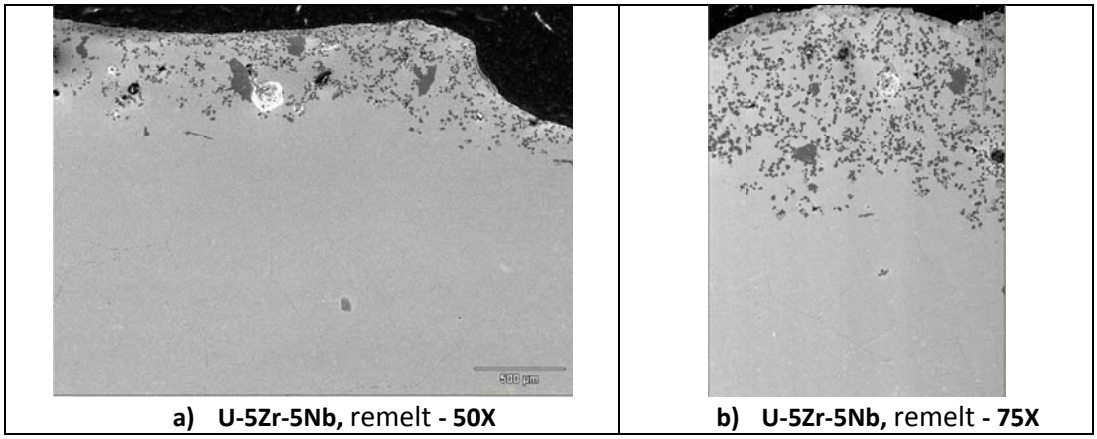

a) U-5Zr-5Nb, remelt **- 50X** **b) U-5Zr-5Nb,** remelt **- 75X**

Figure 3 - Backscattered electrons micrographs of remelted U-5Zr-5Nb a)50x; b)75x

Table 4 shows the EDS microanalysis of U-6Nb, U-5Zr-5Nb and U-2.5Zr-7.5Nb alloys. For the U-5Zr-5Nb, the amount of zirconium and niobium were increased and the uranium content was decreased in the matrix. For the U-5Zr-5Nb and U-2.5Zr-7.5Nb alloys, the precipitates are richer in zirconium and poor in niobium and uranium. In the U-6Nb alloy the precipitates are almost pure niobium.

Table 4 - EDS microanalysis of U-6Nb, U-5Zr-5Nb and U-2,5Zr-7,5Nb alloy after remelting process.

		%Zr (σ)	***%Nb (σ)***	***%U (σ)***
U-6nb	Matrix	-	4,50(0,70)	95,50(0,70)
	Precipitate	-	99,41(0,63)	0,59(0,63)
U-5Zr-5Nb	Matrix	4,05 (0,13)	4,36 (0,15)	91,59 (0,24)
	Precipitate	95,31 (2,69)	2,79 (2,37)	1,9 (0,61)
U-2,5Zr-7,5Nb	Matrix	1,65 (0,12)	6,85(0,11)	91,49 (0,21)
	Precipitate	83,05(10,63)	2,57 (0,37)	14,38 (11,01)

About the precipitates, it can be speculated that they are carbides of the types UC or Nb_2C formed from C impurities contained in the uranium raw material. The formation of such carbide precipitates is thermodynamically favored due the very low solubility of C in uranium. Figure 4 shows the X-ray diffraction of U-6Nb alloy. In this figure, it can be observed, besides the typical pattern of monoclinic α´´ phase, the peak at about 36°, that clear indicates the presence of Nb_2C precipitates, supporting the assumption that the precipitates of the alloys are very stable carbides stable even at high temperature. The experiments have shown that these precipitates could not be vanished even after extensive homogeneous thermal treatments, but only by remelting process proposed at this work. Finally, it could be said that, regardless of the structures of these rich in Zr and Nb precipitates, they deplete the matrix in those elements, altering in this way the properties in relation to the nominal alloy.

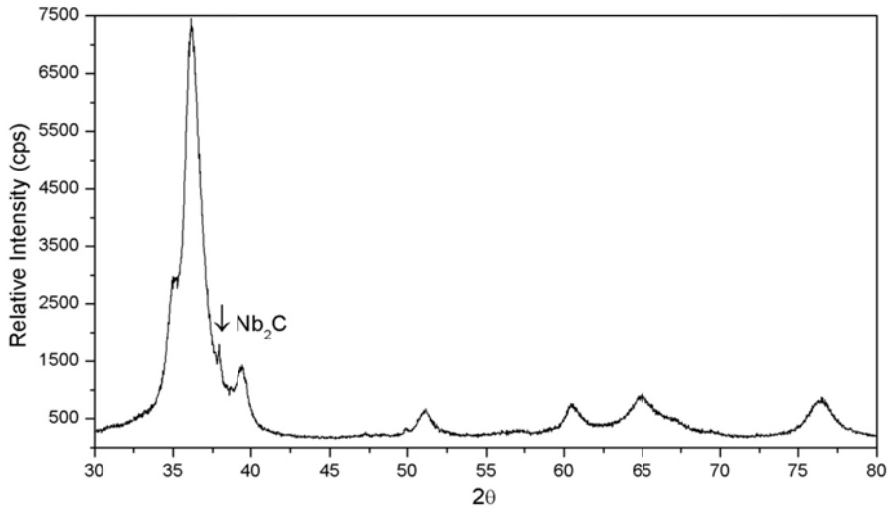

Figure 4 - X-ray diffraction scan of U-6Nb sample.

Conclusions

The thermal treatment applied in this work was effectively to homogenizing the matrix of the alloys. In this way, only the microsegragation, at grain center, was practically dissolved, but the precipitates still continue in the alloy with a big amount of zirconium and niobium. After the remelting process, the precipitates were restricted to a thin layer on the top of the alloy and it can be easily removed, leaving a matrix almost free of precipitates.

The formation of stable precipitates deplete significantly the content of alloying elements in the matrix of the U-Zr-Nb and U-Nb samples. The precipitates have higher content of zirconium than niobium, usually above 80%, and this causes a more pronounced depletion in the content of zirconium when compared with niobium.

References

1. **Leal, J. F.** *Microssegregação de tratamentos téricos de homogeneização em ligas U-Nb.* São Paulo, 1988.

2. *Development status of metallic, dispersion and non-oxide advanced and alternative fuels for power research reactor.*: International Atomic Energy Agency, 2003. Vols. IAEA-TECDOC-1374.

3. *Remelting and Thermal Treatment to homogeneizate U-Zr-Nb and U-Nb alloys.* **M, Aguiar. B.** Lisboa, Portugal, 2010. Reduced Enrichment for Research and Test Reactors.

4. **Choquet, F.** *Contribution a l'etude de l'alliage a haute resistance mecanique U-2,5Nb-2,5Zr.* CEA-R-4291, 1972.

5. *Dispersion type zirconium matrix fuels fabricated by capillary impregnation method.* **A. Savchenko, I. Konovalova, A. Vatulin, A. Morozova, V. Orlova, O. Uferova, S. Ershova, A. Laushkina, G. Kulakova, S. Maranchaka and Z. Petrova.** 2007, Journal of Nuclear Materials, Vol. 362, pp. 356-363.

6. **Burkes, D. E. Prabhakaran, R. Jue, J. Rice, F. J.** Mechanical Properties of DU-xMo with x=7 to 12 Weight Percent. *Metallurgical and Materials Transactions A.* 2009, Vol. 40A, pp. 1069-1079.

7. **Hackenberg, R. E. et al.** *Systhesis and Characterization of Nonbanded U-Nb Plate Material.* January 2007. LA-14316.

SCREENING OF DIFFERENT UMO/AL SAMPLES: PROTECTIVE OXIDE LAYERS, TI ADDITION TO THE MATRIX AND TERNARY U-MO-X ALLOYS

R. JUNGWIRTH , W. PETRY, H. BREITKREUTZ, W. SCHMID
Forschungsneutronenquelle Heinz Maier-Leibnitz (FRM II)
Technische Universität München, D-85747 Garching, Germany

H. PALANCHER, A. BONNIN
CEA, DEN, DEC,
F13108 Saint Paul lez Durance, France

M. GRASSE, C. JAROUSSE, B. STEPNIK
AREVA-CERCA- Les Berauds, B.P. 1114, 26104 Romans Cedex, France

ABSTRACT

It has been shown that the growth of the interaction layer at the UMo/Al interfaces that occurs during in-pile irradiation can be emulated out-of-pile by irradiation of UMo/Al fuel samples with Iodine at 80MeV. The properties of that interdiffusion layer (IDL) are comparable to the one observed after in-pile irradiation. Heavy ion irradiation is therefore a technique that allows the quick screening of different kind of UMo/Al samples to find promising candidates for a future in-pile test.
Different methods to suppress the formation of this undesired IL during irradiation of disperse UMo-Al samples have been suggested:
i) A modified Al-matrix (e.g. by adding Si to the matrix)
ii) A diffusion barrier (e.g. an oxide layer around the UMo particles or a metal coating)
iii) Further alloying the UMo
In this presentation the results of a screening campaign of 20 different U-Mo-X/Al-Y samples are going to be compared and discussed. The samples have been examined before and after irradiation with Iodine at 80MeV by SEM/EDX, laboratory XRD and XRD based on synchrotron radiations. For each sample, the most important results will be presented.

1. Introduction

To define the most promising candidates for a future in-pile test of high density nuclear fuel for research and test reactors, 20 different miniplates have been produced by AREVA-CERCA. They combine the most promising options to avoid the formation of the UMo/Al interdiffusion layer (IDL) during irradiation [1, 2]. From each miniplate a set of samples has been obtained which afterwards has been characterized by TUM and CEA before and after irradiation applying XRD, µXRD and SEM/EDX. Irradiation with heavy ions has been shown to create effects comparable to those observed during in-pile tests [3]. Details on the irradiation procedure have been presented elsewhere [1,4]. First communications have focused on the influence of different Si concentrations inside the Al matrix and on the behaviour of a silicon rich diffusion layer at the UMo7Al interface. In a second step, the influence of 2wt% and 5wt% Bi addition to the matrix on the irradiation behaviour has been shown . Thirdly, the general effects of heavy ion irradiation on samples prepared with ground powder have been discussed [5, 6].

In this paper the results of all 20 miniplates examined will be summed up and compared to the results of other groups. Finally, a general interpretation of the data will be proposed.

2. Sample manufacturing

All samples were produced by AREVA-CERCA through a process comparable to the one applied to produced the IRIS-TUM full size plates [7]. The complete list of samples is presented in Tab. 1. Samples numbered 1 to 17 were prepared with atomized powder provided by KAERI. Samples numbered 17 to 21 were produced with ground UMo powder. The ingot production for the ground powder was followed by a thermal treatment step to increase homogeneity and to retain the γ-UMo phase. Depleted Uranium has been used for all samples.
Secondary element addition to the matrix was achieved by blending very fine high purity powders – except for the Al98Si2 sample.
A part of the samples - labelled "ox" in Tab. 1 - was prepared with UMo powder that had been intentionally oxidized. For this, the UMo powder was heated when exposed to air. Thereby, a thick and homogeneous oxide layer could be created.
Each miniplate was subjected to the same hot-rolling and blister testing procedure making sure that all samples are comparable.
All samples were irradiated with Iodine at 80 MeV to an integral ion fluency of $1 * 10^{17}$ ions/cm² at the MLL tandem accelerator in Garching [8] at a temperature of about 200°C [9].

Sample Nr.	Alloy	Matrix	Comment
MAFIA-I-1	U-7Mo	Al	Reference specimen
MAFIA-I-2	U-7Mo-ox	Al	
MAFIA-I-3	U-7Mo	Al98-Si2	Different Si concentrations to find the best concentration
MAFIA-I-4	U-7Mo-ox	Al98-Si2	
MAFIA-I-5	U-7Mo	Al95-Si5	
MAFIA-I-6	U-7Mo-ox	Al95-Si5	
MAFIA-I-7	U-7Mo	Al93-Si7	
MAFIA-I-8	U-7Mo-ox	Al93-Si7	
MAFIA-I-9	U-7Mo	Al98-Mg2	Mg accelerates formation of IDL. Reproduction of this effect.
MAFIA-I-10	U-7Mo-ox	Al98-Mg2	
MAFIA-I-11	U-7Mo	Al98-Ti2	Study the effect of Ti on IDL formation.
MAFIA-I-12	U-7Mo-ox	Al98-Ti2	
MAFIA-I-13	U-7Mo	Al98-Bi2	Different Bi concentrations to find the best concentration.
MAFIA-I-14	U-7Mo-ox	Al98-Bi2	
MAFIA-I-15	U-7Mo	Al95-Bi5	
MAFIA-I-16	U-7Mo-ox	Al95-Bi5	
MAFIA-I-17	U-7Mo	Mg	Mg matrix, did not work, brittle matrix, matrix with no adhesion to cladding.
MAFIA-I-18	U-7Mo-1Ti	Al	To study principal effect of alloying the UMo on the formation of the IDL.
MAFIA-I-19	U-7Mo-1,5Nb	Al	
MAFIA-I-20	U-7Mo-3Nb	Al	
MAFIA-I-21	U-7Mo-1Pt	Al	

Tab. 1: Complete list of samples examined.

3. Oxidized Particles

Each kind of the samples with secondary element addition to the matrix was produced with and without an oxide layer around the UMo particles. At first, the sample microstructure before irradiation with heavy ions will be considered. Afterwards, the influence of the oxide layer on the fuel behaviour during heavy ion irradiation will be discussed. All samples have

been examined using SEM/EDX and laboratory scale XRD in combination with Rietveld analysis.

a) Pre-irradiation state

Two classes of oxide layers have been found around the UMo particles:

- Thin oxide layers with a thickness <1 µm have been found around some of the particles that have not been intentionally oxidized. In this case, the oxidation must have occurred spontaneously during the sample manufacturing process. Already the thin oxide layers reveal cracks – compare Fig. 1 A.
- Thicker oxide layer with a thickness up to 5 µm have been found around the UMo particles that have been oxidized on air by heating. This kind of oxide layer seems to be very brittle and shows large cracks – compare Fig. 1 B. Furthermore, it seems that the oxidized UMo particles tend to loose contact with the matrix: gaps between the UMo and the oxide layer have been observed. Apparently, the oxide layer sticks rather to the Al matrix than to the UMo particles. This behavior is more obvious at spots where an UMo particle was ripped out during the polishing: the oxide layer remained inside the resulting hole – compare Fig. 1 B.

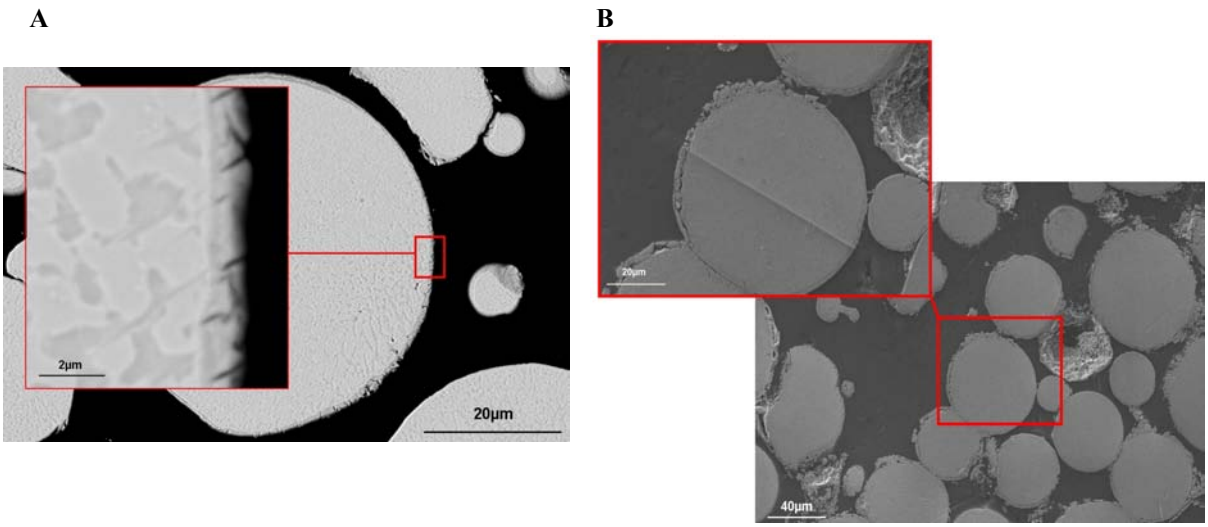

Fig. 1: (A) Thin oxide layer around a UMo particle. (B) Thicker oxide layer and ripped-out particle.

On average a $UO_2/(\alpha\text{–}U+\gamma\text{–}UMo+UO_2)$ ratio of 24±9wt% has been found for samples that were intentionally oxidized. A ratio 10±5wt% has been found for non-oxidized samples. Regarding the XRD diagrams, it seems that the α–U content is higher inside the samples that have been prepared with oxidized powder compared to the ones prepared with non-oxidized powder. This behavior is in accordance with the production parameters since the oxidation was performed by heating the UMo powder.

b) Post-irradiation state

The behavior of the samples with a large oxide layer around the UMo particles after irradiation with heavy ions differed considerably from the behavior of the samples containing atomized powder without or with only a small oxide layer and from the samples containing ground powder. In contrast to the other samples examined, a “glittering” of the irradiated surfaces has been observed upon visual inspection. A more detailed SEM analysis including cross sections through the irradiated surface revealed that the UMo particles had frequently lost contact with the Al matrix and stick out of the surface – see Fig. 2 A. However, particles

covered with thin oxide layers did not loose contact with the Al matrix during irradiation. In these cases, the oxide layer got incorporated into the IDL that grew during irradiation. It seems that the oxide has not moved during irradiation relatively to the original UMo/Al interface: it stayed at the original position – see Fig. 2 B. XRD analysis of the irradiated samples confirmed that in addition to a slight increased UO_2 content due to surface oxidation the only new phase was UAl_3. It can therefore be concluded that also here the IDL consists mainly of this phase.
In contrast, it has been reported before that no IDL has developed after heavy ion irradiation with Iodine at 80MeV inside UMo/Al samples in case a thin oxide layer is present around the UMo particles [12]. The irradiation temperature during the experiment back then was lower than in the case regarded in this work. The fact that a higher irradiation temperature enhances the formation of the IDL [10] can explain this effect. Moreover, the post irradiation examination procedure used nowadays seems to be more adapted to observe even small amounts of an IDL inside heavy ion irradiated samples.

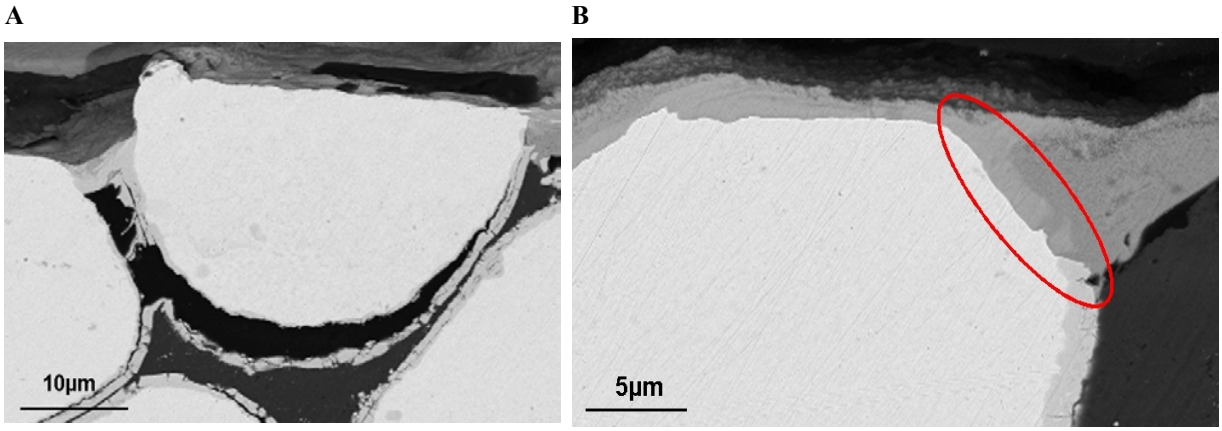

Fig. 2: (A) UMo particle which lost contact during irradiation due to the thick oxide layer. (B) Oxide layer that got incorporated into a conventional IDL (red circle).

An improved irradiation performance - especially a reduction of the IDL growth - of samples prepared with oxidized powder can not be deduced from the heavy ion irradiation experiments. In fact, the irradiation performance during heavy ion irradiation is worse due to the tendency of the UMo particles to loose contact with the matrix. However, this is only a surface effect and will not appear in the bulk material that is used during in pile irradiation.
It can be concluded that the improved swelling behavior of in-pile irradiated plates does not only result from a reduction of the IDL growth but probably from an improved fission gas retainment [11, 12]. The oxide layer gets incorporated into the IDL during burn-up and may positively influence its ability to retain fission gases.

4. UMo/AlTi systems

It seems that Ti retards the uranium-aluminium diffusion. In former studies, the positive effect of titanium could be observed by adding titanium to the aluminium [13], by further alloying the UMo with titanium [11,14,15,16] and by introducing titanium as a diffusion barrier at the interface between UMo and aluminium [17]. The following systems have been examined:

- Conventional dispersed UMo/Al2wt%Ti samples were produced by blending fine powders according to the method described above and irradiated with heavy ions.
- Thin Al/Ti/UMo layer system were produced by DC magnetron sputtering. The compatibility of Ti with Al and UMo in the non-irradiated state has been examined [18,19,20].

- Dispersed samples consisting of ground U7wt%Mo1wt%Ti ternary alloys were produced. The samples have been examined before and after irradiation with heavy ions. Results will be presented in section 6.

a) Matrix addition: UMo/Al2wt%Ti

Blended Al-Ti powder of the finest grain size available was used. Since the solid solubility of Ti in Al is lower than 0.7at% [21], the presence of Ti precipitates in the Al matrix was anticipated. However, the size of the Ti precipitates is larger when using blended powder (5-10 µm) and the distribution is more heterogeneous as would be expected when using melted Al-Ti. No reaction of the aluminium matrix or of the UMo particles with the titanium during the production process could be observed, compare Fig. 3 A.
A surface inspection of the irradiated sample and a cross section examination confirmed that the titanium particles were not affected by the diffusion process: The IDL around the UMo particles forms according to the shape of the Ti particles nearby – see Fig. 3 B . Laboratory scale XRD measurements together with a Rietveld analysis showed that the IDL consists mainly of UAl_3.

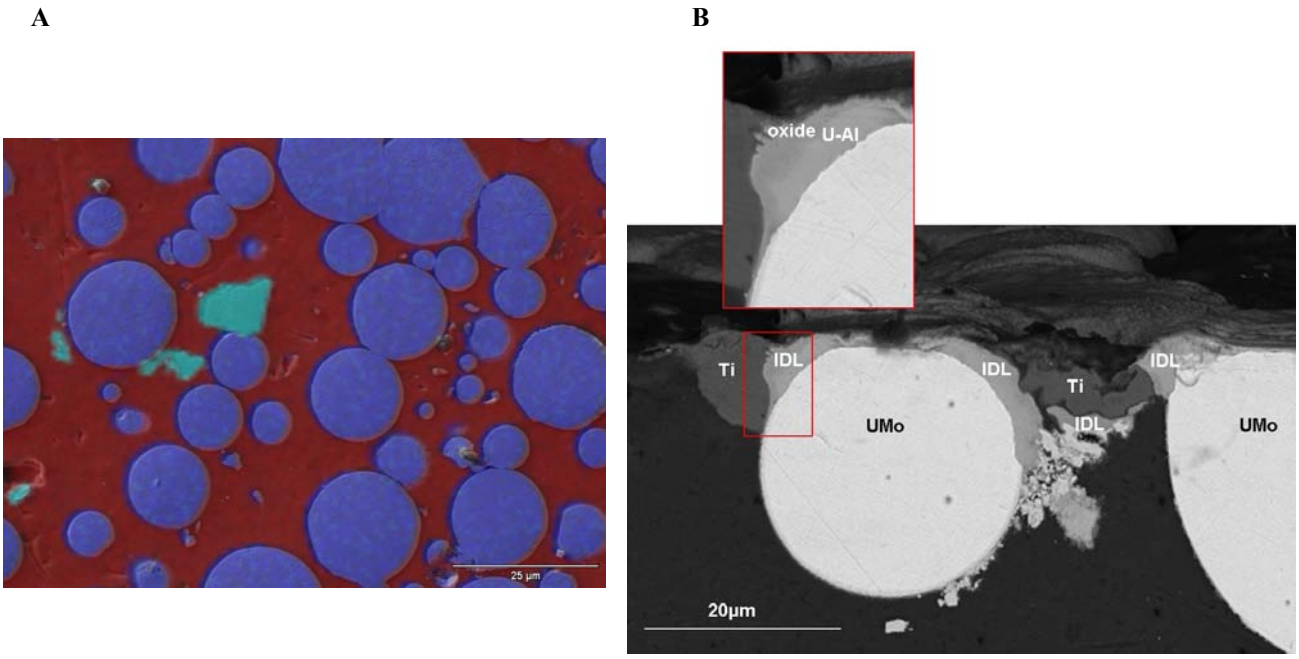

Fig. 3: (A) Colorized SEM image of a fresh UMo/AlTi sample: red indicates aluminum, blue indicates UMo, cyan indicates titanium precipitates. (B) Cross section examination through the irradiated surface: titanium precipitates in contact with UMo and the IDL.

b) Ti as diffusion barrier

Titanium has been considered to be one of the most effective diffusion barriers to stop or delay the UMo/Al diffusion process [17]. Samples produced by DC magnetron sputtering served as model systems: on the one hand the compatibility of titanium with aluminium and UMo has been tested. On the other hand the bond strength of titanium sputtered onto aluminium and of UMo sputtered onto titanium has been determined.
To test the compatibility of titanium with aluminium and UMo, thin layers (each around 5 µm) of titanium and UMo were sputtered onto an aluminium substrate. Cross sections were prepared and examined using SEM/EDX. No interaction of the titanium with the UMo or the

aluminium substrate occurred during the production process. Furthermore, no spontaneous debonding of the sputtered layers has been observed [19].
In a second step, the bonding strength between titanium sputtered onto aluminium substrates and between UMo sputtered onto titanium substrates have been tested by tensile tests. Values between 40-70MPa have been found in the first case, and 67MPa has been found in the second case. The bond strengths of UMo and Ti to the substrate are therefore at least as high as the adhesion between UMo and aluminium that has been reached using conventional techniques [20,22].

c) Discussion

The titanium particles present in the dispersed UMo/Al samples did neither react with the aluminium, nor with the UMo during the production process and during the heavy ion irradiation. Furthermore, no reaction between the titanium and the IDL could be observed after heavy ion irradiation. The positive effect of a titanium addition to the matrix is limited to the fact that as soon as the IDL gets in contact with a titanium precipitate the diffusion stops.
A finer and more homogeneous distribution of titanium in the aluminium matrix as could be achieved by co-melting and casting Al and Ti would be of no avail: the smaller titanium precipitates would most probably be incorporated into the IDL. However, further examinations proofed the compatibility of UMo and aluminium with thin layers of titanium. These result confirm that titanium would be an excellent diffusion barrier.

5. UMo/Al Mg systems

Earlier [13] and recent literature [23] agree that an addition of several wt% of magnesium to the aluminum should be avoided since the UMo/Al diffusion is increased. However, these experiments regarded thermal diffusion at temperatures of 400°C-500°C. To verify this effect also for irradiation induced diffusion, UMo/Al samples with 2wt%Mg addition to the matrix were prepared.
An inspection of the sample surface using SEM/EDX before heavy ion irradiation revealed that the magnesium powder has completely and uniformly dissolved in the aluminium matrix as could be expected from the phase diagram [21]. No Mg particles or precipitates could be found. EDX measurements showed a medial Mg content inside the aluminium of 1.9±0.7wt% which is in good accordance with the expected value of 2wt%.
A cross section analysis of the heavy ion irradiated samples reveals that a diffusion layer has grown around each irradiated UMo particle. However, the diffusion layer is not thicker than the one that has been observed in the reference samples and only slightly thicker than the one that has been observed inside the samples with Si addition to the matrix [5]. This result is clearly in contradiction to what has been found before in diffusion couple experiments: the thickness of the diffusion layer when adding 2-3wt%Mg to the aluminium was at least two times higher compared to the reference samples with pure aluminium and up to 50 times higher compared to the optimal case with 10wt% silicon addition to the aluminium[13,23].
The phase composition of the samples has been compared before and after irradiation with heavy ions using laboratory scale equipment. In addition to the phases present before irradiation - γ-UMo, Al, UO_2 and a slight α-U contamination - UAl_3 was present after heavy ion irradiation. The Mg/(Al+Mg) ratio inside the IDL was 2.6±0.7 which is, within the error bars, the same ratio than in the Al matrix. It can therefore not be concluded that magnesium was preferably built into the IDL compared to aluminium.

6. Ternary UMo alloys – Ground powder

It has been suggested to further alloy the UMo with ternary elements to increase the γ-phase stability and by this mean reduce the UMo-Al interaction. To test this hypothesis, ternary

U8MoX alloys were created where X=1,5wt%Nb, 3wt%Nb,1wt%Ti and 1wt%Pt. The chosen elements and concentrations have shown to be promising in other publications [11,12,16,24,25]. Samples based on ground U8MoX powder were produced by the standard CERCA procedure from these alloy.

a) Pre-irradiation state

All four samples have been examined using SEM/EDX and XRD with Rietveld analysis. On first view, the SEM reveals the typical microstructure of ground powder: particles of irregular sizes and shapes are dispersed in the Al matrix. The particles are oxidized and contain oxide stringers [26].
No signs of Nb or Pt precipitation have been found inside the samples containing U8Mo1.5Nb and U8Mo1Pt. These two additions seem to have dissolved uniformly inside the UMo - compare Fig. 4.

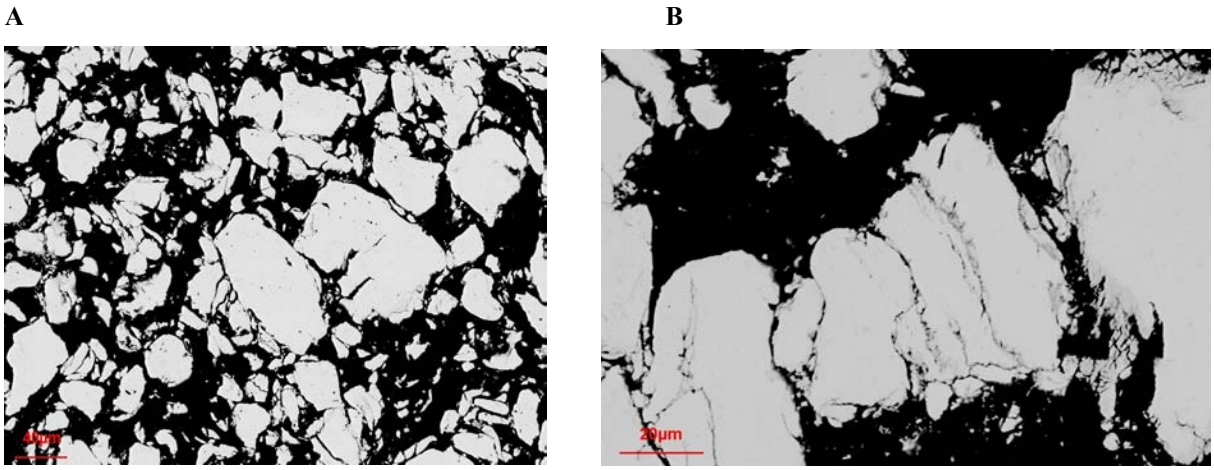

Fig. 4: Ground U8Mo powder with 1.5w\%Nb (A) and 1wt%Pt (B) addition. The third element has been completely dissolved inside the UMo, no precipitation is visible.

In contrast, Nb precipitates (size ~1-5 µm) and larger Nb stringers have been found inside the U8Mo3Nb – see Fig. 5 A . The small precipitates indicate that the solution limit for Nb inside U8Mo may be reached: segregation of small round precipitates of a second phase inside a dominant first phase frequently occurs upon cooling from a single phase towards a two phase regime [21]. The rather large Nb stringers indicate, however, that the initial homogenization step, which consisted of frequent remelting and cooling followed by a final heat treatment of the U8Mo3Nb alloy, was not sufficient to fully homogenize the sample.
The mean composition of the Nb stringers and precipitates has been determined using standardless EDX analysis. While the stringers consist almost exclusively of Nb and contain only traces of Mo and U, the precipitates contain a considerable amount of U and Mo (only precipitates larger than the size of the EDX probe have been considered).
Precipitation has also been found inside the sample containing U8Mo1Ti. Here, Ti rich precipitates of about 1 µm diameter have been found inside the UMo – see Fig. 5 B. In contrast to the U8Mo3Nb alloy, no stringer has been found.
The samples have been investigated using laboratory scale XRD. A full Rietveld analysis has been performed to determine the phases, lattice parameters and phase quantities. Results have been presented before and can be found elsewhere [26].
It is found that further alloying the UMo with a third element can stabilize the UMo γ-phase compared to pure UMo. The addition of 1.5wt% and 3wt% Nb lead to a stabilization of the γ-UMo where the higher alloy composition revealed slightly better results. However, since inside the 3 wt%Nb alloy already precipitation occurred, it is likely that the stabilizing effect has already reached its saturation.

In the case of 1wt%Pt addition, the stabilizing effect is more pronounced. Since no Pt precipitation occurred, it is likely that the effect can be increased by adding more Pt.
In the case of 1wt%Ti addition no effect on the γ-UMo stability compared to unalloyed UMo could be deduced. An explanation for this behavior is most likely the occurrence of Ti precipitates which indicate that virtually no Ti is present inside the UMo lattice.
Regarding the lattice parameters of the α-UMo phase, one finds the same behavior as inside the samples containing pure ground U8Mo: the b-parameter is contracted, the a and c cell parameter are stretched compared to pure α-U. The absolute values are approximately the same as for pure U8Mo samples [26]. From the lattice parameters of the γ-UMo the Mo content of the γ-phase has been calculated. As in the pure U8Mo case the calculated Mo values inside the ternary alloys are higher than what has been expected from the alloys composition.

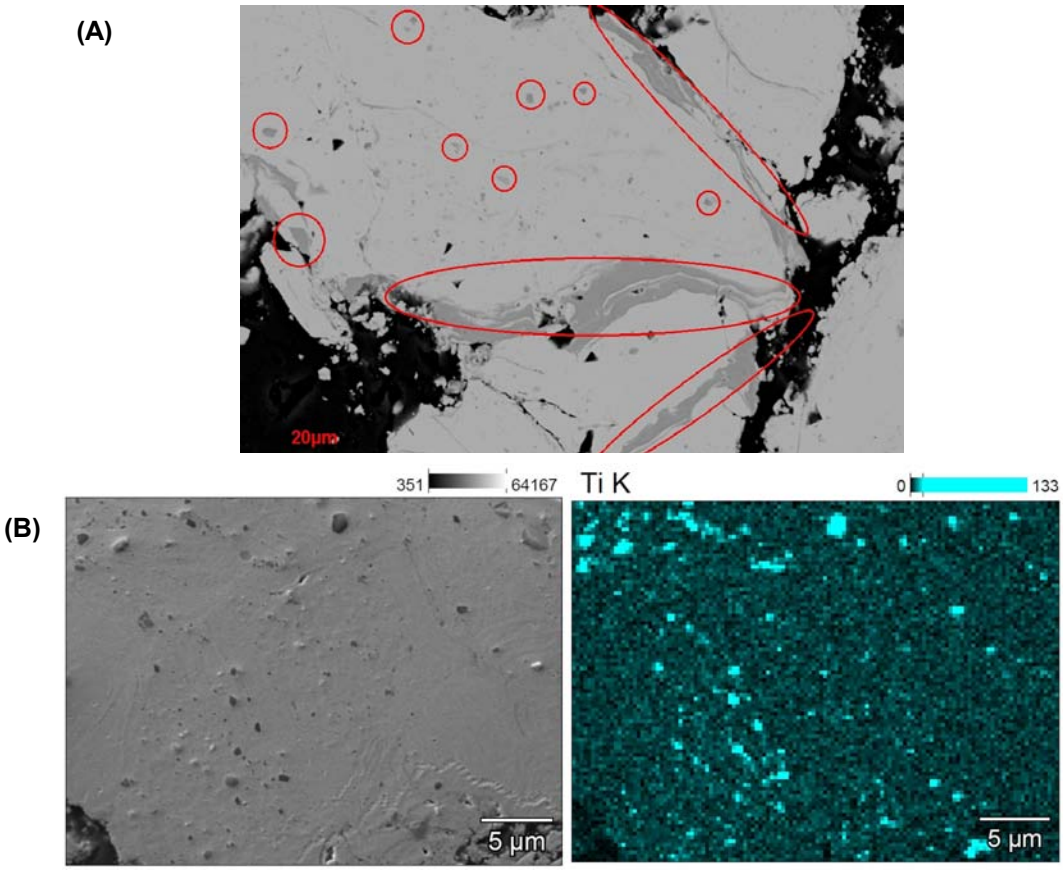

Fig. 5: (A) BSE-image of the U8Mo3Nb alloy ground powder. Nb rich precipitates have formed (red marked positions. (B) BSE image and EDX map on the Ti K-α line: Ti rich precipitates are visible.

b) Post-irradiation state

The general behavior of ground UMo/Al fuels under heavy ion irradiation has already been described before [6]. In addition, it is noteworthy that the IDL Al/(U+Mo) composition has not been influenced by the different ternary alloy compositions. Indeed, no signs of the ternary element could be resolved inside the IDL using EDX, most probably to the low overall content.
Regarding the samples which contained stringers and precipitates inside the UMo before irradiation (U8Mo1Ti and U8Mo3Nb) two different effects have been observed: in case of Nb, the precipitates and stringers have virtually been dissolved inside the IDL and the UMo during irradiation - no signs of precipitates could be found inside the irradiated area.

The opposite effect occurred inside the samples containing Ti precipitates inside the UMo: the Ti precipitates did not dissolve and even got incorporated into the IDL - compare Fig. 6.
The phase composition of the irradiated samples has been determined using laboratory scale XRD together with a Rietveld refinement.
Inside all samples UAl_3 was present additionally after irradiation which indicates that the IDL consists mainly of this phase.
The ratio α-U/(α-U+γ-UMo) is lower than inside the fresh samples. The phase transformation γ-UMo → α'-UMo+γ-UMo wastherefore reversed during heavy ion irradiation. This effect has been observed before after in-pile and heavy ion irradiation [4,27].

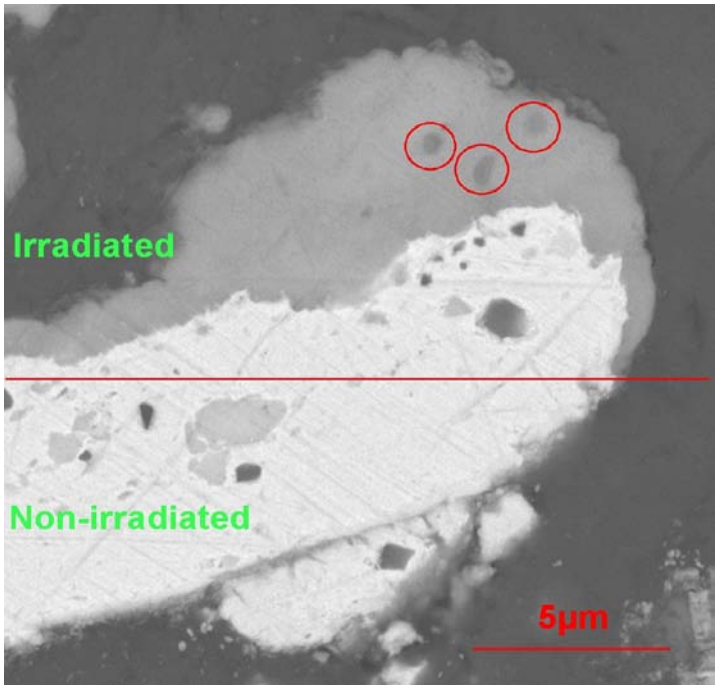

Fig. 6: BSE image of an U8Mo1Ti/Al sample after irradiation with heavy ions. The Ti precipitates present inside the UMo did not dissolve during irradiation and got incorporated into the IDL.

7. Conclusions

Based on the results of this irradiation campaign and results presented before by other groups, the following conclusions can be drawn:

- Additions to the Al matrix and/or additions to the UMo can be reduced to the self-acting formation of a protective layer at the UMo/Al interface in dispersed fuel. These layers form already during the production process or latest during pile irradiation. In case of second element addition to the Al, it is therefore advisable to choose an element with a higher affinity to uranium than to aluminium – as it is the case for a si addition to the matrix. On the other hand, in case of ternary additions to UMo it seems advised to choose elements with higher affinity to aluminum than to uranium. In case additions to the UMo and the aluminum are chosen they should have a very high affinity to form compounds with each other compared to the other elements in the system in order to form a protective layer around the UMo particles [22,23, 28, 29]
- In order not to reduce the available U-density too much, it is desirable to use thin layers in the order of magnitude of 1 µm as diffusion barriers inside dispersed UMo/Al fuels. Thin, stable layers like U-oxide or U-nitride layers seem to be advisable [30]. The other option is to directly apply a reactive layer like Si, USi or ZrN on the UMo

particles before plate production [31]. Since the fission products easily penetrate such a thin layer ion beam mixing will occur. Therefore, these layers will never be able to suppress completely the U-Al diffusion. However, they can control the formation kinetics and lead to the formation of stable diffusion compounds when incorporated into the diffusion layer.

- In case of monolithic fuel, it is possible to insert a rather thick diffusion barrier at the interface UMo-Al. The thickness can be much higher than the penetration depth of the fission products. An order of magnitude is 20 µm. It is advisable to use materials like zirconium, titanium or tantalum that do not easily form compounds with uranium and aluminum. In this way, the UMo-Al diffusion can be completely suppressed. Here, special attention must be paid on the adhesion of the single layers. For example, an oxide layer at the Umo-Al interface would reduce the adhesion. In contrast, a Zr layer enhances the fuel-cladding bonding [20].
- Ternary additions to the UMo in order to stabilize the γ-UMo upon heating seem to be worthless during pile experiments at low temperatures since the decomposition of UMo is reversed. These additions are only valuable in case they form a protective layer at the UMo/Al interface or in case of annealing of the fuel element prior to the irradiation. In the later case, they will reduce or avoid an initially present, thermal grown interaction layer.

8. Acknowledgements

The authors wish to thank the MLL tandem accelerator in Garching for the provision of beam time.

This work was supported by a combined grant (FRM0911) of the Bundesministerium für Bildung und Forschung (BMBF) and the Bayerisches Staatsministerium für Wissenschaft, Forschung und Kunst (StMWFK).

[1] R. Jungwirth, *"Irradiation behaviour of modified high-performance nuclear fuels",* Doctoral thesis, Technische Universität München, 2011
[2] C. Jarousse et.al, *"FRM II and AREA-CERCA common effort on monolithic UMo plate production",* RRFM 2009, Vienna, Austria, 2009
[3] N. Wieschalla et.al., Journal of Nuclear Materials, 357, 191-197,2006; H. Palancher at.al, Journal of Nuclear Materials, 385, 449-454, 2009
[4] E. Welcomme et.al, "*Heavy ion irradiation of U7Mo/Al fuel: methodological approach",* RRFM 2009, Vienna, Austria, 2009
[5] R. Jungwirth et.al., *"Optimization of the Si content in UMo/Al(Si) fuel plates",* RERTR 2009, Bejing, China, 2009
[6] R. Jungwirth et.al, *"Study of heavy ion irradiated UMo/Al miniplates: Si and Bi additions into Al and UMo ground powders",* RRFM 2010, Marrakech, Morocco, 2010
[7] W. Petry et.al, *"UMo full size plate irradiation experiment IRIS-TUM – a progress report"*, RRFM 2008, Hambourg, Germany, 2008
[8] MLL Tandem accelerator, http://www.bl.physik.uni-muenchen.de/
[9] T. Zweifel et.al, *"Heavy ion irradiation of UMo7Al systems: temperature influence and monolithic UMo layers", this conference, 2011*
[10] E. Welcomme, *"Heavy ion irradiation of UMo7/Al fuel: methodological approach",* RRFM 2009, Vienna, Austria, 2009
[11] M. Ripert et.al, *"Results of the {RIS4 irradiation in OSIRIS reactor: oxidized U-Mo particles dispersed in Al (with 0 or 2.1%Si)", RERTR 2009, Bejing, China, 2009*
[12] S. Dubois et.al, *"Development of Dispersed UMo fuel : An Oxide Layer as a Protective Barrier of the UMo Particles",* RERTR 2006, Cape Town, South Africa, 2006
[13] R.O. Williams, *"Terminal report on the ORNL slug rupture problem – causes and prevention",* Oak Ridge National Laboratory, CF-50-7-160, 1950
[14] W.C. Thurber, Oak Ridge National Laboratory, ORNL-2602, 1959
[15] J.M. Park et.al, *"Phase Stability and Diffusion Characteristics of U-Mo-X (X=Si, Al, Zr or Ti) Alloys",* RERTR 2005, Boston, USA, 2005
[16] M. Rodier et.al, *"Effects of Ti in the UMo/Al system: preliminary results",* RRFM 2007, Lyon, France, 2007
[17] D.D. Keiser et.al., *"Characterization and Testing of Monolithic RERTR Fuel Plates",* RRFM 2007, Lyons, France, 2007
[18] W. Schmid, *"Construction of a sputtering reactor for UMo foil coating and tailored sample production",* Doctoral thesis, Technische Universtät München, 2011
[19] H. Juranowitsch, *"Cross Section Examination of Sputtered Uranium-Molybdenum Nuclear Fuels",* Diploma thesis, Hochschule für angewandthe Wissenschaften (FH) München, 2010
[20] S. Dirndorfer, *"Tensile Tests on Monolithic Two Metal Layer Systems for Research Reactor Fuels"*, Diploma thesis, Technische Universität München, 2010
[21] T. Massalski, B*inary alloy phase diagrams*, ASM International, Ohio, 1996
[22] C.R. Clark et.al, *"Update on Monolithic Fuel Fabrication Methods",* RERTR 2006, Cape Town, South Africa, 2006
[23] M. Cornen et.al., *"Physico-chemical aspects of modified UMo/Alinteraction",* RRFM 2007, Lyons, France, 2007
[24] R.J. Van Thyne et.al, *"Transformation kinetics of Uranium-Molybdenum alloys"* , Transactions American Society for Metals, 49, 588-619, 1957
[25] R.J. Van Thyne et.al, Transformation kinetics of Uranium-Niobium and ternary Uranium-Molybdenum base alloys, Transactions American Society for Metals, 49, 576-597, 1957
[26] R. Jungwirth et.al., *"IRIS-TUM: microstructure of the non-irradiated plates",* RERTR 2010, Lisbon, Portugal, 2010
[27] M.L. Bleiberg et.al, Journal of Applied Physics, 27, 11, 1270—1283, 1956
[28] J.H. Yang et.al, *"Effect of Si in Al and third elements in UMo on interaction layer growth during irradiation - KOMO 4 irradiation test results",* RERTR 2010, Lisbon, Portugal, 2010
[29] S. van den Berghe et.al., *"SELENIUM fuel: surface engineering of UMo fuel particles to optimize fuel performance",* RRFM 2010, Marrakech, Morocco, 2010
[30] KAERI, "*U-Mo powder coating",* IFDWG meeting autumn 2010 in Lisbon, 2010

[31] A. Izhutov et.al.,"*The Status of LEU U-Mo fuel Investigation in the MIR Reactor", RERTR 2009, Bejing, China, 2009*

NEW OPPORTUNITIES FOR ENHANCED RESEARCH REACTOR UTILIZATION THROUGH COALITIONS AND NETWORKS

D. RIDIKAS[1], P. ADELFANG[2], K. ALLDRED[2], M. FERRARI[2]

International Atomic Energy Agency (IAEA)
[1]Division of Physical and Chemical Sciences (NAPC)
[2]Division of Nuclear Fuel Cycle and Waste Technology (NEFW)
Wagramer strasse 5, PO Box 100, 1400 Vienna, Austria

ABSTRACT

This paper will give an overview of the IAEA activities related to research reactor (RR) networks and coalitions during the last two years. Both recent achievements and future planed actions will be reported with the major emphasis on enhanced RR utilization through facilitated access to the neighbouring Member States without RRs, created new capabilities leading to potential revenue generation, revised and implemented strategic and business plans, self-monitoring and self-evaluation using comprehensive performance indicators.

1. Introduction

Given the projected decrease in operational research reactors (RRs) from 239 today to between 100 and 150 by 2020, greater international cooperation and networking will be required to assure broad access to such facilities and their efficient use [1]. These networks will also contribute to upgrading existing facilities, developing new facilities and improving access to countries without RRs. If the benefits from RRs are to be realized, then the premises upon which they are built and operated must be reconsidered and updated to fit today's technical, economic and social situation. In this respect, all aspects of research reactor utilization, strategy and life cycle management should be re-examined.

Although a number of RRs is steadily decreasing, more than half of the operational RRs remain heavily underutilized [2], and in most cases, underfunded. In order to continue to play a key role in the further development of peaceful uses of nuclear technology, the decreasing and rather old fleet of RRs needs to ensure the provision of useful services to the community, in some cases with adequate revenue generation for reliable, safe and secure facility management and operation. In a context of declining governmental financial support and needs for improvement of physical security and core conversion to LEU, many RRs are challenged to generate income to offset increasing operational costs.

Among a number of related efforts, during the last three years the IAEA has been promoting networking, coalitions and regional collaboration to improve the efficient and sustainable utilization of RRs [3]. A number of RR coalitions and networks have been developed with IAEA's support as a new model to better utilize RRs and facilitate access for the Member States without such facilities. The coalition/network concept involves putting in place cooperative arrangements among RR operators, user entities, customers and other stakeholders. Ideally, a strong partnership is formed leading to increased utilization of individual RRs through collective efforts, including improved self-sustainability and self-reliability.

2. RR Coalitions and Networks

The IAEA supported coalitions and networks of RRs continued to enhance cooperation among RR facility managers, existing and potential users and other stakeholders. Five such networks, with shared RR facilities and competencies, collectively offered services to regional and international users, and secured entrepreneurial interest and support for

upgrading existing or for developing new facilities and improving access to countries without RRs. With the Mediterranean Research Reactor Network (MRRN), created in September 2010 in Vienna, presently the efforts of RR Coalitions and Networks involve 35 Member States with RRs (out of 56 with RRs) and 12 Member States without RRs (see Fig. 1 and Table 1 for details).

Figure 1: IAEA supported RR coalitions and networks (also see Table 1).

RR coalition/network	Participating Member Sates	Major joint activities
BRRN – Baltic RR Network	Denmark, Estonia, Finland, Germany, Latvia, Lithuania, Norway, Poland, Russian Federation, Sweden	• Education and training • Irradiation services • Neutron beam applications • Waste and decommissioning issues
CRRC – Caribbean RR Coalition	Colombia, Jamaica, Mexico	• NAA
EARRC – EurAsia RR Coalition	Czech Republic, Hungary, Kazakhstan, Ukraine, USA, Uzbekistan	• Radioisotope production, in particular Mo-99 production via neutron capture
EERRI – Eastern European RR Initiative	Austria, Czech Republic, Hungary, Poland, Romania, Serbia, Slovenia	• Education and training • Radioisotope production • Research and applications using neutron beams • Material irradiation and tests
MRRN – Mediterranean RR Network	Azerbaijan, Bulgaria, Egypt, Greece, Italy, Montenegro, Morocco, Portugal, Slovenia, Syria, Tunisia, Turkey	• Education and training • NAA • Neutron radiography

Table 1: Regional Member State representation and major areas of joint activities of RR coalitions.

In 2010 the above RR coalitions have succeeded to achieve very concrete results with some of the selected examples listed below:

- **EERRI:** In 2010, the EERRI, supported by the Agency, organized the second RR Group Fellowship Training Course to assist Member States interested in initiating their first RR projects. The six-week course, including hands-on experimental

exercises and technical visits to different RRs in Central Europe, provided training on RR utilization and safety, operation and maintenance planning and evaluation, including international cooperation. Two additional courses have already been started earlier this year with the third one scheduled for late 2011.

- **CRRC**: In collaboration with the IAEA, a promotional brochure "CRRC: Partnering for Progress" was prepared and published. This publication introduced some of the key peaceful nuclear based technologies, especially in the areas of analytical element determination, production of radioisotopes, radiation protection, etc. that the CRRC can provide to governmental and commercial customers in the region while working in partnership for progress.
- **EARRC:** Through a number of meetings and expert missions, supported by the IAEA, the EARRC was able to finalize its strategic and business plan, including concrete actions towards commercial production of Mo-99 through neutron capture pathway. Some of the trial target irradiation were made and shipped to the radioisotope reprocessing company in the USA as part of the QA/QC process.
- **MRRN:** under coordination of the IAEA, MRRN has collected most of the partner facility information related to the three major activities of the network. This information will be used to create a comprehensive data base on products and services offered by RR facilities in the region and plan/implement future joint activities such as proficiency tests in NAA and neutron radiography or regional group fellowship course on specific RR related topics.

Creation of the new RR Network in Asia-Pacific region under the umbrella of AONSA (Asia-Oceania Neutron Scattering Association) was recently initiated during the IAEA Consultancy Meeting, held in October 2010 in Republic of Korea with 11 Member States representing this region. In addition, in 2010 ANSTO, Australia, with its state-of-the-art neutron-beam facilities associated with the OPAL RR, was re-designated as an IAEA CC for Neutron Scattering Applications, which will further strengthen the access and help build skills in this region through a variety of mechanisms in contributing to expected improvements in the fields of engineering, health and nutrition, and the environment.

Another initiative for creation of the new RR Network in Central Africa around two small power RRs in Nigeria and Ghana (both 30kW, MNSR-type) will be discussed in detail in the regional meeting, scheduled in July 2011 in Accra. Here major focus will be on joint activities such as education and training and NAA to be offered for the neighboring countries without RR facilities.

In summary, although some noticeable results have been obtained in initiating and supporting RR coalitions, much more work needs to be accomplished in order to achieve the objective of increase utilization of individual RRs through collective effort, on a self-sustainable and self-reliant basis. In addition to their individual strategic plans, the coalition partners need to put into place coalition-based common strategic and management plans as a group. They also need to pursue more detailed market analysis and business development to identify specific pay-back opportunities through sustainable commercial activities, through complementary marketing and delivery of irradiation products and services, education and training among other revenue generating applications of RRs.

3. Concept of RRs as International Centres of Excellence or Regional Hubs

Although a few RR facilities have already been established as regional centres of excellence or global providers of products and services, most RR managers still focus their strategy on the fulfilment of national needs and serve national customers and stakeholders. As a matter of fact, more than half of the world's RRs have very low utilization, and many are challenged to obtain appropriate funding. On the other hand, many countries do not have access to RR services and would certainly take the advantage if a facilitated access to these facilities could be arranged. In this context, there is a clear potential for increased international cooperation

for both existing and new RR projects. This should result in facilitated access to foreign nationals, common research and development programmes on a collaborative or commercial basis and more available financial resources for RRs. In addition, being in close contact with the enlarged user community, a shared RR will better understand its needs and be able to tailor services or develop additional capabilities as user requirements evolve. As a result, RRs with a regional or international perspective have access to a much larger user base and diversified funding opportunities. This can be translated into improved sustainability as well as options for increased capabilities or equipment. Non-host countries that subscribe to such RRs would benefit from access to improved capabilities at lower cost than could be achieved by constructing a national facility. To access these benefits, a number of issues at the technical, financial, regulatory, and intergovernmental levels must be resolved. There is a need to envisage and develop sound mechanisms to share RR facilities between countries regionally and internationally. The forthcoming IAEA Technical Meeting (9-13 May 2011) on "Access and Utilization of RR by non-host Member States" is the first step in defining these issues and developing guidelines for their resolution. This meeting is expected to provide a forum to identify existing good practices with international RR facilities and to collate practical experience with both successes and obstacles to such international cooperation as well as other relevant information through presentations and brainstorming discussions.

Another similar initiative is targeting very high-flux RRs, also as multi-user international facilities but with potentially shared ownership. Indeed, a number of such powerful RRs are expected to be brought into service in the next several years (e.g. CARR-China, PIK-Russia, MYRRHA-Belgium, RJH-France, PALLAS-Belgium, MBIR-Russia). Each of these facilities has the potential to be important international centres of excellence and scientific hubs for cutting edge research and materials investigations, though only few are currently so organized (e.g. ILL in France and HBWR in Norway). The applications of these future research centres include development of proliferation resistant fuel cycles, burning of long-lived actinides from thermal reactor fuels, production of advanced radioisotopes, testing of materials, cross section studies, and studying of advanced reactor concepts and advanced fuels. The benefits of developing an international centre of excellence on the basis of the very high flux RRs are twofold:

1. Such infrastructures are expensive, and they are most effective when they are supported intellectually and financially by the World Community. With multilateral support they may be able to complete the needed studies more quickly and cost effectively, avoiding duplication of R&D investments and fragmentation of scientific effort.
2. Each new well-functioning RR ICE builds confidence in the supra-national approach in which a few well-equipped, well-utilized, well-funded, safe and secure facilities can substitute for many comparatively isolated facilities with low utilization and limited funding challenges.

These issues will be addressed in another IAEA Technical Meeting on "Options for using High Flux Research Reactor Facilities as International Centres of Excellence / Regional Hubs" late 2011. As a result of this event and with the follow up activities through 2012-2013 a dedicated technical document or guidelines will be prepared.

4. Strategic and Business Planning for RRs

RRs are facing increasing pressures to become more commercially responsive and above all to increase utilization of their facilities. Whatever the reasons, there is a need for a change in mind-set from the RR facility just "being available" to taking control of the facility's destiny by pro-actively seeking out new users and applications. Therefore, facility managers need a straightforward and cost-effective approach to both increasing utilization and managing efficiently. In that respect, development and implementation of a strategic and business plan is crucial in order to achieve increased utilization, while helping to create a positive safety culture, a motivated staff, a clear understanding of real costs and a balanced budget. One should keep in mind that the IAEA will only support requests for new facilities or equipment

for RR utilization if they are accompanied by a strategic implementation plan clearly demonstrating that the items requested are necessary to achieve the objectives of the plan.

The need for a strategic and business plan is an inseparable part of the IAEA document under preparation on “Specific Considerations and Milestones for a Research Reactor Project”, where the special emphasis is given to assess the Member State’s own status with regard to justification and resourcing for a RR, and the development of the necessary supporting infrastructure. This publication describes the four phases of the implementation programme, and provides guidance on the timely preparation of a RR project through an easy to understand sequential development process. It includes a detailed description of the range of infrastructure issues that need to be addressed and the expected level of achievement (or milestones) at the end of each phase. The document will enable the Member States to prioritize the activities that they need to order, license, construct and then safely operate a RR. This guidance aims to help them to understand their commitments and obligations associated with the RR programme, and clarifies that the responsibility for safe implementation of a RR project rests with the Member State and its organizations and cannot be subcontracted or avoided. Other organizations such as donors, suppliers, nuclear energy agencies and utility organizations may also find this publication useful as a basis for project assessment and follow up. Such assessments could build confidence that the country has the ability to legislate, regulate, construct, efficiently utilize and manage, safely and securely operate a RR.

The justification, conceptual structure and implementation of the RR strategic plan is also now introduced in the RR group fellowship courses, organized by the IAEA in cooperation with the EERRI, as part of the lecture series given by the IAEA staff. Based on the IAEA-TECDOC-1212 “Strategic Planning for RRs” [4], the IAEA has also developed a specific template with explanatory guidelines to facilitate the creation or revision of such a strategic plan for RR facilities. For example, this material, complemented by expert lectures and training workshops, was used to elaborate strategic and business plans for the new-comer Member States, interested in their first RR projects (e.g. Azerbaijan, Sudan and six GCC Member States). The IAEA also is encouraging periodic revision and update of strategic plan documents of already operational RRs by organizing expert review missions or assignments as it was done in 2010 in the case of RR facilities in Egypt, Ghana, Morocco and Ukraine. Last but not the least, in addition to their individual strategic plans, the RR coalition and network partners need to put into place coalition-based common strategic and management plans as a group. As it was already mentioned above, in 2010 the IAEA has already assisted the EARRC in preparation of their strategic and business plan for radioisotope production and commercialization. Thanks to the active regional IAEA TC projects, similar actions will continue in 2011 both in Europe, Africa and Latin America.

5. Performance Indicators for RR Facilities

As it was mentioned in the previous section, the survivability of many RRs around the world will depend upon the development and implementation of an effective strategic and business plan. To assist in the implementation process, the IAEA has recently proposed a set of performance indicators for RR facilities. The need for self-monitoring and self-evaluation is many-fold with the main objectives to

- Provide quantitative base-line of the actual status of a RR facility
- Monitor the performance of the facility on periodic basis and compare the changes with respect to the base-line or the last year results
- Measure the effectiveness and impact of different actions taken on result-based analysis
- Provide guidance for future actions and direct input in a revised strategic plan.

Presently proposed RR performance indicators include the following main areas to be assessed and monitored:

A. Operation Data – 14 variables (e.g. neutron scattering operation, hours/year)
B. Operation Results – 16 variables (e.g. neutron radiography, number of experiments)
C. Shut-down and Maintenance Data – 9 variables (e.g. number of unscheduled shutdowns)
D. Quality and Safety Control – 16 variables (e.g. number of QA/QC audits)
E. Radioactive Dose Records – 6 variables (e.g. average dose per staff member)
F. Radioactive Discharge Records – 9 variables (e.g. iodine release to atmosphere)
G. Financial Records – 10 variables (e.g. revenue generated from NAA)

It is intended that numerical values of various variables will allow implementing semi-automatic analysis according to pre-designed criteria, which can be based on specific priorities and objectives of each facility.

Certainly, some of the information included in the table of performance indicators will be commercially sensitive and intend for internal use only. Hence it should be stated that the IAEA does not expect public disclosure of the information contained therein. The main purpose here is to assist the Member States to develop sound methodologies for self-monitoring and self-evaluation based on quantitative, periodic and comparative analysis.

6. Summary

RRs have played and continue to play an important role within several fields of basic science, in the development of nuclear science and technology, in the valuable generation of radio-isotopes and other products for various applications, in support of nuclear power programmes, including the development of human resources and skills. Nowadays the decreasing fleet of these facilities faces a number of critical issues and important challenges such as underutilization, inexistent or inappropriate strategic-business plans, ageing and needs for modernization-refurbishment, presence of fresh or spent HEU fuel, unavailability of qualified high-density LEU fuels, accumulation of spent nuclear fuel, advanced decommissioning planning and implementation stages, and, in some cases, safety and security issues. In addition to this non-exhaustive list of challenges are the plans to build new RRs by MSs without no or little experience in this domain. In response to these challenges, the IAEA is taking action and designing activities to tackle these issues and make sure that promotion, support and assistance to MSs in the development and uninterrupted operation of strong, dynamic, sustainable, safe and secure RRs dedicated to peaceful uses of atomic energy and nuclear techniques is preserved. The IAEA's efforts related to the support of RR coalitions and networks, promotion of shared-user and shared-ownership facilities, assistance in preparation and revision of strategic and business plans for RRs as well as help in design and implementation of performance indicators for RRs are only a few examples among other on-going activities to address the issues and challenges RRs are facing world-wide.

7. References

[1] IAEA Project D2.01: Enhanced Utilization and Applications of Research Reactors: http://www-naweb.iaea.org/napc/physics/research_reactors/index.html
[2] D. Ridikas, et al., The IAEA Activities Towards Enhanced Utilization, Sustainability and Applications of Research Reactors, Proceedings of the 14th International Topical Meeting on Research Reactor Fuel Management (RRFM2010), 21-25 March 2010, IAEA, Marrakesh, Morocco; available at http://www.euronuclear.org/meetings/rrfm2010/.
[3] Operational RR Data Base (ORRDB), February 2011; the reader is also advised to bookmark the new IAEA RRDB portal at http://nucleus.iaea.org/RRDB/.
[4] "Strategic Planning for Research Reactors" IAEA-TECDOC-1212 (April 2001).

UTILIZATION OF AGN-201K FOR EDUCATION AND RESEARCH IN KOREA

Myung-Hyun KIM
Department of Nuclear Engineering, Kyung Hee University
KHU Reactor Research and Education Center,
Kiheung, Yongin, Gyeonggi-do, 446-701 Rep. of Korea

ABSTRACT

A zero power reactor, AGN-201K has been operated in Kyung Hee University since 1982 and it was refurbished extensively three years ago. In 2008, Reactor Research & Education Center(RREC) was established for student training and research. The primary mission of RREC is an educational service for nuclear engineering students. Since January 2009, short courses were provided 15 times to 160 students from 7 universities. This course has been an one-week dormitory housing program in the name of Reactor Experiment and was designed as an advanced course customized to undergraduate senior-level. It has introductory session, safety guide session, concluding presentation session with six experiment sessions; reactor operation and control, measurement of period for reactivity, criticality approach, rod worth measurement, measurement of temperature feedback coefficient and thermal flux measurement with neutron activation analysis(NAA).

As a R&D effort for future experimental courses, RREC is now seeking for the possibility of reactor utilization for prompt gamma activation analysis, NAA for material mass spectroscopy, and neutron radiography(NR). A feasibility study on NR was done with MCNP simulation on collimator design and showed that calculated thermal flux level was high enough at the object position even though image size is very small, less than 4 cm diameter.

Research activity has been done for sub-criticality measurement with modified neutron source multiplication method(MNSM). For sub-criticality evaluation with this method, three kinds of the neutron flux distributions such as forward, adjoint, fixed source neutron fluxes, which are solution in both eigenvalue and fixed source problems are needed. These flux distributions were calculated by using PARTISN code systems. Physics conditions are highly dependent on the source locations and rod positions as well as detector positions. Recent results showed that this method improved accuracy in rod worth prediction compared with conventional source multiplication method. As an industrial application of reactor, a feasibility of detector calibration is now being studied in depth. An in-core self powered neutron detector module can be calibrated in the glory hole because accessibility to the core center is high even though rated power level of reactor is very low.

1. Introduction

Since 1982, a zero power reactor AGN-201K has been operated in Kyung Hee University for student education with rated power of 0.1 wt. Because of obsolescence of control system, an extensive refurbishment was carried out during the period of 2004 through 2007.[1] Reactor power was up-rated by 100 times and an old analog-type operational console and I&C parts were replaced. Additional shielding walls and a new digital-type console were also installed. The average thermal flux at the glory hole becomes high to 3.0×10^8#/cm^2-sec. Core is a simple cylindrical shape with 9 homogeneous fuel disks made of 19.5w/o UO_2

powders and polyethylene. There is a 1 inch diameter glory hole penetrating the core central zone which is utilized for neutron activation. There are 4 beam ports (8 in total in both direction) which penetrate a 20cm-thick graphite reflector zone outside of core. Reflector zone is surrounded by 10cm-thick lead for gamma shield and 55cm-thick water for neutron shield. Safety against nuclear transients and hypothetical radiation accidents was proved by accident analysis. [2] In 2008, Reactor Research & Education Center(RREC) was established for student training and research. This paper summarized recent accomplishments both in research and education including current activities and future plans for the maximization of reactor utilization.

2. Utilization of AGN-201K for Education

After a decommissioning of TRIGA Mark-II in Korea Atomic Energy Research Institute (KAERI), HANARO and AGN-201K became last two research reactors available for training and education. However, HANARO in KAERI has given too many restrictions in access to students. Reactor experiment course as one of requisite subjects had not been served to nuclear engineering students since 1996. In the period of 2003 through 2008, therefore, selected number of students were sent to Kyoto University Critical Assembly in Reactor Research Institute, Osaka every year for 10 days experimental training. This activity was an excellent example of international collaboration in education between Japan and Korea. In 2008, Kyung Hee University, Reactor Research & Education Center(RREC) was established as a national-wide student training center. One-week short courses were provided to public as dormitory-housing programs.

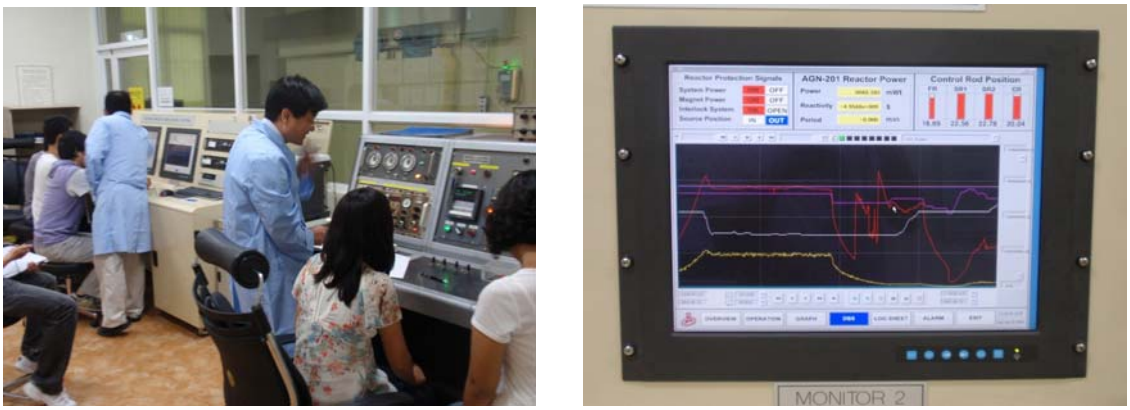

Fig 1. Two reactor consoles (left) and an operational database display in a digital console (right)

The following Table 1 showed a recent achievement in education service. Through 15 times courses, there has been 160 participants. 131 students from 7 outside universities and 18 students from inside completed through 14 courses. One course was served for 11 HANARO operators as continuing education program. Two courses were proceeded in English. Before every experiment one hour lectures were given for background knowledge, and all students should submit reports for all experiment. At the last day, presentation session was arranged for further discussion.

	Education Period	Participants	Number of Trainee
1	Jan. 19-23, 2009	Chosun University UG students	8
2	Feb. 2-6, 2009	Seoul National University UG students & Kyung Hee University Graduate students	6
3	Feb. 16-20, 2009	Jeju National University UG students	13
4	Apr. 27- May 1, 2009	Hanyang University UG students	24
5	Jun 22-26, 2009	KAIST Graduate students	12
6	July 6-10, 2009	KAERI HANARO operators	11
7	Sep.-Nov., 2009	Kyung Hee University UG & Graduate students	11
8	Jan. 27-Feb.2, 2010	Jeju National University UG students & KAIST Graduate student	11
9	Feb.3-9, 2010	Chosun University UG students	12
10	Feb.17-23, 2010	Dongguk University UG students	8
11	Nov.1-5, 2010	Hanyang University UG students	8
12	Sep.-Nov., 2010	Kyung Hee University UG & Graduate students	6
13	Jan.26-Feb.1, 2011	Chosun University UG students & Dankuk University UG student	9
14	Feb.9-15, 2011	Dongguk University UG students	12
15	Feb.16-22, 2011	Jeju National University UG students	9
		total	160

Table 1: Education Record of Short Course - Reactor Experiment

Table 2 summarized the contents of six experiments. At the first day, experiment-1 was given in the afternoon after the introductory session in the morning. This experiment is designed to confirm that reactor have the same control rod position for criticality at different power level. In this experiment, students can operate with two control rod under the supervision of reactor operator. At the day-2, two experiments were performed with busy schedule. Experiment-2 is designed to compare three methods of period measurement from power transient. Least square data fitting and statistical evaluation method were compared with a simple method of two point evaluation. Experiment-3 is a conventional criticality approach based on inverse multiplication. Plot of inverse multiplication for the rod position change was made and interpreted as an estimation of U-235 critical mass by extrapolation technique. At the third day, in an experiment-4 measurement of control rod worth was performed in three techniques; the positive period method for a fine control rod, the compensation method using fine control rod and coarse control rod, and the rod drop experiment applying prompt drop approximation. At the fourth day, experiment-5 was carried out at Monday after the weekend for neutron activation analysis. Gold wire was irradiated on Saturday morning and cooled down through weekend. HP Ge detector was used for absolute activity measurement of irradiated gold samples. Neutron flux distributions in fast and thermal groups were solved with measured cadmium ratios. The last experiment is a measurement of isothermal temperature coefficient with calculated rod worth curve obtained from experiment-4. Replacement of thermal column was done from water to graphite and a reflector effect was measured in core reactivity change.

	Title of Experiments	Activity Goals
1	Understanding RRs & AGN-201K, Reactor Operation Practice	Relation between criticality & power level
2	Measurement of Reactor Period	Handling of measurement errors, Calculation of reactivity with Inhour eq.
3	Critical Mass Approach Experiment	Experiment for subcriticality measurement
4	Control Rod Calibration	Period measurement method, Rod swap method, Rod drop method
5	Thermal Flux Measurement	Au Foil NAA, Evaluation of Cd ratio, MCA counting with HPGe Detector
6	Reflector & Temperature Feedback Effect	Predict the change of reactivity

Table 2: Course Contents of Reactor Experiment

3. Feasibility of AGN-201K for Industrial Services

Because AGN-201K was introduced as an educational reactor, the maximum thermal flux in a glory hole is less than 1E+09 at the maximum power. This level is known to be too small for an industrial application. For a limited application, a feasibility study has been done for AGN-201K including prompt gamma activation analysis.

Although neutron radiography facility is generally installed only at high-flux research reactors, the feasibility of thermal column in AGN-201K was evaluated by using MCNP code. Specially, thermal flux level at the exit of beam line through collimator was evaluated in order to check its feasibility for NRF. Figure 2 shows the cross sectional view of reactor module. The upper part of the core is a thermal column which can be removed. [3]

3.1 AGN-201K Reactor Modeling

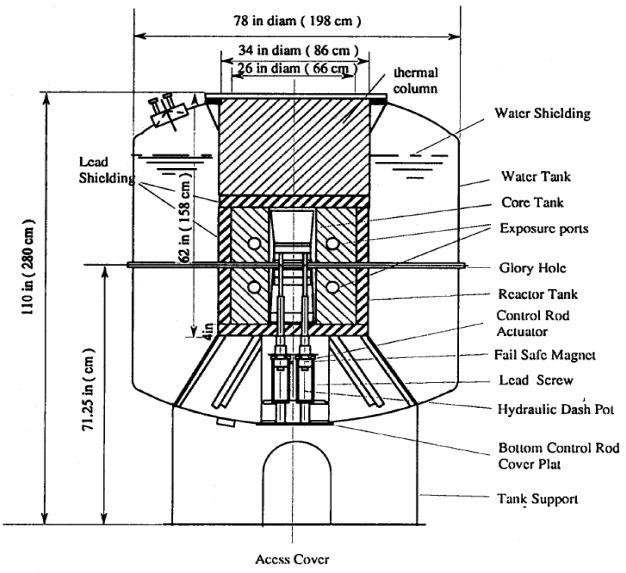

Fig 2. Structure of AGN-201K Reactor

In order to design a collimator for neutron radiography facility, the whole reactor system of AGN-201K was modeled for MCNP code. The following figures show an example of 3-D geometrical model including outside space. Numerical model was compared with experimental data of thermal neutron flux at several locations in glory hole and beam ports. Calculated data from MCNP showed less than 10% error in core region and maximum 20% error at the outer boundary.

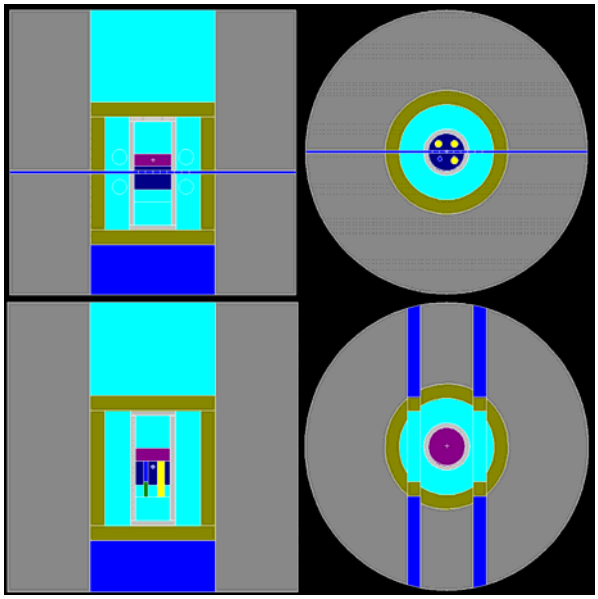

Fig 3. AGN-201K model for MCNP code

3.2 Collimator Design and Evaluation

One of the most important parts of a neutron radiography(NR) facility is the collimator which produce leveled neutron beam. The Collimator characteristics are closely related with resolution and exposure time, that depend on the shape and size of collimator. The idea about the choice of the best shape of the collimator have been changed rapidly with the development of the relatively recent nondestructive technique, as is neutron radiography. In the early years of application of NR, the opinion prevailed that parallel beams of neutrons were needed to obtain an adequate neutron beam flux at the object to be radio-graphed. However, as in early 1967, Barton concluded that a divergent-beam collimator produced the highest resolution. [4]

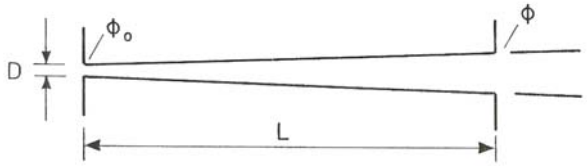

Fig 4. Divergent Beam Collimator

The minimum thermal neutron flux of object needed in NR is about 1.0×10^{5}#/㎠-sec. Based on the formula, the thermal neutron flux is 2.0×10^{8}#/㎠-sec at the entrance of collimator where the collimator ratio cannot exceed more than about 15. In other words, collimator is determined by the length 30cm. Collimator was modeled to be filled with filling gas of helium, after comparison between He and air. For a lining material on the collimator wall was chosen as B_4C (Boron Carbide), after comparison of beam quantity and shape with different material, aluminum, gadolinium and B_4C. The thickness of lining is chosen to be 5mm. Distance from collimator exit to object is 2 cm. Table 3 shows the geometrical design data for collimator and Fig. 5 shows layout of collimator above the core. Fig. 6 shows calculated thermal neutron flux distribution across the object line. Calculated thermal flux level was high enough at the object position even though image size is very small, less than 4 cm diameter.

Entrance Diameter	20 mm
Exit Diameter	34 mm
Collimator Length	300 mm
Collimator Ratio	15

Table 3: Dimension of Divergent Beam Collimator

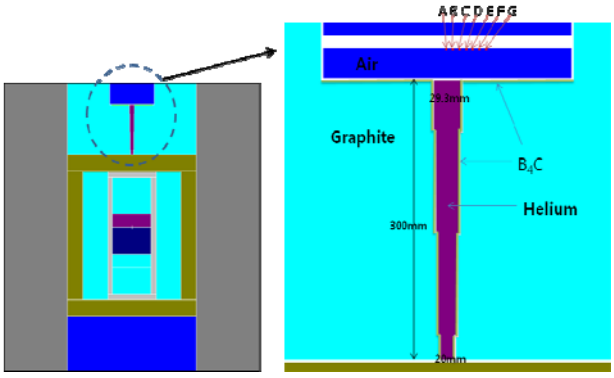

Fig 5. Collimator Design for AGN-201K

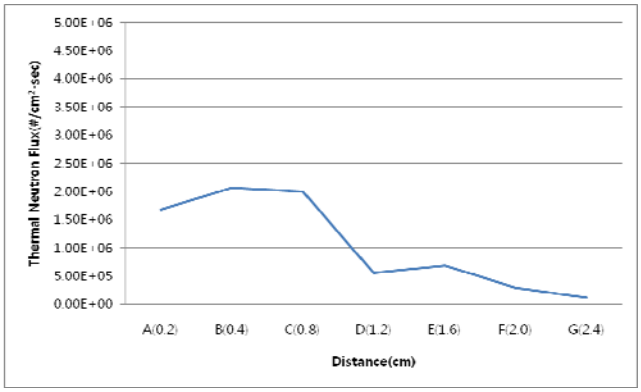

Fig 6. Thermal Neutron Flux Distribution

3.3 Detector Calibration Services

Even though flux level is too small for NAA & NR, AGN-201K has some advantages compared with large-sized research reactors. This reactor is dry itself because there is no coolant in the core zone. There is a high accessibility near to the core. Therefore reasonable flux level can be achieved near to the core compensating low-power core limitation. Neutron detector for ex-core detector system and self-powered neutron detector(SPND) for in-core detector system are now manufactured in Korea. Now there is a demand for detector test and calibration with nuclear reactors. AGN-201K has a high feasibility in this application. There is a scheduled plan to test detector modules in AGN-201K based on requests from domestic companies.

4. Research Application in Subcriticality Measurement

Modified Neutron Source Multiplication method (MNSM)[5] was verified by the various experiments in AGN-201K. This method was tested by computational simulation at Kyung Hee University in 2006. In order to calculate correction factors, reactor analysis code system should be set up for the calculation of neutron fluxes and adjoint fluxes. In 2006, PARTISN code and multi-group cross-section library, ZZ-KASHIL199N was established and validated by the comparison with MCNP.[6] In this study, calculation module for correction factors was invented by using the FORTRAN77 language to handle massive data of flux output from PARTISN code. In addition, the investigation of the correction factor effectiveness was done with various reactor experimental data.

4.1 PARTISN Code Modeling

In a previous study in 2006, PARTISN and ZZ-KASHIL-199N was chosen after a verification study in which results of PARTISN were compared with MCNP and DANTSYS for AGN-201K. PARTISN is a time-dependent, parallel processing, neutron transport calculation code developed at Los Alamos National Laboratory as a expanded version of DANTSYS. ZZ-KASHIL-199N library is a library (of 199-groups for total and 35 groups for thermal) developed for HELIOS code for LWR applications. was chosen to be the best. [7]

The following Fig.7 is a cross-sectional view of AGN-201K and its PARTISN calculation model. Because of complex configuration, an approximate model was established where cylindrical control rod was approximated as a volume equivalent cylindrical node pieces. Total lengths were divided into 31 nodes in R-direction, 10 nodes in theta-direction, 66 nodes in Z-direction.

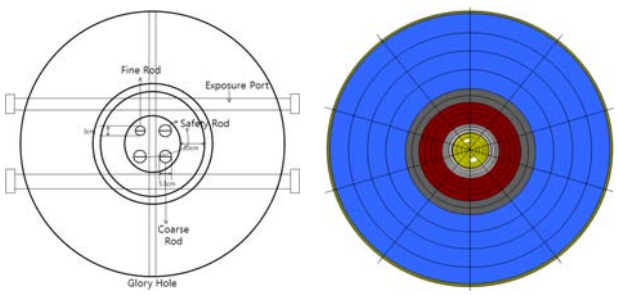

Fig 7. Calculation Mesh for PARTISN

4.2 Calculation of Correction Factors

There have been several methods for measurement of sub-criticality. Neutron source multiplication method(NSM) is an practical method among them. However, this method does not predict an absolute value of certain reactivity. This method always shows relative change of reactivity from a reference state. The NSM method is defined as follows:

$$\rho_n = \rho_{ref}\left(\frac{M_{ref}}{M_n}\right) \qquad (1)$$

where, M_{ref} and M_n are defined as count rate of each reference subcritical state and n-th subcritical state. In other to correct the NSM, MNSM method was proposed by Hokkaido university in Japan several years ago. The MNSM method is defined as follows:

$$\rho_n = \rho_{ref}\left(\frac{M_{ref}}{M_n}\right)C_n^{ext}C_n^{sp}C_n^{im} \qquad (2)$$

where, C_n^{ext} is an extraction correction factor which is defined as a ratio of fundamental mode extraction of reference state to n-state. C_n^{im} is an importance field correction factor which is defined as a ratio of importance weighted source intensity of n-state to reference-state. C_n^{sp} is a spatial correction factor which is defined as a ratio of detector signal from fundamental mode flux of n-state to reference-state. Those three correction factors are defined as ratios of weighted integral sum of eigenvalue fluxes or fixed source fluxes. In this problem weighting has been done by adjoint fluxes. Therefore, for each state of sub-criticality where control rod position are different, eigenvalue multi-group diffusion problems should be solved for normalized real fluxes and normalized adjoint fluxes. For each sub-criticality state, fixed source problems should be also solved for normalized fixed source fluxes. Therefore three kinds of problems should be solved in advance for all kinds of reactor conditions in order to solve three kinds of fluxes. These three kinds of fluxes should be put into formula for three correction factors as a energy-group weighted integrals as well as spatial node-volume adjoint-weighted integrals. At each reactor condition-n, three correction factors C_n^{ext}, C_n^{im}, C_n^{sp} are calculated as a ratio to the reference state.

4.3 Measurement of Sub-criticality

In order to test the correction factor effectiveness, various reactor conditions were tested by six kinds of experiments. Figure 8 shows condition of reactor experiment and Table 4 shows that reactor experiments are classified based on source and detector position.

CASE	Reactor experimental conditions	
s0c0	Reference	Source : Core center location Detector : NE position
s1c0	Source point changes	At Core boundary
s2c0		At Core boundary
s0c1	Detector point changes	At SE Reflector position
s0c2		At SW Reflector position
s0c3		At NW Outside position

Table 4: Experimental Test Cases

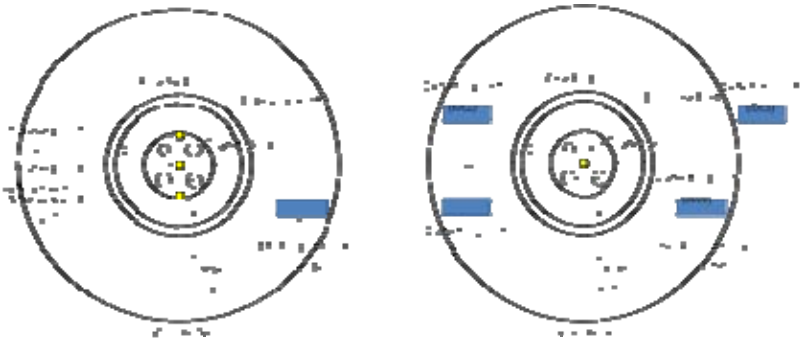

Fig 8. Experimental Cases of Different Source & Detector Positions

In this study, MNSM method was estimated through AGN-201K reactor experiments. To know the effect of correction, it were compared NSM and MNSM method as integral reactivity of respectively subcritical state. Figure 9 shows the result compare NSM and MNSM method as different detector position. And Figure 10 shows the result comparison of NSM and MNSM method as different source position.

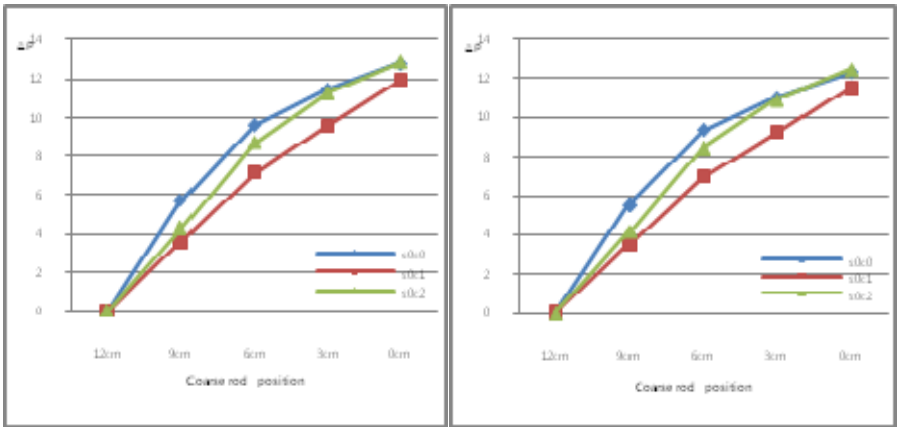

Fig 9. Comparison of integral reactivity for different detector position
(the left: NSM, the right: MNSM)

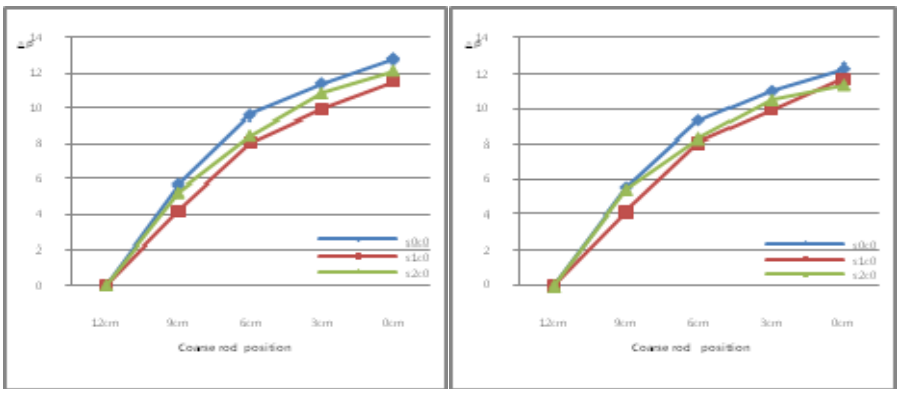

Fig 10. Comparison of integral reactivity for different source position
(the left: NSM, the right: MNSM)

From Fig. 9, it was found that there is no correction effect following the detector position. Even though detector positions were different at each case, the distance from source to detector was the same in this experiment. Therefore correction effect was not shown. However, from Fig. 10 there was a correction effect for the source location changes. At this cases, distant from source to detector were different at each case.

5. Conclusion

Currently utilization of AGN-201K is active only for national-wide education for reactor experiment. However, a feasibility to NAA and NR is now studied for research. The use of reactor for detector calibration is now under way for industrial service.
The use of reactor for research in sub-criticality measurement was successfully done even though research itself did not show a big progress.

References

[1] Myung-Hyun Kim, "Reactor Upgrade of AGN-201 in KHU, Korea," Research Reactor Fuel Management(RRFM-2008), Hamburg, Germany, March 2-6, (2008)
[2] J.Y Lim, M.H.Kim, “Evaluation of Occupational Exposure Dose under a Hypothetical Radiational Severe Accidents of AGN-201K,” HANARO Symposium 2007, Daejon, May 4, (2007)
[3] Charles D. Harmon, Robert D. Busch, Criticality Calculations with MCNP: A Primer, Los Alamos National Laboratory, New Mexico, USA, 1994.
[4] Development of the Neutron Radiography Facility and its Installation in HANARO, KAERI/TR-1981, Deajeon, Korea, 2001.
[5] M. Tsuji, et. al., "Subcriticality Measurement by Neutron Source Multiplication Method with a Fundamental Mode Extraction," J. Nucl. Sci. and Tech., vol. 40, 158-169 (2003)
[6] R. E. Alcouffe, et. al., "PARTISN: A Time-dependent, Parallel Neutral Particle Transport Code System," LA-UR-05-3925, Los Alamos National Laboratory (2005)
[7] C. S. Gil, "KASHILL199N: A Multi-group Library for Thermal Reactor Design and Analysis Based on ENDF/B-Ⅵ," Korea Atomic Energy Research Institute (2005)

Education and Training Programme at the Research Reactor TRIGA Mainz

GABRIELE HAMPEL, KLAUS EBERHARDT

University of Mainz, Institute for Nuclear Chemistry,
D-55099 Mainz, Germany

Abstract

Education and training are important elements for the future of nuclear science, technology and safety. Fields of interest include high-technology applications in nuclear techniques and neutron sources, advances in the areas of power reactor safety, establishing the scientific basis of new reactors, training of personnel needed to operate, maintain, regulate and improve reactors or other facilities associated with nuclear power. Also, creating a knowledgeable public through education usually means less opposition and more support.
Education and training for safeguards, operators, researchers and quality programmes (calibration services, etc.) are one of the main utilisations of TRIGA research reactors. Use of a reactor as a training tool for university students studying nuclear engineering and/or physics, where there is a growing demand at European Universities, is of vital importance. In particular, the TRIGA Mark II reactor, located at the University of Mainz, one of the largest universities in Germany, offers a broad range of nuclear-related courses for training and education.

Introduction

Reseach and training reactors deliver important elements in nuclear science technology, education, training and research infrastructures. Training of personnel is needed to operate, maintain, regulate and improve reactors and other facilities associated with nuclear power activities, and to manage and direct nuclear technology's development and nuclear science research. The basis for advances in power reactor safety and for new reactor designs is well-educated scientists and engineers. Development of high-technology applications in fields such as materials science, fluid dynamics and biomedical science, where neutron sources are needed, can profit through utilisation of research reactors. Due to the dismantling of power and research reactors, radiation protection and knowledge in the handling of radioactivity material becomes even more important.

Due to a decreasing number of students taking nuclear subjects in recent years, the lack of young nuclear scientists, technicians and engineers to replace retiring staff and ageing research reactor facilities being closed and often not replaced, the future of TRIGA reactors which offer excellent training and education possiblities is becoming more and more unsure, especially, as announced recently, there could be a loss in the supply of TRIGA fuel in the coming years.

The Johannes Gutenberg-Universität Mainz, Germany, with about 35,000 students from more than 130 nations, hosts on its campus the research reactor, TRIGA II, which is used intensively for education and training. The reactor can be operated in the steady-state mode with thermal powers up to a maximum of 100 kW and in the pulse mode with a maximum

peak power of 250 MW. To date, more than 17,000 pulses have been performed. When taking into account past and future operation schedules and the typically low burn-up of TRIGA fuel elements (~4g ^{235}U/a for an operation at a power of 100 kW), the reactor can be operated for at least another decade. Due to its utilisation, the TRIGA Mainz will be in operation until at least 2020. For irradiations, the reactor has a central experimental tube, three pneumatic transfer systems and a rotary specimen rack. In addition, four horizontal beam ports and a graphite thermal column, which provides a source of well-thermalised neutrons, are available. Isotope production and Neutron Activation Analysis (NAA) are applied in in-core positions for different applications. A broad spectrum of scientific research and commercial applications are executed [1]. For education and training, various courses in nuclear and radiochemistry, radiation protection, reactor operation and physics are held at the Mainz reactor for scientists, advanced students, teachers, engineers and technicians.

Reactor operation and reactor physics

This course consists of lectures in reactor physics and practical training in reactor operation at steady state power and in the pulse mode. The course focusses on the understanding of the general behaviour of a nuclear reactor. The main objective is to introduce the basics of reactor operation, reactor techniques and physics in practical examples at a research reactor. The participants receive practical experience in operation of a nuclear reactor. The main part of the course includes:

- daily and monthly inspections at the reactor,
- operation of the reactor in the steady state mode,
- reactor pulses with different reactivity insertion,
- neutron flux measurements at different irradiation positions,
- the influence of test samples, such as Cd, to the reactor operation,
- calibration of the control rods,
- fuel inspections,
- function and sensitivity of the compensated ion chamber,
- reactivity measurements and
- error diagnostics.

A complete course is executed in 5 days. The groups are small with the number of participants between 8 and 10 to assure an optimal mentoring. In 2010, the course took place 4 times, two times for students in physics or chemistry of the University of Mainz and two times for the staff of the company AREVA. In 2008, a special 2 weeks reactor Training Course for the University of South Carolina was carried out which included also a lecture at the Mainzer Microton (MAMI) of the physics department of the University of Mainz and a visit to the accelerator at GSI Darmstadt. Due to the success of the course, it will be repeated both as a training course and expanded as an exchange programme between students of both universities.

The requirements for participation on the reactor operation and reactor physics courses are basic theoretical knowledge in nuclear physics, nuclear reactions, fission reactions, production of neutrons, cross sections, chain reaction, moderation, critical size, neutron life cycle and reactor design. The students should have had lessons in Nuclear Chemistry and should have finished the training course in Nuclear Chemistry I.

Every participant receives a printed booklte on the theoretical background, the requirements for the experiments, the experimental procedures, tables for measured values and a description for the analysis and reporting.

Among the most popular experiments is “the reactor pulses with different reactivity insertion”, which can be carried out at TRIGA reactors. Due to the unique characteristics of the Zr-H

moderator used in TRIGA fuel, one can withdraw a control rod completely and suddenly from the critical core. Any other reactor would be severely damaged by this operation, which can be performed routinely at the TRIGA and results in a power pulse or power burst. The property of the Zr-H moderator that makes this possible is that the H-atoms form oscillations around its lattice position. The energy of these oscillations is quantifed similarly to a three-dimensional harmonic oscillator (Einstein oscillator). Incident neutrons are moderated and are then in thermal equilibrium with these atoms. During a power burst, the fuel temperature rises and therefore, the population at higher oscillation energy levels of the moderator atoms increases, thus reducing the moderating effect of the neutrons. The neutrons may even be accelerated by the collisions with the H-atoms and the thermal neutron spectrum is hardened. Therefore, the number of fissions and the reactor power is decreased. The whole procedure takes about 3 ms while the peak power increases to 250 MW.

In the experiment, the reactor power is raised to 50 W moving the shim rod and the regulating rod, the pulse rod stays in its lower position. After switching the control instrumentation to "pulse mode", the pulse rod (maximum reactivity value ~ 2 $!) shoots out of the critical core and the power pulse takes place. The power peak value can be varied by changing the shock absorber position which determines how far the pulse rod is shot out from the core and then determines the amount of reactivity inserted into the critical core. During and after the pulse, the fuel element temperature and maximum power and energy of the pulse can be read from the instrumentation. The procedure may be repeated with the following shock absorber positions: 2 $, 1.75 $, 1.5 $ and 1.25 $. The gamma- and neutron dose rates are measured during the pulse at the platform.

The Cd experiment demonstrates that the reactivity of the reactor can change during operation and be influenced by the samples which are irradiated in the reactor. In this experiment, the effect of different Cd samples which are positioned in a polyethylene capsule is measured. The first samples are empty PE capsule; the second ones, a Cd plate with a mass of 2.9 g and a thickness of 1 mm; the third, two Cd plates on top of each other, each with a mass of 2.9 g; and the fourth, a Cd plate with a mass of 5.8 g and a thickness of 1 mm and at least 5.5 g Cd as acetate. Cd has a high capture cross section for thermal neutrons, σ_{Cd} = 2450 barn. The reactor is operated at a power level of 10 W for a period of 30 s. The changes of the reactivity are determined using the regulating rod calibrations and the results discussed.

Nuclear Chemistry I

In addition to the course “Reactor operation and reactor physics”, a course “Nuclear Chemistry I”, is carried out at the Institute of Nuclear Chemistry. It is based on the course “Experimental Radiochemistry (Praktische Radiochemie)” given in the past by Otto Hahn in Berlin at the Kaiser Wilhelm Institut to teach his students in the handling of radioisotopes. After the foundation of the University of Mainz, this course was established by Fritz Strassmann at the, then, Institute of Anorganic Chemistry (today Institute of Nuclear Chemistry).

The training course is focused on students of chemistry and physics of the 7th semester. It is executed 4 times a year. Each course is two weeks, for a maximum of 18 participants. The course teaches the basics of nuclear chemistry, nuclear physics and radiation protection, as well as the handling of radioactive material, radiochemical preparations and analysis, and the technology to detect radioactive irradiation. Requirements for participation on the course is a certificate of successful attendance at the lecture “Introduction of Nuclear Chemistry”[2]. Each day has its own subject:

- production and measurement of radioactive isotopes produced at the reactor,
- decay and production of isotopes, balance of mother – daughter isotopes,

- the alpha decay,
- the biological effect of radiation and radiation protection,
- experiments for gamma radiation, gamma-spectroscopy,
- beta-decay, utilisation of semiconductor detectors,
- nuclear reactions with neutrons,
- nuclear fission,
- utilisation of radioisotopes, and
- transuranium – the chemistry of neptunium (element 93)

Nuclear Chemistry II

This training course is focussed on research and takes 4 weeks. The participants work in the research groups of the institute under the guidance of a PhD student. The offered subjects depend on the actual situation of the institute.

A course in the NAA has the aim to demonstrate the capabilities of this method for trace analysis of various materials. At the moment, the NAA at the TRIGA Mainz is focused to determine trace elements in different materials belonging to projects in archaeometry, forensics and semiconductors for photovoltaics. The beam ports and the thermal column of the TRIGA Mainz are used for special basic and applied research in medicine, biology, chemistry and physics. Experiments are in preparation to determine the fundamental neutron properties with very high precision using ultra cold neutrons (UCN) produced at the tangential beam port. A second source is under development at the radial piercing beam port. Another experiment under development is the determination of ground-state properties of radioactive nuclei with very high precision using a penning trap and collinear laser spectroscopy. For many years fast chemical separation procedures combining a gas-jet transport system installed in one beam tube with either continuous or discontinuous chemical separation are carried out. In addition the thermal column of the reactor is also used for medical and biological experiments: A project is in progress where patients with liver metastases will be treated, similar to the successful application at the TRIGA reactor in Pavia (Italy). Also cell cultures are irradiated in the thermal column at different neuron fluxes. All these experiments are part of 4-weeks training course in Nuclear Chemistry II [3].

Radiation Protection

Education and training courses in radiation protection are offered for technicians, teachers, students and the fire brigade. Every year courses to receive knowledge in radiation protection are carried out following the requirements of the German Radiation Protection Decree. The experimental programme includes measurements of the neutron- and γ-dose rates at the biological shield and at the near-surface reactor pool. The reactor is operated at different power levels from a few Watts to 100 kW_{th} with dose rate monitoring as a function of reactor power.

For the education and training of students at school, teachers and young scientists, the TRIGA Mainz is working together with the German-Swiss Association of Radiation Protection. Different support programmes are held to advance the knowledge of the young generation and to motivate them to undertake tasks in radiation protection and nuclear field activities [4].

Summary

Education and training is and will be even more so, the main utilisation of the TRIGA Mainz for engineers and technicians, teachers, researchers and especially, as a training tool for university students studying nuclear engineering and/or physics, where there is a growing demand today. Various courses in reactor operation and physics, nuclear and radiochemistry and radiation protection are held. The courses are open for participants of external institutions and companies.

Research reactors, such as TRIGAs, are necessary to fullfill the requirements for nuclear education and training. They provide very useful training to students or researchers in neutron and radiation technologies and engineering education, and they provide powerful tools for the advancement of other academic disciplines.

The training of nuclear personnel, as conducted currently in many TRIGA facilities, is an important contribution not only to the peaceful use of nuclear technologies but to worldwide nuclear safety in general. More significantly, the education and training programmes of TRIGA reactors can have a long term, substantial and sustainable effect on today's anticipated nuclear renaissance.

References

[1] G. Hampel, K. Eberhardt, N. Trautmann, "The Research Reactor TRIGA Mainz", International Journal for Nuclear Power, atw 5 (2006), ISSN 1431-5254
[2] Skript zum Kernchemischen Praktikum I, Institut für Kernchemie, Universität Mainz, 10. Auflage (2000)
[3] G. Hampel, K. Eberhardt, "Utilisation of the Research Reactor TRIGA Mainz", IAEA document in preparation
[4] http://www.fs-ev.de

BIOLOGICAL TESTS FOR BORON NEUTRON CAPTURE THERAPY RESEARCH AT THE TRIGA MARK II REACTOR IN PAVIA

N. PROTTI[1,2], F. BALLARINI[1,2], S. BORTOLUSSI[1,2], P. BRUSCHI[1], A. DE BARI[1,2], S. STELLA[1,2], S. ALTIERI[1,2]

[1] *Department of Nuclear and Theoretical Physics, University of Pavia*
via Bassi 6, 27100 Pavia, Italy
[2] *Nuclear Physics National Institute (INFN), section of Pavia*
via Bassi 6, 27100 Pavia, Italy

J.G. BAKEINE[3], L. CANSOLINO[3], A.M. CLERICI[3], C. ZONTA[3], C. FERRARI[3]
[3] *Laboratory of Experimental Surgery, Department of Surgery, University of Pavia, via Ferrata 9, 27100, Pavia, Italy*

V. CONTE[4], J. ESPOSITO[4], L. DE NARDO[5], D. MORO[5], C. FABRIS[6], M. SONCIN[6], P. COLAUTTI[4], G. JORI[6]
[4] *Nuclear Physics National Institute (INFN), Legnaro National Laboratories (LNL), viale dell'Università 2, 35020 Legnaro, Padova*
[5] *Department of Physics "Galileo Galilei", University of Padova, via Marzolo 8, 35121 Padova*
[6] *Department of Biology, University of Padova, via Bassi 58B, 35121 Padova*

S. GENINATTI CRICH[7], D. ALBERTI[7], S. AIME[7]
[7] *Chemistry Department, University of Torino*
via Nizza 52, 10126 Torino, Italy

ABSTRACT

The thermal column of the TRIGA Mark II reactor of the Pavia University is used as an irradiation facility to perform biological tests and irradiations of living systems for Boron Neutron Capture Therapy (BNCT) research. The suitability of the facility has been ensured by studying the neutron flux and the photon background in the irradiation chamber inside the thermal column. This characterization has been realized both by flux and dose measurements as well as by Monte Carlo simulations [1,2,3]. The routine irradiations concern *in vitro* cells cultures and different tumor animal models to test the efficacy of the BNCT treatment. Some results about these experiments will be described.

1. Introduction

Boron Neutron Capture Therapy (BNCT) is a binary radiotherapy which exploits the synergistic action of a low energy neutron beam and the ^{10}B stable isotope of boron. The tumour is first enriched with ^{10}B thanks to a dedicated molecule which is injected in the blood stream. Then the tumour is irradiated with an external neutron beam. If the energy of the neutron is around 25 meV then the $^{10}B(n,\alpha)^{7}Li$ neutron capture reaction is highly probable (σ=3840 barns). The advantageous features of this reaction are: 1) almost the whole energy (≈ 2.8 MeV) is deposited locally thanks to the charged secondary particles; 2) the ranges of the α-particle and the ^{7}Li ion are of the same order of magnitude of the mean cell diameter (≈ 10 μm). As a consequence, the effect of the irradiation is confined to the single ^{10}B loaded cell: this is the cellular level selectivity peculiar of the BNCT treatment. At the University of Pavia (Italy), an innovative treatment which combined auto-transplantation surgery and BNCT was developed thanks to the thermal column of the T.R.I.G.A. Mark II reactor of the L.E.N.A. laboratory [4]. An isolated organ (a human liver affected by colon adenocarcinoma metastases) was irradiated in the thermal neutron field after being enriched by ^{10}B. Between 2001 and 2003, two patients have been treated by this procedure. In both cases the efficacy of the treatment was clearly demonstrated. The original structure of the T.R.I.G.A. thermal column was modified; in particular, an irradiation chamber of about 40*20*100 cm^3 has been realized inside the column, at about 130 cm from the centre of the core. This chamber is characterized by: 1) a highly uniform thermal neutron flux [1]; 2) a low photon background. Thanks to these characteristics, the irradiation chamber is suitable for a variety of biological tests as well as for prominent studies the BNCT research.

Since the selectivity of BNCT depends on the ^{10}B microscopic distribution, at the Pavia reactor two techniques for ^{10}B quantification have been developed and are nowadays routinely used: α-spectroscopy [5] and neutron autoradiography [6]. Cell culture suspensions are irradiated at different reactor powers to study the efficacy of the BNCT treatment by the survival curve method [7]. To work in a more tissue-like condition, adherent cell cultures will be irradiated in their native Petri flask. The flux uniformity, the mean absorbed dose in the cell layer as well as the mutual effects of the flasks in a multi-flask irradiation set-up were estimated by the Monte Carlo simulations. The suitability of the irradiation chamber as a small animal BNCT-facility has been evaluated both by Monte Carlo calculation and by some preliminary *in vivo* tests.

2.1 Material and methods

In vitro studies

To perform the radiobiological tests, the DHDK12TRb (DHD) colon adenocarcinoma tumour cell line is used. The ^{10}B carrier is the ^{10}BPA-f complex; the cell enrichment is generally obtained from a medium concentration of 80 ppm. Just before irradiation, the ^{10}B enriched medium is removed and a clean one is added. Cell survival is determined by the plating efficiency method. Knowing the absorbed dose received by the cells, it is possible to plot the survival curve. At the moment of the irradiation a cell sample is deposited on a mylar support to get the ^{10}B concentration by the α-spectrometry technique.

In vivo studies

The efficacy of lung BNCT is evaluated. Two animal models are used. 1) $2 \cdot 10^7$ DHD cells are injected intravenously in singenic BD-IX rats; after 10-12 days the tumour is spread in the lungs. 2) lung metastases are induced by the B16F1 tumour cell line (pigmented variant of murine melanoma B16); 10^5-10^6 cells are injected intravenously in C57BL/6 mice; after 14 days the lungs are invaded by the metastases. In both models, the ^{10}B carrier is the ^{10}BPA-f complex and the ^{10}B enrichment is due to a ^{10}BPA-f intra-peritoneal injection (300mg/kg). A pharmacokinetics study is ongoing to determine the ^{10}B distribution in both models. At varying intervals after ^{10}BPA-f infusion, the animals are sacrificed and their organs are collected and frozen in liquid nitrogen. Thin samples of the tissues and of the tumour are analyzed by the α-spectrometry technique to determine the ^{10}B content .

In collaboration with the University of Torino, the feasibility of BNCT mediated by the original adduct Gd/B/LDL [8] is evaluated in a melanoma model. 10^6 B16F10 cells are injected subcutaneously in the back-neck region of C57-BL6 mice; after 7 days a macroscopic localized tumour is present. The ^{10}B enrichment is due to an intravenous injection of 0.1 mmol/kg (Gd content) of Gd/B/LDL. The ^{10}B concentration is measured *in vivo* by Magnetic Resonance Imaging (MRI) thanks to the Gadolinium probe of the molecule. To perform these *in vivo* tests a neutron shield is necessary to protect the healthy animal tissues; in fact, because of the irradiation chamber characteristics, the whole animal will be placed inside the facility. Two shielding materials are under study: 95% ^6Li enriched Lithium carbonate and 99% ^{10}B enriched boric acid. The effectiveness of the first prototype has been characterized only by Monte Carlo simulations, whereas the second one has been already used, as described in [9] and [10]. Because of the powder nature of the materials, a suitable containing structure is necessary. For Lithium carbonate a polystyrene hollow box is under study. For boric acid a home-made container of sticky tape has been built; the final thickness of the shield is about 0.1 cm (correspondent to 0.14 g/cm^2 of boric acid).

Monte Carlo simulations

The Monte Carlo N-Particles (MCNP) code is used to simulate the whole reactor facility as well as the biological systems. The most critical point in the simulations is the reliability of the particle source. The core emission is simulated sampling the neutrons with a uniform distribution in the volume of each fuel element. The energy spectrum is the Watt one. The simulation outputs are normalized thanks to an intensity factor depending on the reactor power of interest (for example: $1.9 \cdot 10^{16}$ s^{-1} at the maximum power of 250 kW). The validation of this source is reported in [1].

Depending of the biological system under study, the irradiation chamber geometry and materials description is changed. *Adherent cell cultures irradiation.* The irradiation position is

at the very end of the chamber. The Petri flask was simulated as a box (about 7.5*9.5*3 cm^3) with walls made by transparent polystyrene (1.05 g/cm^3) of 0.12 cm thickness. At the bottom, a thin layer of water (0.3 cm thickness) simulates the 20 ml culture medium. Some approximations were made to simulate the adherent cells. The cell layer has been described as a continuous layer; the soft tissue composition has been assumed (ICRU-46 [11]: 10.5% H, 25.6% C, 2.7% N, 60.2% O, 1% other elements; 0.987 g/cm^3). Tallies of neutron flux and absorbed dose were set in correspondence of the cell layer. In particular, the single components of the total absorbed dose were estimated: the contribution of the ^{10}B reaction, that of the $^{1}H(n,\gamma)^{2}H$ reaction, the proton contribution from the $^{14}N(n,p)^{14}C$ reaction and from ^{1}H scattering. Moreover, varying the number of Petri flasks, it was possible to study the mutual effect of the flasks in determining the total absorbed dose. *In vivo irradiation set-ups.* The irradiation position is the same of the cell cultures. To plan animal irradiation, very simplified phantoms of the rat (lung metastases BNCT) and of the mouse (Gd/B/LDL BNCT) were designed (Fig. 1A, 1B) starting, respectively, from papers [12] and [9].

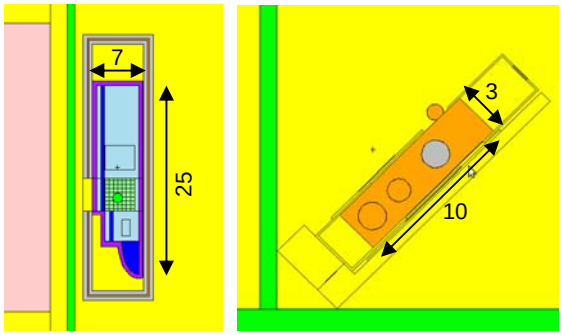

Fig 1. (A) upper rat model vision, (B) lateral mouse model vision, in the irradiation position. In both cases the neutrons come from the left. The phantom dimensions are reported (cm).

The organs were described as geometrical volumes; the tissues were defined as in ICRU-46 [11]. For the lung-BNCT studies, because of the spread structure of the disease, no tumour volume was defined but the lung was voxelized and tallies were set at each element. In the post-processing analysis of the lung outputs the tumour ^{10}B concentration is assumed to evaluate the effects of the treatment on the metastases. On the contrary, since in the Torino model the tumour is localized, the mouse phantom was defined with an external spherical volume (about 0.5 cm of radius). It is necessary to design a suitable neutron shield to protect the animal body. Many geometries and thickness values have been simulated. The incidental side-effects of the shield were evaluated; in particular, the secondary γ-emission from the shielding materials was evaluated (the 2.2 MeV γ-ray emitted by the $^{1}H(n,\gamma)^{2}H$ reaction and the 0.478 MeV γ-ray from the excited $^{7}Li^*$ ion produced in the 94% of the ^{10}B capture reactions).

2.2 Results

In vitro studies

The thermal flux uniformity has been verified. In particular, the decreasing rate along the x direction was estimated. Along the total length of the flask (about 15 cm), the flux decrease is 20%. In the same situation, the cell layer mean absorbed dose has been calculated. In Table 1 (first four columns) the total dose rate and the various contributions are reported at the maximum reactor power (250 kW) and for 1 ppm of ^{10}B in the cells. A linear correlation exists between the power reactor and the calculated neutron flux, as well as between the total dose rate and the ^{10}B concentration. Finally, some multi-flasks set-ups have been studied. In these situations, it was interesting to evaluate the effects on the absorbed dose that each flask produces on the neighbouring one. Because of its interactions, only the photon emission was studied. Due to the large amount of Hydrogen, the important reaction is the radiative capture $^{1}H(n,\gamma)^{2}H$. Secondly, because of the ^{10}B uptake by the cells, another monochromatic γ-ray field of 0.478 MeV is produced. Last column of Table 1 reports the results for the two- and three-flasks cases.

geometry	D (Gy/s)	% (α+^{7}Li)	% (protons)	% (γ)	γ auto-irradiation	γ ext irradiation
1 flask	$6.1 \cdot 10^{-3}$	18%	39%	43%	100%	0%
2 flasks	$6.2 \cdot 10^{-3}$	17.7%	38.7%	43.5%	98.8%	1.2%
3 flasks	$6.2 \cdot 10^{-3}$	17.7%	38.7%	43.5%	96.25%	3.75%

Table 1. Total absorbed dose in the cell layer and its components; in the last two columns, the mutual effects in the gamma fraction in presence of multiple flasks.

In vivo efficacy tests of the BNCT treatment for lung metastases

^{10}B pharmacokinetics. The ^{10}B concentration in the tumour and in the normal lung of the rat model was studied as a function of time. The tumour/lung ratio reaches a quite high value (≈ 3.5) starting 4 hours after ^{10}BPA-f infusion, so this time was chosen for irradiation. Just nowadays, the ^{10}B concentration in the other normal tissues is under study by the α-spectrometry method. In Table 2 some biodistribution results of the B16F1 model (developed by the Padova-Legnaro group) are reported. These values are very preliminary; in particular, they refer only to lung mixed samples. An analysis of the adjacent histology samples is scheduled, to get the correct estimation for the metastases and the normal parenchyma.

time (hours)	^{10}B conc (ppm) [± 20%]
2	4.2
4	4.1
6	2.5

Table 2. ^{10}B pharmacokinetics of the mouse lung metastases

Irradiation set-up. The shield nowadays under study was designed for the rat model. It is a polystyrene box (7*31*7 cm^3, 1.15 cm thickness) with empty walls for the 95% ^{6}Li enriched Lithium carbonate. The required thickness of the layer is 0.15 cm. The lung irradiation will be carried out thanks to a 4*4.5 cm^2 window in one of the box walls. Table 3 reports the estimated total weighted doses in the various organs of the phantom. Various contributions are considered in determining these total doses: the charged particle contribution and the photon contribution from the facility background, from the natural tissue composition as well as from the compound structure of the shielding materials. The reported values refer to the ^{10}B concentration as well as to the RBE and CBE factors measured by Coderre et al. [12]; the tumour uptake was estimated from the normal lung one adopting the 3.5 ratio measured in Pavia. To optimize the treatment, the animal is rotated by 180° at the half of the irradiation. The further development of the shield in planned to get a multi-purpose structure, for example using a removable wall. Building specific patterns of the irradiation windows in the inter-changeable walls, the box would fit different animal models. For example, taking advantage of the small dimensions of the B16F1 mouse model, up to six windows of 1.55*2 cm^2 could be opened. Some MCNP simulations are ongoing; when the pharmacokinetics of this model will be completed, the dose estimations for the described irradiation set-up will be calculated.

(A) rat model				**(B) mouse model**		
tissues	^{10}B ppm	D (Gy_w)	T.D. (Gy)	Tissues	^{10}B ppm	D (Gy)
metastases	76,6	23 – 47.5		tumour bulk	30.8	11.2
lung	21,9	2.9 – 6	7	Liver	55	3.7
heart	21.2	4.8	9.9	Lung	0.7	3.4
brain	11.2	0.4	9.9	Intestine	0.7	3.3
esophagus	32.4	2.4	13	soft tissue	7.7	4.1
intestine	32.4	2.0	18	whole body	8.4	4.0
spinal cord	11.2	1.4	17			
kidney	108.5	8	8.6			
skin inshield	21.5	3	42			

skin outshield	21.5	22.5	42	

Table 3. (A) Estimated total weighted doses in the rat phantom of the DHD lung metastases treated with ^{10}BPA-f; the ^{10}B ppms are from the paper [12] and refer to 4 hours after the BPA-f infusion; the tolerance values come from clinical literature. (B) Estimated total absorbed doses in the B16F10 murine melanoma treated with Gd/B/LDL; the ^{10}B ppms refer to 4-6 hours after the Gd/B/LDL infusion.

In vivo feasibility test of the BNCT treatment mediated by the adduct Gd/B/LDL

The irradiation took place in correspondence of the maximum ^{10}B concentration in the tumour bulk and lasted 7 minutes not to exceed the tolerable limits. The ^{10}B pharmacokinetics of the Gd/B/LDL is reported in [10]. The shield set-up was based on boric acid shields, three for each mouse, so it is able to cover all the body except the neck region. The shields are the same used in [9] To improve the treatment flux intensity, the animals were placed on a 45° rotated support. In this way the estimated flux in the tumour volume was about $5 \cdot 10^9$ cm^{-2}s^{-1}. Table 5 reports the ^{10}B concentrations at 4-6 hours after Gd/B/LDL infusion, as well as the total absorbed doses estimated by MCNP simulations. The follow up of the treated animals has shown that the tumour growth has been considerably reduced with respect to the irradiated control groups (Fig. 2B).

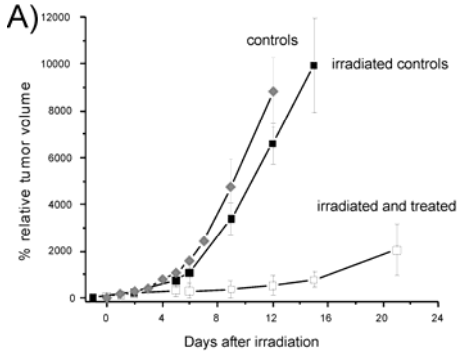

Fig 2. the relative tumour growth as a time function after the irradiation; there were two control groups: the irradiated controls group which was treated by a (neutron irradiation + no ^{10}B enrichment) and the controls group which did not receive any irradiation or any ^{10}B enrichment

3 Conclusions

The suitability of the T.R.I.G.A. reactor thermal column at the University of Pavia has been demonstrated and described. Its flexibility makes possible the implementation of a wide variety of biological experiments, with particular importance for BNCT research.

5 References

[1] Bortolussi S., Altieri S., Med. Phys., 34(12) 4700-4705, 2007
[2] Manera S., degree thesis, University of Pavia, 1994
[3] Carabelli V., degree thesis, University of Pavia,1997
[4] Zonta a. et al., Appl. Radiat. Isot., 67, S67-S75, 2009
[5] Wittig A. et al., Crit. Rev. Oncol. Hematol., 68, 91, 2008
[6] Altieri A. et al., Appl. Radiat. Isot., 66, 1850-1855, 2008
[7]Ferrari C. et al., accepted by Radiat. Res.
[8] Aime S. et al., Org. Biomol. Chem., 6, 4440-6, 2008
[9]Esposito J. et al., Nucl. Instr. And Meth. In Phys. Res. B, 266, 2587-2593, 2008
[10]Geninatti-Crich S. et al., Chemistry. An European journal, in press
[11] Bethesda M.D., ICRU Report 46, 1992
[12] J. Liu Kiger et al., Radiat. Res., 170(1), 60-9, 2008

OPTIMISATION OF THE CORE MANAGEMENT SCENARIO TO REACH HIGH FUEL BURNUP IN THE MYRRHA RESEARCH REACTOR

H. AÏT ABDERRAHIM[1], P. BAETEN[2], G. van den EYNDE[2], V. SOBOLEV[3]
[1]*General Management,* [2]*Advanced Nuclear Systems,* [3]*Nuclear Materials Science*
Belgian Nuclear Research Centre SCK·CEN
Boeretang 200, BE-2400, Mol, Belgium

K. NISHIHARA
Center for Neutron Science, Japanese Agency for Atomic Energy (JAEA)
Muramatsu 124-2, 319-1112 Tokai-Mura, Ibaraki-Ken, Japan

ABSTRACT

An innovative fast spectrum experimental facility MYRRHA has being developed by the Belgian Nuclear Research Centre SCK•CEN. The MYRRHA is an accelerator-driven system with a core loaded with fast reactor MOX fuel and cooled by liquid lead-bismuth eutectic. At this stage the selection of the facility operation mode and the fuel management scenario is of great importance. In the present article two different modes of the MYRRHA core management are compared: at constant power and at constant proton beam current. The results of neutronic and thermo-mechanical modeling are presented. It is shown that safer thermomechanical conditions for the fuel elements are predicted in the case of the core reshuffling with batches of ten fuel assemblies and with the ADS operation mode at a constant proton beam current.

1. Introduction

Since 1998 the Belgian Nuclear Research Centre SCK•CEN has being developed an innovative fast spectrum experimental facility MYRRHA (Multipurpose hYbrid Research Reactor for High-tech Applications). The MYRRHA is an accelerator-driven system (ADS) with a core loaded with fast reactor MOX fuel and cooled by liquid lead-bismuth eutectic (Pb-Bi). It can work in critical and subcritical mode; in the last case it is fed by a spallation neutron Pb-Bi source driven by a proton accelerator [1]. From the beginning this project is in close relation with EURATOM Framework Programs [2]. At this stage the selection of the facility operation mode and the fuel management scenario is of great importance. This can affect the main performances, availability and operation costs. The present article compares scenarios of the MYRRHA ADS core management with two different modes of operation: at a constant core power and at a constant proton beam current. First a general description of the MYRRHA core and its performances is given, then the proposed core reshuffling scheme is explained. In the forth section modeling tools are briefly described. The results of neutronic and thermo-mechanical modeling are presented and discussed in the fifth section. It is shown that the proposed design can achieve the targeted neutronic performances practically in both considered cases, and that a large margin to the fuel melting exists until the end of the targeted fuel residence time of about three years. However, safer thermomechanical conditions for the fuel elements are predicted in the case of the operation mode at a constant proton beam current.

2. MYRRHA core performances at start

The radial schematic view of a variant of the MYRRHA ADS core and schematic axial views of a fuel assembly (FA) and a fuel element (FE) are presented in Figure 1. A space of 3 central hexagons is occupied by a spallation target module. The core can contain up to 183 hexagonal assemblies of which 65 to 97 are FA. 8 positions are occupied by in-pile sections for irradiation devices. Dummy assemblies form a reflector layer around the active zone.

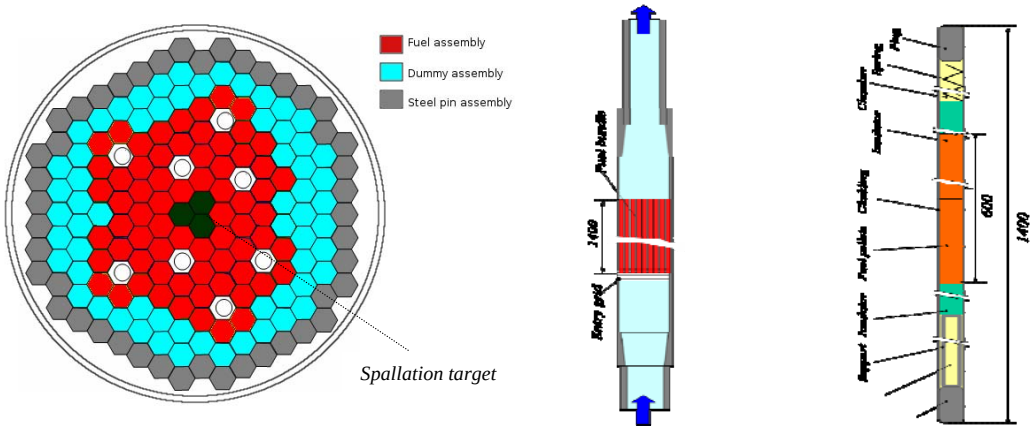

Fig 1. Schematic views of variants of MYRRHA core, fuel assembly and fuel element

Each FA contains 90 FEs with a diameter of 6.55 mm surrounding a central instrumentation rod within a T91 steel hexagonal wrapper (94 mm width). Each FE contains MOX fuel pellets, reflector segments, gas plenums within a cladding made of T91 steel closed from both sides with plugs. A more detailed description of this variant of the MYRRHA core, fuel assembly and fuel element can be found in [3]. The main core parameters are given in Table 1. As MYRRHA is conceived as irradiation facility, the fast neutron flux (~10^{15} cm^{-2} s^{-1}) is considered as the most important characteristic of its performances.

Parameter		Unit	Value
Accelerator:			
Proton beam energy		MeV	600
Proton beam current		mA	3.2
Spallation target:			
Proton beam deposited heat		MW	1.5
Total neutron yield per incident proton			15.3
Core:			
Fuel type		MOX	$(U, Pu)O_{2-x}$
Initial Pu fraction in heavy metal (HM)		wt%	35
Core neutron multiplication factor (k_{eff})			0.955
Thermal power		MW	85
Peak segment linear power		W cm^{-1}	380
Maximum neutron flux:	Φ_{tot}	10^{15} $cm^{-2}s^{-1}$	4.5
	$\Phi_{>0.1\ MeV}$		3.3
	$\Phi_{>1MeV}$		0.78

Table 1: Main parameters of the considered variant of the MYRRHA core at start

The normal operation of the MYRRHA ADS is organized in cycles of 90 days separated by shutdown periods of 30 or 90 days for the reactor maintenance, reloading irradiation devices and the core reshuffling. The normal shutdown period is of 30 days; a shutdown period of 90 days is organised after every three operation cycles.

3. Core reshuffling scheme

In order to compensate the core reactivity loss caused by the fuel burning, it is needed either to add new fuel assemblies, or to replace some partially "burned" assemblies with fresh ones. Different core reshuffling schemes were analysed in the framework of the MYRRHA and EUROTRANS projects [3,4]. Finally a scheme was selected [5], where ten fuel assemblies with close burnup are organised in batches, and each batch is moved after every cycle in the outward radial direction from its initial position to the position of the next batch with lower average burnup. At equilibrium ten fuel assemblies are removed from the core after each cycle and ten fresh fuel assemblies are added.

Two scenarios were selected for more detailed analysis: in the first one the core power is kept constant by means of an increase in the proton beam current; in the second the proton beam current is constant. An intermediate variant is a scenario with a constant neutron flux.

4. Modelling tools

Neutronic modelling was performed with MCNPX [6] using the neutronic data library JEFF3.1 and with the Monte Carlo burn-up code system ALEPH [7] (developed at SCK•CEN), employing the MCNPX, the modified version of the ORIGEN-2.2 burnup code [8] and the ZZ ALEPH-LIB-JEFF3.1 continuous energy multi-temperature nuclear data library. During calculations the used input nuclear data are adapted at each step to the neutronic spectrum calculated by MCNPX at the precedent step.

Thermomechanical modelling of the behaviour of the hottest fuel elements was performed with the FEMAXI-SCK fuel performance code. This code is based on the FEMAXI-V fuel performance code (developed by M. Suzuki at JAERI) [9]). New database for properties of MOX fuel, T91 cladding material and Pb-Bi coolant were introduced and some models were modified in order to apply this code for the preliminary design of the MYRRHA driver fuel and for the estimation of its thermo-mechanical performances.

5. Neutronic analysis

The number of the fresh FAs needed to reach the targeted k_{eff} ~0,95 at start of the reactor operation is 65 in both cases, "constant power" (A) and "constant current" (B). Then, in the case A, the FA number grows up to 83 and fluctuates between 82 and 83; in the case B the FA number increases up to 80 (Fig. 2). Because 10 fuel assemblies belong to a "batch", each batch will reside in the core 8 cycles at equilibrium, except for 2-3 outer FAs in the case A; they are managed independently. A larger number of FAs at equilibrium in the "constant power" case is explained by a slightly higher power density.

The core criticality level at the beginning of each cycle (BOC) is in the interval of 0.954-0.957 (Fig. 2), while the criticality drop per cycle becomes slightly smaller for the later operation because of the larger fuel amount in the core. The averaged criticality drop at equilibrium is about 1550 pcm in the A case and 1400 pcm in the B case.

In the case A, the beam current is strengthened during each cycle to compensate the criticality drop as shown in Figure 3 (left). The maximum current of 4.8 mA and the maximum neutron flux of 5×10^{15} cm^{-2} s^{-1} are reached in the end of the 1st cycle; these values reduce in

the following cycles where the core is larger. In the B case, the core power and the neutron flux reduce in each cycle, as seen in Figure 3 (right).

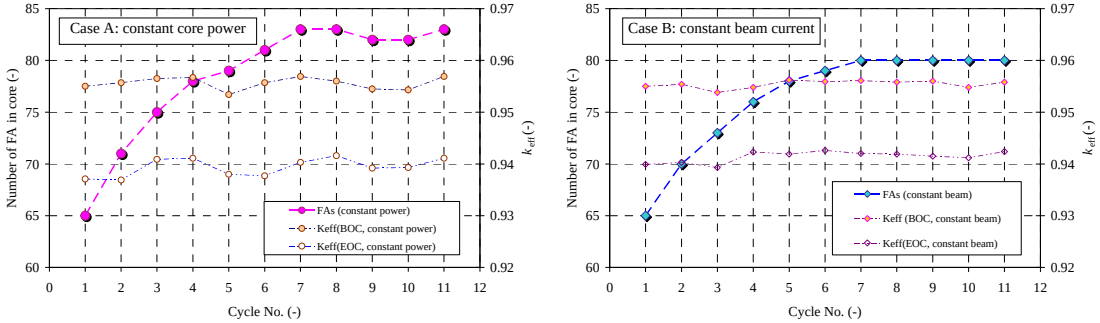

Fig. 2. Number of fuel assemblies in the core and k_{eff} in each cycle at BOC and EOC

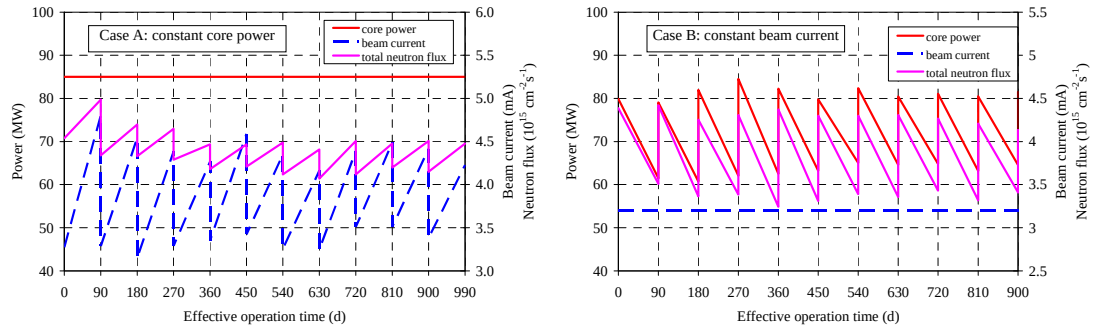

Fig. 3. Evolution of the core power, proton beam current and total neutron flux

Figure 4 provides the fuel linear power, fuel burn-up and clad radiation damage in the hottest segments of the hottest fuel element of the first batch. The fuel peak linear power at start is 380 W cm^{-1} and reduces to about 180 W cm^{-1} in the case A and 150 W cm^{-1} in the case B by the end of the 9th cycle. The fuel burn-up reaches respectively 105 and 90 MWd kg$_{HM}^{-1}$. The radiation damage of the cladding in "atom displacements per atom" (dpa) in the end of the batch residence time is 54 dpa in the case A and 50 dpa in the case B.

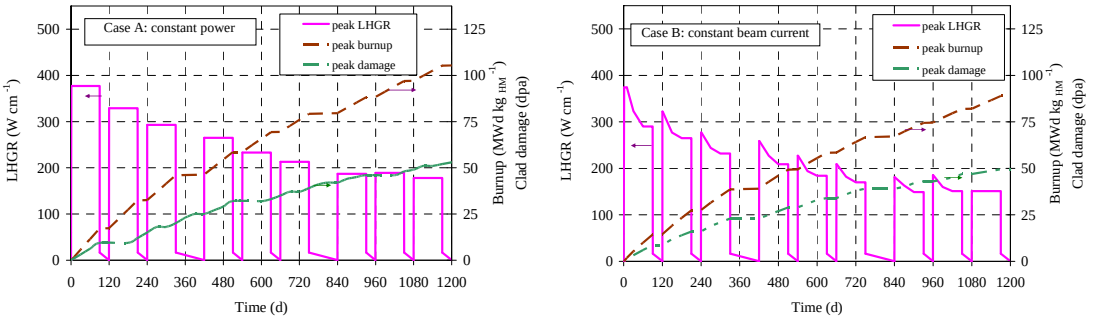

Fig. 4. Evolution of the fuel linear power, fuel burn-up and clad radiation damage in the hottest fuel element of the first batch

6 Thermomechanical behaviour

In the preliminary design of a fuel element of MYRRHA ADS it was aimed to avoid a strong pellet-cladding mechanical interaction (PCMI) during a whole period of fuel operation at the nominal power level. In spite of the fact that PCMI is permitted in traditional power reactors, two peculiarities of MYRRHA-ADS push us to take care of PCMI: the cladding material embitterment and frequent trip/restarts of the proton beam. It is expected that T91 can suffer sever embrittlement under typical MYRRHA conditions; therefore, a "rapid" PCMI can be very dangerous. It was assumed that the fuel lifetime in the MYRRHA core should be limited by the time of the onset of a strong PCMI. The conservative hottest fuel element position in each batch was considered in all cases for thermo-mechanical modelling.

The results of the performed modelling show that in both considered cases, A and B, a large margin to fuel melting exists until the end of the 9th cycle (Fig. 5). The maximum gas pressure within the hottest fuel elements reaches 1.6-1.7 MPa. This is significantly below the estimated permitted level even for the fresh cladding (~20 MPa).

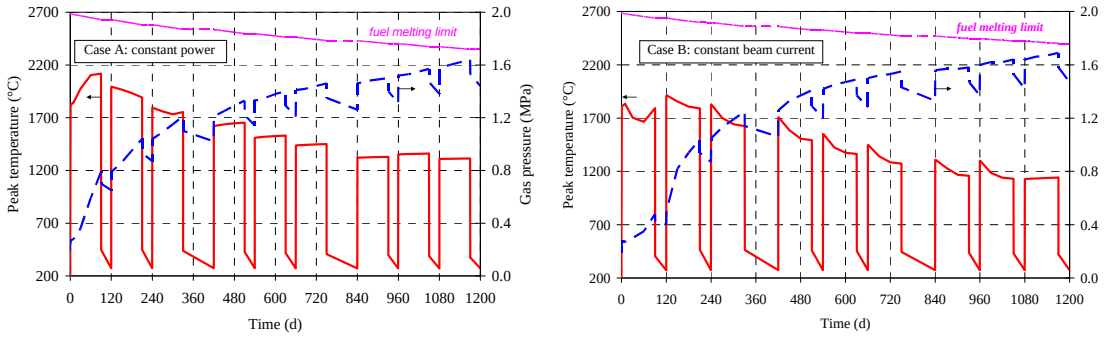

Fig. 5. Peak temperature and gas pressure in the hottest fuel element of the first batch

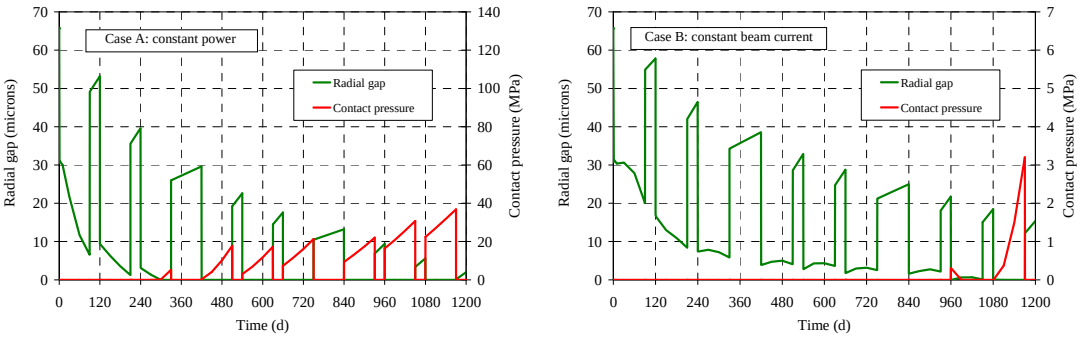

Fig. 6. Radial gap and contact pressure in the hottest fuel element of the first batch

In Figure 6 (left) it can be seen that in the “constant power” case (A) the pellet-cladding gap is closed already in the 3rd cycle and the built contact pressure achieves (~20 MPa) in the end of the 6th cycle (peak burnup ~42 MWd kg_{HM}^{-1}). This contact pressure, however, still remains below the allowed limit for the irradiated at this doses cladding until the end of the residence period of nine cycles. In the “constant beam” case the pellet-cladding gap is completely open until the end of the seventh cycle (peak burnup ~75 MWd kg_{HM}^{-1}). In the 8th cycle the PCMI is very weak and reaches ~3.2 MPa in the end of the 9th cycle (Fig. 6, right).

7 Conclusions

This work presents some results of studies of multi-step fuel re-shuffling in the core of MYRRHA ADS. Two scenarios were analyzed in more details: at a constant core power and at a constant proton beam current. In both cases a batch of ten fuel assemblies with similar burnup is moved after each operation cycle in the outside radial direction. After each cycle, one of the batches is discharged and replaced by fresh one. In the constant power case, the proton beam current is gradually increased during each cycle to partially compensate for the reactivity loss; in the constant proton beam case, this compensation is not done and one has to live with a decreasing power. Starting with a fully fresh core with 65 fuel assemblies, a kind of equilibrium situation is reached with about 80-83 fuel assemblies.

Using the results of the neutronic analysis, the preliminary estimation of the thermomechanical behaviour of the hottest fuel elements was done. The conservative cases were considered where the studied fuel elements were placed in every batch in the hottest position. The obtained results show that in both cases the fuel elements will survive during nine cycles of normal operation, however, the constant proton beam current case would be a better choice from the point of view of safety and simplicity of management. Nevertheless, depending on strategy and needs of the reactor utilisation, one can keep constant either the core power, or the neutron flux in the in-pile irradiation sections, or the proton beam current.

8 References

[1] P. Baeten, R.l Fernandez, D. De Bruyn, *et al.*, MYRRHA, A flexible fast spectrum irradiation facility, in: Proc. Research Reactor Fuel Management (RRFM 2011), European Research Reactor Conference, 20-24 March 2011, Rome, Italy (in press).

[2] J.U. Knebel, H. Ait Abderrahim, L. Cinotti, *et al.*, EUROTRANS, European research programme for the transmutation of high-level nuclear waste in an accelerator driven system, in: Proc. FISA 2006, EU Research and Training in Reactor Systems, Luxemburg, pp. 353-372.

[3] H. Aït Abderrahim, A. Almazouzi, P. Baeten, *et al.*, MYRRHA Project: Multi-purpose hYbrid Research Reactor for High-tech Applications at Mol (Belgium), MYRRHA Technical Description, SCK•CEN, Mol, October 2008.

[4] K. Nishihara, G. Van den Eynde, E. Malambu, *et al.*, XT-ADS Core neutronics & Cycle analysis, Deliverable 1.34 & 1.35, Euratom FP6 IP EUROTRANS, Contract No. FI6W-CT-2004-516629, SCK•CEN, Mol, 2009.

[5] K. Nishihara, D. Maes, V. Sobolev, B. Arien, MYRRHA Flux Update: Optimisation of the MYRRHA core, SCK•CEN Report I-144, Mol, Belgium, 2009.

[6] MCNPX User's Manual, Version 2.5.0, Ed. D. B. Pelowitz, Los Alamos National Laboratory report LA-CP-05-0369, Los Alamos, New Mexico, 2005.

[7] W. Haeck, ALEPH 1.1.2, A Monte Carlo Burn-Up Code, SCK•CEN Report BLG-1003, Mol, Belgium, 2006.

[8] A.G. Croff, ORIGEN2: A Versatile Computer Code for Calculating the Nuclide Compositions and Characteristics of Nuclear Materials, Nucl. Technol. **62** (1983) 335-352.

[9] M. Suzuki, Light Water Reactor Fuel Analysis Code FEMAXI-V, JAERI Report, Tokai-Mura, Japan, January 2001.

RADIATION TRANSPORT SIMULATION FOR BORON NEUTRON CAPTURE THERAPY (BNCT)

M. Ziegner, M. Blaickner
AIT Austrian Institute of Technology GmbH, Health & Environment Department - Molecular Medicine
Muthgasse 11, 1190 Wien - Austria

M. Ziegner, R. Khan, H. Böck
Vienna University of Technology, Institute of Atomic and Subatomic Physics
Stadionallee 2, 1020 Wien - Austria

S. Bortolussi, S. Altieri
Department of Nuclear and Theoretical Physics University of Pavia
National Institute of Nuclear Physics (INFN) Pavia Section, Pavia, Italy
Via Bassi 6, 27100 Pavia - Italy

T. Schmitz, G. Hampel
Nuclear Chemistry, University of Mainz
Fritz Strassmann Weg 2, 55099 Mainz – Germany

ABSTRACT

This work is part of a larger project initiated by the University of Mainz and aiming to use the university's TRIGA reactor to develop a treatment for liver metastases based on Boron Neutron Capture Therapy (BNCT). Diffuse distribution of cancerous cells within the organ makes complete resection difficult and the vicinity to radiosensitive organs impedes external irradiation. Therefore the method of "autotransplantation", first established at the University of Pavia, is used. The liver is taken out of the body, irradiated in the thermal column of the reactor, therewith purged of metastases and then reimplanted. A highly precise dosimetry system is to be developed by means of measurements at the University of Mainz and computational calculations at the AIT.

The stochastic MCNP-5 Monte Carlo-Code, developed by Los Alamos Laboratories, is applied. To verify the calculations of the flux and the absorbed dose in matter a number of measurements are performed irradiating different phantoms and liver sections in a 20cm x 20cm beam tube, which was created by removing graphite blocks from the thermal column of the reactor. The detector material consists of L- α –alanine pellets which are thought to be the most suitable because of their good tissue equivalence, small size and their wide response range. Another experiment focuses on the determination of the relative biological effectiveness (RBE-factor) of the neutron and photon dose for liver cells. Therefore cell culture plates with the cell medium enriched with ^{157}Gd and ^{10}B at different concentrations are irradiated.

With regard to the alanine pellets MCNP-5 calculations give stable results. Nevertheless the absorbed dose is underestimated compared to the measurements, a phenomenon already observed in previous works. The cell culture calculations showed the enormous impact of the added isotopes with high thermal neutron cross sections, especially ^{157}Gd, on the absorbed dose, increasing it by a factor up to 100.

Introduction

It was first shown at the TRIGA reactor in Pavia that the autotransplantation method is feasible in order to cure disseminated liver metastases which are not treatable by the traditional means such as surgery, chemotherapy, external beam therapy or brachytherapy. Neutron Capture Therapy is based on the idea of accumulating a tracer with a high cross

section for neutrons in cancerous tissue to make this tissue more sensitive to neutron irradiation [1]. Therefore it uses a form of biological targeting, i.e. the metabolic properties of the tracer determine the dose distribution pattern whereas in conventional radiotherapy the targeting is of physical form, i.e. altering the irradiation geometry and the spectrum of the photon beam. Boron and Gadolinium isotopes are used for neutron capture at several institutions and huge research effort is spent on suitable carrier molecules [2,3].
The autotransplantation method is thought to overcome the drawbacks of cumbersome redesigning of the TRIGA reactor for beam collimation as well as unwanted dose deposition in healthy tissue [4,5]. To demonstrate the effectiveness of the autotransplantation method and its advantage over external beam radiotherapy in the case of disseminated liver metastases a dose monitoring system has to be established and parameter studies are to be undertaken.

Materials and Methods

The stochastic MCNP-5 Monte Carlo-Code, developed by Los Alamos Laboratories [6], is applied to simulate the neutron and gamma flux from the reactor core through the thermal column. The thermal column of the reactor had been identified in previous parameter studies [7] as the optimal site for the irradiation of the explanted liver. Not only do the dimensions permit an easy placement of the organ with the opportunity of rotation but the column also shows a very constant flux of thermal neutrons in the center. A central beam tube can easily be realized by removing one or more graphite blocks. At a final stage a 40cm x 40cm beam tube is planned, but for preliminary evaluations a 20cm x 20cm beam tube with a 5cm Bismuth gamma shielding has been realized where a box with an explanted liver can be introduced and irradiated.

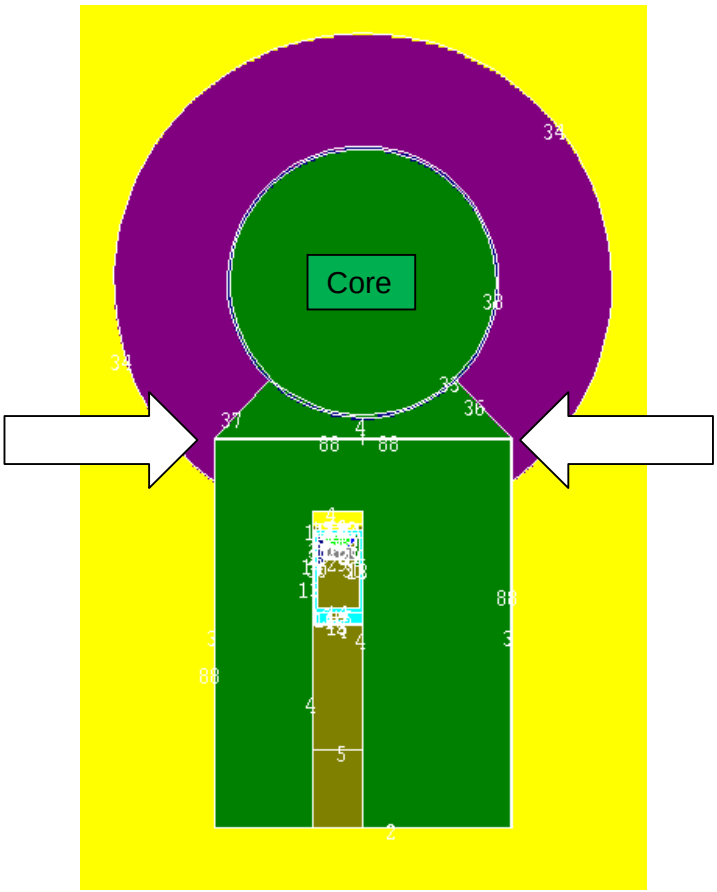

Fig 1: top view of the reactor model where a detailed simulation of the reactor core was replaced by a particle emitting plane (63cm from core) indicated by the two arrows

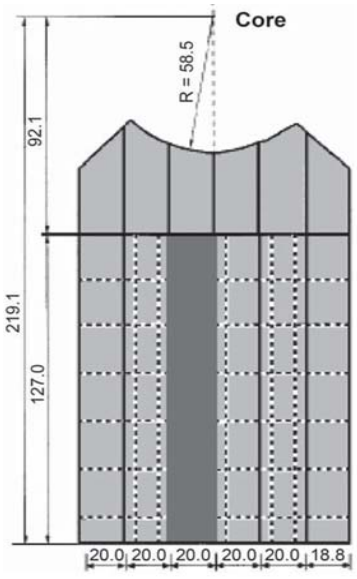

Fig 2: geometry of the thermal column

The very constant neutron and gamma fluxes in the thermal column allow for simplification of the reactor model in the Monte Carlo simulations [8]: The origin of the particles in fuel cylinders of the reactor core can be neglected and a particle emitting plane at the beginning of the thermal column (63cm from the reactor center) can be used instead. This source plane is suggested as a two dimensional isotropic 119.4cm x 119.4cm source with a number of energy bins and particle probabilities which were established and evaluated in previous works [7,9,10,11].

The irradiation experiments that take place at the TRIGA reactor in Mainz and are modelled via MCNP in this work are set up as follows: The dissected liver lobe is cut into slices and alanine dosimeters are shrink-wrapped in PE foil and sewed into it together with gold foils. The irradiated alanine dosimeters are analyzed using an electron spin resonance (ESR) spectrometer [12]. The value of the ESR signal correlates to the number of radicals and to the amount of absorbed dose. The alanine dosimeters are read out at NPL (National Physical Laboratory, UK), applying the Hansen & Olsen model for the alanine detector response [13,14,15,16]. In this way the total absorbed dose in the dosimeters can be assessed.

The second series of irradiation experiments are performed in order to determine the RBE-factors [17] and use cell lines from liver carcinoma with and without ^{10}B- and ^{57}Gd enrichment at different concentrations. For both the liver lobes equipped with detectors as well as the cell cultures the total absorbed dose in the respective volumes will be calculated using the MCNP dose deposition protocols.

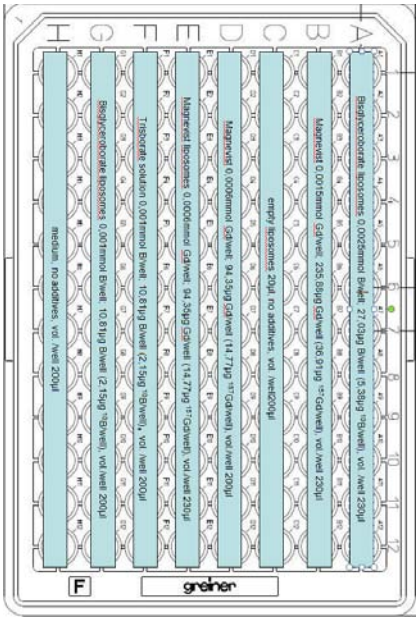

Fig 3: 98well cell culture plate with ^{10}B and ^{157}Gd at different concentrations

Results

The first evaluations of the simulated radiation field for the irradiation of the autotransplanted liver in the thermal column of the TRIGA Mainz show a good correlation between measured and simulated values. Nevertheless a slight underestimation can be observed. This lack of accuracy can be attributed to uncertain geometric dimensions of the liver (simulated as an ellipsoid) and/or other simplifications in the simulation model such as the immediate surrounding..

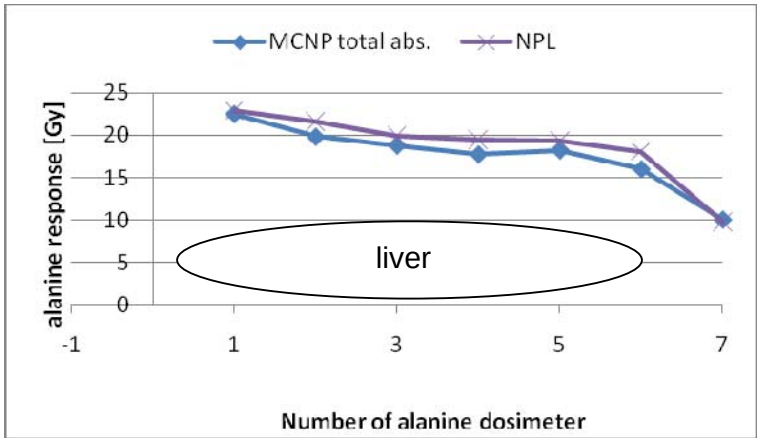

Fig 4: Measured response of the alanine dosimeters (purple) and MCNP simulations (blue) and their relative position in the liver

The cell culture calculations show the enormous impact of the added isotopes with high thermal neutron cross sections, especially ^{157}Gd (254000 barn), on the absorbed dose, increasing it by a factor up to 100!

Further calculations will focus on the dose discrimination between the different contributors to the total absorbed dose. A more effective gamma shielding is to be implemented in the irradiation facility TRIGA Mainz to maximize the therapeutic outcome.

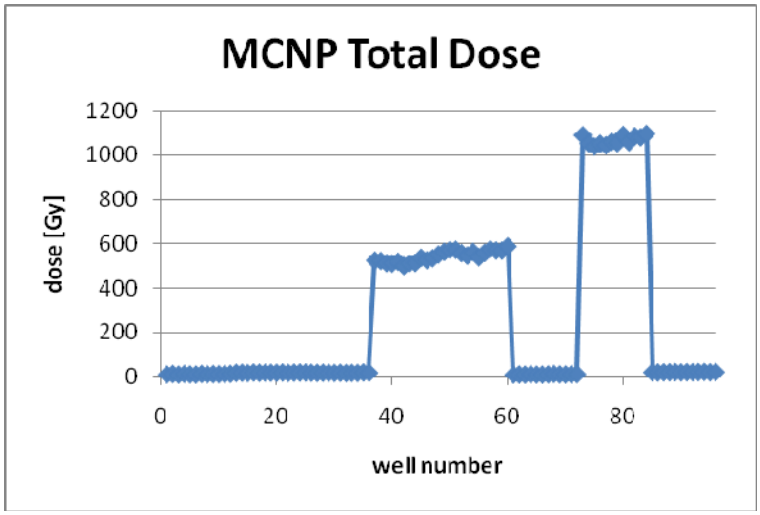

Fig 5: Total absorbed dose in the wells. The two high plateaus correspond to^{157}Gd enriched media

Conclusions

The observed underestimation in simulation of the irradiated liver is still being investigated. Besides liver geometry and boron concentration other causes as oversimplification of the reactor model and inaccurate representation of the source are possible. For further improvement criticality calculations will be performed which crosscheck the currently used data for source strengths and spectra of neutrons and photons. This is done by developing a MCNP criticality calculation which incorporates the burn up history from the first core to the current one. In the course of this work step experience gained at the TRIGA Vienna will be used to model the calculations for the TRIGA reactors in Mainz and Pavia.

References

[1] Locher GL. Biological effects and therapeutic possibilities of neutrons. Am J Roentgenol 1936;36:1 – 13.
[2] Yamamoto T, Nakai K, Matsumura A. Boron neutron capture therapy for glioblastoma. Cancer Lett 2008;262:143 – 152.
[3] Kato I, Ono K, Sakurai Y, Ohmae M, Maruhashi A, Imahori Y, et al. Effectiveness of BNCT for recurrent head and neck malignancies. Topics in Neutron Capture Therapy: Proceedings of the Eleventh World Congress on Neutron Capture Therapy (ISNCT-11). App Radiat Isot 2004;61:1069 – 73.
[4] Zonta A, Prati U, Roveda L, Ferrari C, Zonta S, Clerici AM, et al. Clinical lessons from the first applications of BNCT on unresectable liver metastases. J Phys: Conference Series 2006; 41:484 – 95.
[5] Bortolussi S, Boron Neutron Capture Therapy of Disseminated Tumours, Dipartimento di Fisica Nucleare e Teorica, Università degli Studidi Pavia, Italy 2007, PhD Thesis.
[6] MCNP - a general Monte Carlo N-Particle Transport Code (Version 5),X-5 Monte Carlo Team, Los Alamos National Laboratory, 24 April 2003. http://www-rsicc.ornl.gov/
[7] Wortmann B. Auslegung und Optimierung einer Bestrahlungseinrichtung für die Bor Neutronen Einfang Therapie an autotransplantierten Organen; Fakultät Maschinenwesen,
[8] Khan R, Neutronics Analysis of the TRIGA Mark II Reactor Core and its Experimental Facilities, Faculty of Physics, Vienna University of Technology, Austria 2010, PhD Thesis.
[9] Schmitz T, Dose calculation in biological samples in a mixed neutron-gamma fi eld at the TRIGA reactor of the University of Mainz; Acta Oncologica, 2010; 49: 1165–1169,
[10] Schmitz T, Bestimmung und Simulation der Neutronen- und Gammadosis in der thermischen Säule des TRIGA Reaktors Mainz und Borbestimmung in Blut- und Gewebeproben mittels Prompt-Gamma-Aktivierungsanalyse im Rahmen der Bor-Neutronen-Einfangtherapie, Institut für Kernchemie der Johannes Gutenberg Universität Mainz, Germany 2010; Master's Thesis.
[11] Vogtländer L, Untersuchung von Photonendosis und Neutronenfluss im 20 x 20 x 27cm3 Bestrahlungskanal in der thermischen Säule des TRIGA Reaktors an der Johannes Gutenberg-Universität Mainz, Institut für Kernchemie der Johannes Gutenberg Universität Mainz, Germany 2009; Master's Thesis.
[12] Sharpe P, Sephtan J. An automated system for the measurement of alanine/EPR dosimeters. Appl Radiat Isot 2000;52:1185 – 8.
[13] Hansen JW, Olsen KJ. Theoretical and experimental radiation effectiveness of the free radical dosimeter alanine to irradiation with heavy charged particles. Radiat Res 1985;104: 15 – 27.
[14] Hansen JW, Olsen KJ, Wille M. the alanine radiation detector for high and low LET Dosimetry. Radiat Prot Dosimetry 1987;19:43 – 7.
[15] Hansen JW, Waligorski MPR, Byrski E. Intercomparison of gamma ray X-ray and fast neutron dosimetry using alanine detectors. Radiat Prot Dosimetry 1989;27:85 – 92.
[16] Bassler N, Hansen J.W, Palmans H, Holzscheiter MH, Kovacevic S. The antiproton depth-dose curve measured with alanine detectors. Nuc Instr Meth Phys Res B 2008;26:929 – 36
[17] Butts JJ, Katz R. Theory of {RBE} for heavy ion bombardment of dry enzymes and viruses. Radiat Res 1967;30:855 – 71.

European Nuclear Society
Rue Belliard 65
1040 Brussels, Belgium
Telephone: +32 2 505 30 50 - FAX: +32 2 502 39 02
rrfm2011@euronuclear.org
www.rrfm2011@euronuclear.org